McGill | Faculty of Engineering

DEVELOPMENT OF PARTIALLY BIO-BASED HYBRID HYDROXYURETHANE-CROSSLINKED NETWORKS

Ph.D. Thesis, October 2023

Submitted by:

Mohammad Farkhondehnia

Department of Chemical Engineering
McGill University
Montréal, Quebec, Canada

A thesis submitted to McGill University in partial fulfillment of the requirements for the degree of Doctor of Philosophy

ABSTRACT

Polyurethanes (PUs) are a versatile polymer family that have immense importance in everyday items. PUs are extensively applied in construction, adhesives, coatings, thermoplastics, and thermoset materials. Thermosetting PUs alone accounted for over 70 wt% of total PU production in 2021. PUs possess attractive properties but are associated with harmful isocyanates as precursors. Consequently, there is growing interest in developing safer alternatives through the synthesis of non-isocyanate polyurethanes (NIPUs). Polyaddition of cyclic carbonates with amines yielding poly(hydroxyurethane)s (PHUs) is the most promising route for NIPU synthesis. However, PHUs typically exhibit inferior mechanical properties compared to traditional PUs. The development of hybrid formulations, particularly hybrid PHUs (HPHUs), are one way to enhance the mechanical properties of PHUs. The term "hybrid" in HPHUs can refer to various interpretations, such as chemical structure modifications with inorganic polymers or the use of different polymerization methods for desired functionality. We are effectively using the latter definition for most of this thesis. The first manuscript focuses on using various polymerization techniques with moisture-sensitive silanes as end caps, followed by curing. The subsequent manuscripts in this thesis employ a hybrid approach, combining different polymerization methods. First, moisture-curable HPHUs are prepared. *β*-Myrcene is copolymerized with glycidyl methacrylate (GMA) via free radical polymerization, resulting in copolymers with epoxy pendent groups. The synthesized copolymers are then treated by carbon dioxide (CO_2) to convert epoxy functional groups to cyclic carbonates.

Adding a diamine (e.g., Jeffamine D-4000) forms urethane linkages in the side chains, with the concentration adjusted by varying the initial molar fraction of GMA. Those resins are end-capped via moisture sensitive silanes to provide crosslinked networks but were excessively soft

with Young´s modulus (*E*) values ranging from 32 kPa to 50 kPa. Once this hybridization proof of concept was established, the influence of backbone and side chain rigidity on the mechanical and rheological properties of the crosslinked HPHUs is investigated. Atom transfer radical polymerization (ATRP) is employed to copolymerize C13MA, a vegetable oil-derived alkyl methacrylate with an average side chain length of 13, with GMA, resulting in the formation of a flexible backbone. Then the copolymers are carbonated and then reacted with 1,10-diaminodecane (DAD) to form rigid side chains via hydroxyurethane linkages. By controlling the template functionality, crosslinked networks are obtained, exhibiting a wide range of *E*s from 0.1 MPa to 71.9 MPa. Next, effect of backbone flexibility is investigated by polymerization of binary methyl, ethyl, butyl methacrylate (MMA, EMA, BMA)/GMA mixtures with different GMA initial molar fractions. The copolymers are then treated with CO_2 and then are reacted with Priamine 1074 to form networks crosslinked through urethane linkages. Depending on degree of flexibility of backbones and cyclic carbonate functionality, crosslinked networks showed *E* ranging from 395 MPa to 1250 MPa, displaying brittle behavior. Although a wide range of crosslinked HPHUs are prepared, due to the presence of only two urethane linkages in the side chains, they do not strongly qualify as NIPUs. Therefore, diglycerol dicarbonate (DGC) and D-mannitol biscarbonate (MBC) are polymerized with Priamine 1074 and DAD to synthesize amine-terminated thermoplastic PHUs. These PHUs are then used as crosslinkers with C13MA/GMA templates, forming hybrid crosslinked NIPUs. Hybrid crosslinked NIPUs are achieved with *E*s ranging from 2.35 MPa to 20.85 MPa (DGC-based) and 1.24 MPa to 6.45 MPa (MBC-based). These values show higher *E* values compared to C13MA/GMA templates crosslinked with DAD with the same initial molar ratio of GMA in the templates, due to increased hydroxyl groups.

RÉSUMÉ

Les poly(uréthane)s (PUs) sont des polymères polyvalents d'importance majeure dans la vie quotidienne. Ses applications incluent la construction, les adhésifs, les revêtements, les thermoplastiques et les matériaux thermodurcissables. Les PU thermodurcissables représentaient à eux seuls plus de 70% de la production totale de PU en 2021. Malgré leurs propriétés attractives, les PUs sont associés à l'inconvénient majeur de l'utilisation d'isocyanates nocifs comme précurseurs. Par conséquent, le développement d'alternatives plus sûres par la synthèse de poly(uréthane)s sans isocyanate (NIPUs) suscite un intérêt croissant. La polyaddition de carbonates cycliques avec des amines est la voie la plus prometteuse pour la préparation des NIPUs. Cela mène à la synthèse de poly(hydroxy-urétane)s (PHUs). Cependant, les PHUs ont souvent des propriétés mécaniques inférieures aux PUs traditionnels. Le développement de formulations hybrides, en particulier de poly(hydroxy-uréthane)s hybrides (HPHUs), est un moyen d'améliorer les propriétés mécaniques des PHUs. Le terme "hybride" dans les HPHUs peut avoir différentes interprétations, telles que des modifications de structure chimique avec des polymères inorganiques ou l'utilisation de méthodes de polymérisation variées pour obtenir une fonctionnalité spécifique. Le β-myrcène est copolymérisé avec le méthacrylate de glycidyle (GMA) par polymérisation radicalaire pour former des copolymères avec des groupes époxy pendants. Les copolymères synthétisés sont ensuite traités au dioxyde de carbone (CO_2) pour convertir les groupes fonctionnels époxy, en carbonates cycliques. L'addition ultérieure d'une diamine (Par exemple, Jeffamine D-4000) forme des liaisons uréthane dans les chaînes latérales, la concentration étant ajustée en faisant varier la fraction molaire initiale de GMA. Ensuite, ces résines réagissent avec des silanes sensibles à l'humidité pour former des réseaux réticulés, mais elles étaient relativement souples avec un module d'Young (E) compris

entre 32 kPa et 50 kPa. Ensuite, la polymérisation radicalaire par transfert d'atomes (ATRP) fut utilisée pour copolymériser le C13MA, un méthacrylate d'alkyle dérivé d'une huile végétale, avec le GMA, ce qui entraîne la formation d'une chaine principale flexible. Les copolymères sont ensuite traités au CO_2 via cyclo-addition puis réagissent avec du 1,10-diaminodécane (DAD) pour former des chaînes latérales rigides par l'intermédiaire de liaisons hydroxy-uréthane. En contrôlant la fonctionnalité du modèle, des réseaux réticulés sont obtenus et présentent une large gamme de modules d'Young allant de 0,1 MPa à 71,9 MPa. L'effet de la flexibilité du squelette a ensuite été étudié par polymérisation de mélanges binaires MMA, EMA, BMA/GMA. Les copolymères sont traités au CO_2 et réagissent avec la Priamine 1074 pour former des réseaux réticulés par des liaisons uréthanes. En fonction du degré de flexibilité des squelettes et de la fonctionnalité du carbonate cyclique, les réseaux réticulés présentent une valeur *E* allant de 395 MPa à 1250 MPa. Bien que de nombreux HPHU réticulés soient préparés, leur composition limitée à deux liaisons uréthane dans les chaînes latérales ne les qualifie pas comme des NIPUs. Par conséquent, le dicarbonate de diglycérol (DGC) et le bicarbonate de D-mannitol (MBC) sont polymérisés avec la Priamine 1074 et le DAD pour synthétiser des PHUs thermoplastiques à terminaison amine. Ces PHUs sont utilisés comme agents de réticulation pour former des NIPUs hybrides réticulés en réagissant avec le couple de monomères C13MA/GMA. Les HPHUs réticulés sont obtenus avec des valeurs *E* allant de 2,35 MPa à 20,85 MPa (à base de DGC) et de 1,24 MPa à 6,45 MPa (à base de MBC). Ces valeurs de E obtenues sont plus élevées par rapport aux modèles C13MA/GMA réticulés avec du DAD, malgré le même rapport molaire initial de GMA, ceci s’explique par l'augmentation du nombre de groupes hydroxyle.

ACKNOWLEDGMENTS

Writing this thesis made me to reflect upon the years I have dedicated to my graduate studies. During this period of time, I have had the privilege of meeting numerous individuals whose contributions and support have played a vital role in my personal and professional growth.

First and foremost, I would like to express my sincere gratitude to my supervisor, Prof. Milan Marić, for all the support and guidance throughout my degree. I consider myself fortunate to have had such a kind and supportive individual as my supervisor. Thank you for having me in your research group and for all the opportunities you have provided.

I am forever grateful to Dr. Adrien Métafiot, who mentored me in the lab when I first arrived. He patiently taught me everything I needed to pursue my research, particularly the NMR technique. I would not have been able to accomplish this without your help. Thank you for your kindness and honesty in sharing your knowledge with others-it was always acknowledged and deeply appreciated. Also thank you for writing the French version of the abstract for this thesis.

I would also like to express my appreciation to Mr. Frank Caporuscio and Mrs. Lisa Volpato for their constant help with anything random in the lab. Whenever I encountered any issues with the laboratory equipment, you were always the first people I turned to for help.

To my amazing friend, Dr. Elmira Pajootan, I want to extend my gratitude for your consistent kindness, support, and help whenever I needed it. You have been the best friend I have had the opportunity to meet during my time here in Montreal. Your presence and friendship have made my journey even more enjoyable. Thank you for always being there for me.

To the wonderful individuals with whom I shared the office, Carlee MacInnis and Georges Younes, I consider myself incredibly fortunate to have had the opportunity to work alongside both of you. Your presence in the office and collaboration in the lab have been invaluable. Thank

you for your constant kindness, willingness to help, and for always creating a positive atmosphere.

I would also like to express my appreciation to Chong Yang Du. Thank you for always radiating positivity and optimism. Your cheerful presence has made my experience here at McGill truly enjoyable. I am lucky to have a friend like you by my side throughout this journey.

To all the great lab mates in the Marić lab with whom I had the privilege of learning and working alongside over the years- Sharmaine Luk, Luis Alvarez, Chimdi Chime, Mary Hnatyshyn, Emilio Galindo, Kush Patel, Theo Bride, and Ruixuan Yang - Thank you.

To my dear sister, Houra, I want to thank you for your consistent love and support in every aspect of my life. Your constant encouragement and belief in my abilities have been a driving force behind my achievements. Your confidence in me has given me the strength and determination to pursue my dreams fearlessly. I am truly blessed to have you by my side, and I am deeply grateful for all that you have done for me. I cannot imagine my journey without your love and support. Thank you for being the incredible sister that you are.

Last, but certainly not least, I would like to thank my parents, Simin and Mahmoud, for always being supportive of me. Your consistent love and support during my life has helped me a lot. I am truly blessed to have you as my parents. Moreover, I want to extend a special thank you for your generous financial assistance. I acknowledge that I would not have been able to achieve my goals without your support.

CONTRIBUTIONS OF AUTHORS

This thesis is manuscript-based and contains four original research articles which have been published or submitted in peer-reviewed journals. The author contributions for each manuscript are outlined below.

Article 1 (Chapter 3)

Farkhondehnia, M., Younes, G.R. and Marić, M., Development of Myrcene-Based Resins with Amine Ended Poly (Propylene Glycol) Side Chains Bonded Through Hydroxyurethane Linkages. *Macromolecular Reaction Engineering*, **2023***, 17*, 2200054.

I developed, planned, and executed all experiments in this article. Additionally, I prepared the manuscript for publication and response to reviewers. Georges Younes helped with the writing of the first draft as well as scientific inputs to make the manuscript better. Milan Marić as the principle investigator, conceptualized the idea, advised the progress of research since the beginning, funded the work and aided in the editing of the manuscript before submission.

Article 2 (Chapter 4)

Farkhondehnia, M. and Marić, M., Design of crosslinked networks with hydroxyurethane linkages via bio-based alkyl methacrylates and diamines. *Journal of Applied Polymer Science*, **2023**, *140*, e54039.

I developed, planned, and executed all experiments in this article. Additionally, I prepared the manuscript for publication and response to reviewers. Milan Marić as the principle investigator,

conceptualized the idea, advised the progress of research since the beginning, funded the work and aided in the editing of the manuscript before submission.

Article 3 (Chapter 5)

Farkhondehnia, M. and Marić, M., Effect of alkyl methacrylate/glycidyl methacrylate copolymer backbone structure on mechanical properties of hydroxyurethane-crosslinked networks. *Reactive and Functional Polymers*, **2023**, *191*, 105683.

I developed, planned, and executed all experiments in this article. Additionally, I prepared the manuscript for publication. Milan Marić as the principal investigator, conceptualized the idea, advised the progress of research since the beginning, funded the work and aided in the editing of the manuscript before submission.

Article 4 (Chapter 6)

Farkhondehnia, M. and Marić, M., Utilizing bio-derived amine-terminated thermoplastic polyhydroxyurethanes as crosslinkers for hybrid thermosets, *Journal of Polymer Science*, **2023**, J*ust Accepted,* DOI: https://doi.org/10.1002/pol.20230382.

I developed, planned, and executed all experiments in this article. Additionally, I prepared the manuscript for publication. Milan Marić as the principal investigator, conceptualized the idea, advised the progress of research since the beginning, funded the work and aided in the editing of the manuscript before submission.

TABLE OF CONTENTS

LIST OF FIGURES

LIST OF TABLES

LIST OF SCHEMES

1. INTRODUCTION

Polyurethanes (PUs), which have a global market size of $72.82 billion USD in 2021 [1], are one of the most versatile materials available today, finding applications across a wide array of industries.

Developed in 1937 by Otto Bayer and his co-workers, PUs were initially created as a substitute for rubber during World War II when supplies were scarce. However, their versatility and ability to replace other short-supply materials resulted in their widespread adoption across various applications [2]. This breakthrough was achieved through the polyaddition reaction of diisocyanates and diols (**Figure 1.1**) [2–4]. PUs can be synthesized from a wide range of sources, and thus tailored to various applications. Consequently, PUs can be classified into several distinct categories based on the desired properties, including rigid, flexible, thermoplastic, waterborne materials, binders, coatings, adhesives, sealants, elastomers and thermosets [5]. In addition, they are utilized in biomedical fields for applications such as artificial heart valves and other implants [6]. Although PUs have a wide range of desirable applications, their industrial synthesis involves the use of highly toxic reagents [7–9]. PUs can have adverse environmental effects throughout their lifecycle, starting from the synthesis of their precursors, continuing through the polymerization process, and extending to the end of their usable life [9]. For instance, the synthesis of isocyanates in the polyurethane industry involves the use of phosgene, a highly toxic gas, to convert amines into isocyanates. Additionally, the two commonly used isocyanates in PU production, methylene diphenyl diisocyanates (MDI) and toluene diisocyanates (TDI), are classified as CMR (Carcinogenic, Mutagenic, and Reprotoxic) compounds [10,11]. Finally, at the end of their life cycle, when PUs are disposed, they decompose and release harmful by-products such as isocyanates, hydrogen cyanide, and toxic amines [3,12]. Therefore, with a growing focus on

ecological sustainability in chemical production, significant efforts have been dedicated to explore alternative pathways that are free from isocyanates for the production of PUs [13]. Over the past few years, non-isocyanate polyurethanes (NIPUs) have been subject of interest within the polymer community. NIPUs can be prepared among four general synthetic routes namely, polycondensation, rearrangement, ring-opening-polymerization and polyaddition [9,14]. Summary of all the routes is presented in **Scheme 1.1**.

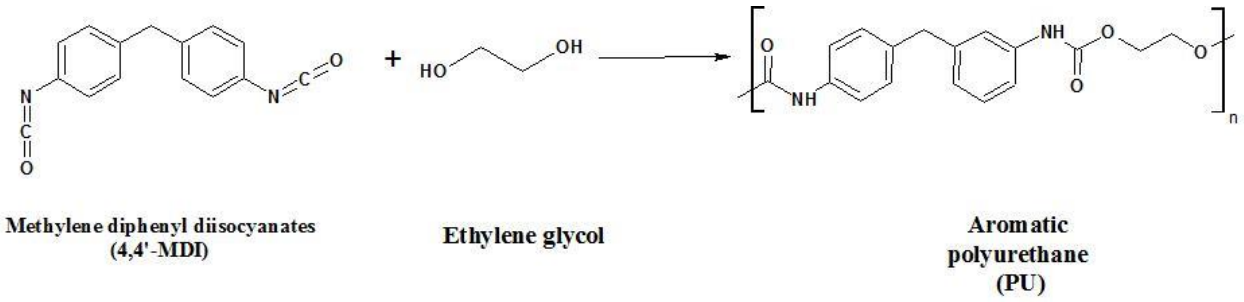

Figure 1.1. Typical reaction of a diisocyanate with a diol to form polyurethane (PU).

Examples of NIPU synthesis through the polycondensation route include the reaction of polychloroformate with polyamine, transurethanization of polycarbamate with polyol, reaction of polycarbamoyl chloride with polyol, and the reaction of polycarbonate with polyamine [15]. However, the polycondensation route cannot be considered environmentally benign due to its inclusion of phosgene or its derivatives in the monomer production process. Moreover, the production of side products such as hydrochloric acid (HCl) or alcohols is considered a significant obstacle to the industrial desirability of this pathway [9,15,16]. The synthesis of NIPUs through rearrangement can be considered more environmentally friendly. However, the utilization of harmful reactants such as acyl azides, carboxamides, and hydroxamic azides makes this route less preferable [15,16]. The third route is ring-opening-polymerization of aliphatic cyclic

carbamates or aziridines. Despite the absence of by-products, the use of phosgene in the synthesis of cyclic carbamates and the toxicity of aziridines pose challenges with this route [15]. The last route is polyaddition of cyclic carbonates with amines. This pathway seems to be the best route to prepare NIPUs since it avoids the use of isocyanate and phosgene in addition to cyclic carbonates themselves not being toxic and not particularly moisture-sensitive, making their storage easy [17]. Moreover, the reaction of cyclic carbonates and amines in this route does not produce any by-products, making it particularly attractive for the coating industry [18].

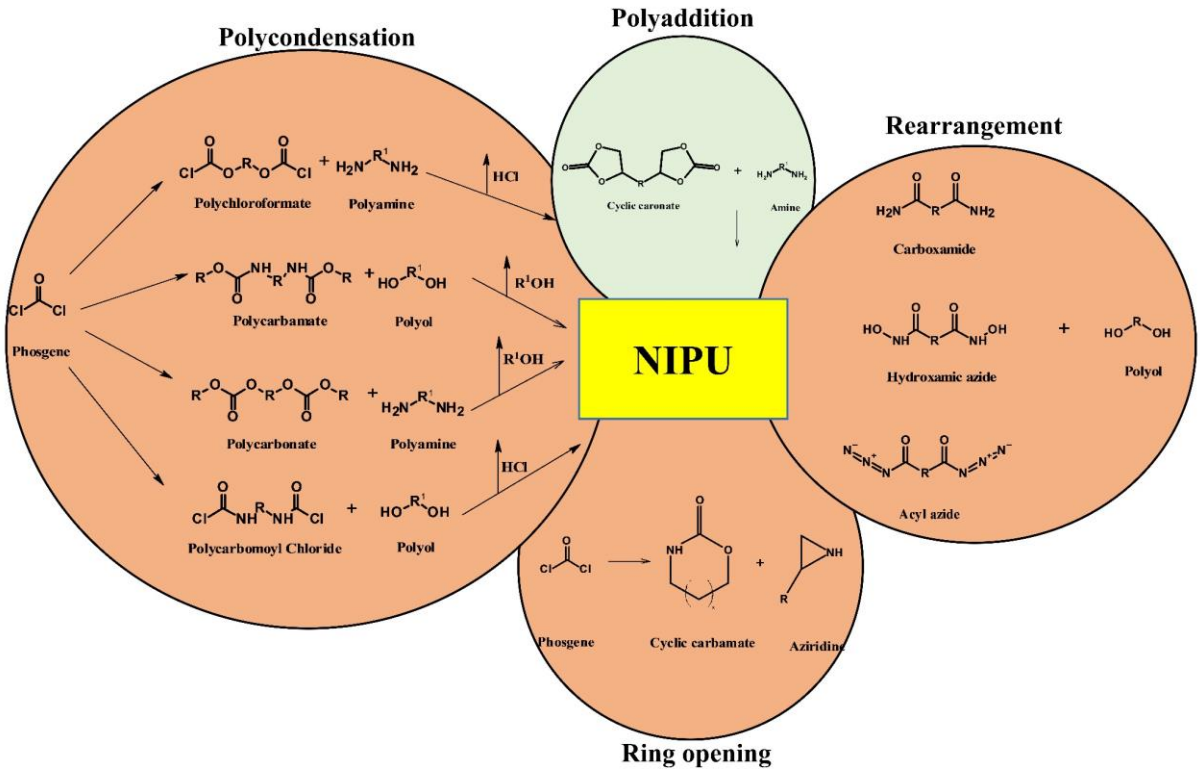

Scheme 1.1. Synthesis of polyurethanes via isocyanate-free routes [15].

Another advantage of this approach is that polyaddition of cyclic carbonates with amines results in formation of urethane linkages with primary/secondary hydroxyl groups in their chain. Therefore, this class of NIPUs are also known as poly(hydroxyurethane)s (PHUs). PHUs exhibit

enhanced chemical and mechanical properties due to intermolecular and intramolecular hydrogen bonds [16,19]. The presence of hydroxyl groups in the structure of PHUs can improve the reprocessability of PHU thermosets by facilitating associative transcarbomylation [20,21]. Precursors used in synthesis of PHUs (cyclic carbonates and amines) are abundant and can be bio-based [19,22–25]. Cyclic carbonates are synthesized from vegetable oils, terpenes, glycerol, sugars, tannin, and lignin [25,26]. While certain precursors containing cyclic carbonate functionalities such as diglycerol dicarbonate (DGC) and sugar-based D-sorbitol and D-mannitol biscarbonates (SBC and MBC, respectively) can be synthesized through the intramolecular etherifications or transesterifications of dimethyl carbonate (DMC) with their respective raw materials [27,28], vegetable oils and limonene, which contain double bonds in their chemical structures, can be epoxidized [29,30], and subsequently, CO_2 can be fixed into the epoxidized vegetable oils to form cyclic carbonates [16,31,32]. Furthermore, extensive research has been conducted on the synthesis of bio-sourced diamines from plant-based fatty acids, leading to the development of several commercially available options [33]. PHUs synthesized via the polyaddition reaction between cyclic carbonates and amines can exist in two forms: linear PHUs, which are valuable as thermoplastics, and crosslinked PHUs (thermoset PHUs), achieved by curing polyfunctional carbonates with di- and polyamines, yielding NIPU thermosets and NIPU rubbers [16]. Thermoplastic PHUs have wide-ranging applications across various industries, whereas thermoset PHUs are specifically utilized in areas such as coatings and sealants, with extensive research conducted to explore their potential [31,34,35]. Thermosets form strong mechanical networks and offer enhanced durability for specific applications [16]. To create thermoset PHUs, the use of multi-functional cyclic carbonates or multi-functional amines is essential.

The ultimate thermomechanical and mechanical properties of PHU thermosets can be influenced by various factors, such as the composition of the building blocks, the choice of cyclic poly(carbonates) and diamines, as well as the cyclic carbonate-to-amine ratio [8,20,36]. Numerous researchers have investigated the crosslinking of carbonated vegetable oils with a variety of diamines, employing different ratios to explore their effects [20,31,35]. However, in all previous studies the focus lies on vegetable oils with a fixed number of cyclic carbonates. The critical factors for manipulating the mechanical properties of thermoset PHUs primarily depends on the structure of the diamine or the amine-to-carbonate ratio.

To address this, the motivation of this thesis is centered around synthesizing diverse hybrid templates that offer the ability to manipulate both cyclic carbonate functionalities and backbone rigidity. The objective is to investigate the extensive range of mechanical and rheological properties that can be achieved through these modifications.

1.1. Objectives

Although there is a rising interest in the development of PHUs, their application in industrial settings is limited due to several significant challenges. For example, PHUs often fail to meet the necessary mechanical and chemical properties that are required for specific applications. To overcome these limitations, a promising approach to enhance the mechanical properties of PHUs has been the design of hybrid formulations (i.e. hybrid poly(hydroxyurethanes) (HPHUs)). The definition of "hybrid" varies. This hybridization can be achieved through diverse methods. These include synthesizing materials that consist of two polymers, with one of them being a PHU. Additionally, introducing inorganic chemicals into the PHUs to enhance their mechanical properties can be considered as hybrid. Furthermore, employing different polymerization techniques, such as radical polymerization combined with polyaddition, allows for the formation

of hybrid PHUs. The main objective of this thesis research was to formulate partially bio-based hybrid networks that are crosslinked through urethane linkages. Therefore, the following specific objectives were pursued:

1. Synthesis of hybrid PHUs through the integration of distinct polymerization techniques, specifically free radical polymerization and polyaddition polymerization.
2. Developing a copolymer formulation with the aim of attaining a diverse spectrum of mechanical properties tailored to accommodate a broad array of applications, spanning from elastomeric to robust engineering coatings/sealants. The initial reference for these mechanical properties is provided by our industrial collaborator, ADFAST Corporation. To achieve this objective, a selection of monomers with varying degrees of rigidity in their polymer structure is employed to strategically modulate the backbone rigidity of the synthesized copolymers.
3. To strategically maximize the incorporation of bio-based precursors while minimizing reliance on petroleum-derived materials, with the aim of addressing sustainability challenges in the current society. The substitution of petroleum-based monomers with sustainably sourced alternatives holds the potential for substantial and enduring socio-economic and environmental benefits. This objective is achieved through the utilization of fully bio-sourced amine-terminated thermoplastic PHUs as crosslinkers, facilitating the formation of robust crosslinked networks. This approach results in the production of crosslinked networks that distinctly qualify as "NIPUs", characterized by more repeating units of urethane linkages within the crosslinked structure.

1.2. Thesis organization

This thesis comprises eight chapters, organized in a manuscript-based format. The next chapter (Chapter 2) thoroughly explores the background of PHUs and HPHUs, providing an in-depth examination of their types (thermoplastic, thermosets, or hybrid thermosets), unique features, and targeted applications. This literature review establishes the fundamental basis on which the subsequent work presented in Chapters 3 through 6 is constructed. Chapter 3 explores the synthesis of templates derived from β-myrcene/glycidyl methacrylate (GMA) copolymers and their subsequent carbonation process, leading to the formation of cyclic carbonate functional groups along the polymer chains. The carbonated copolymers were subsequently reacted with a diamine (Jeffamine® D-4000) to introduce flexible side chains, which were then end-capped with moisture-sensitive silanes to form a crosslinked network. Effect of cyclic carbonate functionality on mechanical and rheological properties of these networks was investigated. Chapter 4 discusses synthesis of partially bio-based "bottle brush-like" networks that are crosslinked through urethane linkages, with rigid side chains and flexible backbones. In Chapter 5, an in-depth investigation is conducted to analyze the influence of the templates' backbone rigidity on the thermal, mechanical, and rheological properties of crosslinked HPHUs. Due to the presence of only two urethane linkages in the side chains of the templates developed in Chapters 3 to 5, they are not formally NIPUs. Consequently, Chapter 6 focuses on the synthesis of fully bio-based amine-terminated PHUs, which serve as crosslinkers for the formation of hybrid thermosets.

Following the manuscripts presented in Chapters 3 to 6, Chapter 7 provides a concise discussion that complements the information already presented in the respective chapters. This chapter offers concluding remarks regarding the achieved objectives and provides recommendations for

future research endeavors. Chapter 8 outlines the original contributions made to the field through this work.

2. LITERATURE REVIEW

PHUs hold significant promise as potential replacements for traditional polyurethanes, offering an alternative to the use of toxic isocyanates as one of the monomers [37,38]. However, despite their promising properties, the industrial development of PHUs has been slowed down by several limitations including challenges related to slow kinetics, limited conversions and molar masses [38,39]. Numerous studies have been conducted to address the challenges associated with PHU synthesis to achieve properties comparable to those of conventional polyurethanes [16,40]. To overcome the limitations associated with PHUs, a new type of PHU was developed, namely hybrid NIPUs and more specifically the hybrid PHUs [40–42].

To accomplish the objectives of this thesis, the research builds upon significant findings documented in the existing literature concerning thermoset PHUs, bio-based PHUs, and HPHUs. The thesis includes a comprehensive background discussion on the synthesis of PHUs, encompassing the factors that influence their final properties. Subsequently, the focus shifts towards the synthesis of HPHUs, exploring the various types of hybrid polyurethanes and their unique characteristics. The examples discussed in this section also highlight significant advancements within the field and help to provide appropriate background material, while also emphasizing areas that are of interest for further investigation.

2.1. Development of polyhydroxyurethanes

Extensive studies have been conducted on the synthesis of PHUs, resulting in a deeper comprehension of the chemistry involved. In addition, a comprehensive analysis of the parameters influencing the ring opening of cyclic carbonates with amines have been conducted to achieve specific targeted properties of the final polymer [25,37,43].

Several pathways for the synthesis of cyclic carbonates have been studied and reported in the literature. The historical route for synthesis of cyclic carbonates involves the reaction between diols and phosgene [44], although alternative, less toxic pathways have also been extensively explored [25]. The main routes to obtain cyclic carbonate monomers from diols, epoxides and alkenes are presented **Scheme 2.1**.

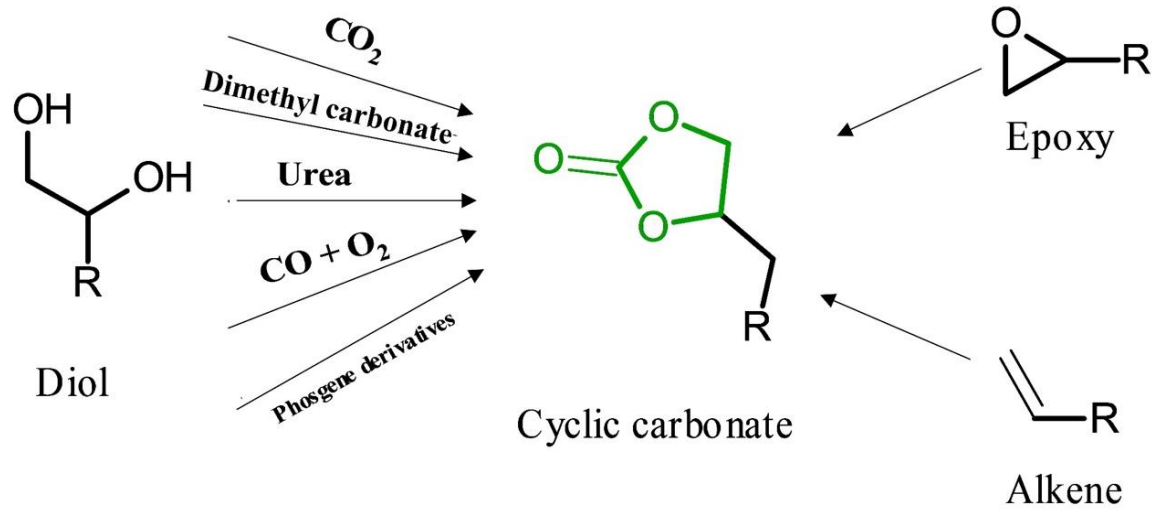

Scheme 2.1. Main routes for the synthesis of cyclic carbonate precursors.

Garipov et al. [45] described a three-step reaction mechanism for the ring-opening of cyclic carbonates with amines. The first step of the mechanism is the nucleophilic attack of the amine at the carboxylic group of the alkylene carbonate, leading to the formation of a tetrahedral

intermediate. Subsequently, the second molecule of the amine participates, deprotonating the tetrahedral intermediate which possesses the characteristics of a bipolar ion. In the final step, the breaking of the carbon-oxygen bond occurs, facilitated by the elevated electron density at the nitrogen atom. The nascent alkoxide ion subsequently undergoes a relatively rapid transformation into the reaction product, resulting in the formation of urethane linkages [45]. Steblyanko et al. [46] conducted studies on the activation energy of the aminolysis reaction between cyclic carbonates and amines and the selectivity towards primary or secondary alcohols (**Figure 2.1**). Since then, many studies focused on the parameters affecting the aminolysis reaction between cyclic carbonates and amines. **Figure 2.2** summarizes the parameters that influence the aminolysis reaction.

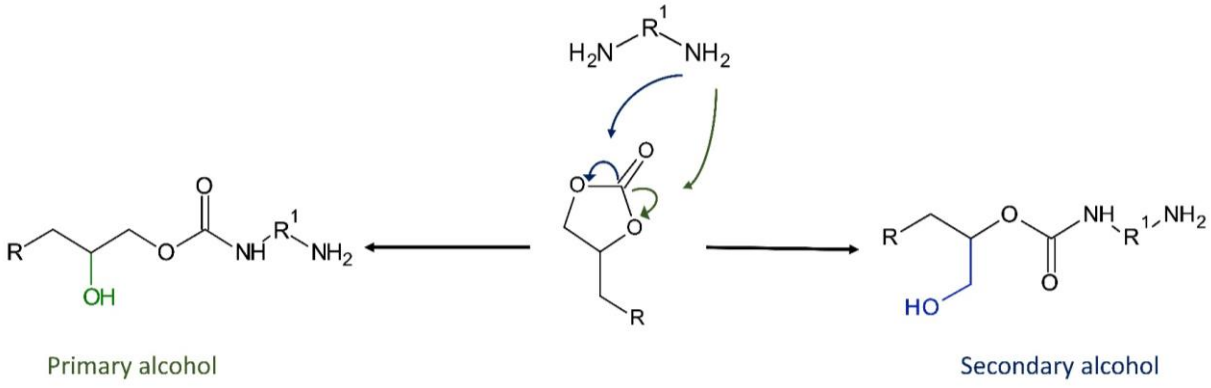

Figure 2.1. Regioselectivity of the addition of amine on cyclic carbonate.

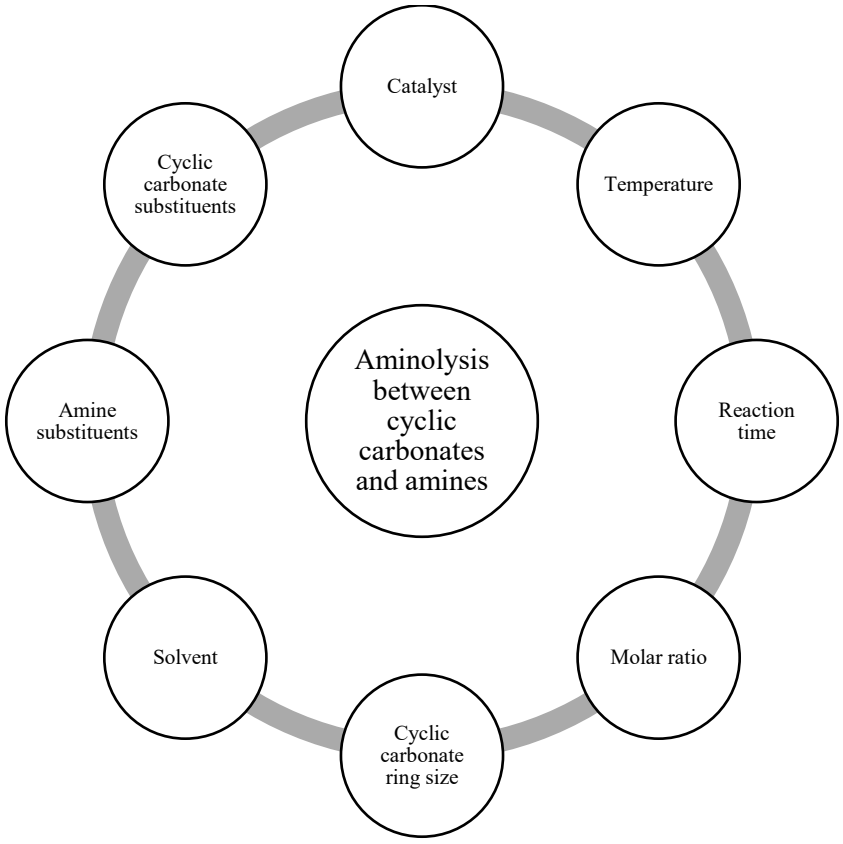

Figure 2.2. Factors affecting the aminolysis reaction between amines and cyclic carbonates.

First, the impact of ring strain on the aminolysis reaction of cyclic carbonates and amines has been investigated, revealing a positive correlation between cyclic carbonate ring size and rate of aminolysis [8,47,48]. Although there is a positive correlation between cyclic carbonate ring size and rate of aminolysis, hazardous reagents such as ethyl chloroformate and triphosgene are involved in the synthesis of six- and seven-membered cyclic carbonates [8,22]. In contrast, five- membered cyclic carbonates can be formed via reaction of carbon dioxide (CO_2) with an epoxide [16,23] and is often considered advantageous as it enables the fixation of CO_2, reducing greenhouse gas effects [49]. In addition, five-membered cyclic carbonates are synthesized with high yields [42,50] and its versatility lies in CO_2 dual functionality as both an aprotic solvent and a reagent [51]. These

distinctive characteristics explains growing interest of researchers to produce PHUs from five-membered cyclic carbonates compared to others.

Another parameter that has a great impact on reactivity of cyclic carbonates is the substituents close to the carbonate rings [15]. Cornille et al. [52] conducted a comprehensive investigation to determine the reactivity scale of various cyclic carbonates towards an amine (commercially available as Jeffamine EDR-148). Based on their findings, they proposed the following reactivity scale: ethyl ester > acetate > trimethylhexanoate > benzoate ethyl ether > phenyl ether > butane. Furthermore, the substituents also affect the regioselectivity of the reaction [53].

Numerous studies have extensively investigated the model reaction between cyclic carbonates and various amines at room temperature since cyclic carbonates could react with the most reactive amines [9,54]. These studies have revealed that the structure of amines has a strong influence on reactivity. For example, Webster et. al. [55] demonstrated that primary amines attached to a primary carbon exhibit higher reactivity compared to primary amines attached to a secondary carbon. In a study by Nohra et. al. [56], aliphatic amines with varying alkyl chain length was used to react with cyclic carbonates and a negative correlation between alkyl chain of amines and their reactivity toward cyclic carbonates was observed.

Studies have showed that increasing the reaction temperature can significantly accelerate the aminolysis reaction, reducing the reaction time from weeks to days. However, high temperature can lead to formation of side-products, such as urea [57,58]. Therefore, use of catalysts are beneficial to increase the rate of aminolysis reaction at moderate temperatures. Various types of catalysts are employed to activate the aminolysis reaction, including Lewis acids [59], bases [60], phosphoric acids [61], carbenes [62], phosphines [63], enzymes [64], guanidines [9], and thioureas [60].

Blain et al. [65] demonstrated that among all catalysts, 1,5,7-triazabicyclo[4.4.0]dec-5-ene (TBD) and phenylcyclohexyl thiourea exhibit the highest effectiveness to improve the reactivity of the aminolysis reaction. **Figure 2.3** depicts the structures of these catalysts.

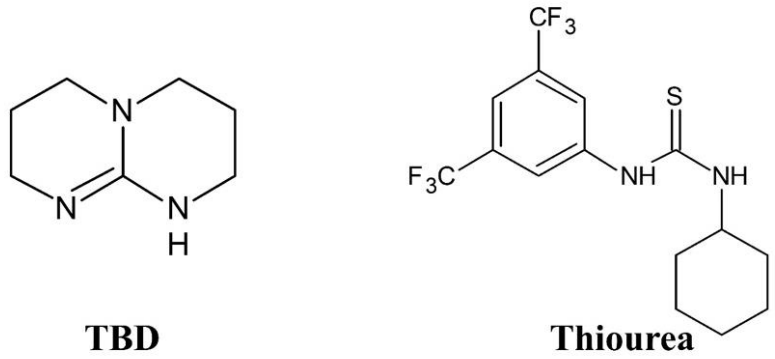

Figure 2.3. Structure of TBD and thiourea catalysts.

2.2. Limitations in synthesis of PHUs

Numerous studies have highlighted the limitations regarding kinetics, conversions and molar masses of thermoplastic PHUs [9,15]. Various side reactions have been documented in the literature for the aminolysis reaction, including amine carbonation, in-situ CO_2 production, urea synthesis, amidation, and oxazolidinone synthesis [9,15,38]. For example, urea formation through transurethanization and amidation is triggered by the nucleophilic attack of amines on carbamates or esters. Bossion et. al. [66] reported that the presence of catalysts, such as TBD, promotes the formation of urea. Typically, all these side reactions occur at temperatures above 100°C and can be facilitated with catalysts. However, it is important to control these reactions as they may result in deviations from the desired stoichiometric ratio, resulting in the synthesis of

PHUs with low molar masses and inferior mechanical properties, including a reduced Young´s modulus.

Furthermore, PHUs possess an additional hydroxyl group close to each carbamate group. The presence of hydroxyl groups in PHUs contributes to the enhancement of mechanical and thermal properties [52]. While hydrogen bonds contribute to improvements in mechanical and thermal properties of PHUs, they can also pose limitations during the PHU polymerization process [52]. For example, studies conducted by Maisonneuve et al. [67] and Rokicki et al. [68] revealed that the polyaddition of cyclic carbonate and diamine at room temperature did not yield thermoplastic PHUs with high molar masses. This can be attributed to the challenge of monomer diffusion during polyaddition polymerization of cyclic carbonates and diamines. The viscosity of the mixture increases with increasing polymer content due to the formation of hydrogen bonds with carbamate groups [9].

The optimization of PHU properties is hindered by challenges associated with the features of aminolysis, including low reactivity, low conversions, side reactions, and a high density of hydrogen bonds. Despite extensive research efforts to tackle these issues, obstacles such as low molar masses, limited reactivity, and incomplete conversion persist as significant issues with no apparent solutions in sight. However, hybrid PHUs emerge as a promising approach to overcome these limitations and attain the desired properties and requirements, providing a potential solution to the challenges faced in conventional PHU synthesis [9,38].

2.3. Hybrid PHUs (HPHUs)

HPHUs have gained significant interest as an attractive alternative to conventional PUs. These hybrid materials possess the ability to hybridize desirable properties from different materials, resulting in a product that can be less toxic and also exhibits improved mechanical properties. Therefore, HPHUs stand out as an appealing alternative. HPHUs can be synthesized through various methods, with the most common main routes involving the utilization of compounds with epoxy, siloxane, and acrylic functionalities. This section aims to provide a comprehensive overview of recent notable works conducted on HPHUs of various types.

2.3.1. Epoxy HPHUs

Epoxide materials are commonly employed in HPHU synthesis due to their reactivity with primary and secondary amine functional groups. The combination of epoxies with PHUs offers the advantage of achieving chemical resistance like epoxies, along with the good mechanical properties of PHUs. There are different routes for synthesis of epoxy HPHUs (**Scheme 2.2**) [38,69]. The first route involves the reaction of partially carbonated epoxy compounds with a polyamine [70]. The second pathway for synthesizing epoxy HPHUs involves the utilization of PHU prepolymers with cyclic carbonate or amine end groups [71]. The third option involves blending a carbonated epoxy resin with an epoxy resin and an amine as a curing agent to form epoxy HPHUs [69]. Finally, the hydroxy urethane modifiers (HUM) are obtained by forming a mono-hydroxy urethane, which then reacts with a polyepoxy to produce the final epoxy HPHUs [9].

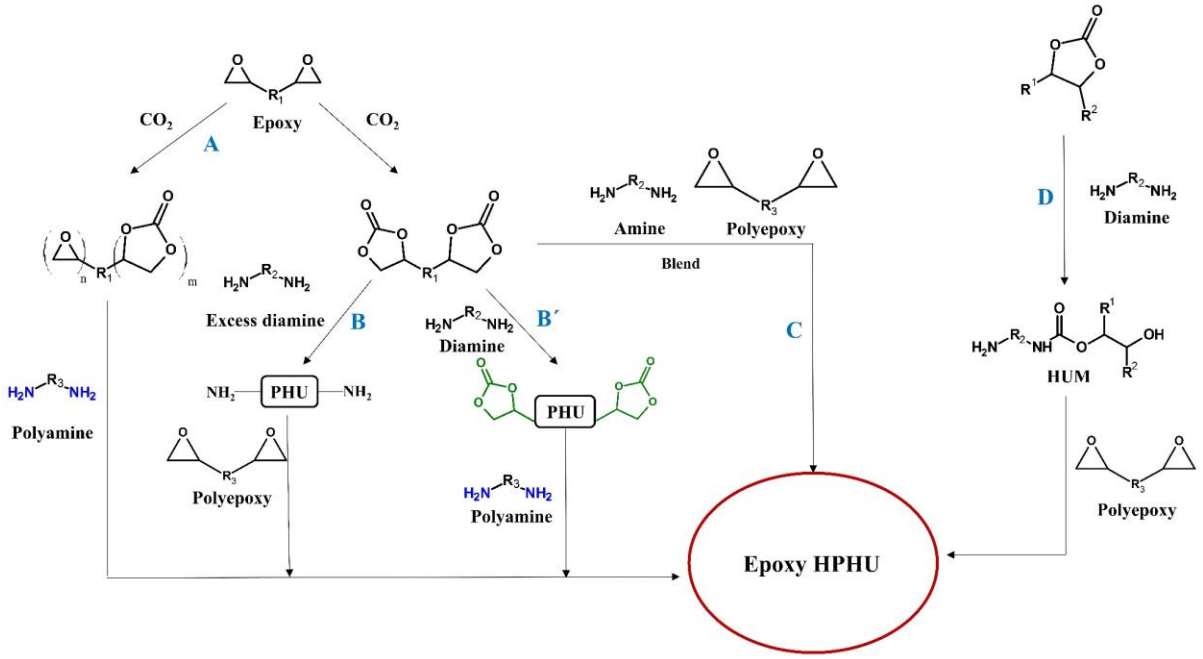

Scheme 2.2. Methods to synthesize epoxy HPHUs: A) the crosslinking of partially carbonated epoxide monomers; B) the crosslinking of PHU prepolymers with carbonate (B) or amine (B′) end groups; C) blending a carbonated epoxy resin with an epoxy resin and D) the crosslinking of hydroxyurethane modifiers (HUM).

2.3.1.1. Epoxy HPHUs synthesized from partially carbonated epoxy compounds

In the late 1980s, Rockicki et al. [72] pioneered the exploration of the chemistry involving polyamines, cyclic carbonates (CCs), and epoxides to obtain hybrid materials. They initiated their study by partially carbonating a bisphenol-A diglycidyl ether (BADGE)-based epoxy resin using CO_2, followed by the reaction with triethylenetetramine (TETA) to prepare a crosslinked network (**Figure 2.4**) [72]. The incorporation of both cyclic carbonates and epoxies in the same molecules avoids the issues linked to reactivity differences. The authors observed a positive correlation between carbonation content and the viscosity of the mixture. This observation was

attributed to the high density of hydrogen bonds formed between the oxygen of the C═O group in the carbonate and the hydroxyl group in the polymer being formed. In another study, Rockicki et al. [73] investigated the effect of carbonation on gelation of crosslinked networks. Increasing the carbonate content resulted in a decrease in gelation time, indicating a higher energetic barrier for the reaction with the epoxy compared to the cyclic carbonate. The functionality of the curing amine influenced its preference to react with either the cyclic carbonate or the epoxy moiety. Primary amines showed a preference for reacting with carbonate moieties, while secondary amines were capable of reacting with both carbonate and epoxy moieties [9,41,74].Better thermo-mechanical properties, including impact resistance, hardness, and compressive strength, were observed in the carbonated epoxy resins compared to the unmodified epoxy resin [73]. However, controlling the partial conversion of epoxies into cyclic carbonates is difficult and can lead to issues with repeatability [38].

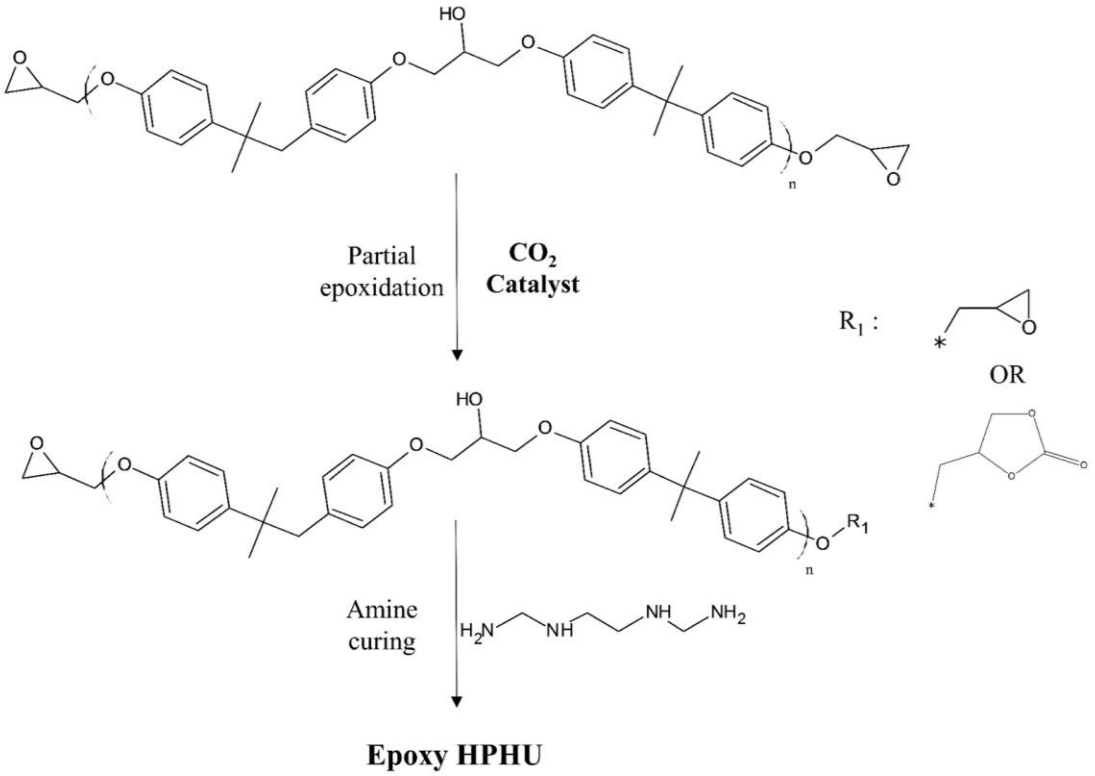

Figure 2.4. BADGE-based HPHU through the amine curing of a partially carbonated epoxy resin.

2.3.1.2. PHU prepolymers

The major pathway to obtain hybrid PHUs involves a two-step procedure: the synthesis of amine-functional or cyclic carbonate functional PHU prepolymers followed by their subsequent reaction with other functionalities such as epoxies and amines. With amine terminated prepolymers, an excess of diamine is used to prepare an amino-telechelic PHU prepolymer. The amino-telechelic PHU prepolymer is crosslinked with an epoxy compound, thus forming a hybrid material [69]. Conversely, a polyamine is added to carbonated functional prepolymers, initiating a ring-opening polymerization reaction between cyclic carbonates and amines. This methodology is attractive for designing materials with well-defined sequences of soft (NIPUs) and hard segments (epoxy) in the resulting crosslinked network [42]. Cornille et al. [42] synthesized

amine-terminated PHU prepolymers with various chain lengths using bis-cyclic carbonates (poly(propylene oxide) oligomers) and varying excess (1.3, 2, 3.3, and 6.5) of 1,2-ethylenediamine (EDA) at 60°C for 12 hours.

In another study, Ke et. al. [75] synthesized a range of epoxy HPHUs with controlled architectures by employing carbonated polypropylene glycol diglycidyl ether (PPGDGE), EDA, and BADGE. Their study aimed to investigate the influence of the amine/epoxy ratio on the microstructure of the resulting hybrid materials. Low NH_2/epoxy ratios led to the presence of unreacted carbonate moieties in infrared spectroscopy (FTIR) analysis and non-homogeneous microstructures observed by scanning electron microscopy (SEM), indicating incomplete crosslinking of the material [75]. Increasing the NH_2/epoxy ratios improved the crosslinking of the material, as confirmed by tensile and swelling tests. Additionally, incorporating excessively high amounts of diamine resulted in more linear structures of HPHUs and increased elongations at break in tensile tests. The presence of additional free ends in the molecular structure allows for greater mobility, consequently lowering the glass transition temperature (T_g) and imparting greater ductility to the network [75].

More recently, Zhang et. al. [76] developed a water-based HPHU by utilizing waterborne amine-terminated PHUs and waterborne epoxy chain extenders. Waterborne HPHUs are prepared by dispersing a PHU prepolymer into water, similar to the synthesis of standard waterborne PUs. This process involves neutralizing the internal dispersion monomer (IDM) present on the PHU prepolymer chain. Waterborne polymers are considered more environmentally friendly as they avoid using volatile organic compounds (VOCs) and their low viscosity aids in coating processes. In this study, PHUs were synthesized using DGC and fatty acid diamine (FDA). The hybrids containing 50 wt% of FDA exhibited two T_gs, indicating phase-separated

microstructures. Moreover, increasing the FDA concentration as the soft segment improved the thermal stability and mechanical strength of the hybrids [76].

Carré et. al. [71] synthesized bio-based thermoplastic HPHUs with aliphatic-aromatic structure using PHU prepolymers containing cyclic carbonate end groups. The prepolymers were subsequently extended with diamines, such as 1,4-butanediamine (BDA) or m-xylene diamine (mXDA). The study revealed that the thermal and mechanical properties of the synthesized HPHUs were strongly influenced by the molar ratio between the monomers as well as the occurrence of side reactions. Specifically, the study revealed that HPHUs prepared with higher concentrations of diamine exhibited longer soft chains, resulting in increased elongation at break values and reduced tensile strengths. Conversely, an increase in the content of rigid building blocks in the HPHUs enhanced the overall tensile strength but led to a decrease in elongation at break [71]. Therefore, the desirable properties typically associated with traditional PUs were not achieved in these HPHUs [71].

2.3.1.3. Hydroxyurethane Modifiers (HUM)

The hydroxyurethane modifiers (HUMs) are synthesized through the reaction between a monocyclic carbonate and a difunctional amine (**Scheme 2.2D**). The unreacted amine obtained from the first step can be subsequently reacted with a polyepoxide in a second step, resulting in a linear polymer with pendant hydroxyurethane functionality. These HPHUs have a comb-like structure [69]. The modified epoxy-amine hybrids were found to exhibit improved curing characteristics and resulted in cured products with enhanced wear resistance, flexibility, well-balanced mechanical properties (hardness, tensile strength), and chemical resistance compared to conventional compositions without HUMs [69]. Wazarkar et. al. [77] synthesized HUMs by reacting

propylene carbonate with ethylene diamine. Subsequently, the obtained HUMs were reacted with commercial epoxies to form hybrid materials, which were further cured using various amines, including isophorone diamine (IPDA), Jeffamine T-401, and diaminodiphenyl methane (DDM). They highlighted the potential of these compounds as corrosion protective coatings, offering a favorable balance between the hardness provided by the epoxy resin and the flexibility imparted by the hydroxyurethane moieties [77].

2.3.2. Siloxane Hybrids

Siloxane-containing HPHUs have been synthesized to impart novel properties to the hybrids, including hydrophobicity, high flexibility, and enhanced thermal stability [69,78]. Various routes exist for incorporating siloxane-based materials into HPHUs. These include the use of polyhedral oligomeric silsesquioxane (POSS) and (3-glycidyloxypropyl)trimethoxysilane (GLYMO), as well as silicon-containing monomers with different functionalities and sol-gel curing routes. The following sections will provide further discussion on these methods.

2.3.2.1. Silicone Monomers

Silicone monomers offer the possibility of synthesizing HPHUs with diverse functionalities. Amine, cyclic carbonate, and hydroxyl-functionalized silicas can be utilized to create hybrid networks with tailored properties. Endo and colleagues employed a carbonation process to introduce CO_2 into BADGE, followed by a direct reaction with a diamine containing siloxane (**Figure 2.5**) [79].

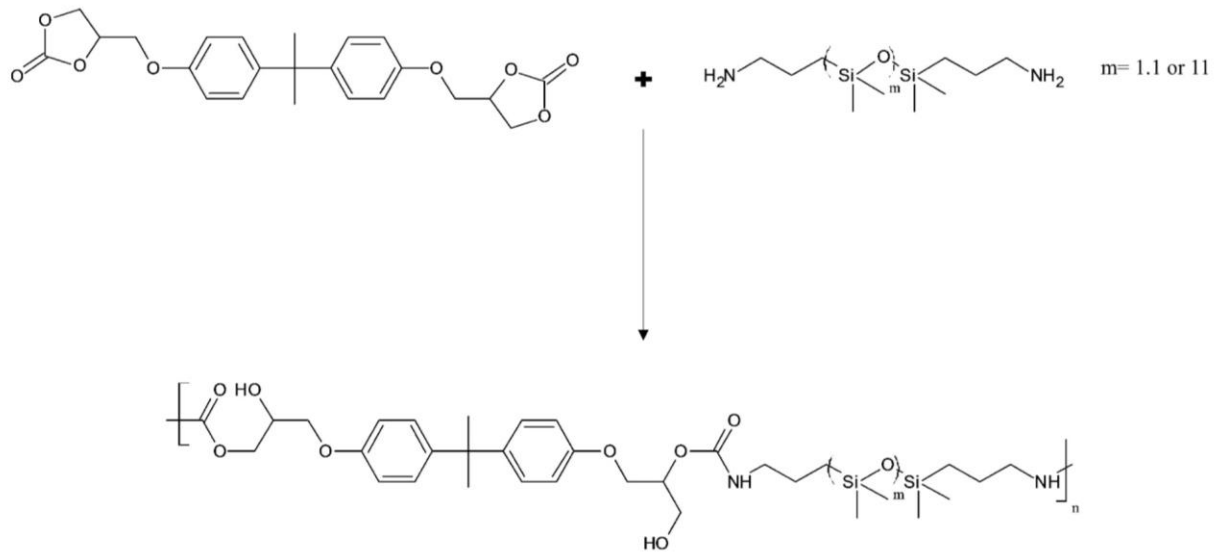

Figure 2.5. PHU containing siloxane-based inner backbone according to Endo and co-workers [79].

By comparison between the siloxane-containing PHUs and a conventional HPHU composed of carbonated BADGE and dodecanediamine, it was observed that higher siloxane content correlated with increased solubility of the resulting products in solvents of low polarity including diethyl ether. Moreover, the water contact angle and flexibility showed an upward trend with increasing siloxane content. Notably, the materials exhibited lower T_gs (1 and 26°C) compared to the dodecanediamine-based HPHUs (40°C) [79].

In another study, Chen et. al. [80] conducted a study on reprocessable HPHUs by incorporating silica nanoparticles with a wide range of surface functionalities as reinforcing fillers. In this particular study, the inability of crosslinked polymers to be recycled due to the presence of permanent crosslinks is considered a negative feature despite the improvement in performance due to the filler. To enhance recyclability of PU materials, incorporation of three distinct types of silica nanoparticles were explored. These include silica nanoparticles with hydroxyl functional groups (OH-silica), with amine-terminated surfaces (NH-silica), and with superhydrophobic properties (SHP-silica) (SHP = superhydrophobic) achieved through proprietary modifications of

the surface hydroxyl groups. These silica nanoparticles were added into PHU networks and reprocessed 2-3 times. It was observed that the involvement of hydroxyl and amine groups in side reactions of OH-silica and NH-silica had a negative impact on the cross-link density and mechanical properties of the PHUs, resulting in inferior performance compared to neat PHUs [80]. The addition of SHP-silica to PHUs resulted in notable enhancements in mechanical properties, and a complete recovery of cross-link density after just one reprocessing step. Hydroxyl groups participate in transcarbamoylation exchange reactions, while amine groups engage in reversible cyclic carbonate aminolysis reactions. These reactions collectively contribute to the reprocessability of PHU networks, offering pathways for controlled loss of cross-link density following reprocessing. This demonstration of a silanized HPHU marks a significant advancement towards the achievement of recyclable polyurethane networks [80].

2.3.2.2. POSS-containing HPHUs

Another way to introduce Si-containing moieties into PHUs is via POSS. The incorporation of this compound can be effective in enhancing the mechanical properties, thermal stability and water tolerance of polyurethanes or polycarbonate composites [81,82]. Liu et. al. [83] incorporated POSS into gallic acid-containing PHU coatings. In this study, the epoxy functional groups of gallic acid-based epoxy resin were converted into cyclic carbonate using CO_2 to form the tetracarbonate functional monomer. The carbonate was reacted with various diamines, and it was also modified with epoxidized-POSS components. The incorporation of POSS enhanced the water resistance of the NIPUs while maintaining properties such as impact resistance, pencil hardness, and flexibility. Generally, the higher loading of POSS resulted in increased material rigidity and improved thermal stability (with a 50% weight loss temperature exceeding 300°C based on thermogravimetric analysis – TGA). This improvement was attributed to the higher

crosslinking density achieved [83]. The authors also investigated the effect of POSS addition into rosin [84]. Rosin-based carbonate compounds were reacted with epoxidized-POSS, carbonated-POSS, and diamines. The impact of POSS on the resulting materials was comparable to that observed in the gallic acid-based HPHUs. Notably, when comparing HPHUs with identical POSS content, it was observed that those incorporating epoxidized-POSS exhibited greater water tolerance compared to those containing carbonated-POSS. This difference can be attributed to the formation of urethane linkages and the presence of hydroxyl groups in the latter systems [84].

2.3.2.3. HPHUs via Sol-Gel Route

Another approach to synthesize siloxane hybrids is through a sol-gel route. In the previously described methods, the siloxane moieties were incorporated as monomers and present in the polymer backbone or network. However, in the sol-gel route, silane groups are introduced at the ends of a polymer chain to cap it and provide silane functionality. The siloxane moieties are capable of crosslinking through the formation of Si–O–Si bridges [69]. In the studies conducted by Younes et. al. [85,86], DGC and MBC were reacted with different diamines, such as Jeffamine D-2000 or telechelic amino-terminated polydimethylsiloxane (PDMS) (2.5k or 5k). The resulting PHUs were characterized, focusing on their chain ends. It was observed that Jeffamine-based PHUs possessed carbonate chain ends, while PDMS-based PHUs predominantly exhibited amine-terminated chain ends. To cap the prepolymers, an amine-containing siloxane (DAMO, N-(2-aminoethyl)-3-aminopropyltrimethoxysilane) was used in the case of Jeffamine, whereas PDMS-based PHUs were functionalized with an epoxy-containing siloxane (GLYMO). Finally, all the end-capped products were cured at 22°C for 24 hours at 20-30% humidity. The PDMS-based HPHUs had very limited swelling in water and showed no signs of leaching from the films, indicating their suitability for outdoor sealant applications. In contrast, the Jeffamine-

based product experienced significant swelling and became excessively soft upon water immersion, making their handling difficult and compromising their suitability for outdoor use [85,86].

2.3.3. Acrylic HPHUs

The combination of toughness and flexibility of PUs with the weatherability and alkali resistance of acrylic polymers has resulted in a widely utilized family of hybrids. These hybrids find extensive applications in various fields such as adhesives, elastomers, and coatings [69,87]. There of different routes to prepare acrylic HPHUs [69]. One approach involves the copolymerization of unsaturated cyclic carbonates, resulting in polymer chains with pendent cyclic carbonates (**Figure 2.6**) [88]. These pendant cyclic carbonates can subsequently react with amines to generate pendant NIPUs. Another approach involves synthesizing hydroxyurethane methacrylates (HUMAs), which can be regarded as equivalents to the HUMs described earlier in epoxy HPHUs. Subsequent acrylic polymerization enables the formation of the final acrylic HPHUs [69].

2.3.3.1. Polymerization of unsaturated cyclic carbonates

Besse et. al. [88] have conducted a comprehensive review on the synthesis of unsaturated cyclic carbonates, and their polymerization behaviors via carbon-carbon double bond reactions. These compounds include a range of materials, including vinyl ether, vinylic, allylic, and allyl ether, as well as styrenic and methacrylic cyclic carbonates [69,87]. Kalinina et. al. [89] conducted a study on the copolymerization of 3-(2-vinyloxyethoxy)-1,2 propylene carbonate (VEOPC) and N-phenyl maleimide in methylethylketone (MEK) using azobis(isobutyronitrile) (AIBN) as an initiator. The resulting copolymers were further post-functionalized with EDA and hexamethylenediamine (HMDA) to form HPHUs, which were applied as coatings. These coatings demonstrated good

solvent resistance and low moisture absorption. However, they exhibited poor adhesion to metal surfaces [89].

Besse et. al. [88] studied polymerization of cyclic carbonate functional methacrylates. There are different pathways to prepare cyclic carbonate methacrylates [69,90]. However, the catalytic fixation of CO_2 onto GMA that has been polymerized via free radical polymerization chemistries is the main alternative.

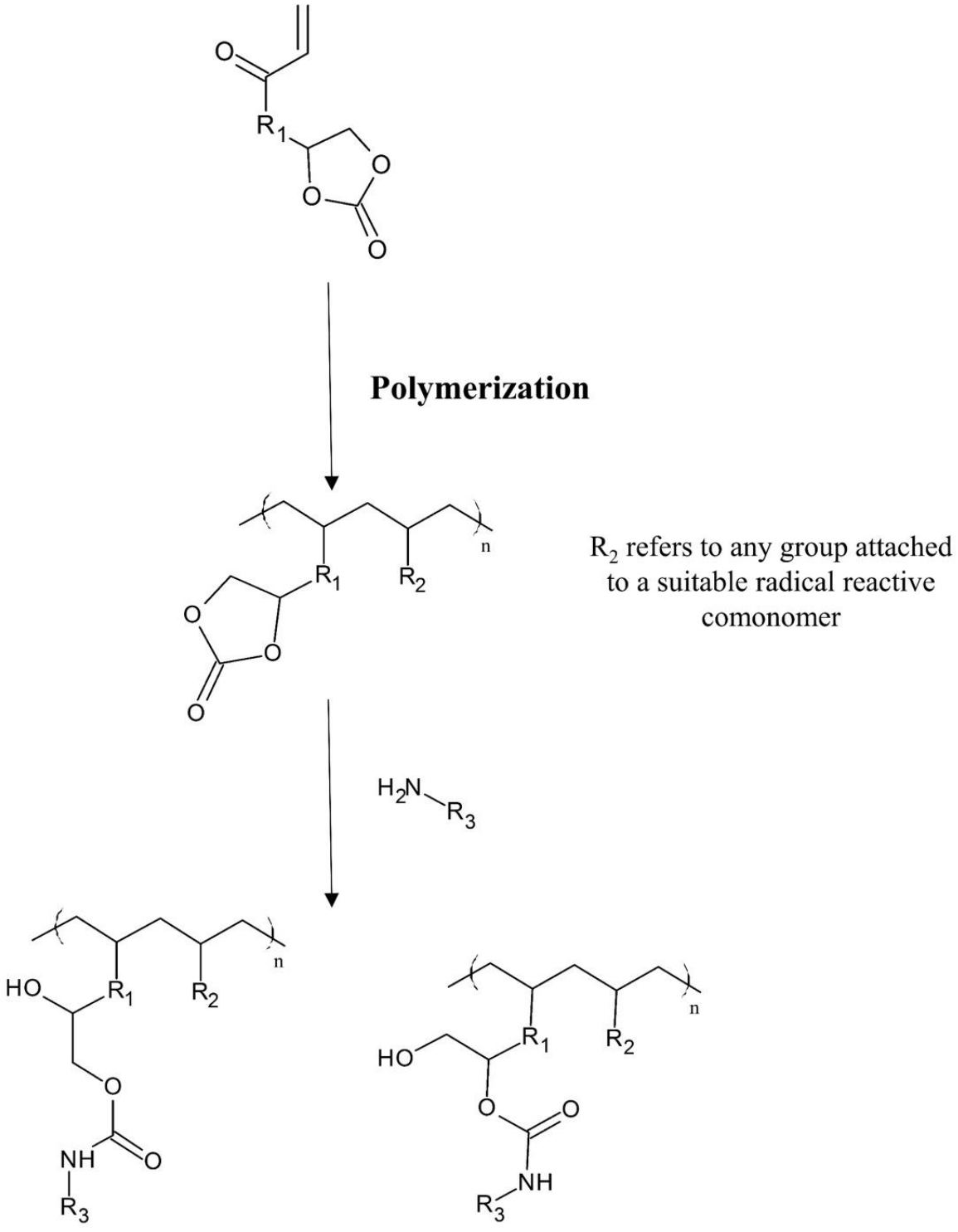

Figure 2.6. Synthesis of HPHUs through polymerization of unsaturated cyclic carbonates.

Kihara and Endo [91] carried out the functionalization of cyclic carbonate methacrylate oligomers using various amines. The primary objectives of their research were to examine the reactivity of different amines towards cyclic carbonates and to investigate the aminolysis of ester groups present in the methacrylates. (2-oxo-1,3-dioxolan-4-yl)methyl methacrylate was synthesized by carbonation of glycidyl methacrylate using CO_2. Radical polymerization of (2-oxo-1,3-dioxolan-4-yl)methyl methacrylate was conducted at 60°C, using 2,2'-azoisobutyronitrile as an initiator in dimethyl sulfoxide (DMSO). Subsequently, the synthesized homopolymer was reacted with the butylamine, benzylamine and cyclohexylamine at room temperature in DMSO for 24 hours, leading to the formation of polymethacrylates with a hydroxyurethane group incorporated in the side chain. Crosslinked networks were obtained using diamines instead of monoamines (e.g. HMDA and benzene-l,3-bis(methylamine). It was observed that an excess of amine was required to achieve complete conversion of the carbonate. However, secondary amines exhibited limited reactivity due to steric hindrance. Gelation occurred after 1.5 hours in dimethylsulfoxide (DMSO) when HMDA was introduced in a 1:1 ratio of repeating units to amino groups. FTIR analysis revealed the presence of traces of both cyclic carbonate and amine, indicating incomplete reaction. The resulting film was described as both hard, flexible and insoluble in any solvent.

2.3.3.2. Hydroxyurethane methacrylates (HUMAs)

Hydroxyurethane methacrylates (HUMAs) are short oligomers, typically dimers or trimers, that are synthesized through the aminolysis of a cyclic carbonate followed by the functionalization of the resulting hydroxyl group (**Figure 2.7**). HUMAs were initially developed as reactive diluents, specifically for applications in UV-curable coatings [92]. Multifunctional HUMAs have been synthesized by employing carbonated BADGE as a key starting material [68]. The tetra-

functionality was achieved by reacting the carbonated BADGE with an amino terminated alcohol, which was subsequently modified with methacryloyl chloride to yield the final products. The synthesized resins had low viscosity and demonstrated both high flexural strength and superior toughness compared to a reference resin used in dental compositions. The high crosslinking density of these resins typically results in elevated hardness.

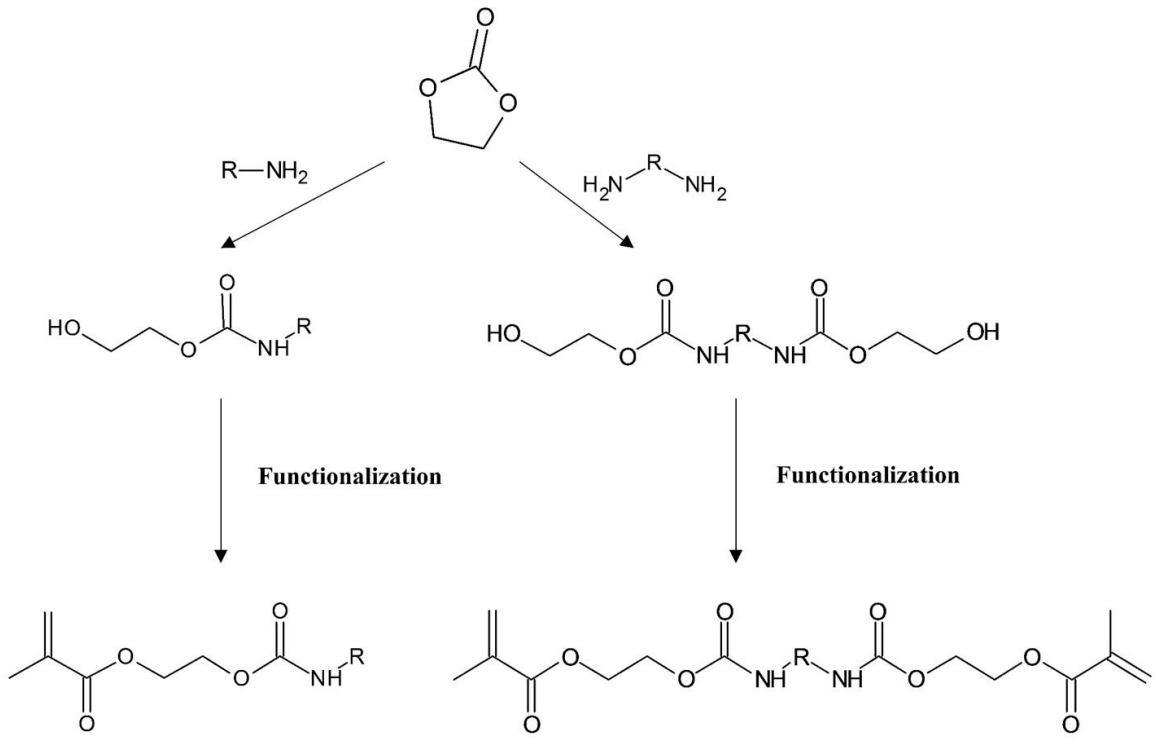

Figure 2.7. Formation of UMAs via the aminolysis of ethylene carbonate followed by subsequent functionalization.

2.4. Conclusion and thesis work considerations

In summary, the examples discussed in the previous sections highlight the progress in synthesis of HPHUs. However, they also reveal existing deficiencies and limitations in this field, calling for further research and improvement. Initially with PHUs, carbonated soybean oil was the first investigated cyclic carbonate, followed by the exploration of various bio-sourced cyclic di and poly(carbonates) [8,15,85,93,94]. Several factors were investigated to assess their impact on the final thermal and mechanical properties of PHU thermosets. These factors include the choice of building blocks, selection of cyclic poly(carbonates) and diamines, and the cyclic carbonate-to-amine ratio. By studying these factors, a comprehensive understanding of their influence on the properties of PHU thermosets can be obtained. However, significant advancements in the field occurred after 2017, with a shift towards developing HPHUs focused on specific industrial applications such as coatings, adhesives, and foams. In this thesis, a hybrid approach is employed to combine the advantageous characteristics of non-isocyanate polyurethane with polymerized methacrylates. The aim is to achieve partially bio-based thermoset hybrid resins containing hydroxyurethane linkages, offering versatile structures and enhanced properties to be tailored to the application. Hence in the next chapter (Chapter 3), a comprehensive investigation will be introduced regarding the hybridization concept of PHUs. This approach involves the integration of free radical polymerization and polyaddition polymerization techniques, coupled with the incorporation of moisture-sensitive silanes, to form thermoset resins. The chapter aims to delve deeper into the experimental methodologies and characterization techniques associated with this hybridization strategy for PHUs. Following the establishment of the proof of concept, Chapter 4 will focus on enhancing the mechanical properties of the resins synthesized in Chapter 3. This will involve the manipulation of the side chain rigidity in the templates produced through radical

polymerization. A thorough investigation of the mechanical and rheological properties will be conducted to gain a comprehensive understanding of the resulting improvements. Chapter 5 is dedicated to investigating the influence of backbone rigidity on the mechanical properties of the thermoset PHUs. In this chapter, templates with varying levels of backbone flexibility were synthesized, and the resulting materials were extensively characterized and compared with previous findings. The chapter aims to provide a comprehensive analysis of how changes in backbone rigidity impact the mechanical behavior of the PHUs, offering valuable insights for the design and optimization of these materials. Lastly, in order to broaden the scope of the study, thermoplastic PHUs were synthesized with diverse backbone structures (Chapter 6). These PHUs were subsequently employed as crosslinkers to form networks, which can be referred to as NIPUs. Comprehensive investigations were conducted to examine the mechanical and rheological properties of these NIPU networks, providing valuable insights into their performance and potential applications.

3. CHAPTER 3

DEVELOPMENT OF MYRCENE-BASED RESINS WITH AMINE ENDED POLY(PROPYLENE GLYCOL) SIDE CHAINS BONDED THROUGH HYDROXYURETHANE LINKAGES

The manuscript of this chapter was published in *Macromolecular Reaction Engineering* in 2023 (Farkhondehnia, M., Younes, G.R. and Marić, M., Development of Myrcene-Based Resins with Amine Ended Poly (Propylene Glycol) Side Chains Bonded Through Hydroxyurethane Linkages. Macromolecular Reaction Engineering, 2023, 17, 2200054.) [1]. This chapter constitutes the proof of concept for the preparation of partially bio-based hybrid moisture curable networks bonded through urethane linkages. This manuscript represents a distinct contribution to the development of NIPU-based hybrid crosslinked networks, which combine the principles of radical polymerization and polyaddition polymerization, along with the silane curing step. We attempted to show here partially bio-based backbones that are largely poly(myrcene) can be used as a template for coupling to diamines and subsequently capping and curing with a silane coupling agent. The results from this initial study were then applied to subsequent iterations in the hybrid resin designs, and improved mechanical properties are detailed in Chpaters 4-6. The supporting information of this manuscript is included in Appendix A.

3.1. Abstract

Hybrid non-isocyanate poly(urethanes) (HNIPUs) are designed from a precursor whose carbonate functionality is derived from epoxy-functional statistical copolymers. Specifically, a bio-based diene (*β*-myrcene) is copolymerized via conventional free radical polymerization with glycidyl methacrylate (GMA) at different molar ratios, producing flexible copolymers with epoxy pendent groups, which are then reacted with carbon dioxide to yield the precursors with cyclic carbonate functionality. Subsequent addition of an amine terminated telechelic poly(propylene glycol) (PPG) forms urethane linkages in the side chains, whose concentration is tuned by varying the GMA initial molar fraction. The NIPUs are end-capped with silanes to enable moisture curing, resulting in HNIPUs with elongations at break up to 150%, and relatively low elastic moduli varying from 32 kPa to 50 kPa as the number of urethane side linkages increases from 6 to 22. Swelling ratio of the NIPUs are also measured in tetrahydrofuran (THF). As the number of urethane side chains increases, the swelling ratio of the NIPUs decreases (710% to 620%), indicating the higher crosslinking density. All samples have gel content of more than 50% in THF, indicating non-crosslinked species in the samples which confirms the relatively low reported values for tensile moduli.

3.2. Introduction

Polyurethanes (PUs), with a global market size of $72.82 billion USD in 2021, play a significant role in everyday applications such as elastomers, foams, adhesives, sealants, coatings, thermoplastics, and thermosets [9,95–97]. However, certain issues with the synthesis and application of PUs have become concerning. Traditionally, PUs are generally made through polyaddition reaction of polyols and isocyanates, the latter of which is toxic and the process used to make it involves toxic phosgene gas, posing severe health risks [9]. These substances are harmful for both environment and human. Along with mentioned serious health concerns, European regulation REACH is concerned about noxiousness of synthesized Pus and in fact most regulations limit the use of some isocyanates [12,98,99]. Moreover, common precursors for the synthesis of polyols are petroleum-based [16,95,100] and thus in addition to the health hazards posed, there is an ecological driver to adapt not only safer but also greener synthetic paths [19,101]. Isocyanate-free methods to produce a new class of PUs have been developed and are known as non-isocyanate polyurethanes (NIPUs). Among all non-isocyanate routes to PUs, the reaction of amine and cyclic carbonate functions is the most common [13,47,67,102–107]. In this route, PUs are synthesized by ring opening of cyclic carbonates with polyamines, leading to the formation of urethane linkages and a secondary hydroxyl group (such polymers are also called polyhydroxyurethanes (PHUs) due to the latter's formation). PHUs synthesized through this method eliminates the issue of isocyanates while also capturing CO_2 in the form of the cyclic carbonates after coupling with the epoxides. The resulting hydroxyl groups form intermolecular and intramolecular hydrogen bonds with urethane carbonyl bonds, which increase the stability of urethane linkages to hydrolysis [16,17,25,67,96,100,108]. The enormous proliferation of NIPU formulations is well documented in the literature [9,67,109,110] . More recently, attention has shifted to hybrid NIPUs [41] to

combat many of the shortcomings of NIPUs, as they still fall short of the performance of conventional PUs in many applications. Hybrid NIPUs are broadly defined as being hybrids in chemical structures (i.e. reacting a suitably end-functionalized NIPU with another monomer), reacting with an inorganic polymer (eg. chain extension with poly(siloxanes)), capping with an inorganic molecule (eg. silanes to introduce moisture-curable groups) or using a different kind of reaction (eg. polyaddition combined with free radical) to improve the properties of the resulting material [41,69,111].Recently, moisture curable NIPUs have been introduced as a new class of hybrid NIPUs which are moisture curable and crosslink properly in ambient temperature [39,86].

Here, we focus on synthesis of hydroxyurethane linkages using a different kind of polymerization (free radical polymerization combined with polyaddition) to combat mechanical and physical property limitations of conventional PUs. This is done by creating a template via statistical radical copolymerization that controls the backbone length and the density of grafting sites. Specifically, a cyclic carbonate functional template is accessed by copolymerization of a diene (to impart flexibility) with glycidyl methacrylate (GMA; to provide epoxy groups) where the latter can be carbonated with CO_2 to provide the requisite cyclic carbonates [112]. Notably, we applied semi-batch conventional free radical polymerization (FRP) to provide more uniform distribution of carbonate sites. The cyclic carbonates along the backbone are then reacted with a diamine (in this case, poly(propylene glycol) diamine – Jeffamine D-4000) to form the urethane grafts. In this work, *β*-myrcene (*Myr*) a terpene-based 1,3-diene was used as a co-monomer with GMA as it provides rubbery characteristics to the copolymer [113]. We also employed bulk conventional free radical polymerization (FRP) with this system, to avoid issues with solvent removal. Further, combination of poly(cyclic carbonate) and diamine with appropriate viscosities were sought to prepare a formulation which can be readily applied onto surfaces [18]. After

carbonation and formation of the urethane linkages, the synthesized myrcene based resin containing hydroxy urethane linkages on the side chains were end-capped using [3-(2,3-epoxypropoxy)-propyl]-trimethoxysilane (known as GLYMO), which is a common moisture sensitive silane and often-used coupling agents, to obtain a moisture-cured formulation containing hydroxyurethane linkages [86]. GLYMO can act as a bridging unit by making interfacial connection through the hydrolysis and condensation of the trialkoxysilane moiety and reaction of epoxy groups with amine functional groups at the same time. Hydrolysis of the methoxy groups in GLYMO gives silanol groups which condense to form the silicone network structures[114,115].The following study focuses on making the templates with distribution of carbonate sites which affects number of urethane linkages along with characterization of resulting PHUs in terms of urethane formation, end-capping efficiency and measurement of physical (swelling) and mechanical properties (**Figure A 1**).

3.3. Results and discussions

3.3.1. Effect of feed composition on My/GMA copolymerization

The goal of this approach to design NIPUs was rooted in the control of the microstructure, from the poly(*Myr*-*co*-GMA) precursor, which defined the locations of the carbonation and thus the attachment points for the amine groups to form the urethane linkages. By controlling the frequency of the carbonate groups via copolymerization between *Myr* and GMA and the length of the diamine attaches, we expected to have a wide latitude into accessing desirable physical and mechanical properties. Thus, the starting point of our investigation was to determine the impact of the initial monomer composition on the final molar composition of poly(*Myr*-*co*-GMA). The *Myr*/GMA copolymerization was studied previously using nitroxide mediated polymerization (NMP) and reversible addition−fragmentation chain-transfer polymerization

(RAFT) and reactivity ratios of the two monomers was estimated by various methods, assuming a terminal copolymerization model [116,117]. Reactivity ratios for *Myr* and GMA by nitroxide-mediated radical polymerization (NMP) were reported as $r_{Myr} = 0.49 \pm 0.13$ and $r_{GMA} = 0.50 \pm 0.13$ with 95% confidence bounds [112], and also reactivity ratios of $r_{Myr} = 0.5181 \pm 0.0620$ and $r_{GMA} = 0.3009 \pm 0.0141$ were reported using RAFT polymerization [117] . These estimates serve as guides for the microstructures we expect for the precursors.

Qualitatively by FTIR, incorporation of GMA in the copolymer structure was indicated by the appearance of a peak at 1725 cm^{-1} corresponding to the C=O stretch of the ester group in GMA. There are also discrete peaks at 890 and 830 cm^{-1}, which corresponded to asymmetric and symmetric oxirane ring bending/deformation, respectively (**Figure 3.1**) [118].

Quantitative determination of copolymer composition was done using ^{1}H NMR. With respect to the *Myr*, literature suggests poly(*Myr*) has varying regioselectivity (**Figure A 2**) [119]. In our case, the regioselectivity of *Myr* in the copolymer was calculated by comparing three peaks at δ= 4.70–4.80 ppm (two vinyl protons of 1,2-addition and two vinyl protons of 3,4-addition), δ=5.00–5.25 ppm (two olefinic protons of 1,4-addition, one olefinic proton of 1,2-addition and one olefinic proton of 3,4-addition), and δ=5.30–5.50 ppm (one olefinic proton of 1,2-addition) [112]. We found > 89.6% of the poly(*Myr*) exhibited 1,4 addition under the conditions studied (**Table 3.1**). The two-step degradation of synthesized copolymers could be due to different microstructures (**Figure A 3 and Table A 1**) [119].

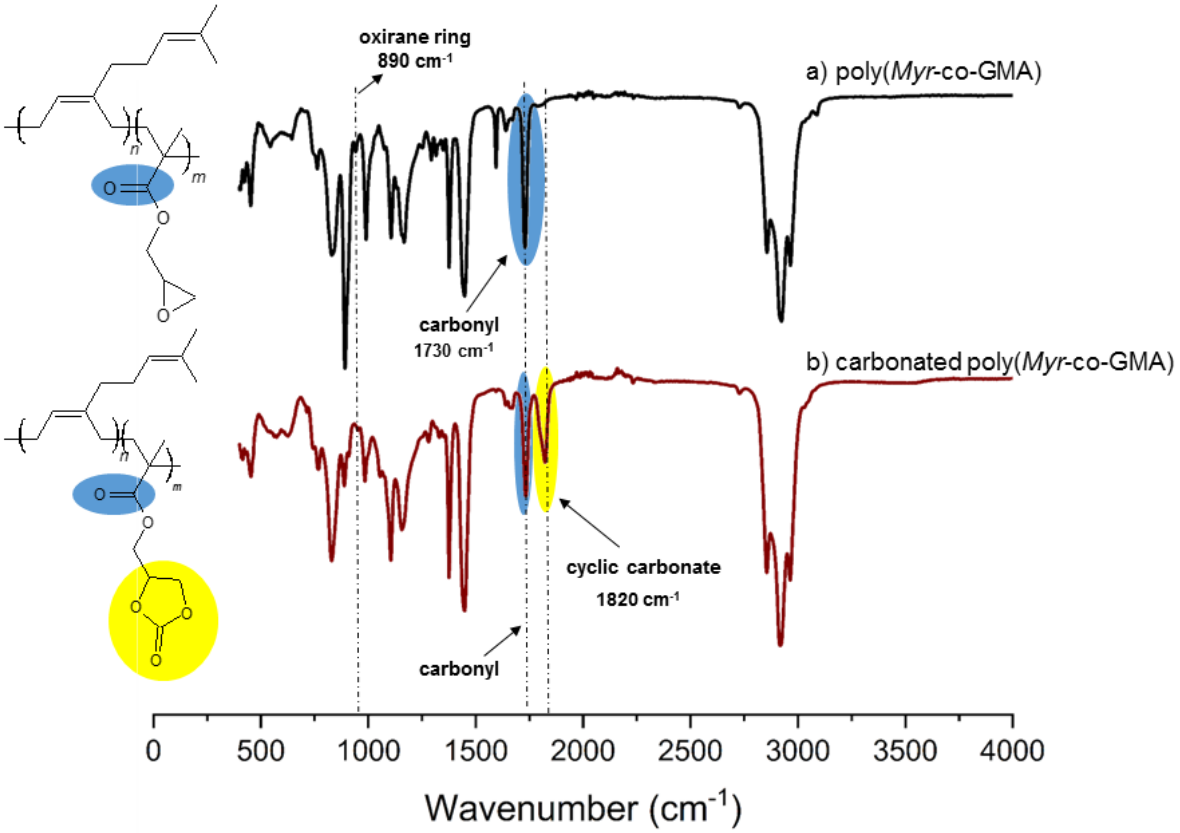

Figure 3.1. FTIR spectra for *Myr*/GMA copolymer before and after carbonation, FTIR spectra for a) *Myr*/GMA-90, b) carbonated *Myr*/GMA-90.

Table 3.1. Molecular Characterization and Myrcene Selectivity at the End of the Experiments.

Sample ID [a)]	F_{Myr}	X_{Miyr} [b)] (%)	X_{GMA} [c)] (%)	$X_{copolymer}$ [d)] (%)	M_n [e)] (g mol^{-1})	$Đ$	1,4 addition (%)	1,2 addition (%)	3,4 addition (%)
Myr/GMA-100	1	62.2	-	62.2	6200	3.12	94.6	4.1	1.3
Myr/GMA-90	0.91	55.3	65.9	56.4	5500	3.26	93.6	5.2	1.2
Myr/GMA-80	0.84	59.2	58.8	59.2	7500	3.31	92.7	6.7	0.6
Myr/GMA-70	0.77	74.0	73.0	73.7	7200	3.99	90.7	7.7	1.6
Myr/GMA-60	0.61	68.1	72.8	70.0	10500	4.12	89.6	9.5	0.90

([a)] Experimental identification given by *Myr*/GMA-XX, where XX refers to the rounded % initial molar fraction of *Myr* in the mixture ($f_{Myr,0}$)); ([b)] X_{Myr} represents myrcene conversion in poly(*Myr-co*-GMA)); ([c)] X_{GMA} is GMA conversion in poly(*Myr-co*-GMA)); ([d)] $X_{copolymer}$ is total conversion of the synthesized copolymer at the end of the reaction); ([e)] Target number average molecular weight for all experiments ($M_{n,theoritical}$)=10000 g mol^{-1} , all reported molecular weights were converted to absolute molecular weight using Mark- Houwink- Sakurada (MHS) coefficients [120–123]).

Reactivity ratios from previous studies suggested that *Myr*/GMA behaved in a statistical fashion [8]. However, we noticed compositional drift with the GMA being incorporated more rapidly (which suggests why we adopted a semi-batch approached towards adding the GMA to get a more uniform distribution of functional groups). Kinetic data may explain some of the trends exhibited in **Table 3.1** and **Figure A 4**, such as an increase in $Đ$ with increasing GMA content in the feed. For instance, the composition drift can be partially explained by the difference in propagation rate constants of the individual monomers. Although *Myr* propagation rates are not known, isoprene is expected to behave similarly and we used that to approximate the propagation rate constant for *Myr*. Isoprene propagation rate constant ($k_{p,isoprene}$) was estimated to be 125 ± 30 L mol^{-1}s^{-1} at 5°C in bulk with peroxide initiator [124]. Later, $k_{p,isoprene}$ by bulk radical polymerization measured with pulsed laser initiated polymerization (PLP) was reported as 99 L

mol^{-1} s^{-1} at 50°C [125]. By PLP, the GMA homopropagation rate constant $k_{p,GMA}$ = 1230 L mol^{-1} s^{-1} at 50°C [126]. This order of magnitude difference influences the faster rate of consumption of the methacrylate versus diene and was reflected in the composition. For this reason, semi-batch addition was adopted for a more regular placement of GMA in the backbone (**Figure A 5**). Lastly, the effect of initial molar ratio of GMA in the feed upon the viscosity of the final copolymer was investigated as it affects leveling, a relevant property for sealant applications. Leveling is a critical factor to achieve a smooth and uniform coating and it is favored by low melt viscosity of the polymer [127]. Poly(*Myr*-*co*-GMA) viscosities were optimized by manipulation of epoxy content in the chain and limiting its number average molecular weight to <10000 g mol^{-1}. The steady shear viscosities of the poly(*Myr*-*co*-GMA) were determined at room temperature, with the viscosity of *Myr*/GMA-90 increasing from 410 mPa s to 1780 mPa s compared to *Myr*/GMA-70 (**Figure A 6**). The increase in viscosity is not surprising as the methacrylic co-monomer makes the copolymer stiffer (The T_g of poly(GMA) homopolymer is 85°C [128]). All poly(*Myr*-*co*-GMA)s, as seen in **Figure A 6**, have Newtonian plateaus for shear rates between 0.1 to 10 s^{-1}, indicating they are all below their entanglement molecular weight (M_e) (M_e of poly(*Myr*) is reported as 17 kg mol^{-1} [129] in the literature). Additionally, the viscosity of synthesized poly(*Myr*-*co*-GMA)s linearly scales with their molecular weight since they are all below their M_e.

3.3.2. Structural identification of carbonated *Myr*/GMA copolymers

Once the series of poly(*Myr*-*co*-GMA)s were prepared, they were treated with CO_2 and TBAB, to form the cyclic carbonate groups [130]. TBAB employs nucleophilic attack by the bromide ion to the oxirane, and then adds to CO_2. Finally, the oxyanion reallocates the bromine, giving the five-membered cyclic carbonate [104,131].The production of the five-membered cyclic carbonate group by CO_2 fixation to the epoxide ring of the GMA monomer of poly(*Myr*-*co*-GMA) was confirmed using FT-IR, and ^{1}H NMR (**Figure 3.1b** and **Figure A 7**).

Figure 3.1a and **Figure 3.1b** show the FTIR spectra of poly(*Myr*-*co*-GMA) before and after CO_2 fixation (after 18h). The epoxy group vibration band appears at 910 cm^{-1} in poly(*Myr*-*co*-GMA). At 1730 cm^{-1}, the stretching vibrations of both carbonyls corresponding to the ester groups of GMA units can be seen. The intensity of the epoxy peak at 910 cm^{-1} decreases after 18 hours of CO_2 fixation, and a new peak appears at 1800 cm^{-1} due to the creation of the cyclic carbonate [95]. The absence of the 910 cm^{-1} peak for the epoxy bonds and the presence of signals related to cyclic carbonate bonds at 1801 cm^{-1} proved that the cyclic carbonated poly(*Myr*-*co*-GMA) was prepared nearly quantitatively. ^{1}H NMR analysis also demonstrated the formation of the cyclic carbonate groups (**Figure A 7**). The signals at 4.25-4.45 ppm are assigned to the protons of the cyclic carbonate and signals at 2.55-3.25 ppm are assigned to the protons of the methylene group of the epoxy ring. These observations confirm the generation of cyclic carbonate groups through the reaction of poly(*Myr*-*co*-GMA) and CO_2. Using ^{1}H NMR, the carbonation conversion was almost 95% after 18 hours of CO_2 bubbling (**Figure A 7** and **Figure A 8**).

3.3.3. Synthesis of NIPUs

With the successful preparation of carbonated poly(*Myr*-*co*-GMA), a series of NIPUs were synthesized via polyaddition reaction with diamines. It should be mentioned that NIPU in this work refers to the formulation in which urethane linkages are formed on the side chains after addition of diamine to cyclic carbonate. Depending on the ring-opening locations of cyclic carbonates, urethanes with primary and secondary hydroxyl moieties were formed [132,133]. **Figure 3.2** depicts the normalized GPC profile for Jeffamine D-4000, carbonated poly(*Myr*-*co*-GMA) and synthesized NIPU (NIPU-70, where 70 refers to the NIPU synthesized from *Myr*/GMA copolymer with 70 mole % of Myr). As seen from **Figure 3.2**, a small shoulder appears for the synthesized NIPU at the higher molecular weights indicating the presence of NIPU in the polymer mixture, and the shoulder intensifies from NIPU-pre-0 (sample taken right after addition of Jeffamine D-4000 at room temperature) to NIPU-6 (sample taken after six hours, which is end of the reaction). The GPC chromatogram suggests that urethane linkages were formed after 6 hours. Excess Jeffamine D-4000 is observed from the left-most peak in the GPC profile. The fraction of Jeffamine D-4000 that is chemically bound to the carbonated poly(*Myr*-*co*-GMA) can be calculated using **Equation A 1**, **Equation A 2** and **Equation A 3**The fraction of Jeffamine D-4000 that is chemically bounded can be calculated using (about 55% of Jeffamine D-4000 was not chemically bound to the carbonated *Myr*/GMA-70) (Supporting Information, **Figure A 9** and **Table A 2**) [134]. It was not possible to remove excess Jeffamine D-4000 from the mixture. Both synthesized NIPU and Jeffamine D-4000 are liquids and no solvent could be found to act as a non-solvent for either the synthesized NIPU or Jeffamine D-4000. **Table 3.2** shows approximate molecular weights for synthesized NIPUs with different number of side chains (NIPU-90, NIPU-80, NIPU-70).

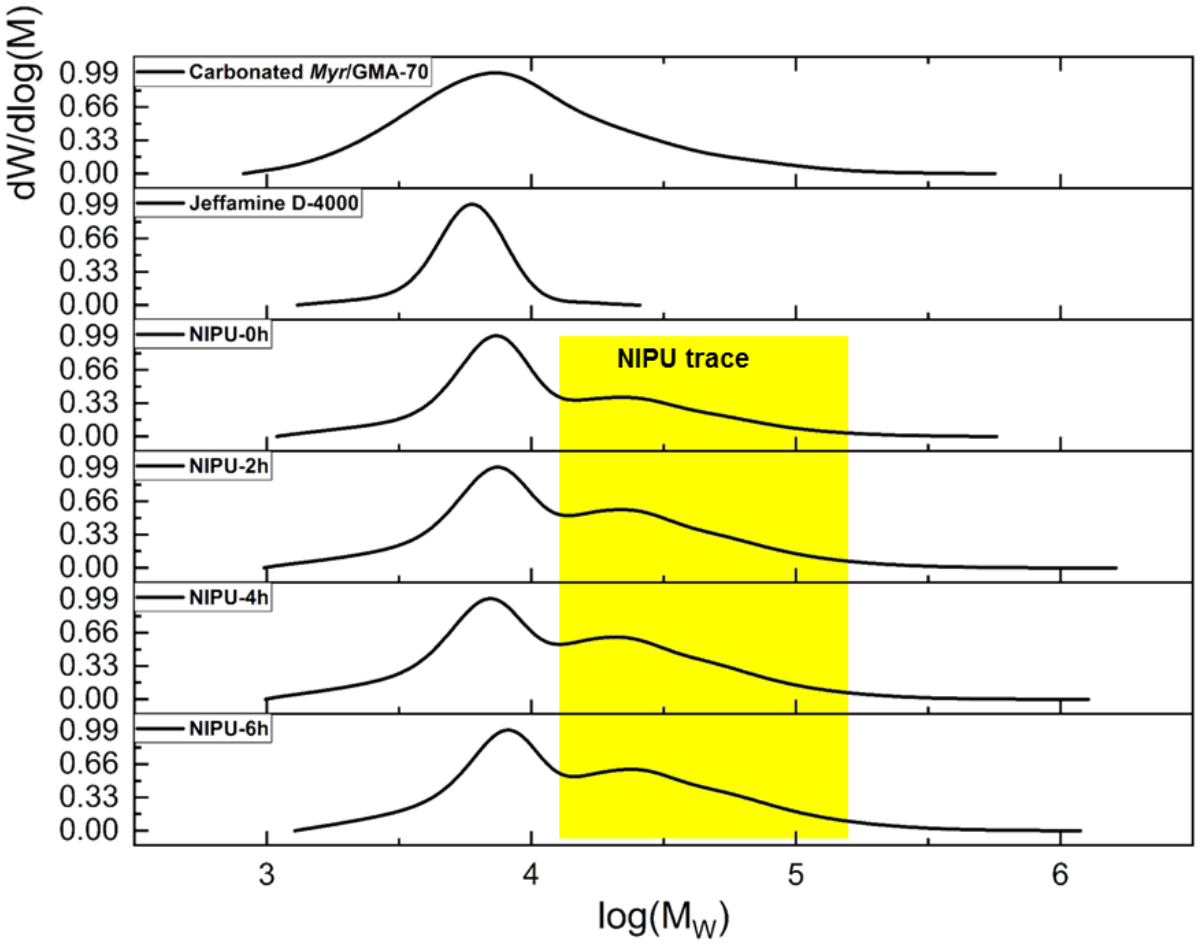

Figure 3.2. Normalized GPC traces for carbonated *Myr*/GMA-70, jeffamine D-4000 and NIPU-70 at various times at T=40°C.

Table 3.2. Molecular weight and physical properties of the synthesized NIPUs.

NIPU	Used diamine, temperature (°C), time (h)	M_n (g mol^{-1})[a)]	Physical state
NIPU – 90[b)]	Jeffamine D4000, 120, 6	26000	viscous liquid
NIPU – 80	Jeffamine D4000, 120, 6	38000	viscous liquid
NIPU - 70	Jeffamine D4000, 120, 6	55000	viscous liquid

([a)] Reported molecular weights are estimated using GPC by integrating the peak assigned to NIPU (values are approximate besides having bimodal distribution). The molecular weights are relative to PMMA standards); ([b)] Experimental identification given by NIPU-XX, where XX refers to the % initial molar fraction of *Myr* in the synthesized *Myr*/GMA copolymer ($f_{Myr,0}$)).

After addition of Jeffamine D-4000, the samples were analyzed by FTIR which show the intensity of the cyclic carbonate peak (1800 cm^{-1}) decreasing (**Figure 3.3**) but still present, indicating that the reaction between cyclic carbonate and Jeffamine D-4000 was incomplete [135]. It is also reported that cyclic carbonate conversion to urethane linkage was higher than at the higher carbonate to amine ratio, although the conversion was not complete [35]. To convert all cyclic carbonates to urethane linkages reaction would probably need longer time or higher temperatures or both. However, longer times at high temperatures could cause side reactions [136,137]. In our system, excess diamine was added to the mixture to increase the steric hindrance and lower the chance of crosslinking while reaction was occurring. This could prevent the diamine reacts on both ends and the NIPU was not crosslinked at the end of the reaction which is six hours.

^{1}H NMR also confirmed the presence of the urethane linkage in the structure of synthesized NIPUs (**Figure 3.4**) (δ= 3.55 ppm and 5.10 ppm). At 3.55 and 5.10 ppm, two different chemical

shifts in the ^{1}H NMR spectra appeared, attributable to the protons of freshly generated primary and secondary hydroxyl groups, respectively [138]. The ^{1}H NMR spectra also indicated that the cyclic carbonates on the backbone of the carbonated poly(*Myr*-*co*-GMA) had been partially converted to NIPUs via ring-opening polyaddition, as the protons associated with the cyclic carbonate peaks were still present (δ = 4.45 -4.65 ppm). Since the cyclic carbonate peak (δ = 4.45 -4.65 ppm) overlaps with the hydrogens peaks of the carbon which is connected to the hydroxyl group of the synthesized NIPU (δ = 4.2 -4.6 ppm), it is not possible to quantify the percentage of unreacted cyclic carbonates.

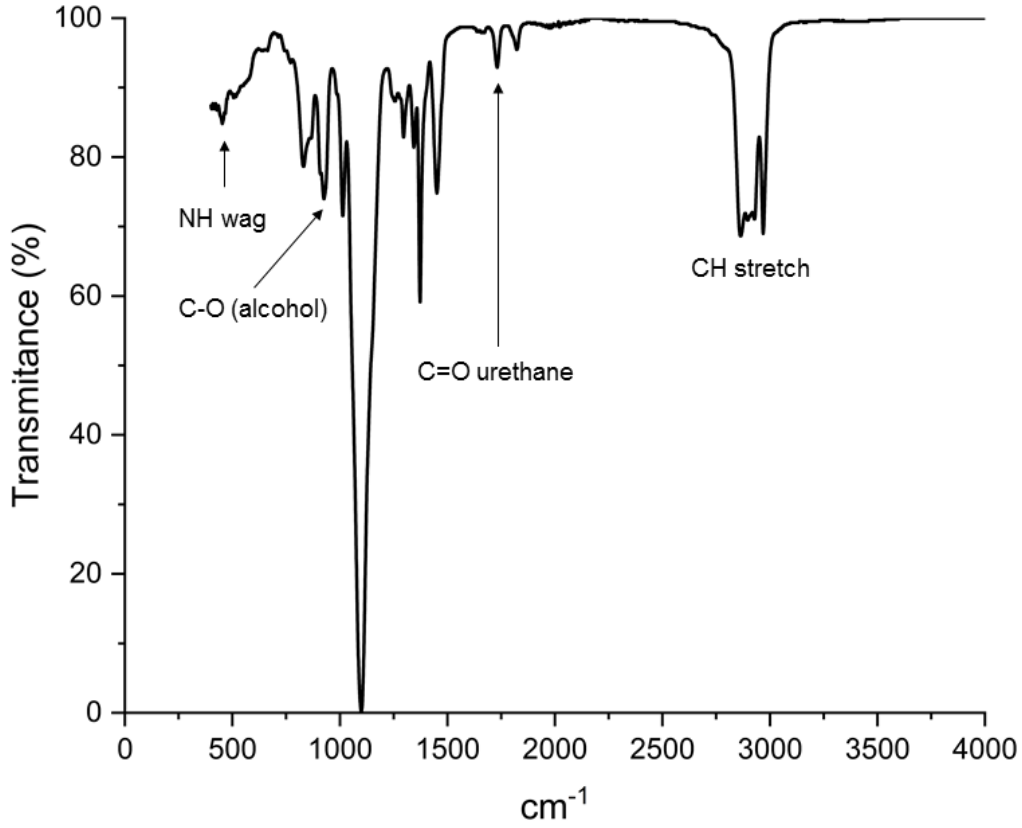

Figure 3.3. FTIR spectra for NIPU-90 and Myr/GMA-90, a) FTIR spectrum of NIPU-90 after six hours, b) carbonated *Myr*/GMA-90.

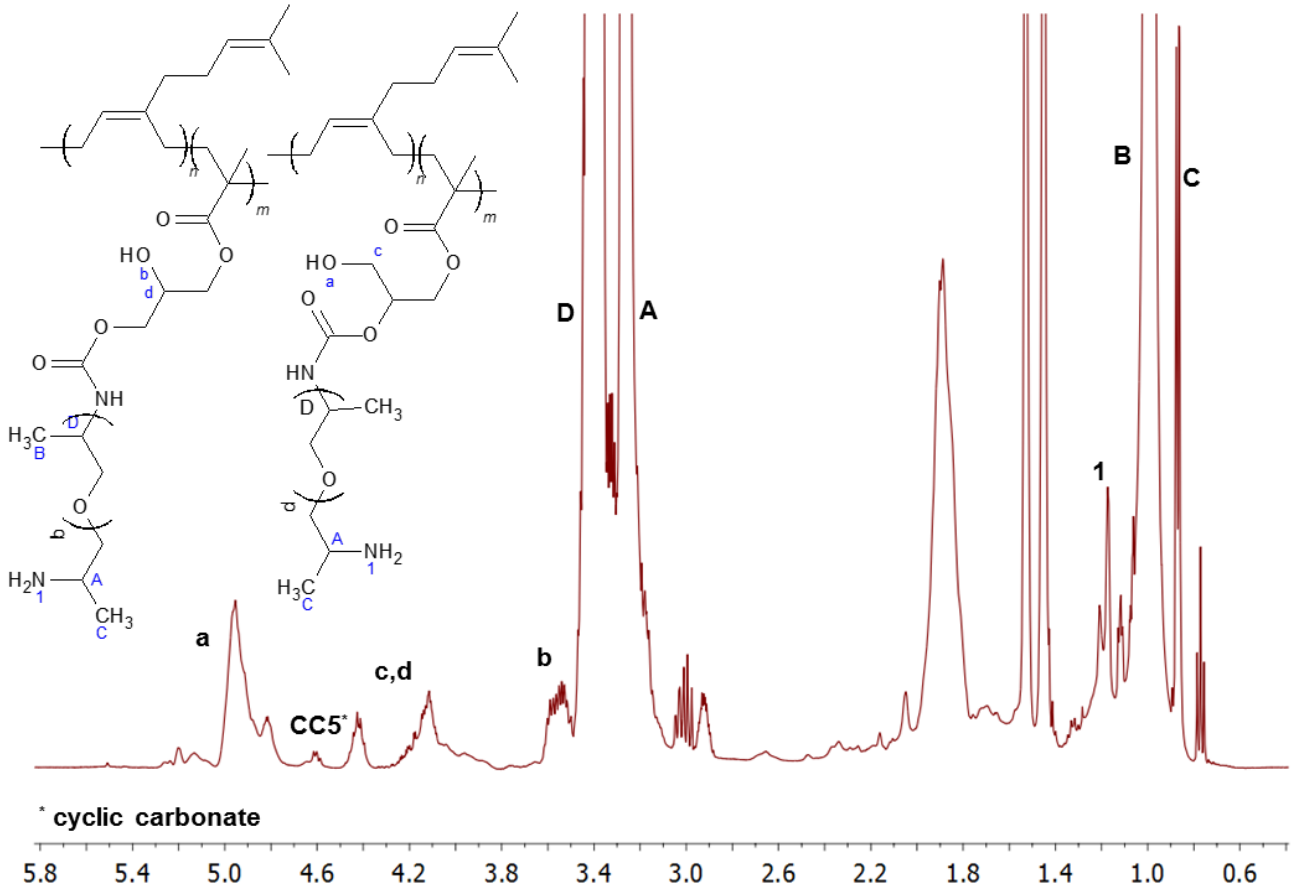

Figure 3.4. [1]H NMR spectrum of NIPU-90 after six hours.

3.3.4. End-Capping and Crosslinking NIPUs

Kinetic studies were investigated on the end-capped NIPUs and combined results are summarized in **Figure 3.5**.

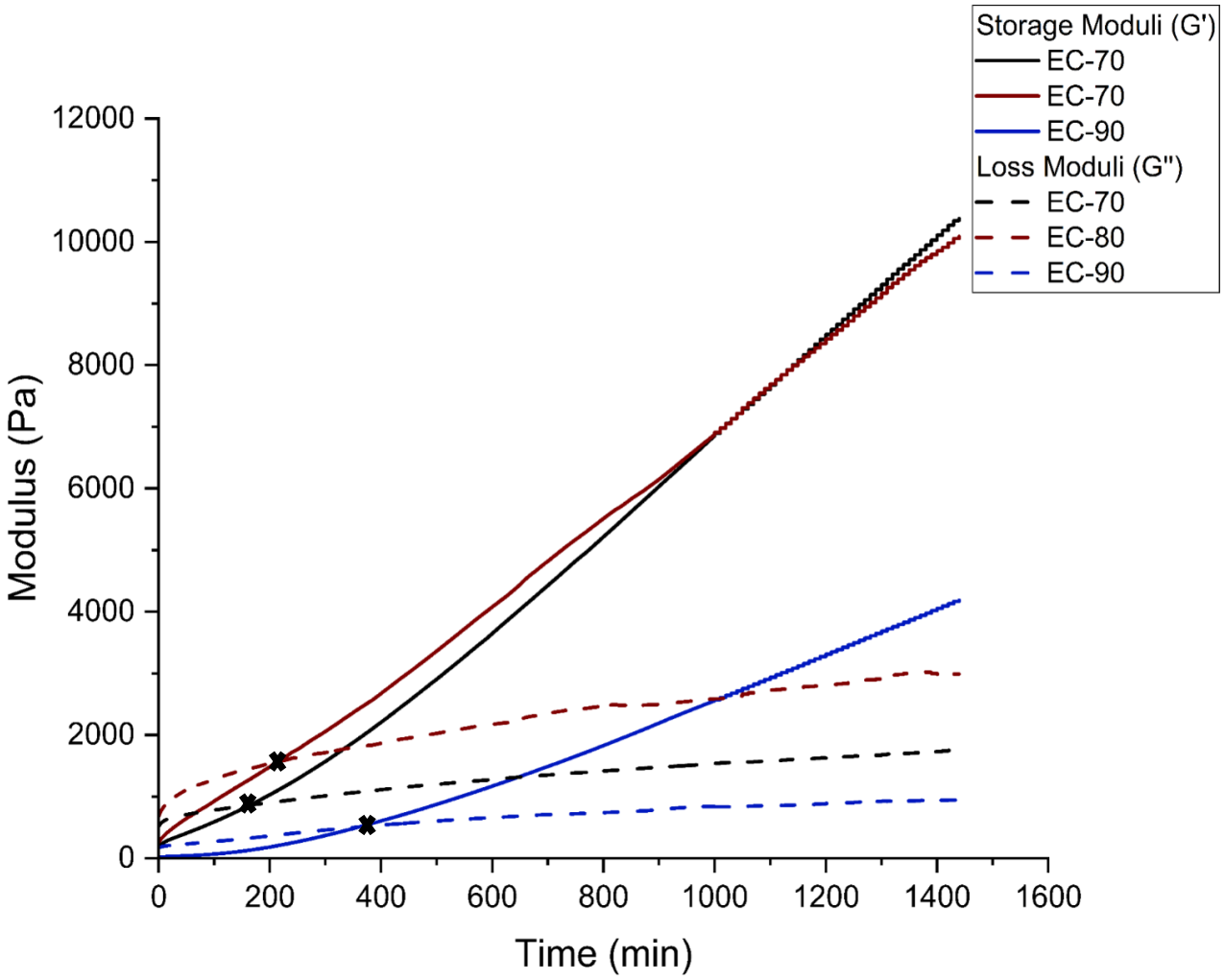

Figure 3.5. Curing kinetics of end-capped NIPUs (EC-70 , EC-80 and EC-90) ascertained by measurement of storage (G') and loss (G'') moduli (Pa) at a frequency of 1 Hz and a strain of 1% for 24 h. Measurements were done at 22°C with humidity of 22.3% (SD 1.25). The gel points are indicated as *X*.

As shown in **Figure 3.5**, EC-70, whose parent *Myr*/GMA copolymer contains 22 units of epoxy functional groups on the backbone ($f_{Myr} = 0.7$), has a gel time of 165 minutes (intersection of G' with G'') which indicates film forming when exposed to ambient conditions (20%-30% humidity at 22°C). In contrast, EC-80 and EC-90 cured more slowly compared to EC-70 due to the lower concentration of side chains emanating from the backbone. All films were left at ambient condition for a week to fully cure. Although the samples were soft and relatively weak due to the presence of excess Jeffamine D-4000 in the samples, DMTA was used to see if the films are sufficiently cured. **Figure 3.6** shows the temperature dependence of storage modulus (E'_r) of the end-capped NIPUs. All end-capped NIPUs had a nearly level plateau in the observed temperature test range, confirming their crosslinked structure. Estimates of the average molecular weight between crosslinks (M_c) using **Equation 3.3,** which are tabulated in **Table 3.3.** End-capping information of EC-90, EC-80 and EC-70., is indirectly proportional to the values of storage modulus at rubbery plateau region (E'_r). These results are consistent with the swelling ratios (*SR*) of end-capped NIPUs provided in **Table 3.4**. The *SR* gives information on the cross-linking density of the cured NIPUs with high *SR* corresponding to greater penetration of solvent. While EC-90 swelled to a higher degree due to the presence of longer chains between crosslinks, EC-70 swelled less, implying a tighter network [139]. This is consistent with the incorporation of Jeffamine D-4000 that increases the length between crosslinking nodes and increases crosslinking density. Furthermore, moderate gel content (*GC*) of end-capped NIPUs indicates a relatively high concentration of free species which are not chemically bonded to the polyurethane network [39,42,50].

Table 3.3. End-capping information of EC-90, EC-80 and EC-70.

NIPU	End-capper	# of urethane side branches on each backbone [a)]	Gel time (min)	$n_{GLYMO}/n_{Jeffamine}$	Temperature (°C)-time (h)	M_c (g mol^{-1})
EC-90	GLYMO	3	360	1	120-1	27000
EC-80	GLYMO	8	214	1	120-1	14800
EC-70	GLYMO	14	165	1	120-1	12000

([a)] Number of urethane linkages are calculated by: Number of Jeffamine D-4000 reacted with cyclic carbonates of the backbone (almost 50% of Jeffamine D-4000 reacted which is determined by GPC) × number of cyclic carbonates on the backbone).

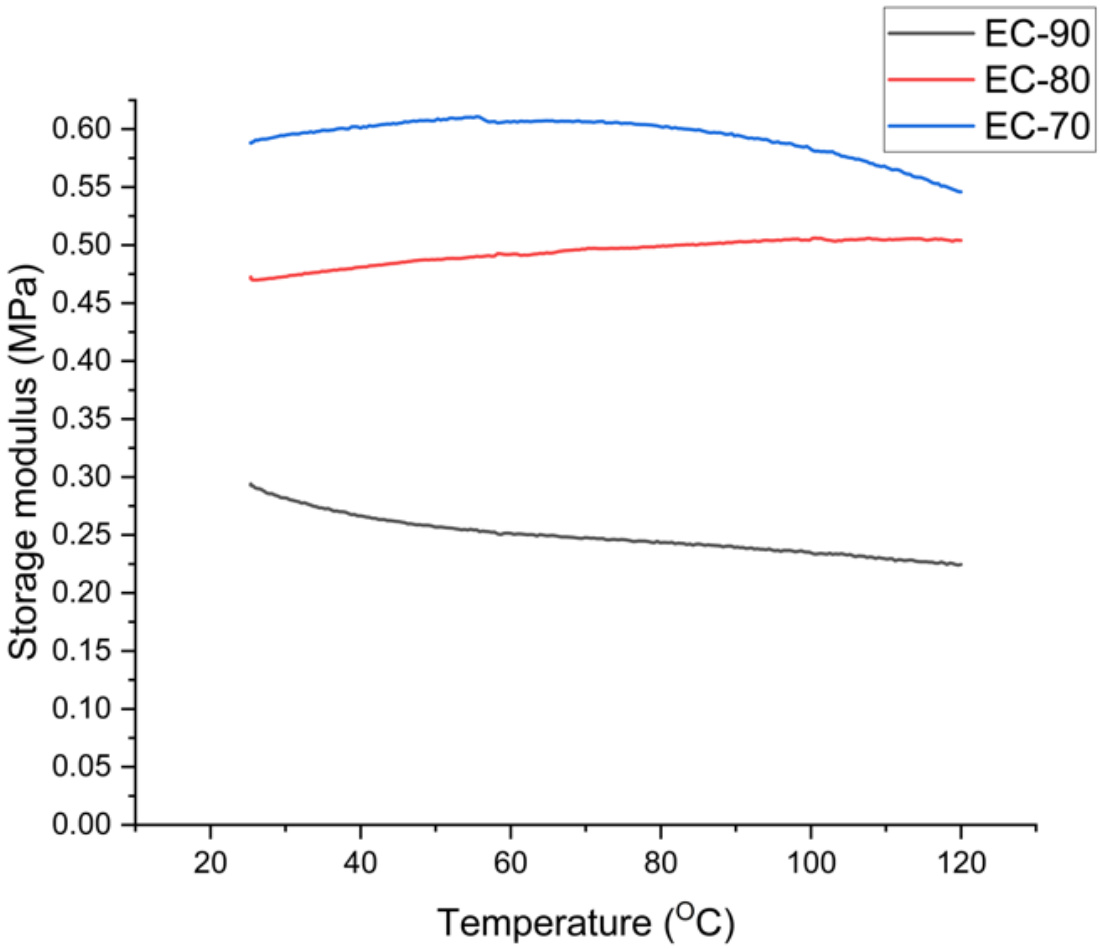

Figure 3.6. DMTA results of EC-90, EC-80 and EC-70.

Table 3.4. Swelling properties of the end-capped NIPUs in THF and water.

End-capped NIPU	THF		Water	
	SR (%)	*GC*(%)	*SR*(%)	*GC*(%)
EC-90	710±18.3	52±2.1	3.5±0.3	>99
EC-80	690±6.4	58±1.4	8.2±0.8	>99
EC-70	620±7.2	59±2.3	6.3±1.7	>99

Swelling studies on the end-capped NIPUs in purified H_2O were done to investigate the sensitivity of the materials to moisture (**Table 3.4**). Samples have low swelling ratios (approximately 3%-9%) and high *GC* values (≈100%) in water after a week. Jeffamine D-4000 is a PPG-based diamine which is a polymer with both hydrophilic and hydrophobic groups in its molecular structure. PPG is generally hydrophilic but becomes water-insoluble when its molecular weight is higher than 740 g mol^{-1} [140]. Also, myrcene is a hydrophobic acyclic monoterpene which can be another reason for high *GC* values in water for the synthesized NIPUs [141]. High *GC* values of samples is an indication of high resistance of cured NIPUs in moist environments. The nature of the diamine and the backbone material used to synthesize the NIPUs obviously play a role in dictating the final properties of the cured material. Although the fully cured NIPUs were soft and mechanically weak, samples were nevertheless cut out of the mold for mechanical testing, and the results are presented in **Figure A 10** and **Table 3.5**.

Table 3.5. Mechanical properties of cured samples[a)]

Cured NIPU	*E* (kPa)	σ_{max} (kPa)	*EB*[b)] (%)
EC-90	32.6±3.5	49.1±6.2	150±11
EC-80	46.2±0.9	60.9±1.1	132±2
EC-70	50.7±1.1	81.6±8.0	159±10

([a)]Three samples were cut out of the mold from each cured NIPU to provide an estimate of error); ([b)] Elongation at break).

Young´s modulus increased with higher number of branches. That is, the higher concentration of epoxy functional groups on the *Myr*/GMA backbone, the higher is the crosslinking density of the film which increases the strength of the films. EC-90 has the lowest crosslinking density (highest SR – see **Table 3.5**) it has the lowest Young´s modulus of 32.6 ± 3.5 kPa. In contrast, EC-70 has the densest crosslinked network and has the highest Young´s modulus (50.7 ±1.1 kPa). Low values of measured Young´s moduli are the result of the inability to remove the excess unreacted Jeffamine D-4000 in the films, making the films mechanically poor. It also could be due to chains entrapped in crosslinking nodes during GLYMO addition which causes that some chains do not participate in end-capping reaction.

As seen from **Figure A 11**, all end-capped NIPUs exhibit almost the same degradation behavior, showing that it is not affected by density of crosslinks for each cured sample. Cured NIPUs show two step degradation which could be due to two different microstructures of their initial *Myr*/GMA copolymer and unreacted Jeffamine D-4000 in the mixture (**Table A 1**). Also, the cured samples do not degrade completely according to TGA and have a residual of almost 1% which is due to the inorganic tin-based catalyst used to accelerate the curing at room temperature.

3.4. Conclusion

Partially bio-based hybrid NIPUs based on poly(*Myr-co*-GMA) were synthesized using bulk polymerization at moderate temperatures. *Myr*/GMA free radical copolymerization was conducted in a semi-batch polymerization to ensure that almost all chains contained epoxy functional groups (as the GMA reacted faster and was used up earlier during the copolymerization). Solvent-free coupling of epoxides of poly(*Myr-co*-GMA) with CO_2 was done with TBAB catalyst with complete conversion of carbonation reaction was achieved after 18 hours. Synthesized carbonated poly(*Myr-co*-GMA) were then reacted with Jeffamine D-4000 to prepare NIPUs with different number of urethane linkages on the chains.

From the NIPUs, end-capping reactions using moisture-sensitive silanes were conducted at moderate temperatures. Curing kinetics of the end-capped NIPUs revealed gel times of 165 minutes to 360 minutes at 22°C with 20%-30% humidity with shorter gel times corresponding to higher crosslinking densities, as revealed by swelling experiments. The tensile strength was weakly correlated to the number of urethane linkages. Young's moduli of the samples improved from 32.6 kPa to 50.7 kPa as the number of urethane linkages on the backbone increased from 6 to 22 (overall degrees of polymerization ~ 60 backbone units). Samples exhibited poor mechanical properties since excess diamine added to the carbonated poly(*Myr*-co-GMA) was used to prevent excessive crosslinking from the amine-carbonate reactions (the goal intended was to make hybrid moisture-curable silane-capped NIPUs). The excess diamine could not be removed but it could still be cross-linked with the silane together with the NIPU units branching from the backbone. Nevertheless, the samples were still mechanically weak. Samples immersed in water and THF exhibited good water resistance but moderate swelling in THF (50-60%) indicating incomplete curing. We are currently examining other backbone systems, where we

have been able to remove excess diamine and have observed more promising mechanical properties.

Probing deeper, the results in this paper also provide a strong foundation for future work in synthesis of sealants with better mechanical properties. Many different monomers can be substituted for *Myr* to make the initial copolymer backbone stiffer, leading to synthesis of sealants with tunable mechanical properties. For example, we are polymerizing more rigid methacrylates with GMA, and after carbonation, the copolymers with the resulting grafted NIPU are separated from the unreacted diamine more easily. This will be detailed in a succeeding report.

3.5. Experimental Section

Materials: β-myrcene (*Myr*), basic alumina (Al_2O_3, Brockmann, Type II 150 mesh), calcium hydride (CaH_2, 90-95% reagent grade), 2,2′-azobis(2-methylpropionitrile) (AIBN), tetrabutylammonium bromide (TBAB) and deuterated chloroform ($CDCl_3$, 99.8%) were purchased form Sigma-Aldrich and used without further purification. Poly(propylene glycol) with terminal amino groups (Jeffamine D-4000) with M_w = 4000 g·mol^{-1} was obtained from Huntsman. Toluene (>99%), methanol (MeOH, >99%), tetrahydrofuran (THF, 99.9% HPLC and certified grades) were purchased from Fisher Scientific as used as received. Glycidyl methacrylate (GMA) was obtained from Sigma-Aldrich and was purified by passing through a column of basic alumina mixed with 5 wt % calcium hydride and then kept in a sealed flask under nitrogen atmosphere in a refrigerator. Syntheses were all carried out under nitrogen atmosphere with high purity (99.99%, Praxair). Carbon dioxide (CO_2) with a purity of 99.99% was purchased from Praxair and used as received.

Myr/GMA copolymerization by free radical polymerization (FRP): All copolymerization reactions were done in a 250-ml three-necked round-bottom flask. *Myr* and AIBN were placed into the reactor, equipped with a thermal well and a magnetic stir bar. The whole setup was placed on a heating mantle on a magnetic stirrer. Next, the mixture was purged with nitrogen to minimize oxygen contamination. A condenser was used to prevent evaporation of monomer and venting of the purge was done via a needle at the top of the condenser. A thermocouple connected to a temperature controller was inserted into the thermal well and the reactor was heated to the desired polymerization temperature of 90°C. When the mixture reached 80°C, previously purified GMA was pumped into the reactor using a NE-1000 programmable single syringe pump at a rate of 5 mL h^{-1} and the polymerization was allowed to continue for six hours. After six hours, the reaction mixture viscosity increased and the heating to the reactor was turned off. Once cooled and after exposing the synthesized polymer to air, the polymer was precipitated in excess methanol to remove unreacted monomers from the final product. The purification was by proton nuclear magnetic resonance (^{1}H NMR) of the product to confirm removal of monomer (additional methanol was added until the supernatant layer was clear to reprecipitate the polymer). Finally, the copolymer was dried in a vacuum oven at 40°C overnight. All formulations for *Myr*/GMA copolymers are tabulated in **Table A 3**.

For every reaction, the initial molar ratio of monomers to initiator (AIBN) was calculated to give *Myr*/GMA copolymer with target number-average molecular weight $M_{n,theoretical} = (f_{GMA,0}M_{GMA}+f_{My,0}M_{Myr})DP_n$= 10000 g mol^{-1} at complete overall conversion (X =1), where $f_{Myr,0}$ and $f_{GMA,0}$ are the initial molar fractions of *Myr* and GMA, and DP_n is number average degree of polymerization, respectively. A specific formulation for *Myr*/GMA : 90/10 mol% is given as an example (experiment *Myr*/GMA-90, **Table A 3**). *Myr* (127.61g, 0.9367 mol), AIBN (5.26g,

0.0320 mol) were added into the reactor and then the setup was prepared as mentioned above. When the reactor reached 80°C, GMA (23.11g, 0.1626 mol) was pumped into the reactor using a pump for four hours at the prescribed flow rate to ensure that epoxy functional groups were evenly distributed along the polymer chains, since *Myr* concentration is higher than GMA leading to nearly full conversion of GMA after almost three hours (**Scheme A 1** compares *Myr*/GMA ideal copolymer microstructures in two different polymerization processes of batch and semi-batch). Samples were taken periodically until the end of the experiment. For each sample withdrawn, NMR and gel permeation chromatography (GPC) were used to determine composition and molecular weight distribution. The (overall) monomer conversions (X_{Myr} and X_{GMA}) were determined by ^{1}H NMR. The aliphatic protons of the monomer (δ=2.15–2.30 ppm, 4H) and the protons of the two methyl groups of monomer and polymer (δ=1.55–1.75 ppm, 6H) were used to compute myrcene conversion. To find conversion of GMA, vinyl protons of the monomer (δ=5.6-6.15 ppm, 2H) and the methine proton of the oxirane ring (δ=3.05-3.30 ppm, 1H) was used. The microstructure of copolymer was found by integrating the non-equivalent protons of the methylene bonded to the ester oxygen (δ=4.20–4.50 and 3.65– 4.00 ppm, 2H), the methine proton of the oxirane ring (δ=3.05– 3.30 ppm, 1H), and the protons of the methylene of the oxirane ring (δ= 2.75–2.90 and 2.55–2.70 ppm, 2H) for GMA and vinyl protons (δ=4.65-5.45 ppm, 2H) for myrcene (**Figure A 12**).

The overall conversion (using **Equation 3.1)** was $X_{copolymer} = 0.56$ (individual conversions: $X_{GMA} = 0.65$ and $X_{Myr} = 0.55$) at the end of the experiment (t = 360 min). Also, FTIR was used to confirm the presence of GMA in the copolymer. The molar composition of GMA in the final abovementioned copolymer was F_{GMA}=0.093.

$$X_{copolymer} = X_{Myr} f_{Myr,0} + X_{GMA} f_{GMA,0} \quad (3.1)$$

The final copolymer was found to have M_n= 6200 g mol^{-1} and dispersity ($Đ$) of 3.2, using gel permeation chromatography (GPC), calibrated relative to narrow molecular weight distribution poly(methyl methacrylate) (PMMA) standards (M_n range of 875 to 1677000 g mol^{-1}, Varian Polymer). **Figure A 1a** shows the schematic of the copolymerization and its carbonation reaction alongside with diamine addition to the carbonated copolymer.

Carbonation of Myr/GMA copolymers: The synthesis of carbonated *Myr*/GMA copolymer was carried out by an addition reaction of CO_2 with poly(*Myr-co*-GMA) using TBAB as catalyst (**Figure A 1b**). TBAB (0.0034 mol, 5 mol% with respect to number of epoxy groups on a chain) was added to a 150 ml three-necked round-bottom flask containing poly(*Myr-co*-GMA) (95.42 g). The reactor was equipped with a thermal well and a magnetic stir bar and the whole setup was placed on a heating mantle on a magnetic stirrer. Next, the mixture was purged with CO_2 to de-oxygenate the reactor. After 30 minutes of purging with CO_2, the temperature was increased to 120°C and the mixture was stirred under a stream of CO_2 (5 psi) for 24 hours. To monitor the reaction conversion, samples were taken every 6 hours and were characterized by NMR. Finally, the final product was precipitated in excess methanol to remove the catalyst entrained in the polymer (additional methanol was added until the supernatant layer was clear to reprecipitate the polymer) and the polymer was then dried in the vacuum oven at 40°C overnight. The overall conversion was calculated as $X_{carbonation}$= 0.97 at the end of the reaction by NMR.

Synthesis of non-isocyanate polyurethane (NIPU) from Jeffamine D-4000: An example is given showing the addition of Jeffamine D-4000 to a carbonated poly(*Myr*-co-GMA). Jeffamine D-4000 (53.12 g, 0.0060 mol) was added to a 150 ml three-necked round-bottom flask containing carbonated *Myr*/GMA-90 (23.63g) (diamine / cyclic carbonate: 1.2:1). Jeffamine D-4000 was added in excess to prevent any crosslinking reactions during polyaddition of diamine to cyclic carbonate. Since it was experimentally observed that cyclic carbonate-to-amine ratio of 1, leads to crosslinked polymer in the reactor over the time of the reaction. The reactor was equipped with a thermal well and a magnetic stir bar and the whole setup was placed on a heating mantle on a magnetic stirrer. Next, the mixture was purged with nitrogen to de-oxygenate the contents. After 30 minutes of purging, the temperature was increased to 120°C while continuing nitrogen purging. **Figure A 1c** shows reaction of the cyclic carbonates with Jeffamine D-4000 to produce the corresponding NIPUs. The reaction ran for six hours in order to prevent crosslinking reactions in the reactor. It should be mentioned that NIPU in this work refers to the formulation in which urethane linkages are formed on the side chains after addition of diamine to cyclic carbonates.

End-Capping of synthesized NIPUs: Synthesized NIPUs with *Myr*/GMA backbones containing 10%, 20% and 30% of GMA in the initial monomer mixture (NIPU-10, NIPU-20 and NIPU-30) were chosen for end-capping as their respective viscosities were suitable for further reactions occurring in bulk. The amount of end-capper to be used was set to one molar equivalent per mole of diamine used in the respective NIPUs to make sure that there is enough GLYMO to react with all amine functional groups. NIPU-90 (14.65 g) was added to a 50 ml three-necked round-bottom flask. The reactor was equipped with a thermal well and a magnetic stir bar and the whole setup was placed on a heating mantle on a magnetic stirrer. Next, the mixture was purged with nitrogen

for 30 minutes to de-oxygenate the contents. Once the mixture reached 120°C, it was mixed with one molar equivalents of GLYMO, depending on the moles of Jeffamine D-4000 in the NIPUs. The reactions were run for one hour and then 2 wt% of the catalyst with respect to NIPUs weight was added to the mixture and mixed for five minutes. Finally, the end-capped polymer was applied on a Teflon sheet. The reaction time was optimized for this step. Gelation was observed for reaction times of more than one hour. The mechanism of the end-capping reaction using moisture sensitive silane (GLYMO) is shown in **Figure A 13**.

Proton Nuclear Magnetic Resonance (^1H NMR) Spectroscopy: Solution-phase NMR spectra were recorded on a Bruker 500 MHz spectrometer (32 scans) at ambient temperature using $CDCl_3$ as solvent.

Fourier Transform Infrared (FTIR) Spectroscopy: A Nicolet iS50 FTIR Spectrometer equipped with a single bounce diamond attenuated transmission reflectance (ATR) for solids. Thirty-two scans were recorded for each sample over the range 4000-500 cm^{-1} with a normal resolution of 4 cm^{-1}.

Size Exclusion Chromatography (SEC): Gel permeation chromatography (GPC, Water Breeze, differential refractive index RI 2414 detector, 40°C) using HPLC grade THF as the mobile phase (flow rate 0.3 mL min^{-1}) was used to determine the number-average molecular weights (M_n) and dispersities ($Đ = M_w/M_n$). M_n values were calculated relative to narrow molecular weight distribution PMMA standards (Varian Polymer Standards, molecular weights ranging from 875 to 1677000 g mol^{-1}). It should be noted that poly(*Mry*) and poly(GMA) contribution to M_n extracted from GPC were converted to absolute molecular weight using Mark- Houwink-Sakurada (MHS) coefficients. MHS coefficients for PMMA at 35°C with THF eluent [120] are: $K_{PMMA} = 12.19 * 10^{-5}$ dL g^{-1}, $\alpha_{PMMA} = 0.683$, MHS coefficient for P(*Myr*) at 30°C with THF

eluent [121] are: $K_{P(Myr)} = 0.746 * 10^{-4}$ dL g^{-1}, $\alpha_{P(Myr)} = 0.772$, MHS coefficients for GMA at 30 °C [122] with THF eluent: $K_{GMA} = 27.8 * 10^{-5}$ dL g^{-1} , $\alpha_{GMA} = 0.537$. Thus, M_n reported are calculated by the Mark-Houwink relationship [123] using **Equation 3.2**:

$$M_{n,MHS} = F_{Myr}[(\frac{K_{P(MMA)}}{K_{P(Myr)}})M_{n,GPC}^{\alpha_{P(MMA)}+1}]^{1/(\alpha_{P(Myr)}+1)} + F_{GMA}[(\frac{K_{P(MMA)}}{K_{P(GMA)}})M_{n,GPC}^{\alpha_{P(MMA)}+1}]^{1/(\alpha_{P(GMA)}+1)} \quad (3.2)$$

where F_{Myr} and F_{GMA} are the final molar fraction of *Myr* and GMA in the copolymer, respectively. *Thermogravimetric Analysis (TGA):* A TA Instruments Discovery 5500 thermo-gravimetric analyzer was used to analyze the degradation of synthesized materials at a heating rate of 10°C min^{-1} from ambient temperature to 700°C under a nitrogen atmosphere in platinum pans. *Rheology:* Viscosity and curing studies were conducted using an Anton Paar Instruments Rheometer (MCR 302) with parallel plates of 25 mm diameter (PP 25) configuration with gap of 1 mm. The curing kinetics of the NIPUs were assessed using the same geometry. This evaluation was conducted at a frequency of 1 Hz and a strain level of 1%. The measurements were performed under ambient conditions (approximately 22 °C) with a humidity range of 20–30%. The evolutions of key parameters including storage modulus (G'), loss modulus (G'') and damping factor ($tan\delta = G''/G'$) were continuously monitored over a period of 24 hours. Prior to conducting these measurements, the samples were allowed to equilibrate to room temperature. Dynamic mechanical thermal analysis (DMTA) was conducted on the cured samples using torsion configuration (SRF 12) with a temperature ramp rate of 5°C min^{-1} (from 25 to 120°C), with an oscillation strain of 1% and a frequency of 1 Hz. Molecular weight between crosslinks (M_c) can be calculated using **Equation 3.3** [142,143]:

$$M_c = \frac{3RT\rho}{E_r'} \quad (3.3)$$

where E_r' is the storage modulus in the rubbery region from the DMTA experiments, R is the gas constant, T is the absolute temperature, and ρ is the density of the cured NIPUs.

Mechanical testing: Tensile properties were measured at ambient temperature using an EZ Test (Shimadzu) tensile machine at speeds of 5 mm min^{-1} on the cured samples. Young´s modulus (E), tensile strength (σ_{max}), and elongation at break ($EB\%$) were determined by the average of at least three repeated samples. Three dog-bone shaped samples with dimensions shown in **Figure 3.7** were cut out to perform tensile testing. **Figure A 7** shows the actual dog-bone shaped samples which were cut from the cured NIPUs.

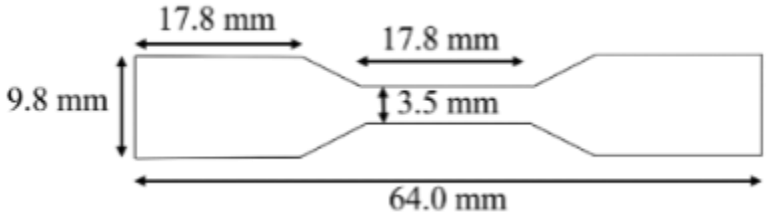

Figure 3.7. Dog-bone shaped samples dimensions for tensile testing.

Swelling ratio: Three samples of around 30 mg each were separately put in THF and purified water for 24 hours. The swelling ratio (SR) was calculated using **Equation 3.4**:

$$SR = \frac{m_2 - m_1}{m_1} \quad (3.4)$$

where m_1 and m_2 are the initial mass of the material and mass of the material after swelling in THF or water, respectively.

Gel content: After *SR* measurements, the three samples were dried in a vacuum oven at room temperature for 24 hours. The gel content (GC) was calculated using the **Equation 3.5**, where m_3

and m_2 are the mass of the material after drying in the oven and the initial mass of the material, respectively.

$$GC\% = \frac{m_3}{m_2} \times 100 \tag{3.5}$$

4. CHAPTER 4

DESIGN OF CROSSLINKED NETWORKS WITH HYDROXYURETHANE LINKAGES VIA BIO-BASED ALKYL METHACRYLATES AND DIAMINES

Following the successful establishment of the hybridization proof of concept, the focus shifted towards enhancing the mechanical properties of the crosslinked networks. It was observed that the *Myr*/GMA crosslinked networks displayed poor mechanical performance attributed to the inherent flexibility of both the backbone and side chains. To address this limitation, a network featuring a flexible backbone and rigid side chains was synthesized in this chapter. The primary objective was to investigate the influence of side chain rigidity on the mechanical properties of the resulting networks. This study aimed to uncover valuable insights into the relationship between the structural characteristics and mechanical behavior of the crosslinked networks, paving the way for the development of materials with improved performance in various applications. The manuscript of this chapter was published in *Journal of Applied Polymer Science* in 2023 (Farkhondehnia, M. and Marić, M., Design of crosslinked networks with hydroxyurethane linkages via bio-based alkyl methacrylates and diamines. Journal of Applied Polymer Science, 2023, 140, e54039) [144]. The supporting information of this publication is given in Appendix B.

4.1. Abstract

Hybrid methodology to combine the favourable properties of non-isocyanate polyurethane (NIPUs) with polymerized methacrylates is used to attain partially bio-based thermoset hybrid resins with hydroxyurethane linkages (HNIPU)s which are environmentally benign and are synthesized from cyclic carbonated copolymer templates derived from atom transfer radical polymerization (ATRP) of alkyl methacrylate (C13MA with average side-chain length of 13)/glycidyl methacrylate (GMA) mixtures (initial GMA mol fraction = 0.1-0.4). The resulting flexible resins with pendent epoxy functional groups were subsequently carbonated and then reacted with 1,10-diaminodecane (DAD) (90°C, 24 h) to form rigid side chains via hydroxyurethane linkages. By manipulating template functionality (2-11 urethane linkages out of 35 backbone units), crosslinked networks were achieved with Young's moduli ranging from 0.1 MPa to 71.9 MPa and decreasing tensile elongation at break from 105% to 10%. Also, swelling ratios (*SR*) of the networks in tetrahydrofuran (THF) decrease as the number of urethane linkages increases, indicating tighter networks, consistent with the rheologically obtained molecular weight between crosslinks (M_c, ranging from 3400 to 1700 $g \cdot mol^{-1}$). Gel content (*GC*) indicated less than 15% of the networks are soluble in THF. Expectedly, tighter crosslink networks limited polymer chain intermolecular mobility, resulting in glass transition temperatures (T_g) increases of the networks.

4.2. Introduction

Polyurethanes (PU)s, with a global market size of $72.82 billion USD in 2021, are an extremely versatile family of polymers [8,97,105,145]. Depending on the precursors used to make PUs, they can be utilized in foams, sealants, adhesives, coatings and stimuli-responsive polymers [5,146]. PUs are commonly synthesized by polyaddition reactions of di- or multi-functional isocyanates and di- or multi-functional alcohols [9,147]. However, toxicity issues associated with the production and use of isocyanates raises major environmental and health-related concerns [8,34,148]. Hence, an acute need has emerged to develop thermoplastic and thermoset isocyanate-free PUs that avoid these dangers.

Non-isocyanate polyurethanes (NIPUs) have surfaced as a contending replacement for conventional PUs. Although there are different methods to prepare NIPUs [9,149], reaction of amine and cyclic carbonate groups is the most prevalent one [13,102,106,150–152]. Both linear and branched or crosslinked networks can be synthesized via polyaddition reaction of cyclic carbonates and amines (e.g. thermosets are prepared via reaction of multi-functional cyclic carbonates and amines which is similar to reaction of multi-functional isocyanates and diols in traditional PUs). A significant benefit of this method is that the majority of cyclic carbonates and amines used in NIPUs are safer than isocyanates, which minimizes the need for special handling due to safety concerns [153]. Another advantage is that polyaddition of cyclic (poly)carbonates with (poly)amines leads to formation of urethane linkages with secondary hydroxyl groups in their chain, thereby giving NIPUs an alternative classification as poly(hydroxyurethane)s (PHUs). PHUs exhibit higher stiffness, improved chemical and mechanical properties compared to conventional PUs due to intermolecular and intramolecular hydrogen bonds [16,19]. To synthesize PHUs, five-, six- or seven-membered cyclic carbonates are typically used to react with amines

[154]. Previous investigations showed that ring strain is important, as addition reaction rate increases with increasing cyclic carbonate ring size [48]. Although six- and seven-membered cyclic carbonates are more reactive, hazardous reagents are used to prepare them [22], while the synthesis of five-membered cyclic carbonates is often favored, as such rings can be prepared via reaction of carbon dioxide (CO_2) with epoxides [155]. The carbonation step is often viewed as an advantage since fixation of CO_2 can alleviate greenhouse gas effects [49], and the relative abundance of CO_2 makes it a cost-effective reagent [136].

Recently, more sustainable methods to prepare NIPUs from bio-based precursors have emerged to complement the lower toxicity expected of NIPUs. In this context, bio-based alternatives for cyclic carbonate containing reagents such as the use of vegetable oils, bio-polyols and terpenes have been extensively studied [34,151]. Synthesis of bio-sourced diamines from plant-based fatty acids has been also investigated and some of them are commercially available [33]. Therefore, it can be said that PHUs are a promising alternative to conventional PUs since their precursors can be derived from bio-based materials and the use of cyclic carbonates eliminates production of by-products such as urea, water and CO_2 [9,35,151]. The final properties of PHUs are manipulated by the choice of cyclic (poly)carbonates, diamines and the cyclic carbonate-to-amine ratio [8,47]. For example, Javni et al.[35] investigated curing of carbonated soybean oil with a variety of diamines and different amine-to-carbonate ratios to produce crosslinked NIPUs with tensile strengths varying from 0.49 MPa to 5.77 MPa. Bähr et al.[151] also studied polyaddition of blends of carbonated linseed oil and carbonated soybean oil at different ratios with various rigid diamines to prepare crosslinked PHUs spanning a wide range of Young's moduli from 2 MPa to 1460 MPa. However, most examples of these thermoset PHUs are from vegetable oils with a fixed number of cyclic carbonate functionality in their structures and the factors which can alter the

mechanical properties of crosslinked PHUs are generally limited to diamine-to-carbonate ratio and type of diamine.

To improve the properties of synthesized bio-based NIPUs, hybrid NIPUs have become increasingly prominent [38]. The definition of hybrid NIPUs varies. It could be hybrid in the chemical structure, reacting with an inorganic polymer, for example, by introducing moisture-sensitive silanes into the structure. Alternatively, utilizing a different kind of polymerization method to incorporate desired functionality can be termed as a hybrid too (e.g combination of radical polymerization and polyaddition) [69,111].

Previously, we investigated synthesis of partially bio-based resins with flexible side chains which are bonded through urethane linkages to a flexible backbone. Those resins were end-capped via moisture sensitive silanes to provide crosslinked networks but were excessively soft [1]. However, in this study our goal is to use the chemistry of polyaddition of multi-functional cyclic carbonates with amines to produce a network with rigid side chains and a flexible backbone in which the concentration of cyclic carbonates can be manipulated easily and thus improve the range of mechanical properties desired.

Specifically, we aim to synthesize a hybrid crosslinked network which is bonded through urethane linkages using a different kind of polymerization. Atom transfer radical polymerization (ATRP) is used to copolymerize C13MA (a vegetable oil-derived alkyl methacrylate) with GMA to make a soft backbone in which epoxy functional groups are introduced via GMA. GMA provides grafting sites on the copolymer and manipulation of GMA content in the copolymer can control the density of the grafting sites. Then, CO_2 is fixed into the synthesized poly(C13MA-*co*-GMA)s to provide the required cyclic carbonate sites [8,156]. Cyclic carbonates in the synthesized copolymers were then reacted with 1,10-diaminodecane, which is a diamine that can be derived

from castor bean oil [157], to form urethane linkages. The final network, which is crosslinked through urethane linkages, exhibits interesting properties due to its specific microstructure. First, as shown in **Figure B 1**, C13MA is a hydrophobic methacrylate monomer with an average aliphatic side chain length of 13 carbon units. This "bottle-brush" structure provides a greater impact resistance and due to steric hindrance of these relative long alkyl side chains and hydrophobicity of C13MA, the access of water molecules to the crosslinked urethane network is limited, making it promising for moisture-resistant applications [158]. Secondly, since a short chain diamine is used to form the urethane linkages, the final crosslinked network has stiff side chains attached to the flexible backbone (**Figure B 1**). Moreover, in contrast to our prior study where *β*-myrcene was copolymerized via free radical polymerization (FRP), the current study utilizes C13MA copolymerized with GMA through atom transfer radical polymerization (ATRP). The implementation of ATRP instead of FRP resulted in a more uniform distribution of polymer chains, leading to formation of crosslinked samples with a more homogeneous network. The networks formed with poly(C13MA) can exhibit higher resistance to oxidation when compared to those formed with poly(myrcene), attributed to the absence of carbon double bonds in its structure. Using this paradigm, we intend to show the wide mechanical property window that can be attained using the combination of stiff grafts and flexible backbones via the density of cyclic carbonate sites to make partially bio-based HPU networks.

4.3. Results and discussion

4.3.1. Preparation of C13MA/GMA copolymers

A partially bio-based copolymer was synthesized as a template with distribution of epoxy groups that can be subsequently carbonated and then made into a crosslinked network with hydroxyurethane linkages [8]. The copolymerization of C13MA/GMA at different feed ratios was conducted using atom transfer radical polymerization (ATRP). It is important to note that temperature control in conventional radical polymerization is critical in bulk or concentrated solution since most free radical polymerizations are exothermic. Therefore, these polymerizations require good heat transfer characteristics; without proper heat removal, polymerizations may run away and one effect is a broadening of molecular weight distribution and unexpectedly higher average molecular weight [159]. Initially, we applied conventional free radical polymerization to synthesize C13MA/GMA copolymers both in bulk and solvent (50 wt% with respect to the weight of monomers), but was extremely exothermic, with the reaction temperature exceeding the temperature set-point by 50°C, leading to a highly viscous mixture in less than five minutes (**Figure B 2**). As it can be seen from **Figure B 2**, after only two minutes, the copolymers synthesized via free radical polymerization had M_n values of approximately 12000 g mol^{-1} with an overall conversion of more than 90%. Thus, ATRP which is a reversible deactivated radical polymerization (RDRP), was used to overcome this issue. ATRP was chosen as it is an efficient route to synthesize polymers with well-controlled composition, active chain ends and narrow molecular weight distributions [160]. The fast and reversible equilibrium between radicals and dormant species results in comparatively low radical concentration, virtually eliminating autoacceleration effects, and enabling control of microstructure with relatively short polymerization times [161]. The characterization of all synthesized copolymers are reported in

Table 4.1 and the copolymer conversions were calculated by ^{1}H NMR (**Figure 4.1**). The copolymers had M_n= 6500-10500 g mol^{-1} and $Đ$=1.19-1.47 (relative to poly(methyl methacrylate) (PMMA) standards by GPC in THF at 40°C, **Figure B 3**). Although all copolymers were synthesized under the same conditions, GMA-rich copolymers had higher apparent molecular weights which can be due to differences in propagation rates and monomer concentrations, leading to faster reaction. Reported values of bulk propagation rate coefficients (k_p) of GMA and the C13MA-related C17MA at 50°C via pulsed laser polymerization, revealed k_ps of 1249 L mol^{-1}s^{-1} and 910 L mol^{-1}s^{-1}, respectively [162,163], and it must be mentioned that there is a positive correlation between ester side chain length of methacrylates and k_p [162]. Furthermore, the reactivity ratios of C13MA and GMA with a terminal copolymerization model were reported using nitroxide mediated polymerization (NMP) using different calculation methods [164]. The reported reactivity ratios are r_{GMA} = 1.17±0.09 and r_{C13MA} = 0.65±0.09 [164], indicating that C13MA/GMA behaved in an essentially statistical fashion. Kinetic results are shown in **Figure B 4**. **Figure B 4b** shows that both C13MA and GMA have conversions below 100% at the end of the reaction, indicating that the epoxy groups are generally distributed through the copolymer chains. We did not observe significant compositional drift as observed previously in methyl methacrylate (MMA)/GMA, C13MA/GMA and β-myrcene/GMA copolymerizations [1,164,165]. Notably, since the GMA concentration in the mixture is lower than C13MA for our study, sequence distribution of the copolymer will favor C13MA incorporation at high conversions, as progressively less GMA is available to react with the growing macroradical. **Figure B 4c** indicates that the $Đ$ of copolymers changes from 1.19 to 1.37 as the GMA initial molar fraction increases from 0.1 to 0.6. Such behavior has been reported for both copolymerizations of MMA/GMA using ATRP and C13MA/GMA by NMP [164,165]. It was suggested that side reactions

including chain transfer reactions and termination, which affected the broadening of *Đ*, became more prevalent as the GMA molar fraction increased [165].

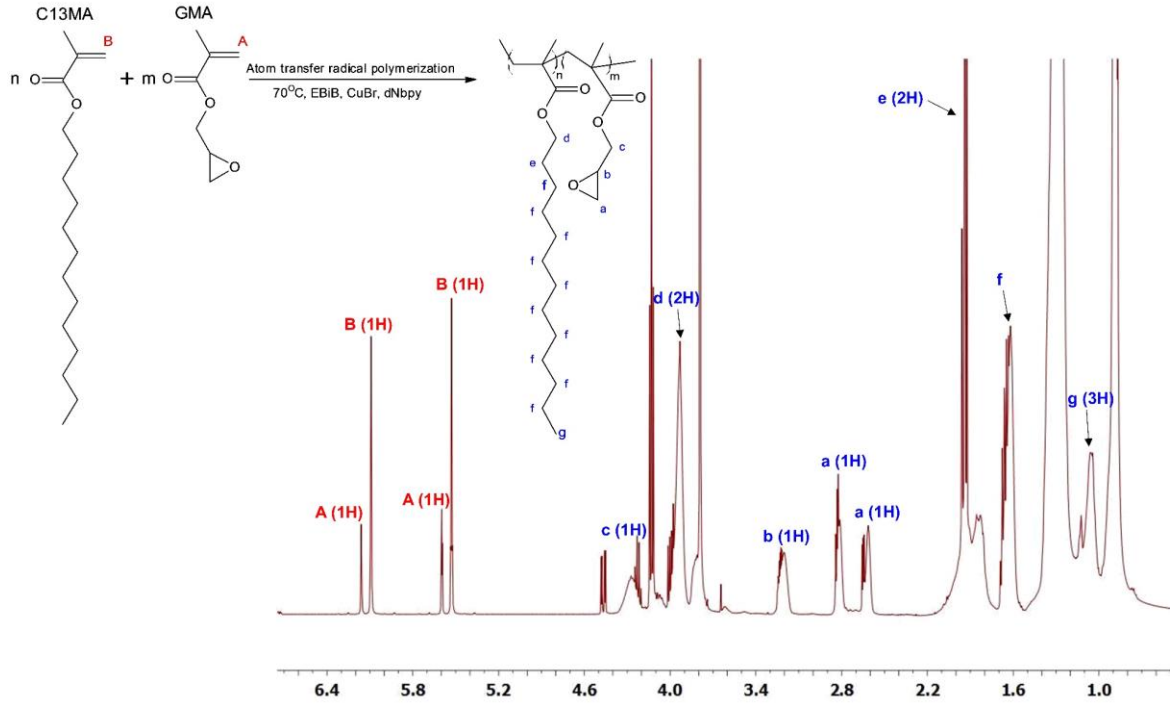

Figure 4.1. ^{1}H NMR spectrum for C13MA/GMA-70 after two hours polymerization at 70°C. ^{1}H NMR ($CDCl_3$, ppm): 6.13-6.20 ppm (m, $1H^{GMA}$), 6.04-6.12 ppm (m, $1H^{C13MA}$), 5.50-5.65 ppm (m, $1H^{GMA}$), 5.48-5.61 ppm (m, $1H^{C13MA}$), 4.20-4.45 ppm (m br, $1H^{P(GMA)}$), 3.87-3.98 ppm (s, $2H^{P(C13MA)}$), 3.10-3.30 ppm (s, $1H^{P(GMA)}$) , 2.80-2.90 ppm (s, $1H^{P(GMA)}$), 2.55-2.70 ppm (s, $1H^{P(GMA)}$), 1.83-2.10 ppm (m, $2H^{P(C13MA)}$), 1.57-1.75 ppm (m, $23H^{P(C13MA)}$), 1.05-1.28 ppm (m, $3H^{P(C13MA)}$).

Table 4.1. Copolymer characterization for statistical C13MA/GMA copolymers using ATRP in 70°C.

ID [a]	f_{C13MA}	F_{C13MA}	X_{C13MA} (%)	X_{GMA} (%)	$X_{copolymer}$ (%)	M_n [b] (g·mol^{-1})	$Đ$
C13MA/GMA-100	1	1	50	-	50	6500	1.20
C13MA/GMA-90	0.9	0.91	80	90	90	8000	1.19
C13MA/GMA-80	0.8	0.87	94	72	90	7800	1.21
C13MA/GMA-70	0.7	0.66	97	95	96	9300	1.25
C13MA/GMA-60	0.6	0.56	97	92	95	8800	1.26
C13MA/GMA-50	0.5	0.48	98	95	96	9600	1.29
C13MA/GMA-40	0.4	0.37	100	100	100	10500	1.37
C13MA/GMA-0 [c]	0	0	-	98	98	7800	1.47

([a] Experimental identification given by C13MA/GMA-XX, where XX refers to the rounded % initial molar fraction of C13MA in the mixture ($f_{C13MA,0}$)); ([b] Target number average molecular weight for all experiments ($M_{n,theoritical}$)=5000 g mol^{-1} , all reported molecular weights (M_n) and dispersity ($Đ$) were determined using GPC relative to poly(methyl methacrylate) (PMMA) standards in tetrahydrofuran (THF) at 40°C); ([c] Reaction was performed for 1.5 hours since the polymer became highly viscous and thus the reaction was terminated earlier to facilitate removal).

The thermal stability of synthesized C13MA/GMA copolymers were analyzed by DSC and TGA to investigate the effect of carbonation and diamine addition on thermal stability and T_gs of the products produced in the succeeding steps. This is also beneficial towards selecting a proper window of curing temperatures (T_{cure}) for the thermoset networks. It is ideal to run the reactions above T_g of the polymers to have the maximum reaction rate, since chain mobilities in the glassy state are limited and the reaction/cross-linking reaction rates will be decelerated [166]. **Table 4.2** reports the T_gs, melting temperatures (T_m)s and decomposition temperatures (T_{dec})s. DSC curves for synthesized poly(C13MA-*co*-GMA)s and carbonated poly(C13MA-*co*-GMA)s are also shown in **Figure B 5a** with -64°C<T_g<-33°C and -44°C<T_g<60°C measured for poly(C13MA-*co*-GMA)s and carbonated poly(C13MA-*co*-GMA)s, respectively. By comparison, T_g = 44-76°C for poly(GMA) (M_n range of 9600 g mol^{-1} to 20400 g mol^{-1}) and T_g = -46°C poly(tridecyl

methacrylate) (M_n = 48 kg mol^{-1}) [167–170]. Poly(C13MA-*co*-GMA) copolymers showed two different T_gs when F_{GMA}> 0.5. Initially, two T_gs suggest possible microphase separation or a blend of two homopolymers. The solubility parameters (δ) of C13MA/GMA (δ_{C13MA} = 15.43 MPa$^{0.5}$ and δ_{GMA} = 19.25 MPa$^{0.5}$) are different enough to suggest possibility of micro-phase separation [171] but the statistical nature of the microstructures seems to preclude micro-phase separation while the GPC traces indicated monomodal peaks and contamination with a homopolymer was not observed. The T_gs at higher temperatures can be due to backbone segmental motion and T_gs at lower temperatures can be attributed to alkyl side chains [172–174]. T_ms for statistical poly(C13MA-*co*-GMA)s were also observed, when F_{C13MA}>0.5 in the copolymer composition. The appearance of T_m in the synthesized C13MA/GMA copolymers was due to crystallization of alkyl chains of C13MA, which has been reported elsewhere. [164,175–177]. Decomposition temperatures are also listed in **Table 4.2** and TGA curves are plotted in **Figure B 6a**. Different peaks were observed in the TGA curves and their derivatives. The first decomposition peak was in the temperature range of 170-200°C and the second peak was between 300°C and 350°C. Appearance of more than one degradation peak in the TGA curves of GMA-based copolymers is common [164,178]. The first degradation peak could be due to degradation of poly(GMA) breaking into smaller fragments as observed in previous studies concerning copolymerization of bis[4(2-hydroxy-3-methacryloyloxypropoxy)phenyl]sulfide with GMA [179]. The second decomposition peak could be associated with the degradation of ester bonds and loss of CO_2 and eventually degradation of the copolymer [164,179]. Generally, epoxy rings are insensitive to thermally induced ring-opening cross-linking. However, the presence of quaternary carbon atoms in the chains due to the GMA moieties facilitates decomposition by an unzipping mechanism [180]. As seen from **Table 4.2**, as the C13MA content increased in the

copolymer, maximum decomposition temperature ($T_{dec,max}$) shifted to higher temperatures but no correlation was observed between GMA or C13MA content and T_{dec} for 10% weight loss ($T_{dec,10\%}$).

Table 4.2. Thermal characterization of C13MA/GMA copolymers via ATRP in anisole as solvent.

Sample ID	T_g [a)] (°C)	T_m [a)] (°C)	$T_{dec,10\%}$ [b)] (°C)	$T_{dec,max}$ [b)] (°C)	$T_{dec,1}$ [b)] (°C)	$T_{dec,2}$ [b)] (°C)	$T_{dec,final}$ [b)] (°C)	F_{GMA} [c)]	Ash content (%)
C13MA/GMA-90	-32.5	-22	193	374	211	374	506	0.17	0
C13MA/GMA-80	-44	-29	195	351	171	351	564	0.29	0
C13MA/GMA-70	-53.5	-36	199	350	172	350	590	0.44	0
C13MA/GMA-60	-58	-38	195	348	185	348	543	0.53	0
C13MA/GMA-50	-60, 0.5	-	183	338	175	338	460	0.62	0
C13MA/GMA-40	-64, 1.5	-	185	335	178	354	595	0.71	0
Carbonated C13MA/GMA-90	-44	-30	242	351	-	345	522	0.17	0
Carbonated C13MA/GMA-80	-50 8.5	-36	249	352	-	347	560	0.29	0
Carbonated C13MA/GMA-70	-53, 31	-	246	335	-	340	562	0.44	0
Carbonated C13MA/GMA-60	-52, 50	-	275	330	-	341	573	0.53	0
Carbonated C13MA/GMA-50	-56, 60	-	260	341	179	344	528	0.62	0
Carbonated C13MA/GMA-40	59	-	257	340	153	322	595	0.71	0.2

([a)] Glass transition temperature (T_g) and melting temperature (T_m) determined by DSC under nitrogen atmosphere using three cysle (heat/cool/heat) with heating rate of 5°C min^{-1}); ([b)] $T_{dec,10\%}$ (decomposition temperature for 10% weight loss), $T_{dec,max}$ (temperature at maximum decomposition rate), $T_{dec,1}$ and $T_{dec,2}$ (the first and second peaks in derivative weight (%/°C) versus temperature (°C) obtained from TGA) and $T_{dec,final}$ (temperature at the end of decomposition) measured by TGA under nitrogen purge at a heating ramp rate of 10°C min^{-1}); ([c)] Final molar composition of GMA in C13MA/GMA copolymers).

Lastly, the effect of GMA mole fraction on poly(C13MA-*co*-GMA) was investigated (**Figure B 7**) as it affects the leveling of the final synthesized polyurethanes. Leveling is a critical factor to achieve a smooth and uniform coating and it is favored when the polymer melt viscosity is low [127]. Viscosity measurements were done for the samples which were soft at ambient temperature. As seen in **Figure B 7a**, there was a positive correlation between GMA content in the copolymer and the viscosity. The viscosity of C13MA/GMA-90 increased from 4000 mPa s to 3×10^6 mPa s for C13MA/GMA-60 (**Figure B 7b**), as more GMA in the copolymer made the chains stiffer. The same trend was also observed in copolymerizations of *tert*-butyl acrylate with GMA and acrylonitrile with GMA [181]. Since C13MA/GMA-60 has higher GMA incorporation compared to C13MA/GMA-90, it was more viscous. It is also expected that C13MA/GMA-60 has higher T_g compared to C13MA/GMA-90. However, as it can be seen from **Table 4.2**, C13MA/GMA-60 has a lower T_g; and also two T_gs for copolymers with $F_{GMA}>0.5$ was observed (with the higher GMA incorporation, the higher the second observed T_g). The higher T_g can be attributed to the segmental motion of the copolymer backbone, while the lower T_g is caused by the crystallization of alkyl side chains (e.g. C13MA/GMA-40 has two T_gs of -64°C and 1.5°C). Lower T_g for C13MA/GMA-60 compared to C13MA/GMA-90 could be due to overlapping of the T_gs of C13MA/GMA-60 with the T_m of the copolymer (C13MA/GMA-60). Thus, the T_g measured for these copolymers must be treated with precaution, but are generally in agreement with previous studies [164].

All poly(C13MA-*co*-GMA)s and carbonated poly(C13MA-*co*-GMA)s have Newtonian plateaus for shear rates between 0.1 to 10 s^{-1}, indicating that they are all below their entanglement molecular weight (entanglement molecular weight (M_e) for a comparable poly(n-dodecyl

methacrylate) is 155 kg mol^{-1}, and a positive correlation between alkyl group length and M_e values was reported [182]).

4.3.2. Synthesis of carbonated poly(C13MA-*co*-GMA)s

After synthesizing the series of poly(C13MA-*co*-GMA) copolymers, they were treated with CO_2 and tetrabutylammonium bromide (TBAB) to convert the epoxy groups to cyclic carbonates [151]. Carbonation of poly(C13MA-*co*-GMA)s was confirmed using FTIR and ^{1}H NMR (**Figure B 8, Figure B 9** and **Figure B 10**). FTIR analysis of poly(C13MA-*co*-GMA) and carbonated poly(C13MA-*co*-GMA) (**Figure B 9**) show the disappearance of characteristic epoxy group peaks at 845 cm^{-1} and appearance of new peaks associated with cyclic carbonate groups at 1800 and 1050 cm^{-1}, which are assigned to C=O carbonyl stretching and C-O stretching of cyclic carbonate functionalities [95]. Carbonation was also confirmed using ^{1}H NMR via the disappearance of the peak at 2.55 ppm assigned to the epoxy ring and appearance of new peaks at 4.65 ppm attributed to the C-H resonance in the α-position of the cyclic carbonate groups. The carbonation conversion was also determined by integrating the two aforementioned peaks (2.55 ppm for epoxy and 4.65 ppm for cyclic carbonate) using **Equation 4.1**.

$$X = \frac{A}{A+B} \tag{4.1}$$

Where A is the integral of the signal assigned to cyclic carbonate (4.65 ppm) and B is the integral of the signal for epoxy functional group (2.55 ppm).

Finally, it can be concluded that the carbonation reaction was complete after 24 hours at 120°C without any thermal degradation since the GPC peak for the carbonated copolymer remains

monomodal and does not broaden significantly compared to the pre-carbonated copolymer (**Figure B 11**). There is a slight shift in the carbonated copolymer's chromatogram due to the different solubility of the carbonated copolymer in the eluent.

Once carbonation of the copolymers was done, thermal stability of the carbonated copolymers was investigated using TGA and T_gs and T_ms were extracted using DSC. **Figure B 5b** shows the DSC curves for the carbonated poly(C13MA-*co*-GMA)s. T_gs of the carbonated poly(C13MA-*co*-GMA)s are tabulated in **Table 4.2**. The T_g values of the carbonated copolymers are clearly higher compared to the T_gs of C13MA/GMA copolymers. This increase in T_g is derived from the cyclic carbonate groups limiting polymer chain mobility. This trend was also observed in carbonation of poly (BA-*co*-MMA-*co*-GMA), poly(GMA-*co*-styrene) and poly(GMA-*co*-butyl acrylate) [156,183]. Appearance of two T_gs for the carbonated copolymers is likely similar to that observed with the pre-carbonated copolymers. The T_g at lower temperatures (e.g. -50°C for carbonated C13MA/GMA-80) is attributed to the alkyl side chains of C13MA while the T_g observed at higher temperatures (e.g. 8.5°C for carbonated C13MA/GMA-80) is due to backbone segmental motion. Melting points for the carbonated copolymers are due to the crystallization of alkyl chains as mentioned before and observed elsewhere [176,177].

Decomposition temperatures are listed in **Table 4.2** and TGA plots are shown in **Figure B 6b**. The polymers with higher cyclic carbonate concentration showed a two step degradation in their TGA profiles. This is due to the elimination of CO_2 from the cyclic carbonate rings at first, followed by degradation of the polymer backbone. Based on **Figure B 6b**, the rate of decomposition increased sharply after almost 260°C ($T_{dec,10\%}$) which is likely due to the release of CO_2 from the cyclic carbonate structure [184,185].

Rheological studies were also done on the carbonated copolymers in order to choose samples with appropriate viscosity to be used for subsequent hydroxyurethane coupling. Carbonation of copolymers led to a significant increase in viscosity (**Figure B 6b**). For example, the viscosity of C13MA/GMA-90 increased from 4×10^3 mPa s to 10^6 mPa s after carbonation at 30°C (carbonated C13MA/GMA-90). The rise in viscosity is due to the intermolecular hydrogen bonding between carbonyl groups of cyclic carbonate, leading to a decrease of mobility of the carbonated copolymers [151]. Samples with lower viscosities and lower cyclic carbonate content were chosen for the diamine addition reaction step to prepare crosslinked networks bonded with urethane linkages, since high viscosity causes processing problems and samples with higher cyclic carbonate functionalities lead to much shorter gel times, especially when reacting with a reactive diamine such as DAD. This led to challenges in molding into desired shapes such as tensile bars [151].

4.3.3. Synthesis of crosslinked networks bonded with urethane linkages using 1,10- diaminodecane

After preparation of carbonated poly(C13MA-*co*-GMA)s, a series of crosslinked networks were synthesized via polyaddition with 1,10-diaminodecane (**Scheme 1a**, prepared samples are called NIPU-xx, where xx refers to the rounded % initial molar fraction of C13MA in poly(C13MA-*co*-GMA)). Since the reactivity of cyclic carbonates with amines is quite low, the reaction rate can be accelerated by increasing temperature or diamine concentration [8,152,186]. For example, by increasing the amine:carbonate ratio, the conversion of cyclic carbonate groups to urethane was increased in polyaddition of carbonated soybean oil with *p*-xylylene diamine [35]. However, excess diamine can form amine terminated urethane linkages which do not participate in the crosslinked networks, leading to lower tensile strengths. Excess diamine can also react with ester groups

available in the C13MA structure or carbonated GMA structure and form amides, providing a network with lower crosslinking density, containing unreacted free species due to aminolysis of the ester groups which cannot be removed from the network (**Scheme 1b**) [187]. Doley et al.[187] investigated the effect of amine:carbonate ratio on mechanical properties of NIPUs produced from polyaddition of carbonated sunflower oil and different diamines such as 1,2-ethylenediamine (EDA). Lower tensile strengths were observed for NIPUs with higher amine-to-carbonate ratios due to ester group aminolysis. Therefore, an amine: carbonate ratio of 1:1 was chosen to achieve better mechanical properties by avoiding formation of free species in the network and amine-terminated urethane linkages.

Reaction rates between diamine and cyclic carbonate functional groups are accelerated at higher temperatures, which led to attainment of higher viscosities faster. This makes stirring and subsequent processing difficult (eg. shaping the product into tensile bars) [152]. Therefore, the crosslinking conditions were subsequently kept at 90°C (above the melting point of 1,10-diaminodecane) for 24 hours with the cyclic carbonate: amine ratio = 1.

In **Figure 4.2**, the FTIR spectra of NIPU-70 (the crosslinked networks which are bonded through urethane linkages are called NIPUs here although a polymeric repeating unit containing multiple urethane linkages is not present) and carbonated C13MA/GMA-70 are shown. Characteristic absorption peaks for the synthesized network are observed at 3370 cm^{-1} due to the OH stretching of the hydroxyl group, 1720 cm^{-1} due to C=O stretching of the urethane group which is formed by the ring-opening of cyclic carbonate groups, and 1525 cm^{-1} due to the NH deformation of the urethane group (**Figure 4.2b**). A weak peak of residual carbonate at 1800 cm^{-1} was observed, suggesting that the conversion of cyclic carbonate to urethane was not complete, which has been seen elsewhere [8,47,52,188,189]. For example, unreacted cyclic carbonate groups were also observed

in polyaddition of carbonated soybean oil with *p*-xylylene diamine and addition of hexamethylenediamine to carbonated soybean oil [8,35]. The absence of an absorption peak at approximately 1650 cm^{-1} for the amide indicates that the aminolysis of ester groups did not occur.

Noticeably, the graft copolymers derived from carbonated poly(C13MA-*co*-GMA)s with higher cyclic carbonate concentration needed a lower degree of cyclic carbonate conversion to reach the gel point. In order to investigate the gel points of the crosslinked networks, curing tests were done at 90°C for 24 hours. As shown in **Figure 4.3**, gel time of the crosslinked networks decreased as the number of cyclic carbonates on the backbone increased. NIPU-60, whose parent C13MA/GMA copolymer contained 11 units of epoxy functional groups on the backbone, has a gel time of 0.8 minutes (intersection of G' with G'' or where $\tan\delta < 1$). In contrast, NIPU-90, NIPU-80 and NIPU-70 cured more slowly due to lower concentration of pendent cyclic carbonate groups. The gel times for the synthesized networks are tabulated in **Table 4.3**.

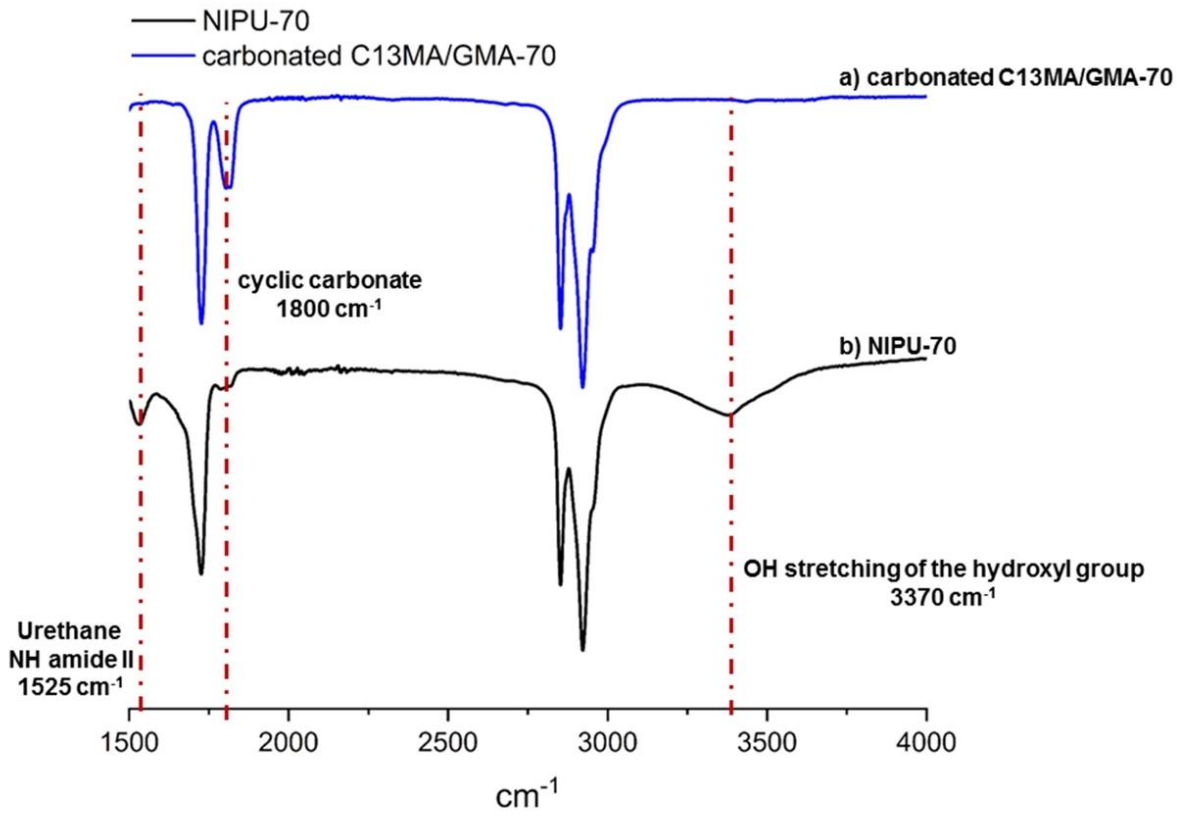

Figure 4.2. FTIR spectra for carbonated C13MA/GMA-70 and NIPU-70; a) carbonated C13MA/GMA-70, b) NIPU-70.

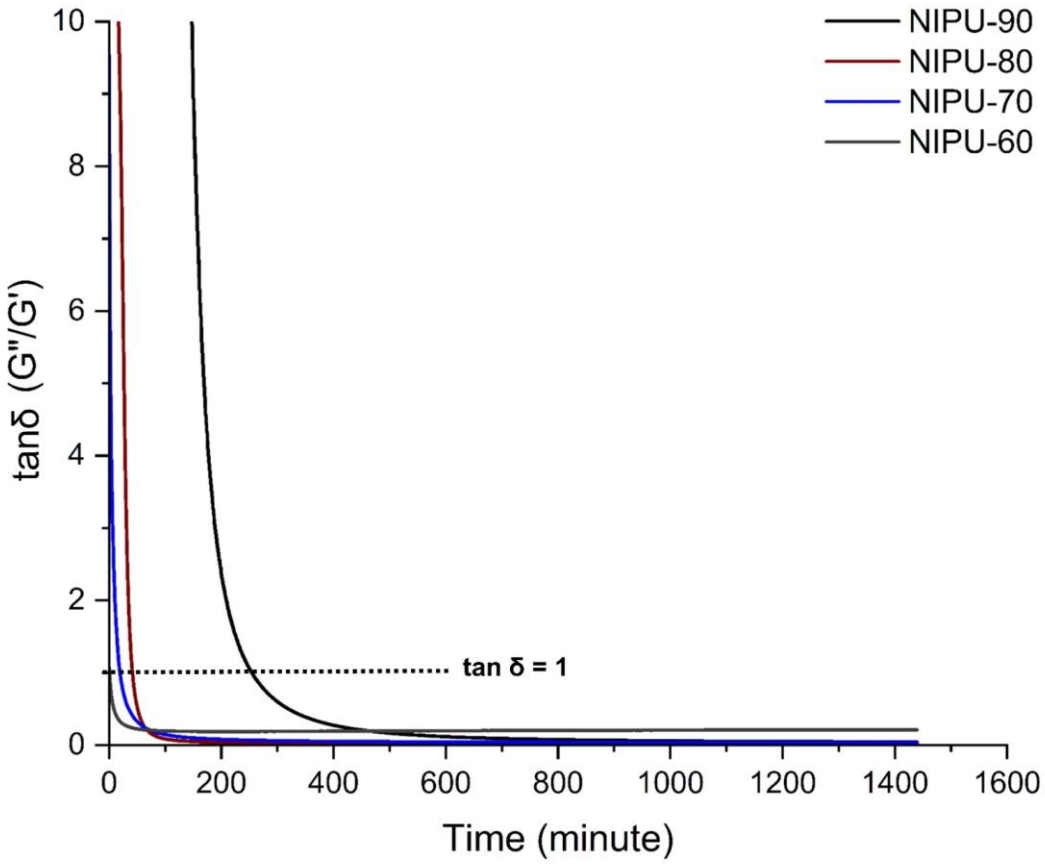

Figure 4.3. Loss factor as function of time for the crosslinked networks (experimental identification given by NIPU-xx, where xx refers to the rounded % initial molar fraction of C13MA in poly(C13MA-*co*-GMA)).

Table 4.3. Gel time and mechanical properties[a)] of crosslinked NIPUs.

Sample ID[b)]	# of urethane linkages on each backbone	Gel time (min)	E[c)] (MPa)	EB[d)] (%)	Ultimate stress (MPa)	T_g (°C)	M_c (g mol^{-1})	Swelling ratio in THF (%)	Swelling ratio in water (%)	Gel content (%)
NIPU-90	2	254	0.08 ± 0.02	105 ± 12	0.05 ± 0.03	61	3400	490.9 ± 26	37.27 ± 5.61	95.2 ± 2.1
NIPU-80	5	41.7	0.31 ± 0.02	95 ± 11	0.28 ± 0.02	73	3000	392.1 ± 27	32.76 ± 4.24	98.3 ± 1.5
NIPU-70	9	19.5	14.4 ± 0.1	29 ± 2	4.45 ± 0.1	77	2030	301.9 ± 21	25.32 ± 3.23	88.4 ± 1.6
NIPU-60	11	0.83	71.9 ± 1.1	10 ± 0.5	7.34 ± 0.5	79	1700	175.5 ± 31	19.73 ± 5.19	85.8 ± 3

((a) Three replicates for each crosslinked NIPU were applied); (b) Experimental identification given by NIPU-xx, where xx refers to the rounded % initial molar fraction of C13MA in poly(C13MA-*co*-GMA)); (c) Young's modulus, E values are calculated in the linear region of stress-strain curve for 2% elongation); (d) Elongation at break))

The viscoelastic properties of the crosslinked networks were characterized via DMTA at constant strain of 1% and frequency of 1Hz at various temperatures. **Figure 4.4a** and **Figure 4.4b** show storage moduli of the networks and tanδ response, respectively. For the crosslinked networks, T_g increased as the number of urethane linkages increased in the backbone. T_g for NIPU-60, with 11 urethane linkages on the backbone, is 18°C higher than NIPU-90 which contains only two urethane linkages on its backbone (**Table 4.3**). Among all crosslinked samples, the highest T_g was observed in NIPU-60 and can be attributed to the lower average molecular weight between

crosslinks (M_c) [8], since NIPU-60 has the highest urethane linkage concentration and thus the densest network.

Variations in the cross-link density in the synthesized networks which contain urethane linkages are seen in **Figure 4.4a**. Using the theory of rubber elasticity [190], the relationship between average molecular weight between cross-links (M_c) and G' is given by the equation provided in experimental section**.** M_c values for all crosslinked networks are given in **Table 4.3**. It can be seen that the predicted M_c are in agreement with the trend in T_g which was extracted from the tanδ response.

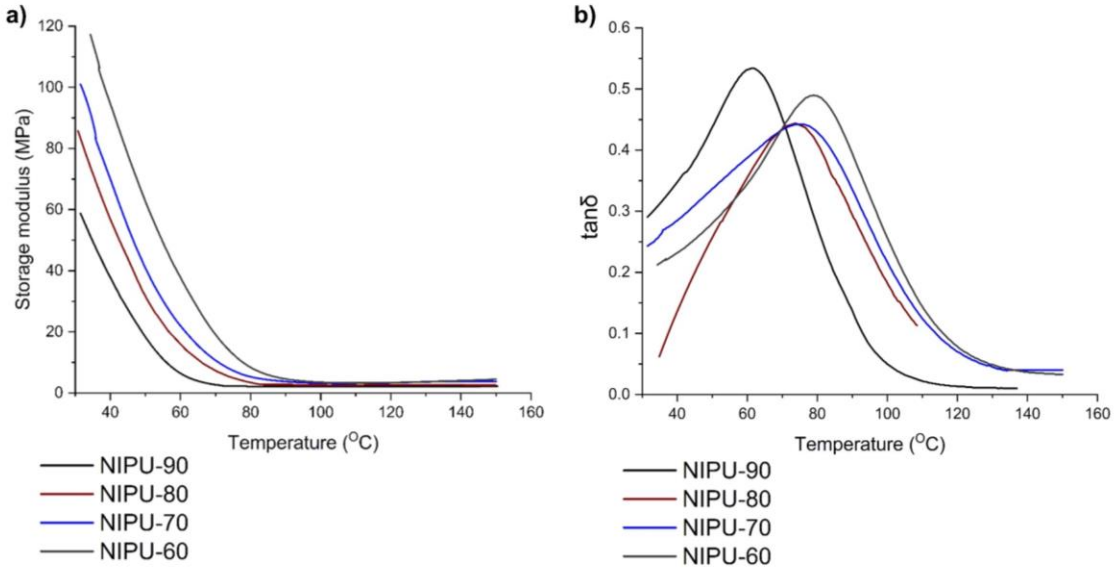

Figure 4.4. DMTA results of the crosslinked samples showing a) storage modulus versus temperature, b) tanδ as function of temperature.

Swelling test experiments were also conducted on the cured samples to evaluate the cross-linking density. **Table 4.3** shows the swelling ratio of the crosslinked samples in THF and water. Extracted swelling ratios (*SR*) in THF are consistent with the DMTA results. NIPU-90 swelled to a higher degree due to the presence of longer chains between crosslinks but NIPU-60 swelled less, signifying a tighter crosslink network [139]. Swelling ratios in water were also measured. Water uptake is an important factor for the application of NIPUs, since they contain hydroxyl functionalities, which increases with higher cyclic carbonate content. The reported swelling ratio values in water are close to the reported values for conventional polyurethanes [151]. Although NIPU-60 has the highest hydroxyl group content, it showed the lowest water uptake which is due to incorporation of the more hydrophobic DAD into its crosslinked network.

Gel content (*GC*) values are also reported in **Table 4.3**. All the reported *GC* values are above 85%, indicating that soluble material in THF was less than 15%. This implies relatively high cyclic carbonate conversion to urethane linkages. The lower *GC* value for NIPU-60 is due to higher viscosity of its carbonated copolymer parent, retarding the movement of the chains.

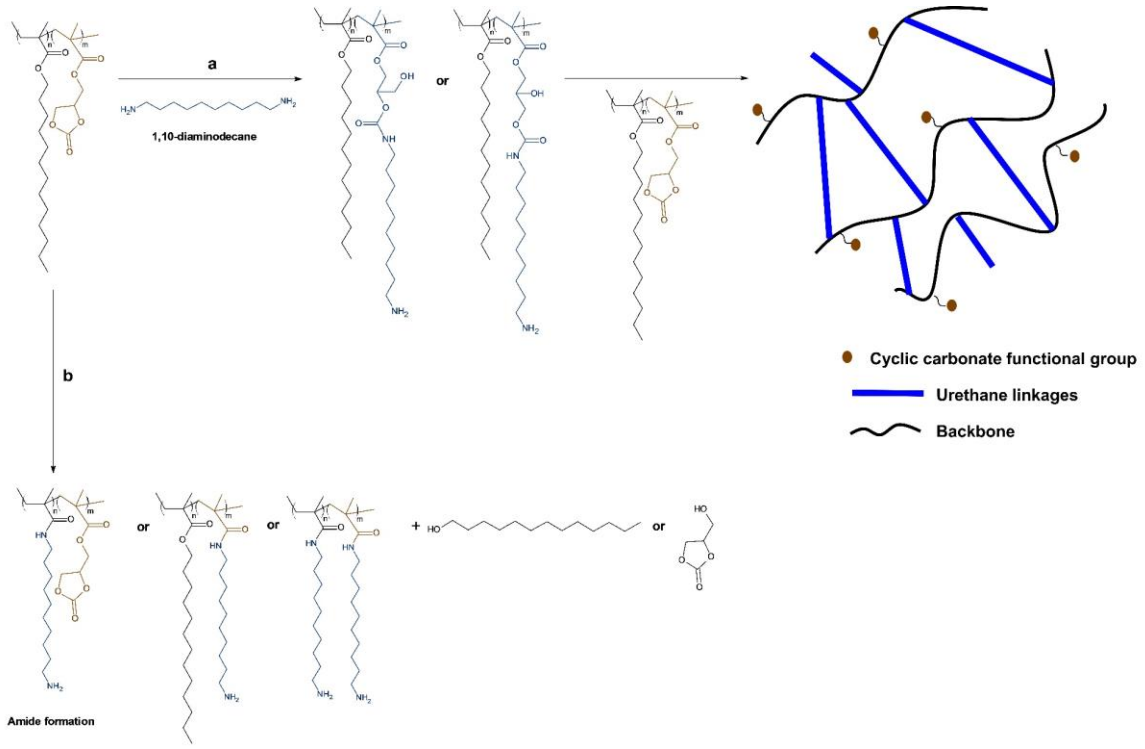

Scheme 4.1. Reaction of cyclic carbonate with DAD to form a) urethane and b) amide.

The mechanical properties of the four crosslinked networks were characterized using tensile tests. Engineering stress-strain curves are shown in **Figure 4.5**. The stress-strain data showed different behavior based on the crosslink density of the network. As expected, a positive correlation between Young′s moduli of the crosslinked networks and the number of urethane linkages on the backbone (i.e. density of the crosslinked networks) was observed.

The brittle behavior of samples with lower M_cs, is related to their relatively high cross-link densities. Polymer chain molecular mobility and chain disentanglements are limited with cross-links [8]. For example, NIPU-60 with the highest crosslink density showed elongation at break of 10%, whereas NIPU-90 with the lowest crosslink density had elongation at break of 105%. These results are consistent with expectations based on the differences in cross-link density. Young′s moduli and elongation at break for all samples are provided in **Table 4.3**.

NIPU-60 was the toughest crosslinked network (highest ultimate stress), which has the highest crosslink density and urethane linkage concentration, enhancing the toughness of the network. It is well-known that intermolecular hydrogen bonding between urethane groups improves the toughness of the NIPUs by converting mechanical energy to heat by breaking and forming of hydrogen bonds [191].

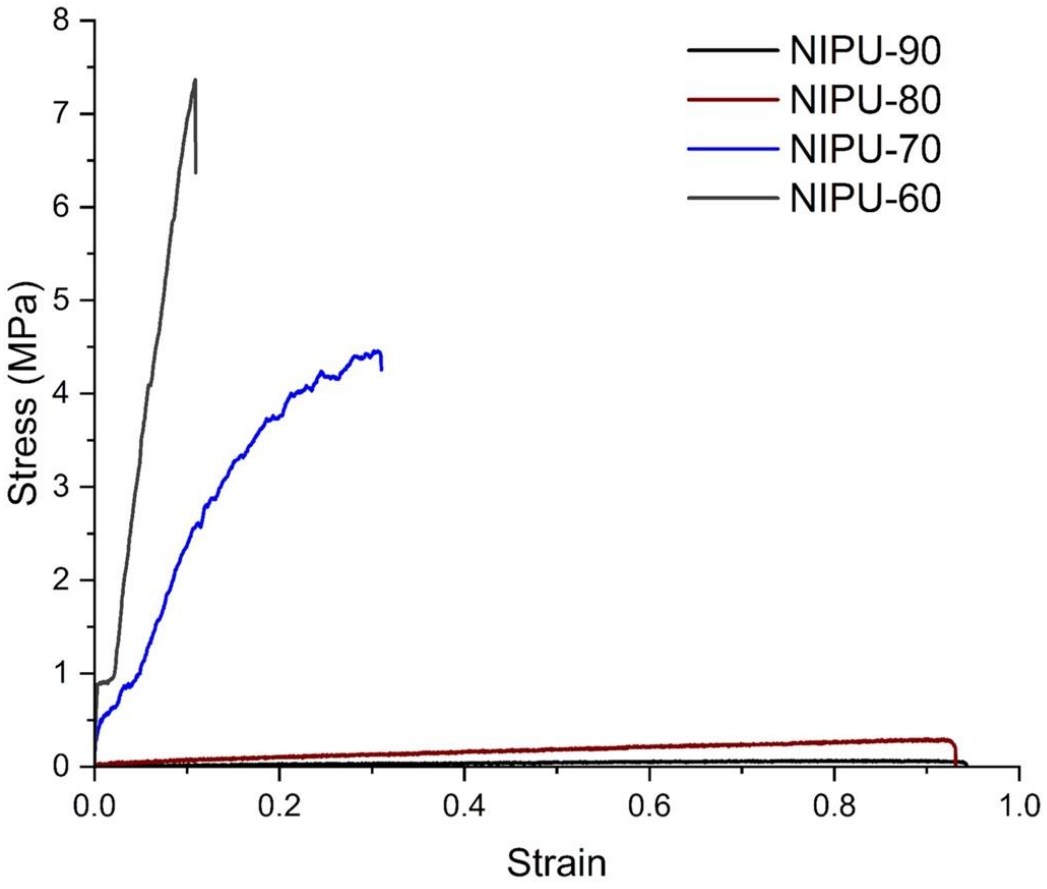

Figure 4.5. Engineering stress-strain results for crosslinked networks bonded through urethane linkages.

Finally, thermal stability of the four samples were characterized using TGA under nitrogen atmosphere. TGA curves are presented in **Figure B 12** and decomposition temperatures for different levels of weight loss are summarized in **Table 4.4**. As reported in **Table 4.4**, crosslinked networks showed slightly higher thermal stability compared to their parent carbonated copolymers. As an example, $T_{dec,10\%}$ for NIPU-60 is 7°C higher than carbonated C13MA/GMA-60.

Table 4.4. Decomposition temperatures for crosslinked networks.

Sample ID	$T_{dec,5\%}$ (°C)	$T_{dec,10\%}$ (°C)	$T_{dec,50\%}$ (°C)	$T_{dec,final}$ (°C)
NIPU-90	278	305	380	590
NIPU-80	260	295	394	595
NIPU-70	271	298	398	625
NIPU-60	237	282	400	620

4.4. Conclusion

Partially bio-based thermoset NIPU-like networks derived from poly(C13MA-*co*-GMA) precursors were studied. C13MA/GMA copolymers were synthesized via atom transfer radical polymerization (ATRP) at moderate temperatures at various compositions. Epoxy functional groups of the copolymers were converted to cyclic carbonate using CO_2 and TBAB as catalyst, with nearly 100% conversion achieved after 24 hours. Synthesized carbonated copolymers were reacted with 1,10-diaminodecane to provide crosslinked networks with varying urethane linkage concentrations and crosslink densities. Curing studies of the crosslinked networks (loosely termed NIPUs here) at 90°C for 24 hours showed that the NIPU with 2 urethane links in the side chains had a gel time of 254 minutes, while the one with 11 urethane links reached the gel point in just 0.84 minutes. Swelling ratio results supported these findings. Young´s moduli of the samples improved from 0.1 MPa to 71.9 MPa as the concentration of urethane linkages increased. Samples with higher urethane linkage concentrations exhibited more brittle behavior due to the limited polymer chain mobility which is the result of a denser crosslink network. Crosslink density also affected the glass transition temperature (T_g) of the synthesized NIPUs. The NIPU with the highest crosslink density had T_g of 79°C, whereas the NIPU with the lowest crosslink density showed T_g of 61°C. Overall, NIPU-60 which had the densest network, provided the toughest and highest strength NIPU from the series studied.

Since synthesized partially bio-based crosslinked NIPUs show varying mechanical properties by altering the number of epoxy functional groups on their parent C13MA/GMA copolymers, they can be engineered for a wide degree of applications, ranging from soft rubbery-like materials to tough coatings. This study investigated crosslinked networks bonded via urethane linkages with only two urethane linkages in the side chains. It is the initial step towards producing NIPUs with

longer poly(urethane) containing side chains. Currently, we are synthesizing bottle-brush polymers using a grafting-to approach with separately synthesized NIPU side chains, and the findings will be reported soon.

4.5. Experimental section

Materials: Basic and neutral alumina (Al_2O_3, Brockmann, Type II 150 mesh), calcium hydride (CaH_2, 90-95% reagent grade), ethyl α-bromoisobutyrate (EBiB, 98%), copper (I) bromide (Cu(I)Br, 99%), 4,4'-dinonyl-2,2'-dipyridyl (dNbpy, 97%), tetrabutylammonium bromide (TBAB), chloroform ($CHCl_3$, >99.8% contains ethanol as stabilizer), deuterated chloroform ($CDCl_3$, 99.8%) and anisole were purchased from Sigma-Aldrich and used without further purification. Methanol (MeOH, >99%), heptane, tetrahydrofuran (THF, 99.9% HPLC and certified grades) and 1,10-diaminodecane (DAD, 98%) were purchased from Fisher Scientific and used as received. Glycidyl methacrylate (GMA, 97%), C13 alkyl methacrylate (C13MA, *n*-alkyl average chain length of 13.0 units, >99%, Visiomer Terra C13-MA) were obtained from Sigma-Aldrich and Evonik (via TRC), respectively. The monomers were purified by passing through a column of basic alumina mixed with 5 wt % calcium hydride and then kept in a sealed flask under nitrogen atmosphere in a refrigerator. Syntheses were all carried out under nitrogen atmosphere with high purity (99.99%, Praxair). Carbon dioxide (CO_2) with a purity of 99.99% was also purchased from Praxair and used as received.

C13MA/GMA copolymerization by atom transfer radical polymerization (ATRP): All copolymerization reactions were done in a 250-ml three-necked round-bottom flask. C13MA, GMA, dNbpy and Cu(I)Br were dissolved in 20 vol.% of anisole and placed into the reactor equipped with a thermal well and a magnetic stir bar. The whole setup was placed on a heating mantle atop a magnetic stirrer. A condenser, which circulates a mixture of ethylene glycol/water

(the water is purified by reverse osmosis) (50:50 vol.%), was used to prevent evaporation of monomers and any solvent. Next, the mixture was purged with nitrogen to minimize oxygen contamination for 30 minutes prior to heating and the purge was vented via a needle through a rubber septum at the top of the reflux condenser. A thermocouple connected to a temperature controller was inserted into the thermal well and the reactor was heated to the desired polymerization temperature of 70°C. When the mixture reached 70°C, EBiB was added to the mixture. After five hours, the highly viscous polymer solution was observed and the polymerization was stopped and cooled down by exposure of the mixture to air and then diluted with chloroform and passed through a column of neutral alumina to remove the copper catalyst. After removing the catalyst, the polymer was precipitated in excess methanol or heptane to remove unreacted reagents from the final product (heptane was used as a precipitant for copolymers with higher concentrations of GMA). Proton nuclear magnetic resonance (^{1}H NMR) was used to confirm the removal of the monomers from the final product (methanol was added to the mixture until the supernatant layer was clear to reprecipitate the polymer). Finally, the copolymer was dried in a vacuum oven at 40°C overnight. All C13MA/GMA copolymers properties are tabulated in **Table 4.1**.

For every reaction, the initial molar ratio of monomers to initiator (EBiB) was calculated to give C13MA/GMA copolymers with target number-average molecular weight $M_{n,theoretical}$= $(f_{GMA,0}M_{GMA}+f_{C13MA,0}M_{C13MA})DP_n$= 5000 g mol^{-1} at complete overall monomer conversion (X =1), where $f_{C13MA,0}$ and $f_{GMA,0}$ are the initial molar fractions of C13MA and GMA, and DP_n is number average degree of polymerization, respectively. C13MA/GMA : 90/10 mol% is given as an example here (experiment C13MA/GMA-90, **Table 4.1**). C13MA (72.40 g, 0.27 mol), GMA (4.26 g, 0.03 mol), Cu(I)Br (0.11 g, 7.49×10^{-4} mol), dNbpy (0.61 g, 0.0015 mol) and anisole

(17.25 ml, 0.154 mol) were added into the reactor and then the setup was prepared as mentioned above. When the reactor reached 70°C, EBiB (2.93 g, 0.015 mol) was added to the reactor to start the polymerization (time = 0). Samples were taken every one hour until the end of the experiment. For each sample withdrawn, NMR and gel permeation chromatography (GPC) were used to determine composition and molecular weight distribution, respectively. The (overall) monomer conversions (X_{C13MA} and X_{GMA}) were determined by ^{1}H NMR. To find conversion of GMA, the nonequivalent protons corresponding of the methylene group of the oxirane ring (δ = 2.55-2.70 ppm and 2.75-2.90 ppm, 2H) was used to calculate the conversion of GMA in the polymer. By the evaluation of the signal corresponding to methylene protons in the C13MA segment (δ = 3.9-4.05 ppm, 2H), conversion of C13MA in the copolymer was calculated (**Figure 4.1**). The microstructure of the synthesized copolymers was also determined by integrating the same signals as mentioned above of the dried, purified copolymers.

Equation 4.2 was used to calculate the overall conversion of the synthesized copolymers, where X_{GMA}, X_{C13MA} and $X_{copolymer}$ are the individual conversions of GMA, C13MA and the overall copolymer conversion, respectively. All conversions for different sets of copolymers along with the determined average number molecular weight (M_n) and dispersity ($Đ$), using gel permeation chromotography (GPC) which is calibrated relative to narrow molecular weight distribution poly(methyl methacrylate) (PMMA) standards (M_n range of 875 to 1677000 g mol^{-1}, Varian Polymer) are tabulated in **Table 4.1**. For example, overall conversion of C13MA/GMA-90 at the end of the experiment was determined 90% ($X_{copolymer}$ = 0.9), where, individual conversions were 82% and 90% for GMA and C13MA, respectively. The final molar composition of GMA in C13MA/GMA-90 was calculated as F_{GMA}=0.093, for example.

$$X_{copolymer} = X_{C13MA} f_{C13MA,0} + X_{GMA} f_{GMA,0} \quad (4.2)$$

Carbonation of C13MA/GMA copolymers: To fix CO_2 onto the synthesized poly(C13MA-*co*-GMA), TBAB was used as catalyst (**Figure B 1**). Carbonation of C13MA/GMA-90 is given as an example. TBAB (0.21g, 6.51×10^{-4} mol, 5 mol% with respect to number of epoxy groups on copolymer chain) was added to a 150 ml three-neck round-bottom flask containing poly(C13MA-co-GMA) (51.37g, 0.0064 mol). The reactor was equipped with a thermal well and a magnetic stir bar and the whole set-up was placed on a heating mantle and was sealed with rubber septa. Next, the mixture was purged with CO_2 to remove oxygen for 30 minutes prior to heating. After 30 minutes of purging, the temperature was increased to 120°C and the mixture was stirred under a stream of CO_2 with pressure < 5 psi for 24 hours. After 24 hours, the reaction was stopped and cooled down by exposure of the mixture to air and the catalyst was removed by precipitating the final product in excess methanol (additional methanol was added until the supernatant layer was clear to reprecipitate the polymer) and the polymer was then dried in the vacuum oven at 40°C overnight. The overall conversion of the carbonation ($X_{carbonation}$) at the end of the reaction was > 95% according to ^{1}H NMR (**Figure B 8**). From **Figure B 8**, the epoxy peaks had disappeared after 24 hours.

Synthesis of urethane functional grafts from 1,10-diaminodecane: Addition of 1,10-diaminodecane (DAD) to carbonated C13MA/GMA-90 is given as an example. Carbonated C13MA/GMA-90 (2.34 g, 2.89×10^{-4} mol) and DAD (0.06 g, 2.99×10^{-4} mol) were added to a 50 ml three-necked round-bottom flask (diamine / cyclic carbonate: 1:1). The reactor was equipped with a thermal well and a magnetic stir bar and the whole setup was placed on a heating mantle on a magnetic stirrer. Next, the mixture was purged with nitrogen to de-oxygenate the contents.

After 30 minutes of purging, the temperature was increased to 90°C, which is higher than the melting point of DAD (70°C). After one hour, the mixture was removed from the reactor and put into tensile test bar molds and pressed to prepare tensile bars with dimensions that are mentioned in mechanical testing section. Once the bars were well-mixed and had homogonous texture, they were placed in an oven at 90°C for 24 hours to make sure that all cyclic carbonates reacted with amines. Appearance of urethane linkage was confirmed by FTIR (**Figure B 13**).

Proton Nuclear Magnetic Resonance (^1H NMR) Spectroscopy: Solution-phase NMR spectra were recorded on a Bruker Avance III HD (500 MHz, 32 scans) spectrometer at room temperature using $CDCl_3$ as solvent.

Fourier Transform Infrared (FTIR) Spectroscopy: A Nicolet iS50 FTIR Spectrometer equipped with a single bounce diamond attenuated transmission reflectance (ATR) for solids was used to identify functional groups involved in reactions. Thirty-two scans were recorded for each sample over the range 4000-500 cm^{-1} with a normal resolution of 4 cm^{-1}.

Size Exclusion Chromatography (SEC): Gel permeation chromatography (GPC, Water Breeze, differential refractive index RI 2414 detector, 40°C) using HPLC grade THF as the mobile phase (flow rate 0.3 mL min^{-1}) was used to determine the number-average molecular weights (M_n) and dispersities ($Đ = M_w/M_n$). M_n values were calculated relative to narrow molecular weight distribution PMMA standards [1].

Differential Scanning Calorimetry (DSC): A TA Instrument Discovery 2500 differential scanning calorimeter using standard hermetic aluminum pans (pan top with a pinhole), calibrated with indium and nitrogen purge was used to measure the glass transition temperature (T_g) and melting point (T_m) of the synthesized copolymers. A heat-cool-heat cycle was conducted with heating rate of 5°C min^{-1} and cooling rate of 10°C min^{-1}. The temperature was increased to

160°C in heating cycles and cooled down to -90°C in cooling cycles. All data was extracted from the second heating cycle. Universal Analysis and Trios software were used to analyze the results.

Thermogravimetric Analysis (TGA): A TA Instruments Discovery 5500 thermo-gravimetric analyzer was used to analyze the degradation of synthesized materials at a heating rate of 10 °C min^{-1} from ambient temperature to 700°C under nitrogen purge in platinum pans. The 5% degradation temperature ($T_{d,5\%}$) and 10% degradation temperature ($T_{d,10\%}$) were extracted from this test.

Rheology: Viscosity and curing tests were conducted on synthesized copolymers and crosslinked networks using an Anton Paar Instruments Rheometer (MCR 302) with parallel plates of 25 mm diameter (PP 25) configuration with gap of 1 mm at 30°C. Dynamic mechanical thermal analysis (DMTA) was conducted on crosslinked networks using torsion configuration (SRF 12) with a temperature ramp rate of 5 °C min^{-1} (from ambient temperature to 120°C), with an oscillation strain of 1% and a frequency of 1 Hz. Molecular weight between crosslinks (M_c) were calculated at room temperature using **Equation 4.3** [142]:

$$M_c = \frac{3RT\rho}{E_r'} \tag{4.3}$$

where E_r' is the storage modulus in the rubbery region from the DMTA experiments, R is the gas constant, T is the absolute temperature, and ρ is the density of the crosslinked samples. All DMTA tests were conducted under a nitrogen atmosphere using a CTD 450 convection oven. It should be mentioned that E' values used in the equation were taken at a temperature 30°C above the T_g as determined from the peak maximum of the tanδ curve.

Mechanical testing: Tensile properties were measured at ambient temperature using an EZ Test (Shimadzu) tensile machine at speeds of 5 mm min^{-1} on the crosslinked urethane functional networks. Young′s modulus (*E*), tensile strength (σ_{max}), and elongation at break (*EB*%) were determined by the average of at least three repeated samples. Three dog-bone shaped samples were cut out to perform tensile testing using ASTM standards (ASTM D638, type V).

Swelling ratio (SR): Three samples of around 30 mg each were separately put in THF and purified water for 24 hours. The swelling ratio (*SR*) was calculated using **Equation 4.4**:

$$\mathrm{SR} = \frac{m_2 - m_1}{m_1} \tag{4.4}$$

where m_1 and m_2 are the initial mass of the material and mass of the material after swelling in THF or water, respectively.

Gel content: After *SR* measurements, the three samples were dried in a vacuum oven at room temperature for 24 hours. The gel content (*GC*) was calculated using the **Equation 4.5**, where m_3 and m_2 are the mass of the material after drying in the oven and the initial mass of the material, respectively.

$$\mathrm{GC\%} = \frac{m_3}{m_2} \times 100 \tag{4.5}$$

Hot press: The pressing was performed with a Carver hydraulic unit model #3925 at 90 °C for the synthesized crosslinked urethane functional networks using three cycles of 5,10 and 15 metric tons for five minutes for each cycle.

Oven: To cure the crosslinked networks at 90°C for 24 hours, a Fisherbrand Isotemp model 281A oven was used.

5. CHAPTER 5

EFFECT OF ALKYL METHACRYLATE/GLYCIDYL METHACRYLATE COPOLYMER BACKBONE STRUCTURE ON MECHANICAL PROPERTIES OF HYDROXYURETHANE-CROSSLINKED NETWORKS

After thoroughly investigating the influence of side chain rigidity on the mechanical properties of the crosslinked networks, the focus of the thesis shifted towards examining the impact of backbone rigidity on both mechanical and rheological properties. This was achieved by synthesizing binary copolymers of methyl methacrylate (MMA), ethyl methacrylate (EMA), and butyl methacrylate (BMA) with glycidyl methacrylate (GMA) providing the epoxy groups that will be carbonated, yielding a methacrylic backbone with multi-functional carbonate macromonomer. It is important to note that the rigidity of the backbone decreases progressively from MMA to BMA, resulting in a range of copolymers with varying levels of flexibility. Additionally, the study delved into characterizing the microstructure of the synthesized copolymers. To this end, the reactivity ratios of EMA/GMA and BMA/GMA were calculated, providing insights into the random nature of the copolymer microstructure. The manuscript of this chapter was published in *Reactive and Functional Polymers* in 2023 (Farkhondehnia, M. and Marić, M., Effect of alkyl methacrylate/glycidyl methacrylate copolymer backbone structure on mechanical properties of hydroxyurethane-crosslinked networks. Reactive and Functional Polymers, 2023, 191, 105683) [192]. The supporting information of this publication is given in Appendix C.

5.1. Abstract

The effect of cyclic carbonate functionalized polymer backbones on mechanical and rheological properties of hybrid thermoset resins with hydroxyurethane linkages via vegetable-oil derived diamine were investigated. Atom transfer radical polymerization (ATRP) of binary methyl, ethyl, butyl methacrylate (MMA, EMA, BMA) mixtures with glycidyl methacrylate (GMA) with various GMA initial molar fractions (f_{GMA} = 0.1-0.9) were performed at 70 °C to create precursor backbones with modulated glass transition temperature (Tg). The copolymer compositions were essentially statistical as demonstrated by estimated reactivity ratios. MMA/GMA reactivity ratios were r_{MMA} = 0.80 ± 0.09 and r_{GMA} = 1.35 ± 0.09, which agreed with earlier studies while previously unreported EMA/GMA reactivity ratios were r_{GMA} = 1.10 ± 0.09 and r_{EMA} = 0.31 ± 0.09 and BMA/GMA reactivity ratios were r_{BMA} = 0.67 ± 0.09 and r_{GMA} = 1.45 ± 0.09. The synthesized copolymers were then carbonated, converting the pendent epoxy functional groups to cyclic carbonates. The carbonated copolymers were reacted with the vegetable oil-derived diamine Priamine 1074 to form relatively rigid side chains via hydroxyurethane linkages to the backbone. Degree of flexibility of backbones and cyclic carbonate functionality were manipulated to synthesize crosslinked networks with Young's moduli ranging from 395 MPa to 1 250 MPa.

5.2. Introduction

Polyurethanes (PUs), which have a global market size of $72.82 billion USD in 2021 [97], are a diverse class of polymers used in foams, coatings, adhesives, sealants and elastomers [193,194]. Among these applications, more than 70 wt% of PUs are used as thermosetting materials [5,36]. Despite the fact that PU use dates back almost a century, their synthesis remains largely unchanged, with the majority of commercially available PUs still being prepared through the polyaddition reaction of di- or multi-functional isocyanates with di- or multi-functional alcohols [16,147]. However, toxicity issues associated with the production and use of isocyanates have become a significant drawback in synthesis of traditional PUs [10,100]. To address this problem in todays's more eco-conscious landscape, researchers have investigated more environmentally benign approaches for PU synthesis, like non-isocyanate polyurethanes (NIPUs).

While several routes have been suggested to prepare NIPUs [9,149], the most promising method is the polyaddition of cyclic carbonates with amines yielding poly(hydroxy urethane)s, PHUs [94,104,108]. Typical PHU thermosets are prepared via reaction of multi-functional cyclic carbonates and amines (similar to reaction of multi-functional isocyanates and diols in traditional PUs), leading to formation of pendent hydroxyl groups adjacent to the urethane linkages [21,195]. The presence of the secondary hydroxyl groups can enhance both the mechanical properties and reprocessability of PHU thermosets by facilitating associative transcarbomylation [20,138].

Five-, six- and seven- membered cyclic carbonates are most commonly used to produce PHUs [8,86,107]. Studies revealed that due to ring strain, addition reaction rate increased with increasing cyclic carbonate ring size [107]. Despite the fact that six- and seven-membered cyclic carbonates exhibit better reactivity, hazardous reagents such as ethyl chloroformate and triphosgene are used to synthesize them [8,22]. In contrast, five- membered cyclic carbonates can be formed via reaction

of carbon dioxide (CO_2) with an epoxide [22,23] and is often considered advantageous as it enables the fixation of CO_2, reducing greenhouse gas effects [49], while also being cost-effective due to the relative abundance of CO_2 [196].

Several factors can influence the ultimate thermomechanical and mechanical properties of PHU thermosets, including the nature of the building blocks, the selection of cyclic (poly)carbonates and diamines, and the cyclic carbonate-to-amine ratio [8,20,36]. Aromatic building blocks impart the necessary rigidity to networks for high-performance applications, whereas aliphatic building blocks typically offer resistance against weather and ultraviolet light [20,138,193]. For example, Janvier et. al. [20] investigated thermoset PHUs using carbonated syringaresinol, which contains aromatic building blocks and two cyclic carbonate functional groups in its structure, and a triamine which led to a thermoset with high T_g of 62 °C and high thermal stability ($T_{d,5\%}$ = 225 °C). However, since the samples were excessively brittle, mechanical testing was not performed. Samanta et. al. [8] also studied the curing of carbonated soybean oil with a variety of diamines with amine-to-cyclic carbonate ratio of 1:1 to produce crosslinked PHUs with tensile strengths varying from 3.6 MPa to 17 MPa. Javni et. al. [35] investigated the effect of amine-to-carbonate ratio on the polyaddition of carbonated soybean oil with various diamines. This study led to preparation of thermosets with Young's moduli of 0.49 MPa to 5.77 MPa. Bähr et al. [104] studied the effect of blends of carbonated linseed and soybean oils at different ratios reacted with several diamines, with a focus on mechanical properties of the resulting thermosets. Their study led to crosslinked PHUs spanning a wide range of Young's moduli from 2 MPa to 1 460 MPa. However, most of the abovementioned examples are vegetable oils in which the number of cyclic carbonates are fixed, and the only critical factors to manipulate the mechanical properties of the thermoset PHUs are diamine structure or amine-to-carbonate ratio.

Recently, a promising approach to enhance the mechanical properties of PHUs has been the design of hybrid formulations (i.e. hybrid poly(hydroxyurethanes) (HPHUs)) [69]. The term "hybrid" can be interpreted in several ways, such as a reaction with an inorganic material or the use of a different polymerization method to incorporate desired functionality (e.g combination of radical polymerization and polyaddition) [1,69]. We are effectively using the latter definition in the study presented here.

We recently reported partially bio-based resins with flexible side chains that are bonded to a flexible backbone via urethane linkages [1]. Additionally, we have created partially bio-based "bottle brush-like" networks that are crosslinked through urethane linkages, with rigid side chains and flexible backbones [144]. However, in many applications, much stiffer yet still somewhat flexible polymers are required, and the work presented here aimed to investigate more deeply the impact of backbone flexibility on the rheological and mechanical properties of networks crosslinked via urethane linkages.

Specifically, we utilized different polymerization methods to prepare our crosslinked networks, in order to better control the compositional uniformity of the template used to make the hybrid materials. Atom transfer radical polymerization (ATRP) was used to copolymerize methyl, ethyl, butyl methacrylate (MMA, EMA, BMA) with glycidyl methacrylate (GMA), resulting in backbones with different degrees of flexibility and varying pendent epoxy functional groups. GMA provides grafting sites, and controlling the content of GMA in the copolymer allows for manipulation of the density of the grafting sites. After preparation of the epoxy-functional copolymers, CO_2 was used to convert the epoxides to cyclic carbonates [8,193]. Then the carbonated copolymers were reacted with a bio-based diamine (Priamine 1074) [197] to form urethane linkages used to crosslink the networks. The final networks are interesting for two reasons. Firstly,

networks with longer alkyl side chains exhibited higher hydrophobicity due to the restricted access of water molecules to the crosslinked urethane network caused by the side chains [198,199]. Secondly, by using Priamine 1074 to form urethane linkages, the resulting networks exhibit relatively rigid side chains that are attached to backbones with varying levels of flexibility. By employing this paradigm, we demonstrate a broad spectrum of mechanical properties can be achieved through the HPU networks, derived from the density of cyclic carbonate sites and the types of monomers used in the prepolymer.

5.3. Experimental section

5.3.1. Materials

Basic and neutral alumina (Al_2O_3, Brockmann, Type II 150 mesh), calcium hydride (CaH_2, 90-95% reagent grade), ethyl α-bromoisobutyrate (EBiB, 98%), copper (I) bromide (Cu(I)Br, 99%), 4,4'- Dinonyl- 2,2'-dipyridyl (dNbpy, 97%), tetrabutylammonium bromide (TBAB), chloroform ($CHCl_3$, >99.8% contains ethanol as stabilizer), deuterated chloroform ($CDCl_3$, 99.8%) and anisole were purchased from Sigma-Aldrich and used without further purification. Priamine 1074 was provided by Cargill and used as received. Methanol (MeOH, >99%), heptane and tetrahydrofuran (THF, 99.9% HPLC and certified grades), ethyl methacrylate (EMA, 99%), butyl methacrylate (BMA, 99%) and *N,N*-Dimethylformamide (DMF) were purchased from Fisher Scientific and was used as received. Glycidyl methacrylate (GMA, 97%) and methyl methacrylate (MMA, 99%) were obtained from Sigma-Aldrich. The monomers were purified by passing through a column of basic alumina mixed with 5 wt % calcium hydride and then kept in a sealed flask under nitrogen atmosphere in a refrigerator. Syntheses were all carried out under a high purity nitrogen atmosphere (99.99%, Praxair). Carbon dioxide (CO_2) with a purity of 99.99% was purchased from Praxair and used as received.

5.3.2. Methods

Monomer conversions (X), carbonation conversion ($X_{carbonation}$) and polymer compositions were characterized by solution-phase proton NMR (^{1}H NMR). ^{1}H NMR spectra were recorded on a Bruker Avance III HD (500 MHz, 32 scans) spectrometer at room temperature using $CDCl_3$ as solvent. Approximately 3 mg of the copolymer was dissolved in 1 ml of $CDCl_3$ and then was transferred into an NMR tube. The analysis was conducted using a zg30 pulse sequence. The resulting spectra were analyzed using Mestrelab MNova software.

Fourier transform infrared (FTIR) was performed on all the synthesized polymers including copolymers, carbonated copolymers and the synthesized crosslinked networks containing urethane linkages. A Nicolet iS50 FTIR Spectrometer equipped with a single bounce diamond attenuated transmission reflectance (ATR) for solids. First, a background reading was performed on a clean diamond to acquire an accurate baseline. Thirty-two scans were recorded for each sample over the range 4000-500 cm^{-1} with a normal resolution of 4 cm^{-1}.

Gel permeation chromatography (GPC, Water Breeze, differential refractive index RI 2414 detector, 40°C) using HPLC grade THF as an eluent with flow rate 0.3 mL min^{-1} was used to determine the number-average molecular weights (M_n) and dispersities ($Đ = M_w/M_n$). The instrument is equipped with three Waters Styragel HR columns: HR1 for molecular weights ranging from 10^2 to 5×10^3 g mol^{-1}, HR2 for molecular weights ranging from 5×10^2 to 2×10^4 g mol^{-1}, and HR4 for molecular weights ranging from 5×10^3 to 6×10^5 g mol^{-1}. It also includes a (RI 2414) refractive index detector and a guard column [200]. The columns were maintained at a temperature of 40 °C while passing an injection of 10 µl of dissolved samples through. The elution time for the samples was 60 min. M_n values were calculated relative to

narrow molecular weight distribution poly(methyl methacrylate) (PMMA) standards (Varian Polymer Standards, molecular weights ranging from 875 to 1677000 g mol^{-1}).

Glass transition temperatures (T_g)s of the synthesized copolymers were measured by Differential Scanning Calorimetry (DSC). A TA Instrument Discovery 2500 differential scanning calorimeter using standard hermetic aluminum pans (pan top with a pinhole), calibrated with indium and nitrogen purge was used. A heat-cool-heat experiment was conducted with heating rate of 5°C min^{-1} and cooling rate of 10°C min^{-1}. The temperature was increased to 160°C in the heating cycles and then reduced to -90°C in cooling cycles. All data was extracted from the second heating cycle after thermal history was removed during the first heating cycle. T_gs were calculated by the inflection method [201]. Universal Analysis and Trios software were used to analyze the results.

Thermal stability of the synthesized polymers was investigated by thermogravimetric analysis (TGA) test. A TA Instruments Discovery 5500 thermo-gravimetric analyzer was used to analyze the degradation of synthesized materials at a heating rate of 10°C min^{-1} from ambient temperature to 700 °C under nitrogen purge in platinum pans. To begin the process, a small platinum pan was cleaned with a blow torch to eliminate any residue from prior samples. The pan is then weighed and tared. After that, 3-10 mg of the sample was added into the pan. Finally, the sample was placed into the furnace chamber and heated under a nitrogen atmosphere. The 5% degradation temperature ($T_{d,5\%}$), 10% degradation temperature ($T_{d,10\%}$), 50% degradation temperature ($T_{d,50\%}$), final decomposition temperature ($T_{d,final}$) and ash content were extracted from this test. Universal Analysis and Trios software were used to analyze the results.

Dynamic mechanical thermal analysis (DMTA) was also conducted on the networks using torsion configuration (SRF 12) with a temperature ramp rate of 5°C min^{-1} (from ambient

temperature to 120 °C under nitrogen atmosphere using a CTD 450 convection oven with air flow of 1 400 NL h^{-1} for the cooling shaft and 850 NL h^{-1} for nitrogen purge to the furnace, It is important to note that the testing of BMA-based crosslinked networks was limited to temperatures up to 90 °C. This was attributed to the inherent softness of the samples, which resulted in their breakage at higher temperatures), with an oscillation strain of 1% and a frequency of 1 Hz on an Anton Paar instruments rheometer.

An EZ Test (Shimadzu) tensile machine equipped with a 500 N load cell was used for tensile tests on the crosslinked networks. Tensile properties of the crosslinked networks were measured at ambient temperature at speeds of 10 mm min^{-1}. Young's modulus (E), tensile strength (σ_{max}), and elongation at break (EB%) were calculated by the average of at least three repeated samples. Three dog-bone shaped bars for each sample with standard dimensions were cut out to perform tensile testing (ASTM 638, type V). For tensile and DMTA tests, crosslinked urethane functional networks were molded into tensile bars and rectangular bars using a Carver hydraulic unit model #3925 at 90 °C. The process included three cycles of applying 5, 10, and 15 metric tons of force for ten minutes for each cycle. Then, the networks were left to fully cure in a Fisherbrand Isotemp model 281A oven at 90 °C for 24 hours.

5.3.3. Copolymerizations of MMA/GMA, EMA/GMA and BMA/GMA by atom transfer radical polymerization (ATRP)

Atom transfer radical polymerization (ATRP) was used to synthesize all sets of copolymers. Monomers, dNbpy and Cu(I)Br were dissolved in anisole at a volume ratio of 20% relative to the total volume of monomers and placed into a 250-ml three-necked round-bottom flask, equipped with a thermal well and a magnetic stir bar (a smaller reactor (50 ml) was used for the experiments which were done to calculate reactivity ratios). The setup was placed on a heating

mantle with a magnetic stirrer for mixing the solution. To prevent evaporation of the monomers and solvent, a condenser, which circulates a mixture of ethylene glycol/ water (purified by reverse osmosis) (50:50 vol.%), was connected to the setup. Next, the mixture was purged with nitrogen for 30 minutes to remove dissolved oxygen and a needle at the top of the reflux condenser was used to vent the nitrogen purge. A thermocouple connected to a temperature controller was inserted into the thermal well and the reaction temperature was set to 70 °C. When the mixture reached 70 °C, EBiB was added to the mixture. After four hours (or less than four hours for the copolymers with higher GMA content), the polymerization was stopped due to the high viscosity of the reaction mixture and cooled down and then diluted with chloroform and passed through a column of neutral alumina to remove the copper catalyst. The color of the mixture transitioned from green to transparent as it passed through the column, indicating the successful removal of the copper catalyst. After removing the copper catalyst, chloroform was removed via rotary evaporation and then excess amount of methanol or heptane (heptane was used for copolymers with higher GMA content) was added to the copolymers to remove unreacted monomers from the mixture and precipitate the polymer. The purification of the copolymers was confirmed by proton nuclear magnetic resonance (1H NMR) (methanol/heptane was added to the mixture until the supernatant layer was clear to reprecipitate the polymer). Finally, the copolymer was dried in a vacuum oven at 40 °C overnight. For every reaction, the initial molar ratio of monomers to initiator (EBiB) was fixed to give a copolymer with target number-average molecular weight (M_n) of 5000 g mol^{-1} at complete overall monomer conversion (X =1) (e.g. $M_{n,theoretical} = (f_{GMA,0}M_{GMA} + f_{MMA,0}\,M_{MMA})DP_n$= 5 000 g mol^{-1}, where $f_{MMA,0}$ and $f_{GMA,0}$ are the initial molar fractions of MMA and GMA, DP_n is number average degree of polymerization, M_{MMA} is molecular weight of MMA and M_{GMA} is molecular weight of GMA).

Copolymerization of MMA and GMA with initial molar ratio of GMA as 10% (MMA/GMA: 90/10%) is given as an example (experiment MMA/GMA-90, where 90 refers to the initial molar ratio of MMA in the feed). MMA (43.1 g, 0.430 mol), GMA (6.85 g, 0.048 mol), Cu(I)Br (0.17 g, 1.2×10^{-3} mol), dNbpy (0.98 g, 2.4×10^{-3} mol) and anisole (10 ml) were added into the reactor and then the setup was prepared as previously mentioned. When the reaction mixture was at 70°C, EBiB (1.95 g, 0.01 mol) was added to the mixture to start the polymerization (time = 0). Samples were taken frequently until the end of the experiment for kinetic study purposes. For each sample withdrawn, copolymer composition, (overall) monomer conversions (X_{MMA} and X_{GMA}) and dispersity ($Đ$) were characterized using NMR and gel permeation chromatography (GPC) (relative to narrow molecular weight distribution PMMA standards (Varian Polymer Standards, molecular weights ranging from 875 to 1 677000 g mol^{-1})). To find conversion of poly(glycidyl methacrylate) (PGMA), the nonequivalent protons corresponding to the methylene group of the ring (δ = 2.55-2.70 ppm and 2.75-2.90 ppm, 2H) were used. Conversion of PMMA was determined by integration of signal corresponding to OCH_3 (δ = 3.55-3.68 ppm, 3H). ^{1}H NMR spectra for poly(MMA-*stat*-GMA) is shown in **Figure C 1**.

^{1}H NMR spectra of poly(EMA-*stat*-GMA) and poly(BMA-*stat*-GMA) are also shown in **Figure C 2**and **Figure C 3**, respectively. The microstructure of the synthesized copolymers was also determined by integrating the same signals (except the ones corresponding to unreacted monomer as they were not present after purification) as mentioned above for the dried copolymers.

It should be noted that EMA/GMA copolymers with $M_{n,target}$ of 10000 g mol^{-1} were used for reactivity ratio calculation. However, EMA/GMA copolymers used for the subsequent carbonation reaction had $M_{n,target}$ of 5000 g mol^{-1}.

5.3.4. Carbonation of the copolymers

After synthesis of the copolymers, the ones with initial GMA molar ratios of 0.1, 0.2 and 0.3 were treated with carbon dioxide (CO_2) and TBAB as catalyst to convert epoxy functional groups to cyclic carbonates. The carbonation reactions of the copolymers were performed in a solvent at high temperatures due to the powdery form of the copolymers and the absence of observed melting points in their DSC analysis. Dimethylformamide (DMF) was chosen as the solvent for the carbonation reaction due to its high boiling point, which allowed the reaction to be done at higher temperatures and increased the carbonation rate. Carbonation of BMA/GMA-80 is given as an example. TBAB (0.45 g, 0.0014 mol, 5 mol% with respect to number of epoxy groups on copolymer chain), poly(BMA-*stat*-GMA) (20 g, 0.0035 mol) and DMF (20 g, 0.27 mol) were added to a 150 ml three-neck round-bottom flask. The reactor was equipped with a thermal well, magnetic stir bar and a reflux condenser, circulating a mixure of ethylene glycol/ reverse osmosis water (50/50 vol.%) to prevent evaporation of the solvent. The whole setup was placed in a heating mantle and rubber septa were used to seal the reactor. Next, the mixture was stirred for 15 minutes to dissolve the copolymer in the solvent. After dissolving the copolymer, the mixture was purged with CO_2 for 30 minutes to remove any oxygen contamination. Then, the temperature was increased to 120°C and the mixture was stirred under a stream of CO_2 with pressure of no more than 5 psi for 24 hours. After 24 hours, the reaction was stopped and cooled down by exposure of the mixture to air and the polymer was washed by methanol to remove the catalyst (additional methanol was added until the supernatant layer was clear to reprecipitate the polymer) and the polymer was then dried in the vacuum oven at 40°C overnight. The overall conversion of the carbonation ($X_{carbonation}$) was calculated via ^{1}H NMR at the end of the reaction. The carbonation conversion for carbonated BMA/GMA-80 was almost 94% after 24 hours.

5.3.5. Synthesis of urethane functional grafts using Priamine 1074

Since the carbonated copolymers were solids and Priamine 1074 is a liquid, ethyl acetate was used as a common solvent for the reaction. Addition of Priamine 1074 to carbonated BMA/GMA-80 is given as an example. Carbonated BMA/GMA-80 (4.12 g, 5.57×10^{-4} mol), which has eight cyclic carbonate functional groups on its backbone, Priamine 1074 (1.2 g, 2.2×10^{-3} mol) and ethyl acetate (6 g, 0.0681 mol) were added to a 50 ml three-necked round-bottom flask (diamine / cyclic carbonate: 1:1, number of cyclic carbonates: 8 per chain). The reactor was equipped with a thermal well, a magnetic stir bar and a condenser and the entire assembly was mounted on a heating mantle with a magnetic stirrer. Next, oxygen was removed from the mixture by purging the contents with nitrogen for 15 minutes at room temperature. After the initial purging, the temperature was increased to 65°C, which is below the boiling point of ethyl acetate (~77°C), while maintaining the purge. After two hours, the mixture was removed from the reactor and dried under air flow for one hour. Next, the mixture was put in a vacuum oven at room temperature for two hours to remove residual ethyl acetate. The dried mixture was put into tensile molds and pressed to prepare tensile bars according to ASTM standards (ASTM D638, type V). To ensure complete reaction of the cyclic carbonates with the diamine, the bars were then placed in an oven at a temperature of 90°C for 24 hours. FTIR was used to confirm the disappearance of cyclic carbonates and appearance of urethane linkages.

5.3.6. Theory

In order to calculate the overall conversion of the copolymers **Equation 5.1** was used (the example is given for MMA/GMA copolymer). In **Equation 5.1**, X_{MMA}, X_{GMA}, f_{MMA}, f_{GMA} and $X_{copolymer}$ are the conversions of MMA, GMA, initial molar ratio of MMA in the feed, initial molar ratio of GMA in the feed and the overall copolymer conversion, respectively.

$$X_{copolymer} = X_{MMA} f_{MMA,0} + X_{GMA} f_{GMA,0} \quad (5.1)$$

Rubber elasticity theory [142] (**Equation 5.2**) was used to calculate molecular weight between crosslinks (M_c) for the crosslinked networks at room temperature:

$$M_c = \frac{3RT\rho}{E_r'} \quad (5.2)$$

In **Equation 5.2** E_r' is the storage modulus in the rubbery region from the DMTA experiments, R is the gas constant, T is the absolute temperature, and ρ is the density of the crosslinked samples. Swelling ratio (SR) of the crosslinked samples was also measured by soaking samples in 2 different media: THF and water for 24 hours. To determine the SR, three samples weighing approximately 30 mg each were individually placed into a glass jar filled with purified water or THF and allowed to soak for 24 hours. SR values were calculated using **Equation 5.3**:

$$SR = \frac{m_f - m_i}{m_i} \quad (5.3)$$

In **Equation 5.3**, m_i and m_f are the initial mass of the material and mass of the material after swelling in THF or water, respectively.

After SR measurements, the samples were placed back into the glass vials. The vials then were placed into a vacuum oven at room temperature for 24 hours. Gel content (GC) values were found using the **Equation 5.4**, where m_d and m_i are the mass of the material after drying in the oven and the initial mass of the material, respectively.

$$GC\% = \frac{m_d}{m_i} \times 100 \quad (5.4)$$

5.4. Results and discussion

5.4.1. Synthesis of MMA/GMA, EMA/GMA and BMA/GMA copolymers using atom transfer radical polymerization (ATRP) and determination of EMA/GMA and BMA/GMA reactivity ratios

Atom transfer radical polymerization (ATRP) was used to synthesize copolymers of MMA/GMA, EMA/GMA and BMA/GMA at various comonomer ratios. We originally aimed to use conventional radical polymerization but the heat generated was problematic under the conditions we used initially (e.g. copolymerization of MMA with GMA with 50 wt% dioxane, we also wished to use minimal solvent). Most radical polymerizations are exothermic with the heat of reaction about 100–200 kJ mol^{-1} and apparent activation energies of about 10–30 kJ mol^{-1} [202] which can lead to autoacceleration effects [159]. Thus, ATRP was employed due to its generally lower active radical concentration in addition to its efficacy in synthesizing polymers with precise composition and narrow molecular weight distributions [203]. We thus synthesized a series of statistical copolymers to serve as precursors for carbonated copolymers.

Statistical copolymers of MMA/GMA, EMA/GMA and BMA/GMA at different comonomer ratios were prepared using ATRP at 70°C. Kinetic studies were done on the copolymers and reactivity ratios of EMA/GMA (r_{EMA} and r_{GMA}) and BMA/GMA (r_{BMA} and r_{GMA}) were calculated as they were not readily available from literature. Some of the synthesized copolymers, which were used as a template with different epoxy distribution in their backbone, were carbonated and subsequently reacted with a diamine to produce crosslinked networks bonded through urethane linkages [94].

All copolymer characterization data for poly(EMA-*stat*-GMA)s, poly(BMA-*stat*-GMA)s and poly(MMA-*stat*-GMA)s are listed in

Table 5.1, **Table 5.2** and **Table 5.3**, respectively. Lower degrees of polymerization were targeted to ease subsequent processing. In all cases, distributions were monomodal and possessed generally narrow molecular weight distributions (MMA/GMA copolymerizations had M_n = 5400-6800 g mol^{-1} and $Đ$ = 1.20-1.25, while the EMA/GMA copolymers had M_n = 7800-9800 g mol^{-1} and $Đ$ =1.28-1.51 and BMA/GMA had M_n = 4400-8700 g mol^{-1} and $Đ$ = 1.21-1.68 (relative to PMMA standards [1]). All kinetic results for the copolymerizations are displayed in **Figure C 4** and **Figure C 5**. **Figure C 4a** and **Figure C 5a** indicate first-order kinetics since the semi-logarithmic plot of conversion versus time is linear. **Figure C 4b** and **Figure C 5b** present M_n versus X for all synthesized copolymers. A similar linear growth of M_n versus X was also observed, but M_n deviated from the predicted values expected if the polymerization was truly living at higher conversions. Three reasons are proposed for the observed deviations: 1) using

PMMA standards to measure M_n values by GPC, 2) poor control during the early stages of polymerization, prior to establishing a sufficiently high concentration of copper to achieve equilibrium between dormant and active chains and 3) the sample preparation step for GPC to remove the copper/ligand complex may result in some fractionation. Copolymerizations with higher f_{GMA} were less controlled, as deemed by the generally broader molecular weight distributions (higher $Đ$) and M_ns as shown in **Figure C 4c** and **Figure C 5c**. This is attributed to the increase in copolymerization propagation rate as f_{GMA} increases [1]. The changes in propagation rate can be inferred from reported values of bulk propagation rate coefficients (k_p) of GMA, MMA, EMA and BMA at 50°C via pulsed laser polymerization (PLP) are 1249 L mol^{-1} s^{-1}, 649 L mol^{-1} s^{-1}, 723 L mol^{-1} s^{-1}, 794 L mol^{-1} s^{-1}, respectively [122]. The influence of the higher $k_{p,GMA}$ is apparent when utilizing Fukuda et al's terminal kinetic model [204] to calculate k_p for the binary copolymerizations, as increasing f_{GMA} leads to higher propagation rate, in alignment with our observations (**Figure C 6**). Details of the predicted k_ps is summarized by **Equation C1** and **Figure C 6** in the supporting information. Another reason for the broadening of the molecular weight distributions could be more prevalent side reactions including chain transfer reactions and termination at higher conversions for copolymers with GMA-rich composition [165]. It has also been reported that methacrylic monomers may contain traces of methacrylic acid due to ester hydrolysis during prolonged storage. These carboxylic acid groups can undergo crosslinking reactions with epoxy groups, which can adversely affect the control of polymerization [205,206]

Table 5.1. Copolymer characterizations for statistical EMA/GMA copolymers using ATRP in 70°C.

ID	f_{EMA} [a]	F_{EMA} [b]	X_{EMA} [c]	X_{GMA} [d]	$X_{copolymer}$ [e]	M_n [f] (g mol^{-1})	Đ [f]	[EBiB] (mol)	[GMA] (mol)	[EMA] (mol)	[dNbpy] (mol)	[CuBr] (mol)
EMA/GMA-90 [g]	0.9	0.87	0.69	0.60	0.68	7800	1.28	0.0008	0.0068	0.061	0.00034	0.00017
EMA/GMA-80	0.8	0.81	0.83	0.81	0.82	8200	1.30	0.0008	0.014	0.053	0.00034	0.00017
EMA/GMA-70	0.7	0.73	0.93	0.95	0.93	8500	1.28	0.0008	0.019	0.045	0.00033	0.00016
EMA/GMA-60	0.6	0.58	0.98	0.99	0.98	9000	1.38	0.0009	0.032	0.048	0.0004	0.0002
EMA/GMA-50	0.5	0.43	0.95	0.94	0.94	9600	1.43	0.0009	0.039	0.039	0.0004	0.0002
EMA/GMA-40	0.4	0.45	0.99	0.99	0.99	9700	1.45	0.0009	0.046	0.031	0.00036	0.00019
EMA/GMA-30	0.3	0.34	0.99	0.99	0.99	9500	1.36	0.0009	0.053	0.023	0.00037	0.00018
EMA/GMA-20	0.2	0.24	0.99	0.99	0.99	9100	1.48	0.0009	0.058	0.015	0.00036	0.00018
EMA/GMA-10	0.1	0.13	0.99	0.99	0.99	9400	1.51	0.0009	0.065	0.0073	0.00036	0.00018
EMA/GMA-0 [h]	0	0	-	0.98	0.98	7500	1.47	0.005	0.17	-	0.0008	0.0004

[a] Initial molar ratio of EMA in the feed

[b] Final molar ratio of EMA in the dried copolymer

[c] Final conversion of EMA

[d] Final conversion of GMA

[e] Final conversion of copolymer

[f] Final averegae molecular weight of the copolymer, target number average molecular weight for all experiments ($M_{n,theoritical}$)=10000 g mol^{-1} , all reported molecular weights (M_n) and dispersity (Đ) were determined using GPC relative to poly(methyl methacrylate) (PMMA) standards in tetrahydrofuran (THF) at 40°C. It should be mentioned that for carbonation reactions $M_{n,target}$ was 5000 g mol^{-1}

[g]) Experimental identification given by EMA/GMA-XX, where XX refers to the rounded % initial molar fraction of EMA in the mixture ($f_{EMA,0}$))

[h] Reaction was ran for 1.5 hours since the polymer was viscouse

To see if there was any compositional drift in copolymerizations, reactivity ratios of EMA/GMA and BMA/GMA were determined since these were not available in the literature. As an initial estimate, Fineman–Ross (FR) [207] and then Kelen–Tüdös (KT) [208] approaches were used to calculate the reactivity ratios (estimates of reactivity ratios were done using samples taken at relatively low overall conversions (X <20% for every copolymerization), assuming a terminal model (**Table C 1** and **Table C 2**)). It should be mentioned that the errors associated with the experimental data were derived from the standard errors associated with the linear fits. As these methods are both linearized fits, they may introduce bias to estimates of the reactivity ratios. Despite considering relatively low monomer conversions, it should be noted that the FR and KT approaches do not account for the potential composition drift that may occur during copolymerization. A direct non-linear least square (NLLS) method was also applied [209] to the Mayo-Lewis equation [210] and it showed a good agreement with the other methods used. Generally, integral methods provide the best estimates for reactivity ratios and were calculated by employing Meyer and Lowry‘s analytical solution of Skeist‘s equation for binary copolymerization (**Equation 5.5**) [211].

$$1 - \frac{M}{M_0} = 1 - \left[\frac{f_1}{f_{1,0}}\right]^{\alpha}\left[\frac{f_2}{f_{2,0}}\right]^{\beta}\left[\frac{f_{1,0}-\delta}{f_1-\delta}\right]^{\gamma} \quad (5.5)$$

In **Equation 5.5**, $^{M}/_{M_0}$ is mole conversion, f_1 and f_2 are the molar compositions of monomer 1 and 2 in the mixture, and $f_{1,0}$ and $f_{2,0}$ are the initial molar ratio of monomer 1 and 2 in the feed. α, β, γ and δ were defined as $\alpha = \frac{r_2}{1-r_2}$, $\beta = \frac{r_1}{1-r_1}$, $\gamma = \frac{1-r_1 r_2}{(1-r_1)(1-r_2)}$ and $\delta = \frac{1-r_2}{2-r_1-r_2}$.

The integral method considered the monomer feed changes during polymerization (compositional drift in the molar feed of GMA with X as depicted in **Figure 5.1**). The reactivity ratios of MMA and GMA were determined by calculating them through NLLS and the analytical solution of Skeist's equation, as the values obtained via the FR and KT methods have already been reported elsewhere [165]. NLLS method led to values of r_{GMA} = 1.51 ± 0.11 and r_{MMA} = 0.77 ± 0.11, while values of r_{GMA} = 1.35 ± 0.09 and r_{MMA} = 0.80 ± 0.09 were calculated via analytical solution of Skiest's equation. For EMA/GMA copolymers, the reactivity ratios via the FR approach were calculated as r_{GMA} = 1.26 ± 0.06 and r_{EMA} = 0.42 ± 0.15 and KT method led to values of r_{GMA} = 0.65 ± 0.13 and r_{EMA} = 0.44 ± 0.18. Using the NLLS method, r_{GMA} = 1.17 ± 0.13 and r_{EMA} = 0.46 ± 0.13 with 95% confidence intervals were calculated (**Figure C 7** shows the plots of parameters for linear models of FR and KT and NLLS approaches). The reactivity ratios of r_{EMA}= 0.31 ± 0.09 and r_{GMA} = 1.10 ± 0.09 were also calculated using an analytical solution of Skeist's equation.

For BMA/GMA copolymers, the FR approach yielded the following: r_{BMA} = 0.55 ± 0.13 and r_{GMA} = 1.49 ± 0.06 and KT method yielded r_{BMA} = 0.67 ± 0.07 and r_{GMA} = 1.15 ± 0.20. Reactivity ratios calculated by the NLLS method are r_{BMA} = 0.67 ± 0.13 and r_{GMA} = 1.67 ± 0.13 with 95% confidence bounds (**Figure C 8**). Finally, the reactivity ratios of r_{BMA} = 0.67 ± 0.09 and r_{GMA}= 1.45 ± 0.09 using an analytical solution of Skeist's equation were calculated. For comparison, reactivity ratios of butyl acrylate (BA) and GMA obtained by ATRP were reported as r_{BA} = 0.16

± 0.07 and r_{GMA} = 2.78 ± 0.32 [212]. **Table 5.4** presents the reactivity ratios calculated using different methods.

The higher value of r_{GMA} than r_{EMA} and r_{GMA} than r_{BMA} indicates higher reactivity of macroradicals toward GMA, raising the possibility of the formation of blockier GMA sequences during the statistical copolymerization.

Table 5.2. Copolymer characterizations for statistical BMA/GMA copolymers using ATRP in 70°C.

ID	f_{BMA} [a)]	F_{BMA} [b)]	X_{BMA} [c)]	X_{GMA} [d)]	$X_{copolymer}$ [e)]	M_n [f)] (g mol^{-1})	Đ [f)]	[EBiB] (mol)	[GMA] (mol)	[BMA] (mol)	[dNbpy] (mol)	[CuBr] (mol)
BMA/GMA-90 [g)]	0.9	0.94	0.68	0.72	0.68	4400	1.21	0.0100	0.0350	0.3200	0.0018	0.0009
BMA/GMA-80	0.8	0.87	0.85	0.83	0.85	5800	1.24	0.008	0.0703	0.2800	0.0018	0.0009
BMA/GMA-70	0.7	0.80	0.90	0.95	0.91	6200	1.32	0.0130	0.1428	0.3249	0.0023	0.0012
BMA/GMA-60	0.6	0.68	0.95	0.92	0.94	5900	1.27	0.0010	0.0140	0.0210	0.0002	0.0001
BMA/GMA-50	0.5	0.65	0.92	0.98	0.95	7200	1.26	0.0015	0.0270	0.0270	0.0003	0.0001
BMA/GMA-40	0.4	0.55	0.99	0.99	0.99	6200	1.32	0.0015	0.0314	0.0210	0.0003	0.0001
BMA/GMA-30	0.3	0.41	0.99	0.99	0.99	8400	1.58	0.0015	0.0360	0.0150	0.0003	0.0001
BMA/GMA-20	0.2	0.24	0.99	0.99	0.99	8000	1.68	0.0020	0.0560	0.0140	0.0004	0.0002
BMA/GMA-10	0.1	0.14	0.99	0.99	0.99	8700	1.60	0.0020	0.0630	0.0070	0.0004	0.0002
BMA/GMA-0 [h)]	0	0	-	0.98	0.98	7500	1.47	0.005	0.17	-	0.0008	0.0004

[a)] Initial molar ratio of BMA in the feed

[b)] Final molar ratio of BMA in the dried copolymer

[c)] Final conversion of BMA

[d)] Final conversion of GMA

[e)] Final conversion of copolymer, reaction time for copolymers with $f_{GMA} > 0.5$ was only 2 hours [f)] Final averegae molecular weight of the copolymer, target number average molecular weight for all experiments ($M_{n,theoritical}$)=5000 g mol^{-1} , all reported molecular weights (M_n) and dispersity (Đ) were determined using GPC relative to poly(methyl methacrylate) (PMMA) standards in tetrahydrofuran (THF) at 40°C

[g)] Experimental identification given by BMA/GMA-XX, where XX refers to the rounded % initial molar fraction of BMA in the mixture ($f_{BMA,0}$)

[h)] Reaction was ran for 1.5 hours since the polymer was viscouse

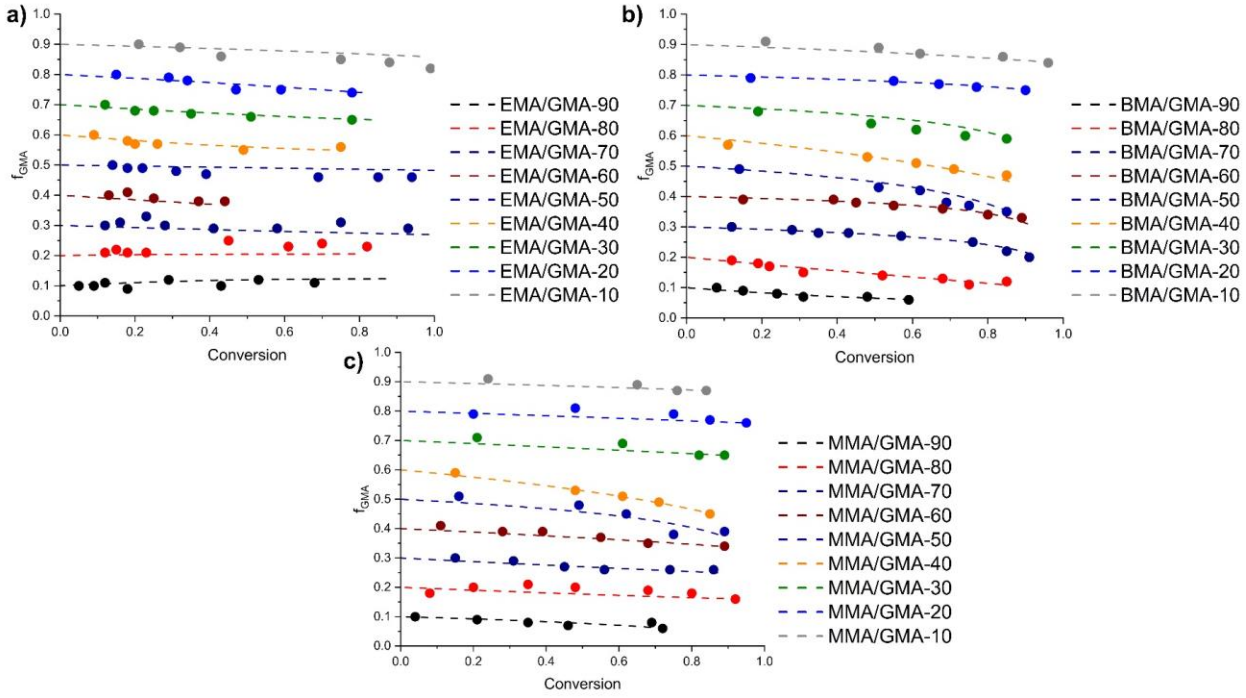

Figure 5.1. Reactivity ratio calculation; a) By utilizing the Meyer-Lowry method, the fitted curves for copolymerization with various ratios of EMA/GMA were determined, taking into consideration the drift in GMA molar feed (f_{GMA}) with monomer conversion. The resulting reactivity ratios r_{GMA} and r_{EMA} were found to be 1.10 ± 0.09 and 0.31 ± 0.09, respectively, b) the Meyer Lowry method was used to determine the fitted curves for copolymerization with various ratios of BMA/GMA, taking into account the drift in GMA molar feed (f_{GMA}) with monomer conversion. The resulting reactivity ratios r_{GMA} and r_{BMA} were determined to be 1.45 ± 0.09 and 0.67 ± 0.09, respectively, c) the Meyer Lowry method was employed to determine the fitted curves for copolymerization using various ratios of MMA/GMA, while considering the drift in GMA molar feed (f_{GMA}) with monomer conversion. As a result, the reactivity ratios r_{GMA} and r_{MMA} were determined to be 1.35 ± 0.07 and 0.80 ± 0.07, respectively.

Table 5.3. Copolymer characterizations for statistical MMA/GMA copolymers using ATRP in 70°C.

ID	f_{MMA} [a]	F_{MMA} [b]	X_{MMA} [c]	X_{GMA} [d]	$X_{copolymer}$ [e]	M_n [f] (g mol^{-1})	Đ [f]	[EBiB] (mol)	[GMA] (mol)	[BMA] (mol)	[dNbpy] (mol)	[CuBr] (mol)
MMA/GMA-90 [g]	0.9	0.92	0.92	0.94	0.92	5400	1.20	0.0100	0.0482	0.4300	0.0024	0.0012
MMA/GMA-80	0.8	0.84	0.87	0.91	0.88	6000	1.25	0.0160	0.1467	0.5968	0.0037	0.0018
MMA/GMA-70	0.7	0.71	0.95	0.98	0.96	6800	1.24	0.0150	0.1950	0.4644	0.0033	0.0017

[a] Initial molar ratio of MMA in the feed

[b] Final molar ratio of MMA in the dried copolymer

[c] Final conversion of BMA

[d] Final conversion of GMA

[e] Final conversion of copolymer (determined from Eq. 1), reaction time for copolymers with $f_{GMA} > 0.5$ was only 2 hours

[f] Final averegae molecular weight of the copolymer, target number average molecular weight for all experiments ($M_{n,theoritical}$)=5000 g mol^{-1} , all reported molecular weights (M_n) and dispersity (Đ) were determined using GPC relative to poly(methyl methacrylate) (PMMA) standards in tetrahydrofuran (THF) at 40°C

[g] Experimental identification given by MMA/GMA-XX, where XX refers to the rounded % initial molar fraction of MMA in the mixture ($f_{MMA,0}$)).

Table 5.4. Summary of calculated reactivity ratios of synthesized copolymers with different methods.

Copolymer / Method	Poly(MMA-*stat*-GMA)		Poly(EMA-*stat*-GMA)		Poly(BMA-*stat*-GMA)	
	r_{GMA}	r_{MMA}	r_{GMA}	r_{EMA}	r_{GMA}	r_{BMA}
FR	1.24 ± 0.02 [165]	0.85 ± 0.03 [165]	1.26 ± 0.06	0.42 ± 0.15	1.49 ± 0.06	0.55 ± 0.13
KT	1.53 ± 0.17 [213]	0.79 ± 0.12 [213]	0.65 ± 0.13	0.44 ± 0.18	1.15 ± 0.20	0.67 ± 0.07
NLLS	1.51 ± 0.11	0.77 ± 0.11	1.17 ± 0.13	0.46 ± 0.13	1.67 ± 0.13	0.67 ± 0.13
Analytical solution of Skeist's equation	1.35 ± 0.09	0.80 ± 0.09	1.10 ± 0.09	0.31 ± 0.09	1.45 ± 0.09	0.67 ± 0.09

5.4.2. Thermal properties of MMA/GMA, EMA/GMA and BMA/GMA copolymers

The thermal properties of synthesized copolymers were analyzed using DSC and TGA to investigate the effect of carbonation and ultimately diamine addition to the copolymers on the thermal stability and T_gs of the final products. Studying the effect of carbonation on T_gs is also beneficial to select a proper temperature window to cure the crosslinked networks (T_{cure}) as the cross-linking should started when chain are more mobile [166]. T_gs and decomposition temperatures (T_d)s of the synthesized poly(EMA-*stat*-GMA)s and their carbonated forms are all tabulated in **Table C 3**. DSC curves for poly(EMA-*stat*-GMA)s are also shown in **Figure C 9a**, with 45°C <T_g<70°C in good agreement with the predicted values from the Fox equation [214] using reported T_g = 44-85 °C for PGMA (M_n range of 9600 g mol^{-1} to 20400 g mol^{-1}, 50°C was used for Fox equation) [167] and T_g = 50-72 °C for poly(ethyl methacrylate) (PEMA) (M_n = 8000-130000 g mol^{-1}, 55°C was used for Fox equation) [215,216] in the literature. Poly(BMA-*stat*-GMA)s had T_g values between 15°C and 52°C (**Figure C 9b** and **Table C 4**), which is in agreement with the predicted values based on Fox equation [214] with T_g = 23 °C for poly(butyl methacrylate) (PBMA) (M_n = 160000 g mol^{-1}) [217]. MMA/GMA copolymers exhibited different T_gs based on initial GMA ratio in the mixture (**Figure C 9c** and **Table C 4**), ranging from 77°C to 107°C, which is consistent with the values reported elsewhere by Neugebauer et al. [165] for MMA/GMA copolymers with M_n > 12000 g mol^{-1} at different MMA-to-GMA ratios.

DSC experiments for all synthesized copolymers revealed that there was a positive correlation between T_g of the copolymers and their epoxide content, which can be attributed to the restriction of the chain mobility of the copolymers with higher epoxide content because of interactions between the polar functional groups [218]. Generally, the T_g values of poly(EMA-*stat*-GMA)s were

higher than poly(BMA-*stat*-GMA)s (poly(MMA-*stat*-GMA)s expectedly had the highest T_gs). As the size of the side-chain substituent in the polymeric backbone increases, the physical separation between the polymeric chains is increased, increasing the mobility between adjacent chains [219].

Decomposition temperatures are also shown in **Table C 3** and **Table C 4** and TGA curves are plotted in **Figure C 10**. For all copolymers, different peaks were observed in their TGA curves and their derivative weight versus temperature plots. Appearance of more than one degradation peak for GMA-based copolymers is common and have been reported in the literature [178,179]. This could be due to the formation of volatile intermediate products, including carbon dioxide, carbon monoxide, acrolein, allyl alcohol and glycidyl methacrylate, during thermal degradation analysis of GMA-based copolymers [178].

The maximum weight loss of the first decomposition peaks for EMA/GMA copolymers were observed from 140-180°C. The second decomposition stage took place between 320-370°C and the third one was at 390-550°C. Thermal stability experiments for BMA/GMA copolymers revealed that the maximum weight loss of the first decomposition peak for the synthesized copolymers was at a temperature range of 140-175°C and the second maximum weight loss was observed between 320-350°C. For MMA/GMA copolymers, the maximum weight loss of the first decomposition peak was in the range of 180-185°C, and the maximum weight loss for the second stage ranged from 350-360°C.

Generally, the overall decomposition process can be summarized in two different reactions: depolymerization to monomer and ester decomposition [178]. The first degradation peak could be due to degradation of PGMA breaking into smaller fragments [179]. The second decomposition

peak (between 320°C to 370°C) could be associated with the degradation of ester bonds and loss of CO_2 [220], while the third one could be attributed to the total degradation of the copolymers [179]. The final decomposition temperature ($T_{d,final}$) for all synthesized copolymers were above 500°C. The thermal stability results were consistent with Kaya et al. [221] work which was mainly focused on synthesis of MMA, EMA and BMA copolymer with GMA (M_n = 440–555000 g mol^{-1}, $Đ$ = 1.28-1.59 and polymer composition of GMA/ MMA [62:38], GMA/EMA [56:44], GMA/BMA [59:41] (mol%/mol%)).

The ash content for all MMA/GMA, EMA/GMA and BMA/GMA copolymers was zero at 700°C. Kaya et al. [221] also reported ash content of 3%, 4% and 4.2% at 500°C for copolymers of GMA with MMA, EMA and BMA, respectively. The residual weight of our synthesized copolymers at 500°C were between 5% to 10%, consistent with the abovementioned studies.

5.4.3. Carbonation of MMA/GMA, EMA/GMA and BMA/GMA copolymers

Some of the synthesized MMA/GMA, EMA/GMA and BMA/GMA copolymers were treated with CO_2 and TBAB catalyst to convert the epoxy functional groups from GMA incorporation to cyclic carbonate [1,8,151]. The proposed mechanism for the carbonation reaction includes the initiation of the epoxide ring opening by the bromide present in TBAB, leading to the formation of an alkoxide. Subsequently, the alkoxide acts as a nucleophile, initiating a nucleophilic attack at CO_2, resulting in the formation of a carboxylate. This step is then followed by a subsequent ring closure, leading to the formation of a five-membered cyclic carbonate [68]. Copolymers with initial GMA molar ratios of 0.1, 0.2 and 0.3 were chosen for carbonation, since high concentration of cyclic carbonate in the copolymer backbone will cause some molding difficulties in the diamine cure addition step, which is discussed in the next section. Carbonations of poly(MMA-*stat*-GMA)s, poly(EMA-*stat*-GMA)s and poly(BMA-*stat*-GMA)s were confirmed

via ^{1}H NMR and FTIR (**Figure 5.2**, **Figure C 11** and **Figure C 12**). The FTIR spectra of MMA/GMA-70 and carbonated MMA/GMA-70 after 24 hours is shown in **Figure 5.2**. As shown in **Figure 5.2a**, the FTIR spectrum of MMA/GMA-70 copolymers exhibits the characteristic peaks for the ester carbonyl at 1720 cm^{-1} and the epoxy group at 845 cm^{-1} [222]. **Figure 5.2b** shows appearance of new peaks associated with cyclic carbonate groups at 1800 and 1050 cm^{-1}, which are assigned to the C=O carbonyl stretching and C-O stretching of cyclic carbonate functionalities [95]. The appearance of a new peak at 1670 cm^{-1} is assigned to residual solvent (DMF) in the mixture [223]. ^{1}H NMR was also used to confirm the carbonation reaction and calculate the carbonation conversion (an example ^{1}H NMR spectrum of carbonated MMA/GMA-90 is presented in **Figure C 12**). In the ^{1}H NMR spectrum, the signal associated with the cyclic carbonate at 4.65 ppm is apparent and the signal associated with epoxy functional groups at 2.55 ppm disappears after 24 hours [1], showing that all epoxy groups were converted to cyclic carbonates. The carbonation conversion was calculated using **Equation 5.6**.

$$Carbonation\ conversion = \frac{A}{A+B} \tag{5.6}$$

In **Equation 5.6**, A is the integral of the signal assigned to the cyclic carbonate groups at 4.65 ppm and B is the integral of the signal assigned to the epoxy groups at 2.55 ppm. For example, carbonation conversion for carbonated EMA/GMA-90 was 71% after almost 12 hours (A = 2.51 and B = 1).

Since the carbonation reaction was done at high temperature (120°C) and its reaction time was long (24 hours), thermal degradation of copolymers is possible. In order to test for occurrence of any possible thermal degradation, GPC peak comparisons before and after carbonation was done. **Figure C 13** shows the GPC traces of MMA/GMA-90, EMA/GMA-90, BMA/GMA-90 and their carbonated forms. New peaks as a results of oligomerization or chain cleavage were not

observed and the peak for the carbonated copolymers did not broaden significantly compared to the non-carbonated copolymers, indicating that thermal degradation during the carbonation reaction was insignificant. The slight shift towards higher elution volumes for carbonated copolymers, is due to different solubility of the carbonated copolymers in the eluent [224].

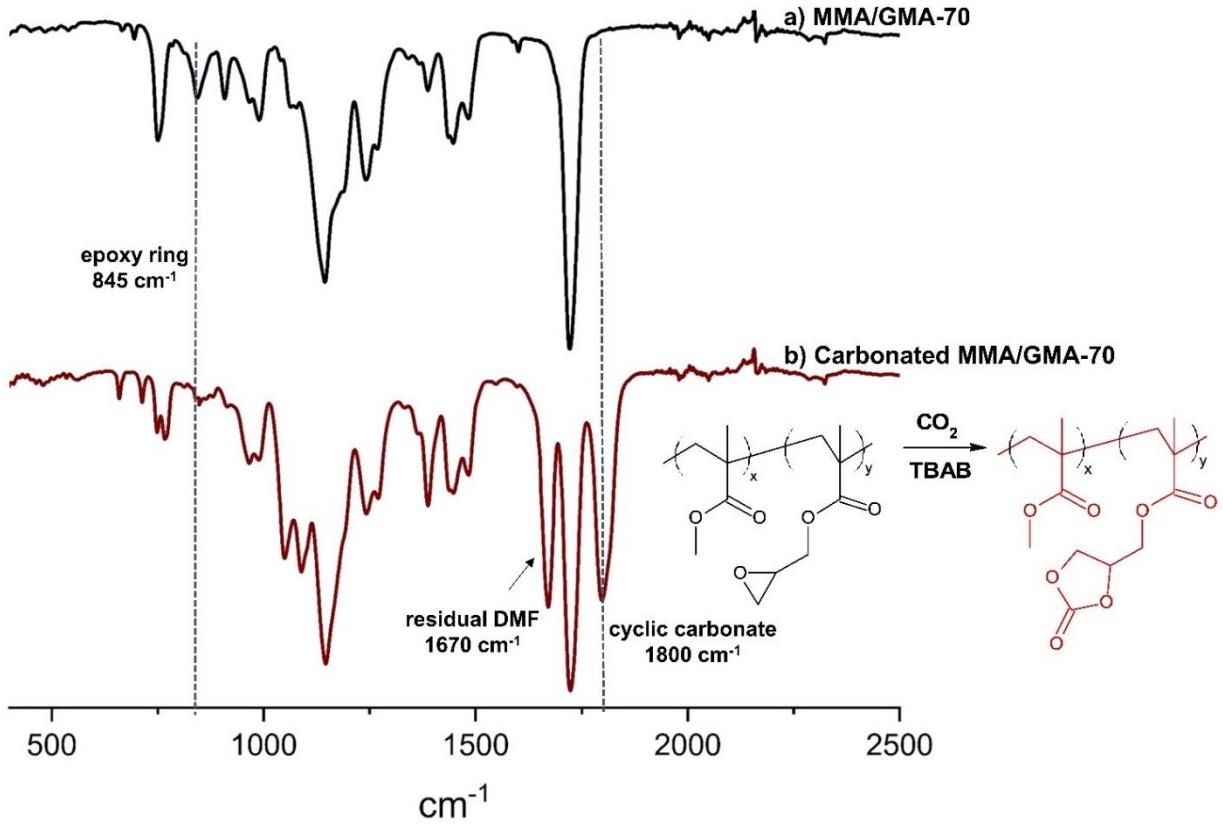

Figure 5.2. FTIR spectra of MMA/GMA-70 before and after carbonation; a) MMA/GMA-70 and b) carbonated MMA/GMA-70 after 24 hours.

The thermal properties of the carbonated copolymers were studied using TGA and DSC. **Figure C 14** shows the DSC curves for the carbonated copolymers and T_gs are also reported in **Table C 3** and **Table C 4**. 105°C < T_g < 117.5°C were measured for carbonated MMA/GMA copolymers. Carbonated EMA/GMA copolymers had T_gs of 50-75°C; and T_gs for carbonated BMA/GMA copolymers were between 28.5°C to 45°C.

In all cases, T_gs of the carbonated copolymers are higher than the pre-carbonated analogs, as their polymer chain mobility becomes more restrictive due to the carbonate rings, as noted elsewhere [156]. For example, T_g of MMA/GMA-90 increased from 78.5°C to 117.5°C after carbonation and T_g of carbonated BMA/GMA-90 was 13°C higher than its pre-carbonated copolymer.

Table C 3 and **Table C 4** list the decomposition temperatures for carbonated copolymers and **Figure C 15** presents the corresponding TGA thermograms. The TGA profile of the carbonated copolymers shows a two step degradation process. This can be attributed to the elimination of CO_2 from the cyclic carbonate rings, which is followed by the degradation of the polymer backbone [184]. The first decomposition peak of carbonated poly(MMA-*stat*-GMA)s, carbonated poly(EMA-*stat*-GMA)s, and carbonated poly(BMA-*stat*-GMA)s showed maximum weight loss at temperature ranges of 200-215°C, 175-198°C, and 168-180°C, respectively. The maximum weight loss of the second decomposition for the same series occurred at 320-360°C, 325-365°C, and 340-345°C, respectively. These decomposition temperature ranges are consistent with those reported previously [225,226]. Finally, the samples were fully degraded at 700 °C.

5.4.4. Synthesis of networks crosslinked through urethane linkages using Priamine 1074

After preparing carbonated poly(MMA-*stat*-GMA)s, poly(EMA-*stat*-GMA)s, and poly(BMA-*stat*-GMA)s, a series of crosslinked networks bonded with urethane linkages were synthesized via polyaddition with Priamine 1074 (**Scheme 5.1**, samples that were prepared with poly(MMA-*stat*-GMA)s are referred to as MMA/NIPU-xx, where "xx" represents the approximate percentage of MMA in the copolymer). Since the polyaddition reaction of cyclic carbonates with amines has been shown to be slow compared to reaction of isocyanates with alcohols [227], different methods were employed to increase the rate of reaction including use of catalyst to promote the nucleophilic attack of the amine on the carbonyl group of the carbonates [228], or increase of temperature or diamine concentration [8,47]. Although there is a positive correlation between reaction rates of cyclic carbonate functional groups with diamine and reaction temperature [194], in our work higher temperatures (higher than 110°C) led to formation of yellowish/brownish discolored networks [229] with short gel times, making processing harder (e.g. when shaping the product into tensile bars, the tensile bars exhibited non-uniformity after hot pressing at higher temperatures, likely due to crosslinking of the networks occurring before achieving a uniform texture in the mold). Therefore, we did not increase the reaction temperature beyond 110°C. A higher conversion of cyclic carbonates to urethane linkages can also be achieved by increasing the amine-to-carbonate ratio [35]. However, an excessive amount of diamine can result in the formation of amine-terminated urethane linkages that do not contribute to the crosslinked networks, ultimately leading to reduced tensile strength and lower gel content. Moreover, excess diamine can react with the ester groups of methacrylates, resulting in the formation of amides [230,231]. This can lead to a network with lower crosslinking density and

contain unreacted free species due to the aminolysis of the ester groups [187]. Carré et al. [232] observed the aminolysis of ester groups during the reaction between sebacic biscyclocarbonate and a bio-sourced dimer-based diamine carried out in bulk at 75°C for 2 hours. Doley et. al. [187] also observed aminolysis of ester groups in reaction of carbonated sunflower oil with excess 1,2-ethylenediamine (EDA), leading to poorer mechanical properties (e.g. lower tensile strength). Therefore, the crosslinking conditions were selected to be 90°C for 24 hours, except for MMA/GMA copolymers, which have a higher T_g and require a temperature of 110°C. In addition, the amine-to-carbonate ratio was set to unity (**Scheme 5.2**).

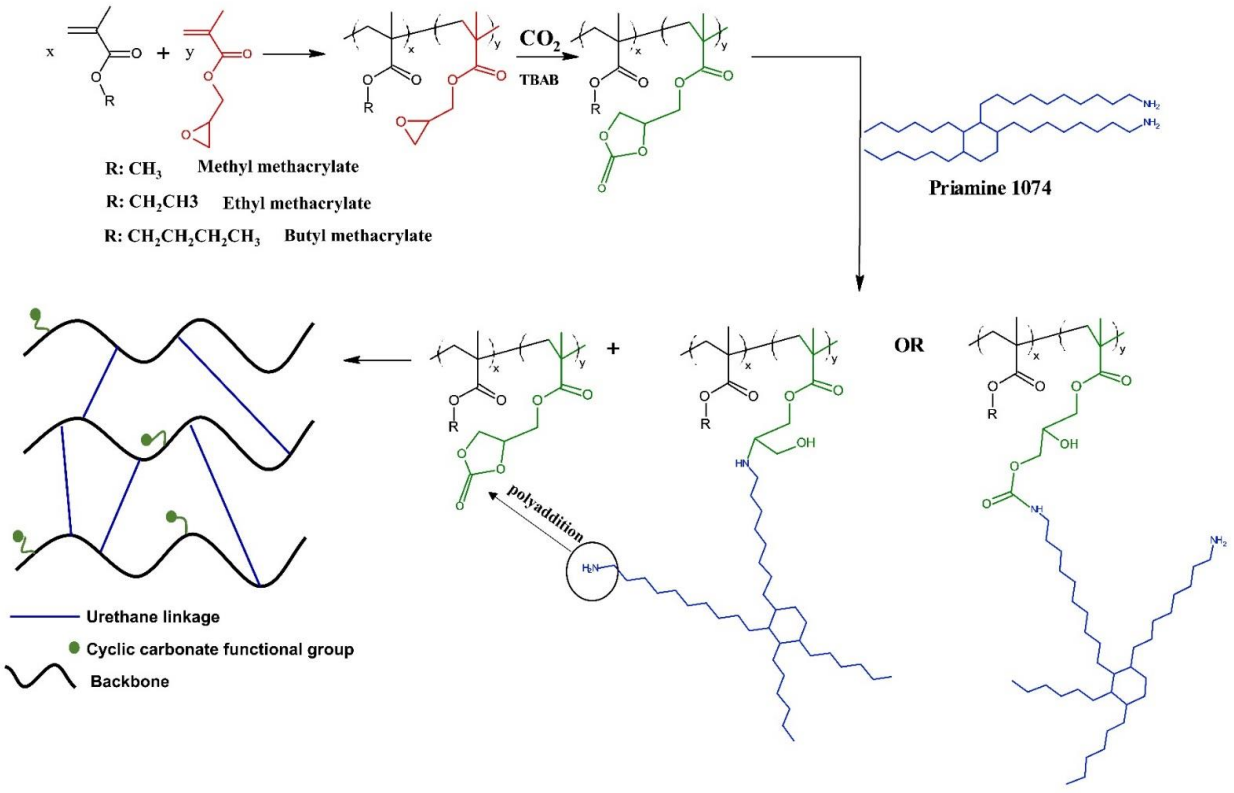

Scheme 5.1. Preparation of networks crosslinked through urethane linkages.

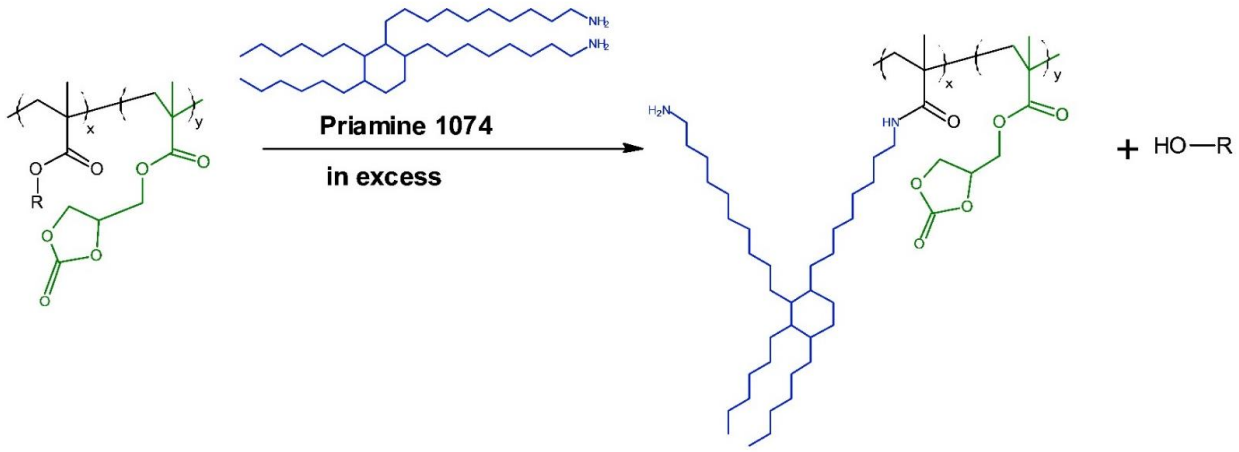

Scheme 5.2. Aminolysis of ester groups due to use of excess diamine (Priamine 1074).

After 24 hours, conversion of cyclic carbonate functional groups to urethane linkages was confirmed via FTIR. **Figure 5.3** displays the FTIR spectra for carbonated MMA/GMA-70 and MMA/NIPU-70. FTIR spectra for other crosslinked samples are presented in **Figure C 16**. FTIR results demonstrate that the characteristic absorption peak of cyclic carbonates at 1800 cm^{-1} for almost most of the crosslinked networks was virtually absent, except for BMA/NIPU-80 after 24 hours. This proves that the cyclic carbonate functional groups reacted with amine functional groups. The weak peak observed for residual carbonate at 1800 cm^{-1} in FTIR spectrum of BMA/GMA-80 suggests that the conversion of cyclic carbonate to urethane was not complete, which was reported elsewhere [8,139]. The presence of a broad signal between 3600 and 3100 cm^{-1} confirmed the formation of -NH and -OH groups [139]. The synthesized network exhibits characteristic absorption peaks at 1720 cm^{-1}, which is attributed to C=O stretching of the urethane group which is formed through the ring-opening of cyclic carbonates. It should be mentioned that the peak at 1720 cm^{-1} overlaps with ester groups present in the methacrylate structure. Additionally, a peak at 1525 cm^{-1} is observed, corresponding to the NH bending of the urethane group [8,139].

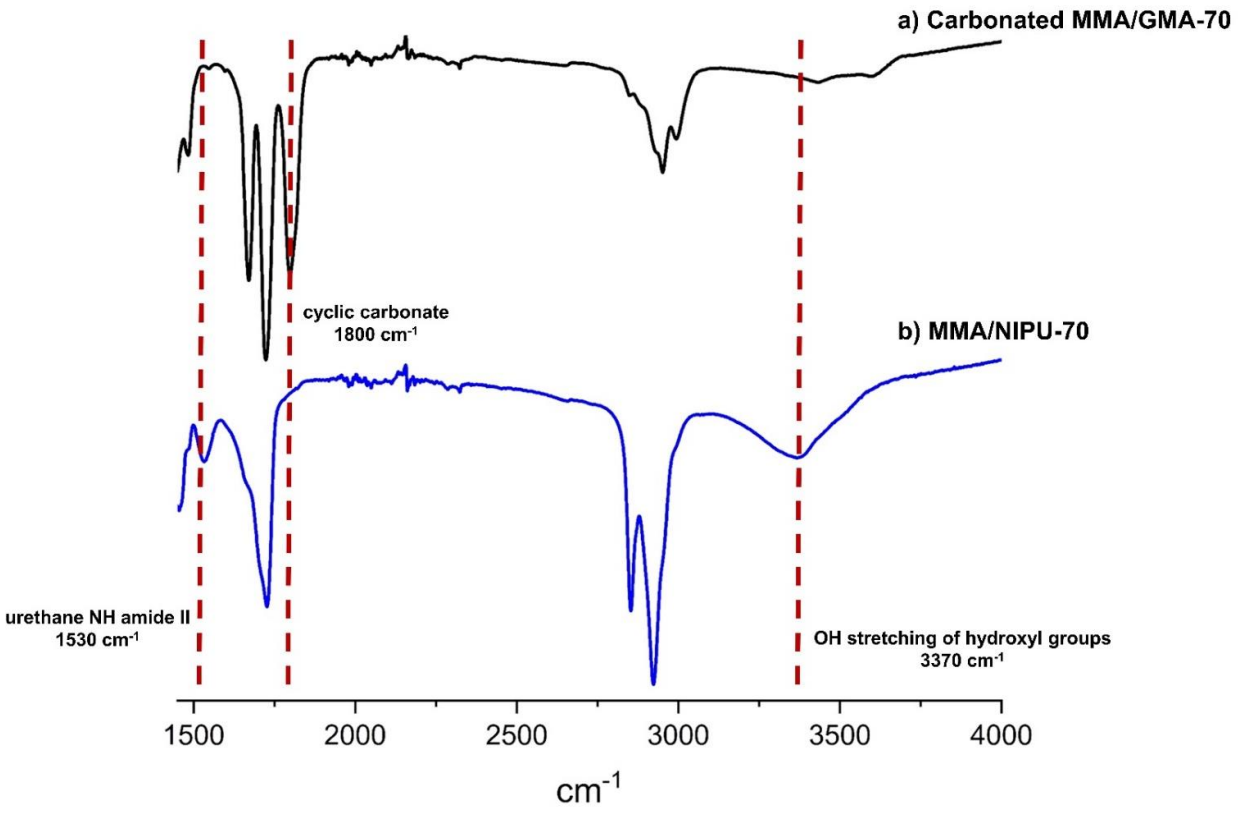

Figure 5.3. FTIR spectra for carbonated MMA/GMA-70 and MMA/NIPU-70; a) FTIR spectrum of carbonated MMA/GMA-70, b) FTIR spectrum of MMA/NIPU-70.

DMTA was used to evaluate the viscoelastic properties of the crosslinked networks at different temperatures. For all the thermosets, only one step change in modulus (**Figure C 17**) and one peak in the tanδ response (**Figure 5.4**) was observed, suggesting no phase separation and absence of unreacted carbonated copolymers or free species in the networks (at the temperature range of room temperature to 150°C) [233,234]. **Figure C 17** illustrates storage moduli (*E'*)s of the crosslinked samples at various temperatures. Crosslinked networks based on MMA/GMA copolymers exhibited a rubbery plateau after almost 105°C, whereas EMA/GMA based networks showed a plateau at 90°C, and BMA/GMA based networks reached a plateau at 70°C. The observed plateau is attributed to the presence of crosslinking points [232]. Furthermore, the storage

moduli of all networks crosslinked with urethane linkages stay constant at above 1 MPa, which is typical for conventional thermosets [232]. As seen from **Figure C 17**, MMA/GMA-based crosslinked networks had a higher E' in the glassy region (T = 30°C), which could be due to having a more rigid backbone compared to EMA/GMA and BMA/GMA based networks [235]. Generally, networks with higher urethane linkage concentration (higher number of cyclic carbonates on their carbonated copolymer backbone), showed higher E' in the rubbery region, and thus tighter crosslinked networks [234,236].

DMTA is also an effective and sensitive method to measure T_g or other structural changes. T_g can be also measured at the maximum peak of the mechanical damping curve (tanδ response) [1]. T_g values obtained from the tanδ response are tabulated in **Table 5.5**. The T_g of the crosslinked networks increased as the number of urethane linkages increased in the backbone. For example, T_g of MMA/NIPU-70, which has 19 urethane linkages on its backbone, is 15°C higher than T_g of MMA/NIPU-90 with 9 urethane linkages on its backbone. However, T_g of MMA/GMA-based networks are generally lower than their carbonated form. This is due to the change in flexibility of the backbone compared to the crosslinking molecule. The tanδ curves provide primary evidence that the addition of Priamine 1074 introduces flexible chains to the structure, resulting in a more flexible structure and a lower T_g to the carbonated MMA-based networks [176,237]. On the other hand, when Priamine 1074 was added to EMA/GMA-based networks and BMA/GMA-based networks, the increase in crosslinking density outweighed the introduction of a more flexible structure to the network, resulting in higher T_g values for the crosslinked networks compared to the carbonated copolymers. In general, both E' and T_g are indications of material rigidity [238]. However, E' and T_g are still different. T_g is a constant value but E' varies with temperature. With increasing temperature, the movement of the polymer chains also increases,

resulting in lower E'. As the temperature increases, the mobility of chains within a crosslinked polymer increases, leading to the gradual disentanglement of physical entanglements. Eventually, a plateau is reached in the storage modulus, indicating the presence of chemical permanent crosslinks. This phenomenon can be attributed to the stabilization of the polymer network by covalent bonds, which resist further changes in the storage modulus. In other words, E' observed in the glassy state can be attributed to a combination of physical entanglements and chemical crosslinks. However, as the temperature increases, E' primarily becomes governed by the presence of chemical crosslinks [237]. However, in **Figure C 17**, we can observe that E' values for crosslinked networks at room temperature do not necessarily follow a trend based on the rigidity of their backbone and number of crosslinks (e.g. E' for EMA/NIPU-90 is higher than EMA/NIPU-70 below almost 70°C (based on **Table 5.5**, EMA/NIPU-90 has lower T_g and lower E' in the rubbery region)). This observation can be attributed to the experimental conditions of the DMTA test, which is conducted between room temperature and 120°C. In this temperature range, the crosslinked networks have not yet reached their plateau in the glassy state. If the test were conducted at a temperature below room temperature, it is likely that the storage moduli of the crosslinked networks would have reached their plateau, making it possible to compare E' values in their glassy state and investigate the effect of physical entanglements and chemical crosslinks. This discrepancy may be explained by the fact that the networks do not have very high T_gs (T_g < 100°C).

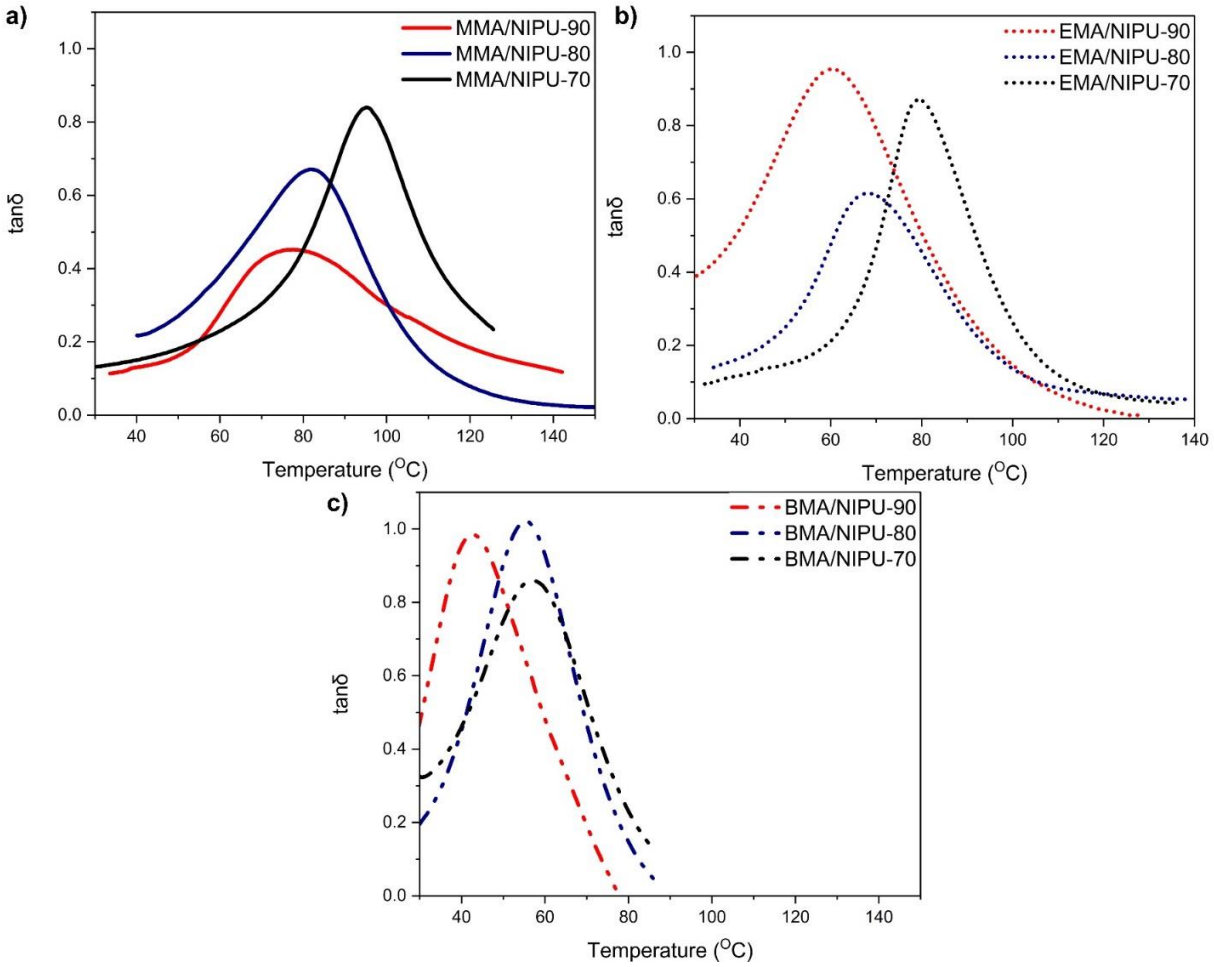

Figure 5.4. tanδ response as functional temperature for crosslinked NIPUs; a) synthesized crosslinked samples based on MMA/GMA copolymers, b) crosslinked samples based on EMA/GMA copolymers and c) crosslinked samples based on BMA/GMA copolymers.

Table 5.5. Gel content and mechanical properties of crosslinked networks.

Sample ID[b)]	# of urethane linkages on each backbone	E[c)] (MPa)	EB[d)] (%)	Ultimate stress (MPa)	T_g (°C)	M_c (g mol^{-1})	Swelling ratio in THF (%)	Swelling ratio in water (%)	Gel content (%)
MMA/NIPU-90	9	1020 ± 40	2.6 ± 0.1	18.36 ± 1.06	80	2900	151.10 ± 13.90	22.56 ± 4.44	93.44 ± 6.31
MMA/NIPU-80	12	1060 ± 45	2.3 ± 0.4	16.35 ± 1.15	85	1900	123.57 ± 8.15	12.75 ± 5.25	81.79 ± 5.03
MMA/NIPU-70	19	1250 ± 40	1.9 ± 0.3	19.67 ± 1.33	95	990	95.53 ± 2.10	11.65 ± 3.21	97.35 ± 1.33
EMA/NIPU-90	8	760 ± 50	3.5 ± 0.1	13.23 ± 2.13	60	3580	285.33 ± 5.67	29.90 ± 5.41	89.65 ± 1.86
EMA/NIPU-80	15	850 ± 30	2.6 ± 0.5	15.46 ± 0.75	70	2200	121.33 ± 11.33	12.80 ± 4.80	86.73 ± 1.08
EMA/NIPU-70	24	1000 ± 35	1.8 ± 0.3	16.25 ± 1.25	85	1550	110.63 ± 6.75	3.11 ± 0.32	83.58 ± 2.34
BMA/NIPU-90	6	395 ± 20	5.9 ± 0.3	9.45 ± 1.20	44	3700	243.67 ± 25.12	36.70 ± 5.71	96.18 ± 0.87
BMA/NIPU-80	8	495 ± 15	4.5 ± 0.4	12.60 ± 2.10	58	3100	155.67 ± 8.33	20.52 ± 4.35	90.34 ± 4.81
BMA/NIPU-70	12	530 ± 20	3.8 ± 0.2	16.15 ± 1.35	63	2200	114.60 ± 6.33	9.45 ± 2.12	94.00 ± 3.24

[a)] At least three replicates for each crosslinked sample were used

[b)] Experimental identification given by methacrylic monomer/NIPU-XX, where XX refers to the rounded % initial molar fraction of methacrylic monomer (MMA, EMA or BMA) in the copolymer

[c)] Young's modulus, E values are determined within the linear region of the stress-strain curve at 2% elongation

[d)] Elongation at break

By employing the theory of rubber elasticity [141], the relationship between the average molecular weight between cross-links (Mc) and E' can be determined using **Equation 5.2** and the M_c for all crosslinked networks are presented in **Table 5.5**. The predicted M_c values are consistent with the trend observed in T_g, which was extracted from the tanδ responses. M_c was positively correlated with the T_g increase. Swelling measurements were used to determine crosslinking density like in other polyurethane networks [239], and were done here in THF and water. After soaking the samples in THF and water, all of them swelled, but none completely dissolved. This observation suggests that all samples were sufficiently crosslinked (swelling ratios (*SR*)s are tabulated in **Table 5.5**). The extracted *SR* values in THF are consistent with DMTA results. The crosslinked networks with lower M_c values exhibited lower *SR*s, indicating a more tightly crosslinked network with shorter chains between the crosslinks [139,240]. For example, EMA/NIPU-90, with M_c = 3580 g mol^{-1}, had a higher degree of swelling (285%), but EMA/NIPU-70 swelled less (110%) due to the presence of shorter chains between the crosslinks (M_c = 1650 g mol^{-1}).

Swelling ratios in water were also measured as increased water uptake of PHUs compared to conventional PUs was suggested to be due to the pendent hydroxyl groups in PHUs [189,241]. Although samples with tighter networks have higher hydroxyl group concentration, they showed lower water uptake. This could be due to higher concentration of hydrophobic Priamine 1074 in the structure of the networks [242].

Both BMA/NIPU-70 and MMA/NIPU-80 have the same number of urethane linkages on their backbones (12 on each backbone). However, BMA/NIPU-70 had slightly lower water uptake by 3.3% (9.45% compared to 12.75%), which could be attributed to differences in the structure of the copolymer backbone, namely that the BMA/GMA copolymers had a longer alkyl side chain compared to the MMA/GMA copolymers. Furthermore, some steric hindrance due to the longer

alkyl side chains in BMA/GMA-based networks may reduce access of water molecules to the crosslinked urethane network, leading to lower water uptake [198,199]. The water uptake of BMA/NIPU-70 with 12 urethane linkages is also lower than EMA/NIPU-80 with 15 urethane linkages, confirming the effect of longer alkyl side chain in BMA/NIPU-70 compared to EMA/NIPU-80 although they both have nearly the same T_gs (T_g of EMA/NIPU-80 is 70°C and T_g for BMA/NIPU-70 is 63°C). Gel content (*GC*) values are also reported in **Table 5.5**. *GC*s were all > 80%, indicating the soluble fraction in THF was less than 20%. From the calculated *GC* values, it can be interpreted that the conversion of cyclic carbonates to urethane linkages was relatively high. The higher *GC* values in BMA/NIPU samples is attributed to the lower T_g of the carbonated BMA/GMA copolymers, resulting in easier chain movement compared to the other carbonated copolymers.

Finally, the mechanical properties of the synthesized networks were characterized using tensile tests, and the resulting engineering stress-strain curves are shown in **Figure C 18**. The first observation was the effect of crosslinking density on the Young´s moduli of the networks as higher crosslinking density increases the Young´s modulus [8]. For instance, BMA/NIPU-70, which has 12 urethane linkages in its backbone, exhibited a Young´s modulus of 530 ± 20 MPa, while BMA/NIPU-90 with 6 urethane linkages had a Young´s modulus of 395 ± 20 MPa. As the crosslinking density increased, the networks exhibited increasingly brittle behavior. For example, MMA/NIPU-90 had elongation at break of 2.6 ± 0.1%, while MMA/NIPU-70 broke at elongation of 1.9 ± 0.3%. These results are consistent with the results extracted from DMTA. Compared to EMA/GMA and MMA/GMA-based networks, the BMA/GMA-based networks showed higher elongations at break (*EB*) (for instance, networks based on BMA/GMA exhibited *EB* values ranging from 3.8% to 5.9%, while those based on EMA/GMA and MMA/GMA

showed lower *EB* values of 1.8%-3.5% and 1.9%-2.6%, respectively), which can be attributed to the copolymer structure. The more flexible backbone of PBMA, with a lower T_g, could explain the higher *EB* values compared to PMMA and PEMA backbones.

Networks with the highest M_cs exhibited the highest ultimate stress. The role of intermolecular hydrogen bonding between urethane groups in improving the toughness of HPUs is well-documented [8,144]. This bonding mechanism converts mechanical energy into heat by breaking and forming of hydrogen bonds. Despite the fact that MMA/NIPU-80 has higher urethane concentration compared to MMA/NIPU-90, MMA/NIPU-80 had lower ultimate stress than MMA/NIPU-90. This observation could be attributed to the difference in copolymer backbone structure, with MMA/NIPU-90 containing a higher proportion of MMA units.

Finally, thermal stability of all crosslinked samples was analyzed using TGA under nitrogen purge. **Figure C 19** displays the TGA curves, and **Table 5.6** summarizes the decomposition temperatures at different levels of weight loss. TGA results showed that all crosslinked networks exhibited good thermal stability below 250°C, with decomposition temperatures at 5% weight losses ($T_{d,5\%}$) ranging from 270°C to 296°C. Not surprisingly, crosslinked networks possessed higher thermal stability compared to their carbonated counterparts.

Table 5.6. Decomposition temperatures for 5%, 10%, 50%, 100% weight loss and $T_{d,max}$ for the crosslinked networks.

Sample ID	$T_{d,5\%}$ (°C)	$T_{d,10\%}$ (°C)	$T_{d,50\%}$ (°C)	$T_{d,max}$ (°C)	$T_{d,final}$ (°C)
MMA/NIPU-90	278	324	438	443	600
MMA/NIPU-80	282	316	434	445	610
MMA/NIPU-70	272	305	437	442	615
EMA/NIPU-90	294	340	450	439	595
EMA/NIPU-80	285	322	437	445	617
EMA/NIPU-70	296	330	445	450	615
BMA/NIPU-90	295	345	430	445	600
BMA/NIPU-80	280	315	423	435	605
BMA/NIPU-70	277	310	431	442	615

5.5. Conclusions

Networks crosslinked with hydroxyurethane linkages were synthesized from a series of poly(alkyl methacrylate/GMA) (alkyl methacrylate = MMA, EMA and BMA) precursors and the effect of the copolymer backbone on rheological and mechanical properties was investigated. The precursors were synthesized via ATRP at moderate temperatures with various compositions to produce epoxy-functional templates that were subsequently converted to cyclic carbonate functional copolymers. The cyclic carbonate functional copolymers were reacted with a vegetable oil-derived diamine (Priamine 1074) to form urethane-linked networks. For all networks, with more urethane linkages, molecular weight between crosslinks increased. Crosslink density expectedly affected the glass transition temperature (T_g) of the networks. For example, the EMA/GMA-based network with highest crosslink density showed T_g of 85°C, whereas the network with the lowest urethane concentration had T_g of 60°C (compared to 70°C and 50°C for carbonated EMA/GMA copolymers). Swelling ratio of the networks confirmed the trend observed via rheological studies. In general, networks with longer alkyl side chains had lower swelling ratios, indicating the hydrophobic effect of the side chain on the crosslinked networks. A positive correlation was observed between the concentration of urethane linkages and the Young's modulus of the samples. Additionally, samples with higher concentrations of urethane linkages exhibited more brittle behavior, attributed to limited polymer chain mobility caused by a denser crosslink network. This study revealed that the mechanical properties (e.g., Young's modulus and elongation at break) of the networks were impacted by the flexibility of the copolymer backbone, resulting in vastly tunable networks (Young's moduli ranging from 395 MPa to 1250 MPa). In addition, the impact of the alkyl side chain of the copolymers on the hydrophobicity of the networks cannot be discounted with respect to the cross-linking density.

6. CHAPTER 6

UTILIZING BIO-DERIVED AMINE-TERMINATED THERMOPLASTIC POLYHYDROXYURETHANES AS CROSSLINKERS FOR HYBRID THERMOSETS

Following the investigation of crosslinked networks bonded through urethane linkages and the exploration of backbone/side chain rigidity effects, the study progressed towards the synthesis of crosslinked NIPUs. The previously synthesized networks, which contained only two urethane linkage, did not fully meet the criteria to be classified as NIPUs. To address this limitation and more fully explore possible advantages of NIPU-rich materials, thermoplastic PHUs were synthesized and utilized as crosslinkers for the C13MA/GMA templates. This approach aimed to enhance the network structure and achieve the desired properties of NIPUs. By incorporating the thermoplastic PHUs as crosslinkers, the resulting networks were expected to exhibit improved mechanical and rheological characteristics, thus fulfilling the requirements for true NIPU materials. The manuscript of this chapter was published in *Journal of Polymer Science* in 2023 (**Farkhondehnia, M.** and Marić, M., Utilizing bio-derived amine-terminated thermoplastic polyhydroxyurethanes as crosslinkers for hybrid thermosets, *Journal of Polymer Science*, **2023**, J*ust Accepted,* DOI: https://doi.org/10.1002/pol.20230382.) [243]. The supporting information of this publication is given in Appendix D.

6.1. Abstract

Bio-sourced amine-terminated polyhydroxyurethanes (PHUs) are obtained by terpolymerizing bio-based diglycerol dicarbonate (DGC) or mannitol biscarbonate (MBC) with Priamine 1074 and 1,10-diaminodecane (DAD). Partially bio-based thermoset non-isocyanate polyurethane (NIPU) hybrids with high biorenewable carbon content (84%-95%) are obtained by using the synthesized PHUs as crosslinkers with cyclic carbonated copolymers derived from epoxy-functional templates. The latter are derived from the atom transfer radical polymerization (ATRP) of an alkyl methacrylate (C13MA, with an average side-chain length of 13) and epoxy-functional glycidyl methacrylate (GMA) mixtures (initial GMA mol fraction = 0.1-0.3). By manipulating template functionality as well as type of crosslinker, crosslinked NIPU hybrids are achieved with Young's moduli ranging from 2.35 ± 0.45 MPa to 20.85 ± 1.73 MPa for DGC-based crosslinkers and 1.24 ± 0.61 MPa to 6.45 ± 1.05 MPa for MBC-based ones. Moreover, with increased density of urethane linkages, networks become tighter as measured by swelling ratios (*SR*) of the networks in tetrahydrofuran (THF), consistent with the estimated molecular weight between crosslinks obtained rheologically. The crosslinked NIPUs display high conversions, ranging from 75% to 95%, despite being solvent- or catalyst-free systems.

6.2. Introduction

Polyurethanes (PUs) are highly versatile materials, renowned for their broad range of structures and properties, such as their ability to exhibit elastomeric, thermoplastic, and thermoset behavior [8,36]. Despite their many advantageous properties, PUs pose distinct environmental and human health concerns. PUs, which are derived from fossil fuels, are associated with significant greenhouse gas (GHG) emissions during their production. Annual GHG emissions of PUs in the United States alone are estimated to be 7.8 million metric tons [36]. Furthermore, conventional PUs are synthesized via polyaddition reactions between poly-isocyanates and polyols [144]. Synthesis of isocyanates involves the use of phosgene, an extremely toxic and lethal gas, making the process hazardous. This method also generates significant amounts of hydrochloric acid (HCl) as a side product [33]. Due to increasing emphasis on ecological sustainability in chemical production, there have been extensive efforts to explore alternatives to isocyanate-free routes for producing PUs [13,85]. Various synthetic pathways can be employed to obtain non-isocyanate polyurethanes (NIPUs) [9]. Despite the wide choice of methods, many still generate significant amounts of side products such as HCl, alcohols, and water [9,108,144]. The polyaddition of cyclic carbonate functional groups with di- or polyamines, resulting in poly(hydroxy urethanes)s (PHUs), is considered one of the most promising synthesis routes. PHUs are highly desirable materials because their polymerization does not result in lower molecular weight byproducts and their precursors are abundant and can be bio-based. Replacing petroleum-based monomers with those derived from sustainable resources can provide long-term socio-economic and environmental benefits.

Sugar-derived compounds and diglycerol are promising renewable resources for the synthesis of cyclic carbonates, which can then be used to produce thermoplastic PHUs [25,108,151,244]. Diglycerol

dicarbonate (DGC) is derived from glycerol, a byproduct of biomass waste hydrolysis and biodiesel production [94]. On the other hand, D-mannitol biscarbonate (MBC) is obtained from sugars derived from glucose processing [19,94]. While thermoplastic NIPUs have a wide range of applications, thermoset NIPUs are required for specific applications such as coatings and sealants [34]. However, their inability to be recycled due to the presence of permanent crosslinks is considered a negative feature. Therefore, there is a significant need to develop thermoset NIPUs that are sustainably sourced and possess recyclability, all while maintaining their mechanical properties. To achieve this, researchers have extensively studied the crosslinking of bio-based carbonated vegetable oils with bio-sourced diamines to form bio-based thermoset NIPUs with tunable mechanical properties. Previous studies have reported that the hydroxyl and carbamate groups present in PHUs, resulting from the reaction between cyclic carbonates and amines, are capable of undergoing dynamic covalent bond exchange. This unique characteristic allows bio-based NIPUs to possess good reprocessing capabilities [245,246]. For example, Javni et al. [35] conducted a study concerning the curing of carbonated soybean oil using various diamines and amine-to-carbonate ratios, resulting in crosslinked NIPUs with Young's moduli ranging from 0.49 MPa to 5.77 MPa. According to Bähr et al. [151], the use of carbonated linseed oil blended with carbonated soybean oil resulted in higher Young's moduli values spanning from 2 MPa to 1460 MPa, which was attributed to the higher cyclocarbonate functionality on the linseed oil. As discussed above, the factors that can modify the mechanical properties of crosslinked NIPUs are generally limited to the diamine-to-carbonate ratio and the type of diamine used.

To enhance the properties of bio-based NIPUs, hybrid NIPUs have gained increasing prominence [41]. The definition of hybrid NIPUs varies, as it could refer to a chemical structure that is hybridized with an inorganic polymer, such as through the introduction of moisture-

sensitive silanes, or it may refer to the incorporation of desired functionality through a different polymerization method, such as the combination of radical polymerization and polyaddition [69,111,144,247].

We recently investigated crosslinking of carbonated copolymers with different diamines to form crosslinked networks bonded via urethane linkages. However, due to the presence of only two urethane linkages in the side chains, they do not strongly qualify as NIPUs [1,144].

In this study, our aim is to synthesize hybrid thermoset NIPUs by combining free radical polymerization with polyaddition, using bio-sourced amine-ended thermoplastic PHUs as crosslinker. First, DGC and MBC were polymerized with Priamine 1074 and 1,10-diaminodecane (DAD) to synthesized amine-ended thermoplastic PHUs. The rheological and thermal behavior of the prepared PHUs were investigated to examine the effects of DGC and MBC backbones on their properties. Second, atom transfer radical polymerization (ATRP) was utilized to copolymerize C13MA, an alkyl methacrylate derived from vegetable oil, with glycidyl methacrylate (GMA), resulting in a soft backbone with epoxy functional groups introduced via GMA. Then, cyclic carbonates are introduced into the synthesized poly(C13MA-*co*-GMA)s by carbonation, transforming CO_2 into value-added chemical feedstock [8,186,225,245]. Cyclic carbonates in the synthesized copolymers were then reacted with the synthesized bio-based amine-ended PHUs to form the requisite thermoset NIPUs. The mechanical properties of the final crosslinked NIPUs varied based on the type of amine-ended PHUs used and the number of cyclic carbonates present on the carbonated C13MA/GMA copolymers.

6.3. Results and discussion

6.3.1. Characterization of synthesized Polyhydroxyurethanes (PHUs)

To achieve a high molecular weight and monomer conversion, the polymerizations were conducted using dioxane as the solvent. Fourier Transform Infrared (FTIR) analysis on purified PHUs confirmed the absence of cyclic carbonate functional groups in the backbone and their conversion to urethane linkages after 24 hours. In the following discussion, we will refer to Mannitol biscarbonate (MBC)-based PHUs as MDP, where M represents MBC, D represents 1,10-diaminodecane (DAD), and P represents Priamine 1074. Similarly, Diglycerol dicarbonate (DGC)-based PHUs will be referred to as DDP, using the same sample naming convention where the first letter refers to the carbonated species. **Figure D 1** displays the FTIR spectra of DGC, MBC, DDP and MDP. The FTIR results indicate that the characteristic absorption peak of cyclic carbonates at 1800 cm^{-1} was visually absent in both DDP and MDP. This proves that the cyclic carbonate functional groups reacted with amine functional groups and led to the formation of amine-ended PHUs. The presence of a broad signal between 3600 and 3100 cm^{-1} confirmed the formation of -NH and -OH groups [139]. The characteristic absorption peaks at 1720 cm^{-1} exhibited by the synthesized PHUs is attributed to the C=O stretching of the urethane group formed through the ring-opening of cyclic carbonates [8]. In addition, a peak corresponding to the NH bending of the urethane group is observed at 1525 cm^{-1} [139]. The absence of a peak at 1650 cm^{-1} indicates that no urea was formed as a side product during the reaction [25,248]. Regioselectivity of ring opening polyaddition was also studied via proton nuclear magnetic resonance (^{1}H NMR) (**Figure D 2** and **Figure D 3**, see supporting information for calculation). **Figure 6.1** illustrates that the nucleophilic attack of a primary amine on the cyclic carbonate moiety provides access to both primary and secondary alcohols. Typically, the signal for a primary alcohol falls within the

range of 4.8-5.3 ppm, whereas a secondary alcohol exhibits a signal between 3.5 and 4.8 ppm. The ratio of secondary to primary alcohol can be found in **Table 6.1**. Secondary to primary alcohol ratios for the synthesized PHUs (0.60/0.40 for DDP and 0.65/0.35 for MDP) indicates a greater tendency for the formation of secondary alcohol over primary alcohol [20]. Theoretical calculations have indicated that the formation of the secondary alcohol is thermodynamically more favorable than that of the primary hydroxyl group [53].

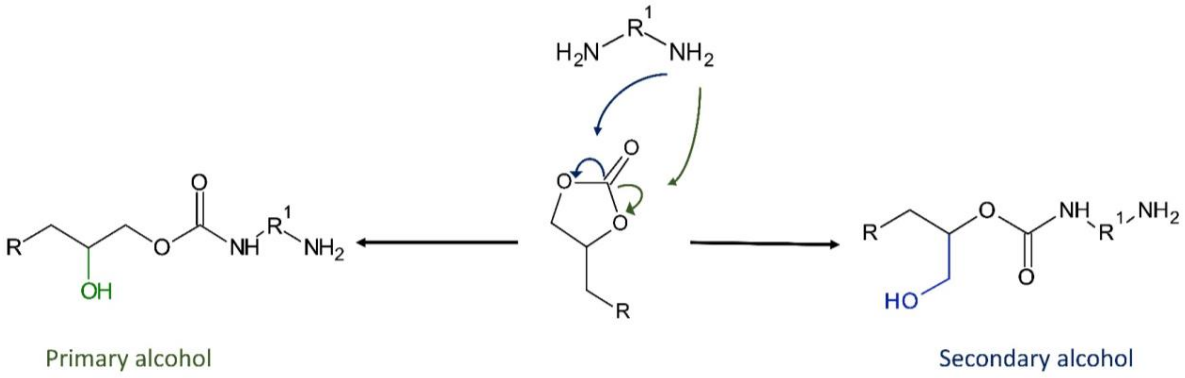

Figure 6.1. Regioselectivity of the addition of amine on cyclic carbonate.

Table 6.1. Structural, microstructural and thermal properties of synthesized PHUs.

PHU	Sec. OH/prim. OH [a)]	M_n [b)] (g mol^{-1})	$Đ$	T_{g1} (°C)	T_{g2} (°C)	$T_{d,10\%}$ [c)] (°C)	$T_{d,50\%}$ [c)] (°C)	$T_{d,final}$ [c)] (°C)
DDP [d)]	0.60/0.40	6200	2.4	-13	29	260	447	550
MDP [e)]	0.65/0.35	5800	2.2	1.5	-	225	445	560

((a) Ratio of secondary to primary alcohols in the synthesized PHUs determined by ^{1}H NMR); (b) Number average molecular weight (M_n) values were extracted by GPC rative to PMMA standards); (c) $T_{d,10\%}$ (decomposition temperature for 10% weight loss), $T_{d,50\%}$ (decomposition temperature for 50% weight loss), and $T_{d,final}$ (end of decomposition) measured by TGA under N_2 atmosphere at a ramp rate of 10 °C min^{-1}), (d) PHU synthesized through terpolymerization of DGC, 1,10-diaminodecane and Priamine 1074); (e) PHU synthesized through terpolymerization of MBC, 1,10-diaminodecane and Priamine 1074).

^{1}H NMR analyses, which were used to study the microstructure of the synthesized PHUs, were then completed with gel permeation chromatography (GPC) to measure the molecular weights. The number average molecular weight (M_n) and dispersity ($Đ$) of DDP were found to be 6200 g mol^{-1} and 2.1, respectively, while MDP had M_n = 5800 g mol^{-1} and $Đ$ = 2.2 (relative to PMMA standards by GPC in THF at 40 °C). The thermal analysis of DDP and MDP was studied using thermogravimetric analysis (TGA) and differential scanning calorimetry (DSC). **Figure D 4** shows TGA traces with two distinct degradation steps. The first one can be attributed to the degradation of the urethane linkages, and the second one can be attributed to the decomposition of carbon chains [249]. TGA results indicated that thermal decomposition of PHUs started at after 220°C (according to the $T_{d,5\%}$), after a slight mass decrease between 0 and 200°C due to the

evaporation of residual and linked water molecules. Both DDP and MDP showed almost similar $T_{d,10\%}$ and $T_{d,50\%}$ (**Table 6.1**). Ash content for both synthesized PHUs were almost zero at 700°C. These PHUs have thermal stability that is consistent with that of other NIPUs/PHUs found in the literature [232,250]. However, it is lower than conventional dimer-based PUs, which typically display decomposition temperatures above 300°C [251,252].

Endothermic or exothermic peaks were not observed in the temperature range examined by DSC (**Figure D 5**), indicating that both PHUs are amorphous. The DSC traces showed two T_gs for DDP, whereas MDP showed a single T_g. The first T_g observed in DDP (-30°C) could be associated with the presence of soft segments due to Priamine 1074 and the second T_g (29°C) could be attributed to the presence of hard segments formed by DAD. The presence of two T_gs in the DSC results for DDP indicates that DDP has a segmented block-like structure with DGC serving as a bridging component between them because if there were two populations of PHUs formed, the GPC traces would have appeared bimodal instead of monomodal (**Figure D 6**) [108]. The two T_gs suggest possible microphase separation. To assess whether the segments are miscible, the Hoftyzer-Van Krevelen method was conducted to estimate the Hansen solubility parameters of DAD/DGC and Priamine 1074/DGC hydroxyurethane linkages [253–255]. Briefly, the cohesive forces in liquids and amorphous polymers depend on dispersion forces, polar forces, and hydrogen bonding, and therefore, estimating the solubility parameter is typically divided into three components : δ_d, δ_p and δ_h, respectively [256]. The difference in solubility parameters ($\Delta\delta$) of DAD/DGC and Priamine 1074/DGC is 4.97 $(MJ.m^{-3})^{0.5}$, which is below the value that polymers are considered miscible ($\Delta\delta < 5$ $(MJ.m^{-3})^{0.5}$) [255] (**Table D 1**). The T_g observed for MDP was higher that the T_{g1} observed for DDP which could be attributed to the presence of the stiffer furan ring in the structure of MDP, making PHU chains less flexible.

In addition, rheological studies were conducted on the synthesized PHUs to investigate the impact of the dicarbonate used in their synthesis. As seen in **Figure 6.2** and **Figure D 7**, both MDP and DDP have similar G' and G'' values, exhibiting solid-like behavior at 25°C with $G' > G''$. MDP generally exhibits higher G' values than DDP, which may be attributed to its stiffer structure resulting from the presence of furan rings. From dynamic mechanical thermal analysis (DMTA) results (**Figure 6.3**), it is interesting to note that a new peak emerges for MDP at a temperature range of 100-120°C. One possible explanation for this phenomenon is that, at elevated temperatures, there may be a re-orientation of MBC-based PHUs due to the presence of furan ring in their structure [94].

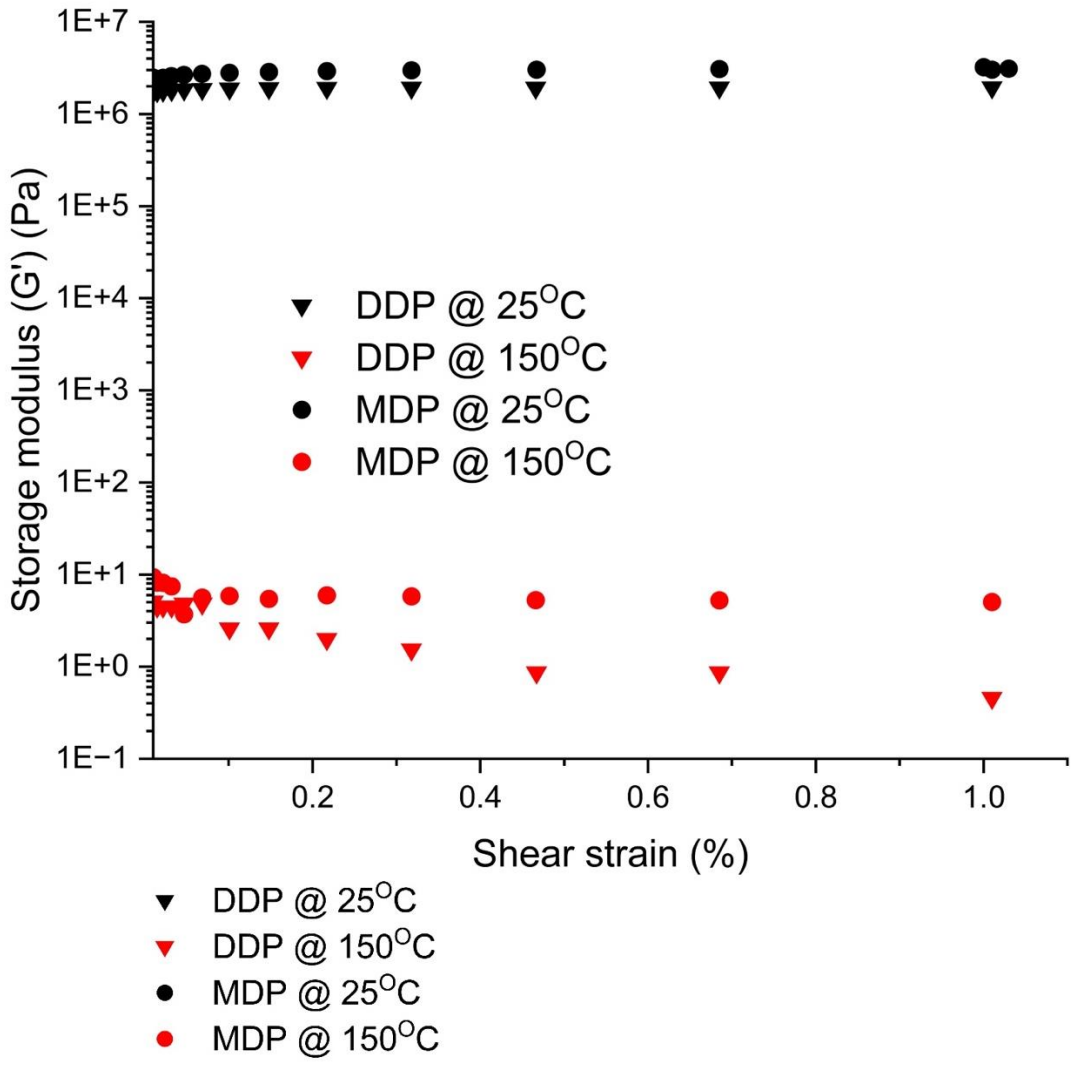

Figure 6.2. Amplitude sweep results performed on the synthesized PHUs at 25°C and 150°C with frequency of 1 Hz.

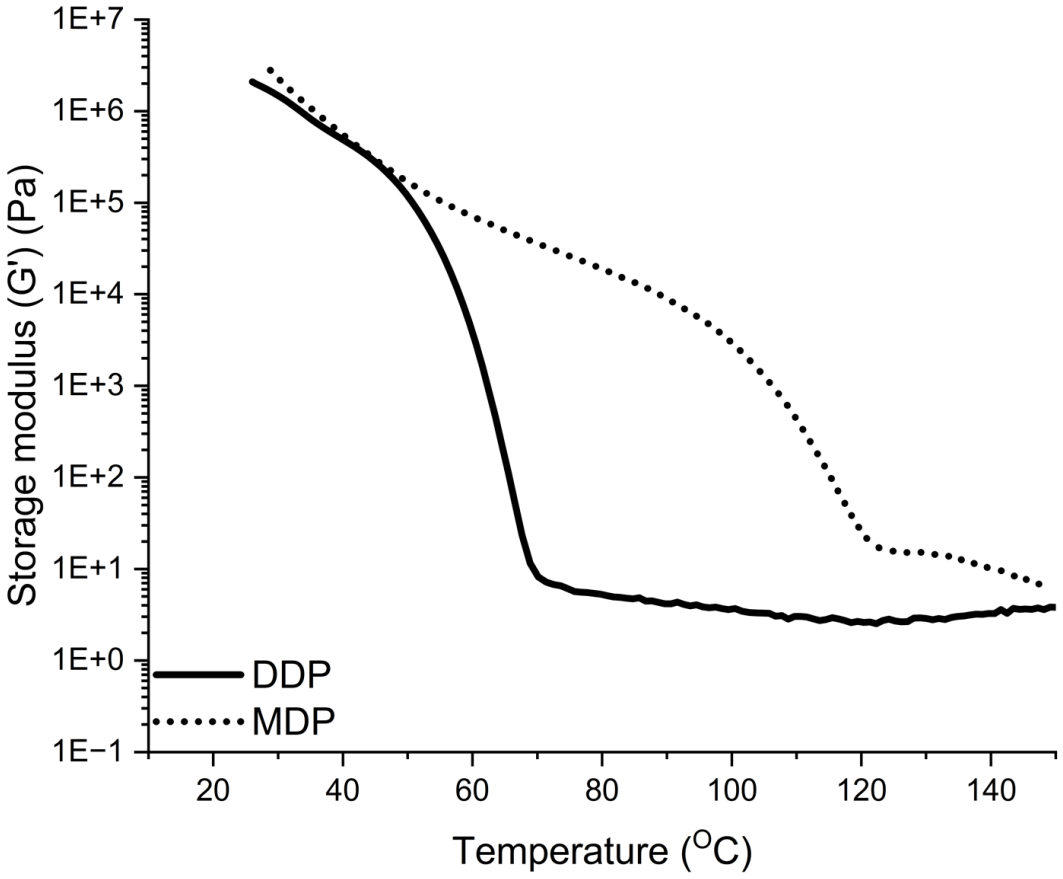

Figure 6.3. DMTA results of the synthesized PHUs in the temperature range of 25-150°C.

6.3.2. Synthesis of crosslinked C13MA-based NIPUs using amine-ended PHUs

Following the preparation of carbonated poly(C13MA-*co*-GMA)s, amine-terminated PHUs (DDP and MDP) were employed as crosslinkers to synthesize thermoset NIPUs (**Scheme 6.1**, prepared samples with DDP are called NIPUDDP-xx, where xx refers to the rounded % initial molar fraction of C13MA in poly(C13MA-*co*-GMA), the MDP-based NIPUs are named using the same naming system as NIPUMDP-xx). The curing process of all NIPUs was carried out at 100°C, using an amine to cyclic carbonate ratio of 1. The polyaddition reaction between amines and cyclic carbonates tends to be slower compared to the reaction of isocyanates with alcohols [257]. To accelerate the reaction rate, various methods can be employed, such as increasing the temperature or adding excess amine [8,65]. It should be noted that while increasing temperature can enhance reactivity of amines towards cyclic carbonates, it can come at the expense of side reactions, such as the production of urea [17]. In the case of excess diamine, amine-terminated urethane linkages can be formed that do not contribute to the crosslinked networks. This can lead to reduced tensile strength and lower gel content in the final product [144]. Additionally, the excess diamine can react with the ester groups of methacrylates, leading to the formation of amides, [187,230,231], resulting in a network having lower crosslinking density with unreacted free species due to the aminolysis of the ester groups. Effects of using an excessive amount of diamine or conducting the reaction at elevated temperatures have been reported elsewhere [187,236]. Therefore, in our study the temperature was set at 100°C and the amine-to-cyclic carbonate ratio was fixed at 1.

The conversion of cyclic carbonates to urethane linkages was confirmed using FTIR. **Figure 6.4** shows the FTIR spectra for NIPUDDP-70 and NIPUMDP-70. As seen from **Figure 6.4**, the

characteristic absorption peak for OH stretching of the hydroxyl group which is formed through the ring-opening of cyclic carbonates at 3370 cm^{-1}, and 1525 cm^{-1} due to the NH deformation of the urethane group, confirmed the conversion of cyclic carbonate functional groups to urethane linkages [8,139,144]. It should be mentioned that the peak at 1720 cm^{-1} attributed to C=O stretching of the urethane group overlaps with ester groups present in C13MA/GMA copolymer structure. The absence of an absorption peak at approximately 1650 cm^{-1} for the amide suggests that there was no aminolysis of ester groups [144].

An observed weak peak of residual carbonate at 1800 cm^{-1} indicates that the conversion of cyclic carbonate to urethane was not fully completed, as noted previously [8,144,188,189]. The conversion of cyclic carbonate functional groups to urethanes is calculated from the FTIR peak absorbance and the results are summarized in **Table 6.2**. The conversions were determined using **Equation 6.1** which calculates the band area ratio between the urethane group and the total of carbonate and urethane groups.

$$Conversion = \frac{\int urethane}{\int carbonate + \int urethane} \times 100 \quad (6.1)$$

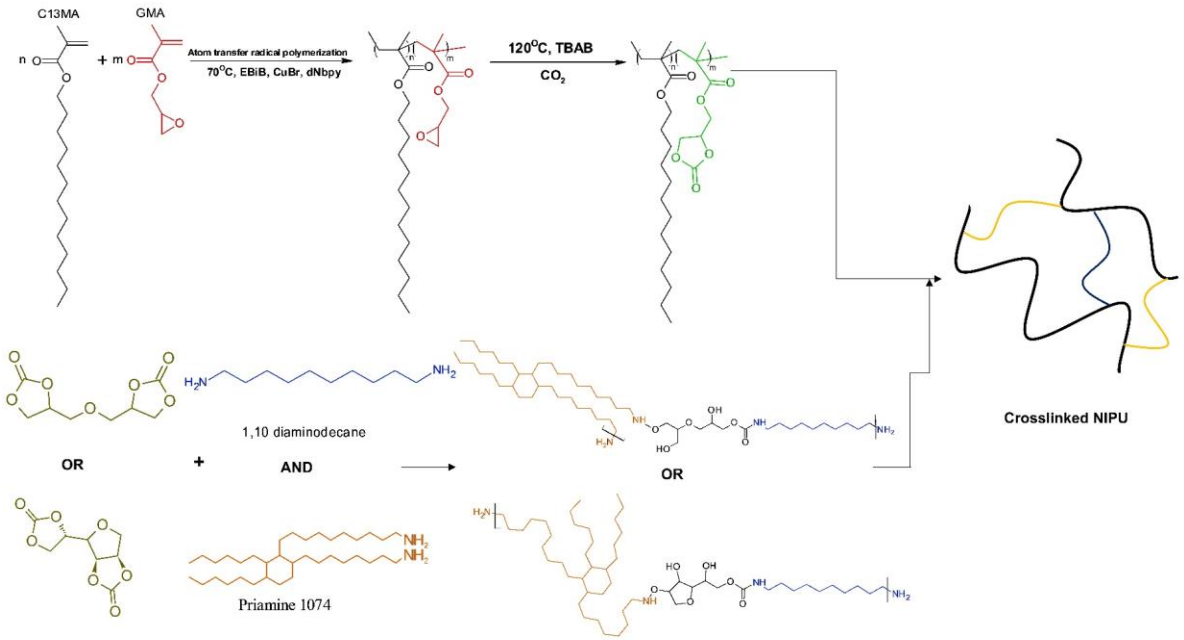

Scheme 6.1. Preparation of thermoset hybrid NIPUs.

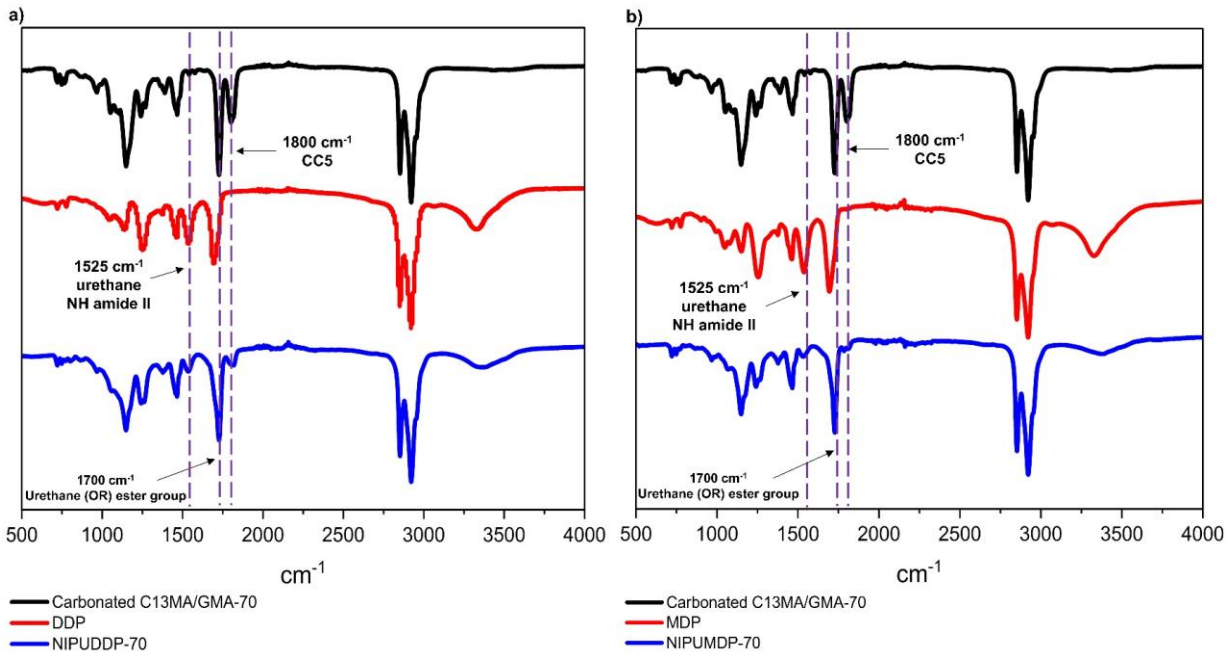

Figure 6.4. FTIR spectra for the crosslinked NIPUs; a) carbonated C13MA/GMA-70, DDP and NIPUDDP-70 and b) carbonated C13MA/GMA-70, MDP and NIPUMDP-70.

The crosslinked NIPUs exhibited high conversions, ranging from 75% to 95%. The conversion of cyclic carbonates to urethanes is known to be limited, due to the high viscosity of growing chains and the presence of hydrogen bonds in the mixture [52,258]. The reported values in this study are high for solvent- or catalyst-free systems [259]. As observed in **Table 6.2**, the conversion of cyclic carbonates to urethane linkages decreases as the number of urethane linkages (which is equivalent to the number of cyclic carbonates on the carbonated C13MA/GMA) increases. This can be attributed to the higher viscosity of the carbonated copolymer parent, which hinders the mobility of the chains. In addition, MDP-based NIPUs had generally lower urethane conversion compared to DDP-based crosslinked NIPUs. This can be associated with the presence of furan rings in the structure of MBC, retarding the movements of the chains.

Table 6.2. Mechanical properties[a)] of crosslinked NIPUs.

Sample ID[b)]	# of urethane linkages on each backbone	F_{C13MA} [c)]	FTIR conversion (%)	E [d)] (MPa)	EB [e)] (%)	Ultimate stress (MPa)	M_c (g mol^{-1})	Swelling ratio in THF (%)	Swelling ratio in water (%)	Gel content (%)	BRC [f)] (%)
NIPUDDP-90 [g)]	2	0.91	95	2.35 ± 0.45	95 ± 10	0.93 ± 0.12	3800	530.45 ± 12.55	9.25 ± 2.35	97 ± 1.8	84
NIPUDDP-80	5	0.87	89	4.43 ± 0.75	90 ± 7	1.55 ± 0.41	2600	470.30 ± 15.21	11.05 ± 1.76	95 ± 2.1	88
NIPUDDP-70	9	0.66	80	20.85 ± 1.73	51 ± 5	4.15 ± 0.37	2200	188.72 ± 3.51	15.31 ± 2.72	89 ± 1.5	95
NIPUMDP-90 [h)]	2	0.91	92	1.24 ± 0.61	50 ± 7	0.28 ± 0.11	8800	397.35 ± 13.27	7.51 ± 2.30	94 ± 1.8	83
NIPUMDP-80	5	0.87	82	2.07 ± 0.24	37 ± 3	0.45 ± 0.13	4500	327.31 ± 7.79	14.74 ± 1.36	87 ± 2.6	88
NIPUMDP-70	9	0.66	78	6.45 ± 1.05	24 ± 4	1.01 ± 0.10	2750	232.57 ± 28.27	18.80 ± 3.78	84 ± 2.3	91

([a)] Three replicates for each crosslinked NIPU were applied, results for every individual samples are taulated in Table S2); ([b)] Experimental identification given by NIPU-xx, where xx refers to the rounded % initial molar fraction of C13MA in poly(C13MA-*co*-GMA)); ([c)] Final molar fraction of C13MA in copolymer composition extracted by ^{1}H NMR); ([d)] Young's moduli, E, are calculated in the linear region of the stress-strain curve for 2% elongation); ([e)] Elongation at break); ([f)] Biorenewable carbon content); ([g)] The crosslinked NIPUs, resulting from the reaction between poly(C13MA-*co*-GMA)s and DDP, are termed NIPUDDP-xx, where xx denotes the approximate initial molar fraction of C13MA in poly(C13MA-*co*-GMA)); ([h)] The crosslinked NIPUs, resulting from the reaction between poly(C13MA-*co*-GMA)s and MDP, are termed NIPUMDP-xx, where xx denotes the approximate initial molar fraction of C13MA in poly(C13MA-*co*-GMA)).

To assess the crosslinking density, swelling tests were also conducted on the crosslinked NIPUs. The swelling ratios in THF and water are tabulated in **Table 6.2**. As seen from the table, NIPUDDP-90 swelled to a higher degree (530.45 ± 12.55%) compared to NIPUDDP-80 and NIPUDDP-70 due to longer chains between crosslinks (188.72 ± 3.51% for NIPUDDP-70 and 470.30 ± 15.21% for NIPUDDP-80), signifying a tighter crosslinked network. Swelling ratios of the crosslinked NIPUs were also measured in water. Presence of hydrophilic primary and secondary hydroxyl groups in the main chain of PHUs can result in poor water resistance [31]. The measured water uptakes in this study are close to the reported values for conventional PUs [31]. It can be seen that NIPUDDP-70 has the highest water uptake (15.31 ± 2.72%) among all DDP-based NIPUs (11.05 ± 1.76% for NIPUDDP-80 and 9.25 ± 2.35% for NIPUDDP-90) which is due to higher number of urethane linkages (higher concentration of hydroxyl groups) in the network. Same positive correlation between number of urethane linkages and water uptake can be seen for MDP-based NIPUs with NIPUMDP-70 having water uptake of 18.80 ± 3.78% compared to 14.74 ± 1.36% for NIPUMDP-80 and 7.51 ± 2.30% for NIPUMDP-90.

Gel content (*GC*) values are also reported in **Table 6.2**. All the reported *GC* values are above 85%, highlighting the high conversion of cyclic carbonates to urethane linkages. The overall lower *GC* values for MDP-based NIPUs compared to DDP-based ones could be due to MDP being more viscous, limiting the movement of the chains.

DMTA was used to analyze viscoelastic behavior of crosslinked NIPUs. Storage moduli of the NIPUs as well as their tanδ response are presented in **Figure 6.5**. DDP-based NIPUs exhibited a noticeable peak in their tanδ response, suggesting the presence of a T_g. In contrast, no such peak was observed in the tanδ response of MDP-based NIPUs within the tested temperature range of 30-150°C.A positive correlation was observed between the number of urethane linkages and the

T_g of the NIPUs, as the crosslinks restrict the movement of the chains. The T_g of NIPUDDP-70, which contained 9 urethane linkages on its C13MA/GMA template, was 20°C higher than that of NIPUDDP-90, which contained only 2 urethane linkages on its template, indicating higher crosslinking density, consistent with the swelling ratio values. Using $M_c = 3RT\rho E_r'$ (6.2, M_c values for the crosslinked networks were calculated and they were consistent with *SR* values. For instance, NIPUMDP-90, which had 2 urethane linkages on its C13MA/GMA template, exhibited M_c of 88000 g mol^{-1}, while NIPUMDP-70, which had 9 urethane linkages on its template, displayed a significantly lower M_c of 2750 g mol^{-1}.

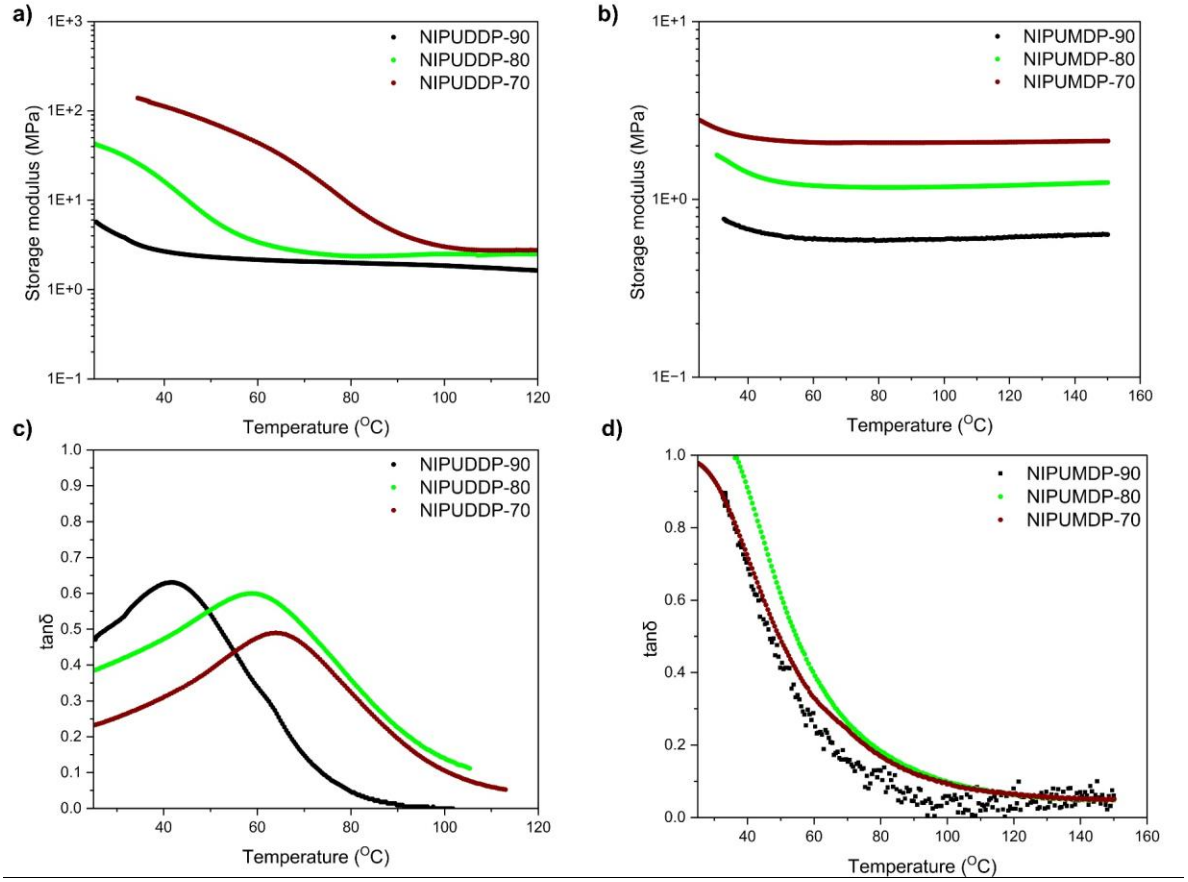

Figure 6.5. DMTA results for the crosslinked NIPUs; a) storage modulus versus temperature for DDP-based NIPUs, b) storage modulus versus temperature for MDP-based NIPUs, c) tanδ response of DDP-based NIPUs and d) tanδ response of MDP-based NIPUs.

Tensile tests were performed on the samples to characterize the mechanical properties of the crosslinked NIPUs. **Figure 6.6** shows engineering stress-strain curves for all crosslinked NIPUs. The stress-strain data exhibited varying behavior depending on the crosslink density of the network. A positive correlation between Young´s moduli (*E*) of the NIPUs with concentration of urethane linkages was observed. As the number of urethane linkages on the C13MA/GMA template increased from 2 to 9, the *E* values of DDP-based NIPUs increased from 2.35 ± 0.45 MPa to 20.85 ± 1.73 MPa. A similar trend was observed in MDP-based NIPUs, where the Young's moduli increased from 1.24 ± 0.61 MPa to 6.45 ± 1.05 MPa with an increase in urethane linkage concentration from 2 to 9 on each chain. In general, the Young's moduli observed in this study were higher than those in our previous study, where crosslinking of carbonated C13MA/GMA templates was done with 1,10-diaminodecane (for the same number of urethane linkages) [144]. The higher concentration of hydroxyl groups in the crosslinkers used in this study (DDP and MDP) could have contributed to the observed increase in Young's moduli, as the increased presence of hydroxyl groups could lead to greater molecular interaction. Samples with higher crosslinking density exhibited more brittleness, which is due to the limited molecular mobility and chain disentanglement resulting from the crosslinks [8]. For instance, NIPUMDP-70, which had the highest crosslink density, demonstrated an elongation at break of 24 ± 4%, while NIPUMDP-90, with the lowest crosslink density, had an elongation at break of 50 ± 7%. NIPUDDP-70 and NIPUMDP-70, which had the highest concentration of urethane linkages, exhibited the greatest toughness (highest ultimate stress) due to intermolecular hydrogen bonding between the urethane groups. This bonding improved the toughness of the NIPUs by converting mechanical energy to heat through the breaking and forming of hydrogen bonds [191].

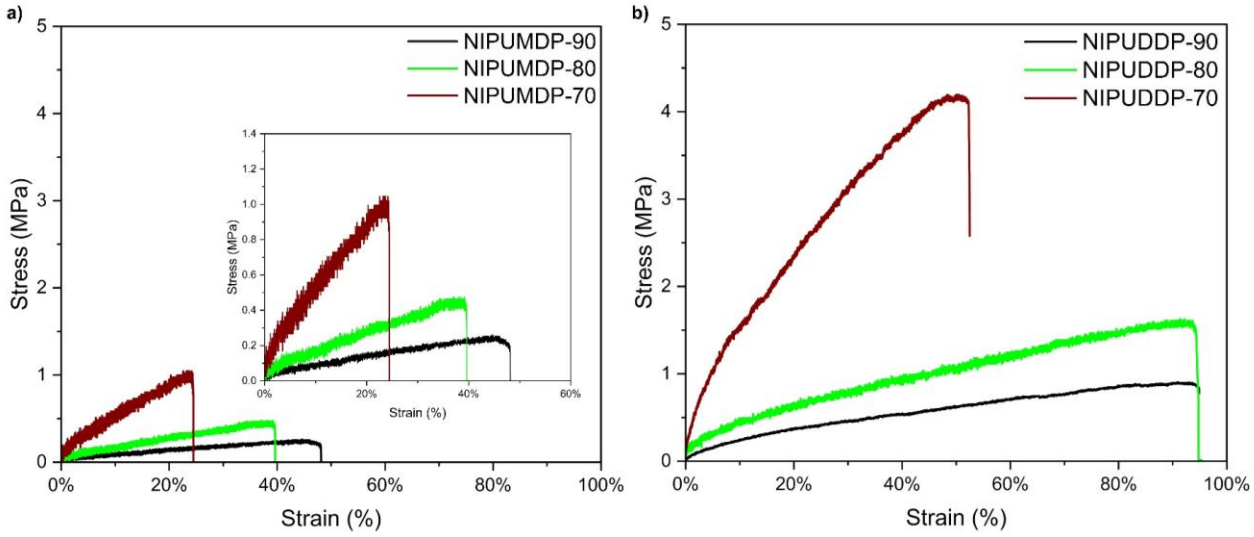

Figure 6.6. Engineering stress-strain results of the crosslinked NIPUs; a) crosslinked MDP-based NIPUs and b) crosslinked DDP-based NIPUs.

Lastly, thermal stability of the crosslinked NIPUs was analyzed using TGA. TGA thermograms are shown in **Figure D 8** and decomposition temperatures are tabulated in **Table 6.3**.

Table 6.3 reports that the crosslinked NIPUs exhibited higher thermal stability than their parent carbonated copolymers [144] as well as DDP and MDP PHUs. For example, $T_{d,10\%}$ of NIPUDDP-70 is 46°C higher than DDP and 31°C higher than carbonated C13MA/GMA-70 [144].

Table 6.3. Decomposition temperatures for 5%, 10%, 50% and 100% weight loss for the crosslinked NIPUs.

Sample ID	$T_{d,5\%}$ (°C)	$T_{d,10\%}$ (°C)	$T_{d,50\%}$ (°C)	$T_{d,final}$ (°C)
NIPUDDP-90 [a)]	275	305	399	645
NIPUDDP-80	285	309	415	602
NIPUDDP-70	304	306	428	615
NIPUMDP-90 [b)]	277	308	399	635
NIPUMDP-80	267	290	405	600
NIPUMDP-70	247	267	428	615

([a)] The crosslinked NIPUs, resulting from the reaction between poly(C13MA-*co*-GMA)s and DDP, are termed NIPUDDP-xx, where xx denotes the approximate initial molar fraction of C13MA in poly(C13MA-*co*-GMA)); ([b)] The crosslinked NIPUs, resulting from the reaction between poly(C13MA-*co*-GMA)s and MDP, are termed NIPUMDP-xx, where xx denotes the approximate initial molar fraction of C13MA in poly(C13MA-*co*-GMA)).

6.4. Conclusion

Amine-terminated polyhydroxyurethanes (PHUs) were synthesized via the terpolymerization of Priamine 1074 and 1,10-diaminodecane (DAD) with either diglycerol dicarbonate (DGC) or mannitol biscarbonate (MBC). Rheological and thermal properties of the synthesized PHUs were studied. Regardless of the type of dicarbonate used, the PHUs exhibited similar rheological and thermal behaviors. The PHUs were then used as a crosslinkers to react with carbonated copolymer templates to synthesize a set of thermoset non-isocyanate polyurethanes (NIPUs). To provide the carbonated copolymers, C13MA/GMA copolymers with varying compositions were synthesized via atom transfer radical polymerization (ATRP) at 70°C. The pendent epoxy functional groups available on the backbone of the copolymers were then converted into cyclic carbonates using CO_2 and TBAB catalyst with nearly 100% conversion and were subsequently reacted with the synthesized amine-ended PHUs to produce crosslinked NIPUs with varying concentrations of urethane linkages. Young's moduli of the NIPUs based on MBC crosslinker improved from 1.24 ± 0.61 MPa to 6.45 ± 1.05 MPa as the number of urethane linkages increased from 2 to 9. A similar trend was also observed for NIPUs which were crosslinked with DGC-based crosslinkers with E values ranging from 2.35 ± 0.45 MPa to 20.85 ± 1.73 MPa. The samples with higher concentrations of urethane linkages were more brittle, attributed to the denser crosslink network, which limited polymer chain mobility. The thermoset NIPUs crosslinked with DGC-based PHUs exhibited a T_g range of 40°C to 60°C, which depended on the number of urethane linkages present on the C13MA/GMA template. The NIPU with the highest crosslink density had the highest T_g (60°C), whereas the NIPU with the lowest crosslink density showed the lowest T_g (40°C).

Finally, this study represents the first investigation of amine-ended PHUs synthesized from bio-sourced precursors via terpolymerization, and their use as crosslinkers to produce thermoset NIPUs. By modifying the number of epoxy functional groups on their parent C13MA/GMA copolymers and use of DGC- or MBC-based PHUs, the partially bio-based crosslinked NIPUs display varying mechanical properties, enabling them to be tailored for a broad range of applications, spanning from soft, rubbery-like materials to tough coatings.

6.5. Experimental Section

Materials: Diglycerol (DIG, ≥80% α, α, impurities consist of mono-, α, β-di-, β, β-di, and triglycerol) was obtained from Tokyo Chemical Industry (TCI). Dimethyl carbonate (DMC, ≥99%, anhydrous) and potassium carbonate (K_2CO_3, 98%, anhydrous powder) were purchased from Acros. Basic and neutral alumina (Al_2O_3, Brockmann, Type II 150 mesh), calcium hydride (CaH_2, 90-95% reagent grade), Ethyl α-bromoisobutyrate (EBiB, 98%), copper (I) bromide (Cu(I)Br, 99%), 4,4'- Dinonyl- 2,2'-dipyridyl (dNbpy, 97%), tetrabutylammonium bromide (TBAB), chloroform ($CHCl_3$, >99.8% contains ethanol as stabilizer), deuterated chloroform ($CDCl_3$, 99.8%), anisole D-mannitol (≥98% powder) and 1,5,75-triazabicyclo[4.4.0]dec-5-ene (TBD, 98%), 1,4-dioxane (>99%, ACS reagent) were purchased form Sigma-Aldrich and used without further purification. Priamine 1074 was provided by Cargill and used as recieved. Methanol (MeOH, >99%), heptane and tetrahydrofuran (THF, 99.9% HPLC and certified grades), ethyl acetate (EtOAc, certified grade), dimethyl sulfoxide (DMSO) and 1,10-diaminodecane (DAD, 98%) were purchased from Fisher Scientific and used as received. Glycidyl methacrylate (GMA, 97%), C13 alkyl methacrylate (C13MA, *n*-alkyl average chain length of 13.0 units, >99%, Visiomer Terra C13-MA) were obtained from Sigma-Aldrich and

Evonik (via TRC), respectively. The monomers were purified by passing through a column of basic alumina mixed with 5 wt % calcium hydride and then kept in a sealed flask under nitrogen atmosphere in a refrigerator. Syntheses were all carried out under nitrogen atmosphere with high purity (99.99%, Praxair). Carbon dioxide (CO_2) with a purity of 99.99% was purchased from Praxair and used as received.

Diglycerol dicarbonate (DGC) synthesis: The synthesis of DGC was performed using procedures reported elsewhere [85,94]. First, DIG (29.19 g, 0.175 mol), DMC at a 10:1 molar ratio of DMC: DIG (158.5 g, 1.75 mol) and potassium carbonate as a catalyst at 0.5 wt% of the DIG (0.14 g) were added to a 250-ml three-necked round-bottom flask equipped with a thermal well and a magnetic stir bar. The setup was placed on a heating mantle on a magnetic stirrer for mixing the mixture. To prevent evaporation of the monomers, a condenser was utilized, which circulated a 50:50 volume mixture of ethylene glycol and purified water via reverse osmosis. The temperature of the condenser was set to 5°C. The mixture was then purged with nitrogen for 15 minutes to eliminate any contamination, and a needle at the top of the reflux was used to vent the nitrogen purge. Next, nitrogen purged was stopped and a thermocouple was inserted into the thermal well and connected to a temperature controller. The reaction temperature was then adjusted to 80°C and the mixture was allowed to react for 24 hours.

After 24 hours, the reaction was stopped and cooled down and then filtered with a vacuum pump to remove the catalyst. The filtrate was left under air flow overnight to remove methanol formed during the reaction. Afterward, 100 ml of reverse osmosis (RO) purified water, previously refrigerated, was added to the mixture and mixed for almost an hour to dissolve any unreacted DIG and facilitate the crystallization of DGC. The resulting mixture was once again filtered using a vacuum pump, and the precipitated powder was collected and dried overnight in a

vacuum oven at 40°C. Proton nuclear magnetic resonance (^{1}H NMR) was used to confirm the synthesis of DGC (**Figure D 9**). The DGC yield was determined to be 55% based on the amount of DIG used in the reactor.

Mannitol biscarbonate (MBC) synthesis: MBC was synthesized according to the procedure provided in the literature [94]. D-mannitol (29.14 g, 0.16 mol), DMC (100.87 g, 1.11 mol, or 7 molar equivalents with respect to D-mannitol) and 5 mol% of TBD with respect to D-mannitol (1.11 g, 7.9 mmol) were added to a 250-ml three-necked round-bottom flask equipped with a thermal well and a magnetic stir bar. The setup was positioned on a heating mantle and connected to a condenser, and the mixture was stirred using a magnetic stirrer. After purging the mixture with nitrogen for 15 minutes, a thermocouple was inserted into the thermal well and connected to a temperature controller. The reaction temperature was then set to 80°C and maintained for 16 hours. After 16 hours, the reaction was stopped and cooled down to ambient temperature. Subsequently, the mixture was filtered using a vacuum pump to remove the catalyst. The remaining DMC and any methanol formed during the reaction were then evaporated by exposing the mixture to air overnight. Next, refrigerated RO purified water was added to the mixture and mixed for almost two hours. After two hours, the precipitated MBC was filtered using a vacuum pump and subsequently dried overnight in a vacuum oven at 40°C. The MBC synthesis was confirmed using ^{1}H NMR (**Figure D 10**). The yield of MBC was 60% based on the amount of D-mannitol added to the reactor.

Polyhydroxyurethanes (PHUs) synthesis: The PHU terpolymers were synthesized using polyaddition of DGC with Priamine 1074 and DAD, with a fixed molar ratio of 0.6/0.4 for Priamine 1074 to DAD. The same ratio was used for the polyaddition of MBC with Priamine 1074 and DAD. It should be noted that the high viscosity of the mixture required addition of a

solvent. Thus, dioxane was added as a solvent at a concentration of 50 wt% with respect to DGC/MBC. To ensure that the PHUs are terminated with NH_2, an excess amount of Priamine 1074 was added.

Here preparation of MDP is given as an example. MBC (10.23 g, 0.047 mol), DAD (4.75 g, 0.023 mol), Priamine 1074 (18.5 g, 0.035 mol) and dioxane (5 g) were added to a 150-ml two-neck round-bottom flask, equipped with a thermal well and a high viscosity magnetic stir bar. To remove any contamination, the mixture was purged with nitrogen for 15 minutes before increasing the temperature to 85°C. After 24 hours the reaction was stopped and cooled down to ambient temperature. The mixture was then dissolved in chloroform and filtered with vacuum pump to remove undissolved MBC. Next, excess heptane was added to remove the excess diamines while precipitating the polymer. The formation of PHUs and absence of cyclic carbonate were confirmed using ^{1}H NMR and FTIR (**Figure D 1**-**Figure D 3**).

Copolymerization of C13MA/GMA by atom transfer radical polymerization (ATRP): The procedure outlined in a previous study was used to synthesize C13MA/GMA copolymers with different initial molar ratios of GMA ranging from 0.1 to 0.3 [144]. The targeted number average molecular weight ($M_{n,target}$) for the copolymers was 10000 g mol^{-1}. The copolymerization resulted in the synthesis of copolymers with M_n ranging from 8500-9400 g mol^{-1} and dispersity ($Đ$) between 1.19-1.25 relative to PMMA standards [144]. The conversions for all copolymers were more than 90%.

Carbonation of the copolymers: After synthesis of the copolymers, they were treated with carbon dioxide (CO_2) and TBAB as catalyst to convert epoxy functional groups to cyclic carbonates, as reported elsewhere [144]. An example of carbonation is provided using C13MA/GMA-90. TBAB (0.21g, 6.51×10-4 mol, 5 mol% relative to epoxy groups on copolymer chain) was introduced

into a 150 ml three-neck round-bottom flask containing poly(C13MA-*co*-GMA) (51.37g, 0.0064 mol). The setup, including a thermal well and magnetic stir bar, was positioned on a heating mantle and sealed with rubber septa. After purging the mixture with CO_2 for 30 minutes to eliminate oxygen, the temperature was raised to 120°C. Stirring the mixture continued under a CO_2 stream with pressure < 5 psi for 24 hours. The carbonated copolymers had M_n values ranging from 9500-10500 g mol^{-1} and $Đ$ between 1.20-1.35 relative to PMMA standards [144]. The overall conversion of the carbonation ($X_{carbonation}$) was calculated using ^{1}H NMR via the disappearance of the peak at 2.55 ppm assigned to the epoxy ring and appearance of new peaks at 4.65 ppm attributed to the C-H resonance in the α-position of the cyclic carbonate groups. The conversions for all carbonated copolymers were more than 95% after 24 hours. **Figure D 11** shows the ^{1}H NMR spectrum of carbonated C13MA/GMA-80 (samples are referred to as C13MA/GMA-xx, where "xx" represents the approximate percentage of C13MA in the copolymer). It should be noted that only the peak at 4.65 ppm was utilized for carbonation conversion, as the peak at 4.10 ppm, also associated with cyclic carbonate groups, could potentially overlap with any remaining initiator or solvent (anisole) in the copolymer. The calculation for carbonation conversion is detailed in the Supplementary Information. Furthermore, based on the GPC results, the peak for the carbonated copolymer remains monomodal and exhibits negligible broadening in comparison to the pre-carbonated copolymer (**Figure D 12**). This indicates no thermal degradation occurred. Additionally, a minor shift is observed in the chromatogram of the carbonated copolymer, attributed to its different solubility in the eluent.

Synthesis of crosslinked non-isocyanate polyurethanes (NIPUs) from amine-ended PHUs: In order to achieve adequate mixing of carbonated C13MA/GMA copolymers with the synthesized

amine-ended PHUs, ethyl acetate was used as a solvent to dissolve both the carbonated copolymers and PHUs. Here, an example of DDP addition to carbonated C13MA/GMA-90 is provided. In a 50-ml three-neck round-bottom flask, carbonated C13MA/GMA-90, which contains an average of three cyclic carbonate functional groups per chain (4.96 g, 5.25×10^{-4} mol), DDP (4.25 g, 8.5×10^{-4} mol), and ethyl acetate (5 g, 0.057 mol) were added. The ratio of amine functional groups to cyclic carbonate functional groups was at 1:1. A thermal well, a magnetic stir bar, and a condenser were installed in the reactor, and the entire setup was placed on a heating mantle with a magnetic stirrer. Next, oxygen was eliminated from the mixture by purging the contents with nitrogen for 15 minutes. After 15 minutes of purging, the temperature was increased to 65°C, which is below the boiling point of ethyl acetate (~77°C). After one hour, the mixture was removed from the reactor and dried under air flow for an additional hour. The mixture was then placed in a vacuum oven at room temperature for two hours to eliminate any residual ethyl acetate. The mixture was then poured into tensile molds and then placed in an oven at a temperature of 90°C for 24 hours to ensure complete reaction of the cyclic carbonates with the amine-ended PHUs. FTIR was utilized to confirm the disappearance of cyclic carbonates and appearance of urethane linkages.

Proton Nuclear Magnetic Resonance (^1H NMR) Spectroscopy: ^{1}H NMR was used to characterize the synthesized copolymers, carbonated copolymers, PHUs, DGC and MBC. 3-5 mg of polymer was dissolved in 1 ml of $CDCl_3$ and subsequently transferred to a NMR tube. DMSO-d_6 was the solvent used for the characterization of DGC and MBC.

Solution-phase proton NMR spectra were recorded on a Bruker Avance III HD (500 MHz, 32 scans) spectrometer at room temperature. The analysis was done with a zg30 pulse sequence, and the resulting spectra was analyzed using Mestrelab MNova software.

Fourier Transform Infrared (FTIR) Spectroscopy: FTIR was performed on PHUs and the crosslinked NIPUs. The instrument used was a Nicolet iS50 FTIR Spectrometer, which was equipped with a single bounce diamond attenuated transmission reflectance (ATR) for solids. First, a background reading was performed on a clean diamond to acquire an accurate baseline. Thirty-two scans were recorded for each sample over the range 4000-500 cm^{-1} with a normal resolution of 4 cm^{-1}.

Size Exclusion Chromatography (SEC): The synthesized PHUs and copolymers were dissolved in HPLC grade THF at a concentration of 2.5 g L^{-1} in a 1-dram glass vial. Gel permeation chromatography (GPC, Water Breeze, differential refractive index RI 2414 detector, 40°C) using HPLC grade THF as an eluent with flow rate 0.3 mL min^{-1} was used to determine the M_n and $Đ$. The instrument is equipped with three Waters Styragel HR columns: HR1 for molecular weights ranging from 10^2 to 5×10^3 g mol^{-1}, HR2 for molecular weights ranging from 5×10^2 to 2×10^4 g mol^{-1}, and HR4 for molecular weights ranging from 5×10^3 to 6×10^5 g mol^{-1}. Additionally, it is equipped with a refractive index detector (RI 2414) and a guard column. The columns were maintained at a temperature of 40°C while passing an injection of 10 µl of dissolved samples through. The elution time for the samples was 60 min. M_n values were calculated relative to narrow molecular weight distribution poly(methyl methacrylate) (PMMA) standards (Varian Polymer Standards, molecular weights ranging from 875 to 1677000 g mol^{-1}).

Differential Scanning Calorimetry (DSC): Glass transition temperatures (T_g)s of the synthesized PHUs were measured by Differential Scanning Calorimetry (DSC). For the analysis, a TA Instrument Discovery 2500 differential scanning calorimeter using standard hermetic aluminum pans (pan top with a pinhole), calibrated with indium and nitrogen purge was used. A heat-cool-heat experiment was conducted with heating rate of 5°C min^{-1} and cooling rate of 10°C min^{-1}.

During the heating cycles, the temperature was increased to 200°C, whereas in the cooling cycles, it was decreased to -90°C. All data was extracted from the second heating cycle after thermal history was removed during the first heating cycle and inflection method was used to measure T_gs. Universal Analysis and Trios software were used to analyze the results.

Thermogravimetric Analysis (TGA): Thermal stability of the crosslinked NIPUs were investigated by thermogravimetric analysis (TGA). A TA Instruments Discovery 5500 thermo-gravimetric analyzer was used to analyze the degradation of synthesized materials at a heating rate of 10°C min^{-1} from ambient temperature to 700°C under nitrogen purge in platinum pans. The process begins by cleaning a small platinum pan with a blow torch to remove any residual material from prior samples. The pan is subsequently weighed and tared, following which 3-10 mg of the sample is added. The pan containing the sample is then placed in the furnace chamber and heated in a nitrogen atmosphere. The 10% degradation temperature ($T_{d,10\%}$), final decomposition temperature ($T_{d,final}$) and ash content were extracted from this test. Universal Analysis and Trios software were used to analyze the results.

Rheology: Rheology tests were run on PHUs and the crosslinked NIPUs. Dynamic mechanical thermal analysis (DMTA) was conducted on the networks using a torsion configuration (SRF 12) with a temperature ramp rate of 5°C min^{-1} (from ambient temperature to 150°C under nitrogen atmosphere using a CTD 450 convection oven with air flow of 1400 NL h^{-1} for the cooling shaft and 850 NL h^{-1} for nitrogen purge to the furnace), with an oscillation strain of 1% and a frequency of 1 Hz. The tests were done in an Anton Paar Instruments rheometer (MCR 302). **Equation 6.2** [142] was used to calculate molecular weight between crosslinks (M_c) for the crosslinked networks at room temperature.

$$M_c = \frac{3RT\rho}{E_r'} \quad (6.2)$$

In **Equation 6.2**, E_r' is the storage modulus in the rubbery region from the DMTA experiments, R is the gas constant, T is the absolute temperature, and ρ is the density of the crosslinked samples.

DMTA and amplitude sweep tests were also performed on the PHUs. For these tests, PHUs were shaped into disks of 25 mm diameter and a thickness of 1−2 mm using a hot press. The pressing was performed with a Carver hydraulic unit model #3925 at 100°C using three cycles of 5, 10, and 15 metric tons for 10 minutes each. Amplitude sweep measurements and DMTA analyses were conducted on the PHU samples using the 25 mm diameter parallel plate configuration (PP25). Amplitude sweep measurements were all conducted at ambient temperature and 150°C at a frequency of 1 Hz and a shear strain ranging from 0.001 to 1%. The DMTA was also done with a temperature ramp rate of 5°C min^{-1} (from ambient temperature to 150°C under nitrogen atmosphere using a CTD 450 convection oven with air flow of 1400 NL h^{-1} for cooling shaft and 850 NL h^{-1} for nitrogen purge to the furnace), with an oscillation strain of 1% and a frequency of 1 Hz.

Mechanical testing: For conducting tensile tests on the crosslinked networks, an EZ Test (Shimadzu) tensile machine equipped with a 500 N load cell was utilized. Tensile properties were measured at ambient temperature at speeds of 5 mm min^{-1} on the crosslinked networks. Young's modulus (E), tensile strength (σ_{max}), and % elongation at break (EB%) were calculated using the average of at least three repeated samples. Three dog-bone shaped samples for each formulation with standard dimensions were cut out to perform tensile testing (ASTM638, type V).

Swelling ratio (SR): THF and water swelling tests were also performed on the crosslinked networks. The swelling ratio (*SR*) was determined by placing three samples weighing approximately 30 mg each into separate glass jars filled with either purified water or THF, and allowing them to soak for 24 hours. The *SR* was calculated using **Equation 6.3**:

$$SR = \frac{m_f - m_i}{m_i} \quad (6.3)$$

In **Equation 6.3**, m_i and m_f are the initial mass of the material and mass of the material after swelling in THF or water, respectively.

Gel content: After *SR* measurements, the samples were placed back into the glass vials. The vials then were placed into a vacuum oven at room temperature for 24 hours. Gel content (*GC*) values were found using the **Equation 6.4**, where m_d and m_i are the mass of the material after drying in the oven and the initial mass of the material, respectively.

$$GC\% = \frac{m_d}{m_i} \times 100 \quad (6.4)$$

In **Equation 6.4**, m_1 and m_2 are the initial mass of the material and mass of the material after swelling in THF or water, respectively.

Oven: The crosslinked NIPUs were cured at 90°C for 24 hours using a Fisherbrand Isotemp model 281A oven.

Biorenewable Carbon Content (BRC): Biorenewable carbon (*BRC*) content was calculated according to **Equation 6.5**.

$$BRC\ (\%) = \frac{Bio\ sourced\ carbon}{Bio\ sourced\ carbon + Fossil\ carbon} \times 100 \quad (6.5)$$

Using Equation 5, BRC values for the thermoset NIPUs were calculated, with non-biobased carbon atoms introduced through the use of GMA monomer. C13MA (with a bio carbon content of 76%) is sourced from pine sap [260], DAD can be produced from bio-based precursors with high yields [261], DGC can be easily prepared from bio-based diglycerol [85], MBC is sugar based and Priamine 1074 is a bio-derived diamine from dimer fatty acids [262]. The molecular weight of each component (e.g. C13MA/GMA copolymers and amine-terminated PHUs) and the molar ratio of bio-based and non-biobased components in the crosslinked NIPUs were identified, and BRC values were reported using **Equation 6.5**.

7. DISCUSSION AND FUTURE WORK

This section aims to provide a brief analysis of the results presented in Chapters 3 through 6, highlighting their key findings. Subsequently, some recommendations for future studies are provided.

7.1. Discussion

This thesis proves the versatility of NIPUs/PHUs as thermoset materials by demonstrating a wide range of mechanical properties via combination of polyaddition and free radical polymerization chemistries. The findings indicate that these materials can serve as competitive alternatives to traditional PUs. Although there has been significant research focus in this area in recent years, many advancements in the field have been limited to the synthesis of bio-based thermoset PHUs from vegetable oils with a fixed number of cyclic carbonates. Moreover, the exploration of mechanical properties has primarily been restricted to variations in diamine structure or the ratio of diamine to carbonate. In contrast, the present thesis introduces a comprehensive approach for the development of thermoset NIPUs. It presents a methodology for preparing templates with the ability to easily manipulate the number of cyclic carbonates, thereby enabling tailored properties for specific applications.

The first manuscript presented in Chapter 3, describes the synthesis of a series of partially bio-based copolymers through radical polymerization of *β*-myrcene (*Myr*) and glycidyl methacrylate (GMA) with varied initial molar fractions of GMA. The *Myr*/GMA copolymerization was conducted in semi-batch mode to ensure that almost all chains contain GMA, since GMA reacted faster and was used up earlier than *Myr*. Next, the copolymers were treated with carbon dioxide (CO_2) and TBAB as catalyst to convert the epoxy functional groups, incorporated through GMA, into cyclic carbonates. The synthesized carbonated poly(*Myr*-*co*-GMA) copolymers were

subsequently reacted with Jeffamine D-4000 to prepare NIPUs with varying numbers of urethane linkages along the polymer chains. Those resins were end-capped via moisture sensitive silanes to provide crosslinked networks. The influence of the epoxy functional group concentration in the parent copolymers of *Myr*/GMA on the mechanical properties of the resulting crosslinked networks was studied. As expected, a positive correlation was observed between the concentration of epoxy functional groups and the Young's moduli (*E*) of the crosslinked networks. However, due to the inherent rubbery and soft nature of both the *Myr*/GMA copolymers and Jeffamine D-4000, the resulting product exhibited a combination of soft backbones and side chains, resulting in low *E* values ranging from 32 kPa to 50 kPa.

In the second manuscript presented in Chapter 4, the objective was to improve the mechanical properties of the resins as well as to investigate the influence of side chain rigidity on the mechanical properties of the synthesized crosslinked networks. To achieve this, a vegetable oil-derived alkyl methacrylate, C13MA, with an average side chain length of 13, was copolymerized with GMA using atom transfer radical polymerization (ATRP) to produce copolymers with flexible backbones. To introduce rigidity to the side chains of the copolymers, 1,10-diaminodecane (DAD) was employed as a diamine instead of Jeffamine D-4000. To be more specific, copolymers of C13MA/GMA were synthesized with varying concentrations of GMA. These copolymers were then treated with CO_2 to introduce cyclic carbonates on the polymer chains. Subsequently, the carbonated C13MA/GMA copolymers were reacted with DAD to create crosslinked networks with different *E* values and significantly higher compared to the initial design presented in Chapter 3.

The resulting crosslinked networks exhibited a range of *E* values from 0.1 MPa to 72 MPa, depending on the number of urethane linkages present in the side chains. The study included an

investigation of not only the mechanical properties but also the rheological properties of the networks. Dynamic mechanical thermal analysis (DMTA) was conducted on the crosslinked networks to assess the impact of the number of cyclic carbonates on each chain. Parameters such as gel time, molecular weight between the crosslinks (M_c), and glass transition temperature (T_g) were investigated. As the number of cyclic carbonates on the carbonated copolymer chains increased from 2 to 11, the gel times showed a significant decrease from 254 minutes to 0.84 minutes. A negative correlation between the number of cyclic carbonates on each chain and the M_c values was observed, indicating the formation of tighter crosslinked networks. With decreasing M_c values from 3400 g mol^{-1} to 1700 g mol^{-1}, the networks exhibited increased tightness, resulting in restricted chain movements. This restricted mobility led to an increase in T_g of the networks from 61°C to 79°C, as T_g is correlated with the mobility of polymer chains. In the third manuscript presented in Chapter 5, the focus shifted to study the influence of the copolymer backbone rigidity alone on the mechanical and rheological properties of the resulting crosslinked networks. To achieve copolymers with different backbone rigidity, binary copolymers of methyl methacrylate (MMA), ethyl methacrylate (EMA), and butyl methacrylate (BMA) with GMA were synthesized using various initial molar fractions of GMA. Additionally, the reactivity ratios of EMA/GMA and BMA/GMA were determined, revealing that the microstructure of the copolymers was predominantly statistical, which had not been reported previously. Following the carbonation of the synthesized copolymers, the epoxy functional groups were converted into cyclic carbonates. Subsequently, the carbonated copolymers were reacted with a bio-based diamine (Priamine 1074) to create networks crosslinked through urethane linkages. The networks based on MMA exhibited E values ranging from 1020 MPa to 1250 MPa, depending on the number of urethane linkages present in the side chains. For the

EMA-based networks, the *E* values decreased to the range of 760 MPa to 1000 MPa, while the BMA-based networks exhibited *E* values spanning from 395 MPa to 530 MPa. These results demonstrate the significant impact of backbone rigidity on the mechanical properties of the resulting product. All networks were brittle, as observed by their low elongation at break (*EB*) values ranging from 1.9% to 5.9%. This brittleness can be attributed to the inherent nature of the backbones. The gel content (*GC*) values, which serve as an indicator of the insoluble crosslinked networks or the conversion of cyclic carbonates to urethane linkages in this study, exceeded 80%. These high *GC* values suggest relatively high level of conversions. The influence of alkyl side chain length, ranging from MMA to BMA, on the water uptake of the crosslinked networks was investigated, revealing intriguing findings. The BMA-based crosslinked networks exhibited the lowest water uptake compared to their MMA and EMA counterparts. This observation can be attributed to the steric hindrance caused by the longer alkyl side chains in the BMA-based networks, which restricts the access of water molecules to the crosslinked urethane network, resulting in reduced water uptake.

One notable aspect of this study is that although various crosslinked networks bonded through urethane linkages with different mechanical and rheological properties were synthesized, it should be noted that these networks cannot be termed strictly as NIPUs (non-isocyanate polyurethanes) due to the absence of multiple repeating units of urethane linkages denoted by the term "poly". In these studies, the carbonated copolymers, which contained cyclic carbonates on their backbones, were reacted with diamines. The resultant structure demonstrated a crosslinked network consisting of chains interconnected by the diamines. Notably, each amine functional group reacted with one cyclic carbonate, leading to the chains being linked only by two urethane linkages. This aspect will be further explored in the next chapter.

In the fourth manuscript presented in Chapter 6, the aim was synthesis of crosslinked "NIPUs", serving as an extension of the work described in Chapters 3 through 5.

The polymerization of diglycerol dicarbonate (DGC) and D-mannitol biscarbonate (MBC) with Priamine 1074 and DAD was carried out to synthesize amine-terminated thermoplastic poly(hydroxyurethanes) (PHUs). These amine-terminated thermoplastic PHUs were subsequently utilized as crosslinkers with C13MA/GMA templates, resulting in the formation of hybrid crosslinked NIPUs. Hybrid crosslinked NIPUs exhibited *E*s ranging from 2.35 MPa to 20.85 MPa (DGC-based) and 1.24 MPa to 6.45 MPa (MBC-based). These values indicate higher *E* values compared to C13MA/GMA templates crosslinked with DAD using the same initial molar ratio of GMA. The increased *E* in the crosslinked NIPUs compared to the C13MA/GMA-based networks crosslinked with DAD, can be attributed to the higher concentration of hydroxyl groups present in these materials compared to the previous HPHUs.

7.2. Future work

Based on the findings and outcomes presented in this thesis, some recommendations are proposed for future areas of study.

Self-healable hybrid NIPUs

While thermoplastic NIPUs have found many applications, there is a distinct demand for thermoset NIPUs in specialized fields such as coatings and sealants. Nevertheless, their lack of recyclability due to the presence of permanent crosslinks is considered a drawback. Consequently, there is a compelling requirement to develop thermoset NIPUs that are derived from sustainable sources and exhibit recyclability, without compromising their mechanical properties. The reprocessability of PUs has been effectively addressed through the emergence of vitrimers [263]. Vitrimers represent a category of thermosetting materials that exhibit characteristics

of permanently cross-linked structures at ambient temperatures but trigger dynamic chemical crosslinking bond exchange at certain temperatures. During the dynamic cross-linking process of vitrimers, the simultaneous fracture of original covalent bonds and the formation of new covalent bonds take place, ensuring that the reaction process does not result in a decrease in network junctions or the generation of small molecular chain segments. This unique behavior allows vitrimers to maintain a specific polymer viscosity and achieve comparable reprocessability to thermoplastic materials. By preserving network integrity while enabling bond exchange, vitrimers offer enhanced flexibility and processability without compromising their properties [263]. Our hybridization concept can be effectively integrated with the synthesis of templates using a combination of radical polymerization and polyaddition polymerization techniques. The radical polymerization pathway enables the efficient incorporation of monomers with desired reactivity and functionality, while the polyaddition polymerization pathway facilitates the formation of cross-linked networks with excellent mechanical and thermal properties. In the initial stage, various bio-sourced bis-cyclic carbonates, such as DGC and MBC, will undergo polymerization with excess diamines that can be bio-based including 1,10-diaminodecane, hexamethylenediamine, and Priamine 1074 (a commercially available bio-based diamine) to form amine-terminated PHUs. This polymerization process will be conducted using either an extruder or an internal mixer, aiming to attain high molecular weight PHUs. The subsequent torque mixer measurements will be employed to evaluate and monitor the polymerization process [264]. The microstructure of the synthesized PHUs will be carefully examined. Key aspects to be examined include the primary-to-secondary alcohol ratio within the polymer chains and the characterization of end-groups. After successful synthesis of the high molecular weight PHUs, the next step will involve the preparation of templates in which the PHUs will be utilized as

crosslinkers. In order to attain enhanced mechanical properties, it is important to synthesize templates with high molecular weights (M_n = 60 kg mol^{-1}). To achieve this objective, C13MA will be copolymerized with (2-acetoacetoxy) ethyl methacrylate (AAEMA) via atom transfer radical polymerization (ATRP) [265]. The synthesized copolymers will be carefully characterized using characterization techniques including GPC, ^{1}H NMR, DSC and TGA. Subsequently, the synthesized PHUs will react with the prepared templates using an internal mixer. The progress of the crosslinking reaction will be monitored and evaluated through torque mixer measurements. The mechanical and rheological properties of the crosslinked polymers will be comprehensively investigated to gain a thorough understanding of their performance characteristics. Various mechanical tests, such as tensile testing, hardness measurement, and impact testing, will be conducted to evaluate the strength, stiffness, toughness, and other mechanical parameters of the crosslinked polymers. Additionally, rheological analysis, including viscosity measurements and dynamic mechanical thermal analysis (DMTA), will be performed to assess the flow behavior, viscoelastic properties, and temperature-dependent response of the polymers.

Following the initial characterization, the crosslinked polymers will undergo a recycling process to evaluate their reprocessability and the impact on their mechanical and rheological properties. The recycled polymers will be compared to the original materials to assess any changes or degradation that may occur during recycling. In parallel to the aforementioned investigations, the gel time of the crosslinking reaction between the templates and PHUs will be measured at several distinct temperatures, which can be modeled with a pseudo-Arrhenius equation to calculate the activation energy of the reaction, a key parameter that characterizes the temperature dependence of the reaction rate and thus the network formation process. The calculated activation energy will be compared to existing literature data to validate the consistency and

reliability of the experimental findings, providing valuable information for understanding the underlying mechanisms of the crosslinking process.

8. CONCLUSION AND ORIGINAL CONTRIBUTIONS

The work presented in this thesis includes several noteworthy contributions to the field of thermoset non-isocyanate polyurethanes. In summary, the key original contributions made in this study are as follows:

1. The development of partially bio-based hybrid thermoset crosslinked networks, as described in Chapter 3, represents the successful proof of concept for the hybridization of radical polymerization with polyaddition polymerization in synthesis of hybrid PHUs. These networks demonstrate the unique capability to cure functionalized polymers under ambient conditions, without the need for external heating. This innovative approach combines both radical polymerization and polyaddition polymerization, paving the way for new possibilities in thermoset materials.
2. The investigations conducted in this thesis regarding the synthesis of thermoset poly(hydroxyurethanes) (PHUs) represent a significant advancement in the field. Unlike previous studies that focused on the reaction of carbonated vegetable oils with fixed numbers of cyclic carbonates, this work introduces a novel approach. Specifically, the templates used in this study were synthesized with varying cyclic carbonate functionalities, allowing for precise control over the mechanical properties of the resulting materials. By manipulating the number of cyclic carbonates on the templates, a direct correlation with the mechanical properties was established, thereby expanding our understanding of structure-property relationships in PHUs.
3. The investigation presented in this thesis encompasses a broad spectrum of mechanical properties achieved through the manipulation of the backbone rigidity of the templates.

4. The random microstructure in the ethyl methacrylate/glycidyl methacrylate and butyl methacrylate/glycidyl methacrylate copolymers was confirmed through the calculation of reactivity ratios.
5. Saccharide-based thermoplastic poly(hydroxyurethanes) (PHUs) were successfully synthesized and employed as crosslinkers in the formation of crosslinked non-isocyanate polyurethanes (NIPUs) with a wide range of mechanical properties.

NOMENCLATURE

^1H *NMR*: Proton Nuclear Magnetic Resonance, 57
AIBN: Azobisisobutyronitrile, 25
Al_2O_3: Alumina, 52
ATRP: Atom transfer radical polymerization
BADGE: Bisphenol-A diglycidyl ether, 16
BDA: 1,4-butanediamine, 20
BMA: Butyl methacrylate
CaH_2: Calcium hydride, 52
CC: Cyclic carbonate, 16
CO_2: Carbon dioxide
Đ: Dispersity, 38
DAD: 1,10-diaminodecane
DAMO: N-(2-aminoethyl)-3-aminopropyltrimethoxysilane, 24
DDM: Diaminodiphenyl methane, 20
DGC: Diglycerol dicarbonate
DMF: Dimethylformamide, 106
DMSO: Dimethylsulfoxide, 28
DMTA: Dynamic mechanical thermal analysis, 58
dNbpy: 4,4'-dinonyl-2,2'-dipyridyl, 87
DP_n: Degree of polymerization
E: Young's modulusi
E': Storage modulus, 130
EB: Elongation at break, 49
EBiB: Ethyl α-bromoisobutyrate, 87
EDA: 1,2-ethylenediamine, 19
EMA: Ethyl methacrylate
f: Initial molar fraction of monomer in mixture, 69
F: Final molar fraction of a monomer in copolymer, 38
FDA: Fatty acid diamine, 19
FRP: Free radical polymerization, 34
FTIR: Fourier Transform Infrared, 57
G': Storage modulus, 46
G″: Loss modulus, 46
GC: Gel content, 47
GLYMO: (3-Glycidyloxypropyl)trimethoxysilane, 21
GMA: Glycidyl methacrylate
GPC: Gel permeation chromatography, 54
HCl: Hydrochloric acid, 2
HMDA: Hexamethylenediamine, 25
HPHU: Hybrid poly(hydroxyurethane)
HUM: Hydroxy urethane modifiers, 15
HUMA: Hydroxyurethane methacrylate, 28
IDM: Internal Dispersion Monomer, 19
IPDA: Isophorone diamine, 20
k_p: Propagation rate constant, 38
MBC: D-mannitol biscarbonate
M_c: Molecular weight between crosslinks, 47
MDI: Methylene diphenyl diisocyanates, 1
M_e: Entanglement molecular weight, 39
MEK: N-phenyl maleimide in methylethylketone, 25
MHS: Mark- Houwink- Sakurada coefficients, 38
MMA: Methyl methacrylate
M_n: Number average molecular weight, 38
mXDA: m-xylene diamine, 20
Myr: *β*-myrcene, 34
NIPU: Non-isocyanate polyurethane
NMP: Nitroxide mediated polymerization, 35
PDMS: Polydimethylsiloxane, 24
PHU: Poly(hydroxyurethane)
PLP: Pulsed laser initiated polymerization, 38
POSS: Polyhedral oligomeric silsesquioxane, 21
PPG: Poly(propylene glycol), 32
PPGDGE: Polypropylene glycol diglycidyl ether, 19
PU: Polyurethanei
r: Reactivity ratio, 35
R: Gas constant, 58
RAFT: Reversible addition−fragmentation chain-transfer polymerization, 35

REFERENCES

(1) Farkhondehnia, M.; Younes, G.R.; Marić, M.. Development of Myrcene-Based Resins with Amine Ended Poly (Propylene Glycol) Side Chains Bonded Through Hydroxyurethane Linkages. *Macromolecular Reaction Engineering* **2023**, *17* (2), 2200054.

(2) Akindoyo, J. O.; Beg, M. D. H.; Ghazali, S.; Islam, M. R.; Jeyaratnam, N.; Yuvaraj, A. R. Polyurethane Types, Synthesis and Applications-a Review. *RSC Advances* **2016**, *6* (115), 114453–114482. https://doi.org/10.1039/c6ra14525f.

(3) Prof. Dr. Otto Bayer. Das Di-Lsocganat-Poluadditionsverfahren (Polyurethane). *Angewandte Chemie* **1947**, *59* (9), 257–272.

(4) Seymour, R. B.; Kauffman, G. B. Products of Chemistry - Polyurethanes: A Class of Modern Versatile Materials. *Journal of Chemical Education* **1992**, *69* (11), 909–910. https://doi.org/10.1021/ed069p909.

(5) Szycher, M. *Szycher's Handbook of Polyurethane*; 2013.

(6) Kim, S.; Liu, S. Smart and Biostable Polyurethanes for Long-Term Implants. *ACS Biomaterials Science and Engineering* **2018**, *4* (5), 1479–1490. https://doi.org/10.1021/acsbiomaterials.8b00301.

(7) Kreye, O.; Mutlu, H.; Meier, M. A. R. Sustainable Routes to Polyurethane Precursors. *Green Chemistry* **2013**, *15* (6), 1431–1455. https://doi.org/10.1039/c3gc40440d.

(8) Samanta, S.; Selvakumar, S.; Bahr, J.; Wickramaratne, D. S.; Sibi, M.; Chisholm, B. J. Synthesis and Characterization of Polyurethane Networks Derived from Soybean-Oil-Based Cyclic Carbonates and Bioderivable Diamines. *ACS Sustainable Chemistry and Engineering* **2016**, *4* (12), 6551–6561. https://doi.org/10.1021/acssuschemeng.6b01409.

(9) Cornille, A.; Auvergne, R.; Figovsky, O.; Boutevin, B.; Caillol, S. A Perspective Approach to Sustainable Routes for Non-Isocyanate Polyurethanes. *European Polymer Journal* **2017**, *87*, 535–552. https://doi.org/10.1016/j.eurpolymj.2016.11.027.

(10) Bello, D.; Herrick, C. A.; Smith, T. J.; Woskie, S. R.; Streicher, R. P.; Cullen, M. R.; Liu, Y.; Redlich, C. A. Skin Exposure to Isocyanates: Reasons for Concern. *Environmental Health Perspectives* **2007**, *115* (3), 328–335. https://doi.org/10.1289/ehp.9557.

(11) Diller, W. F. Pathogenesis of Phosgene Poisoning. *Toxicology and Industrial Health* **1985**, *1* (2), 7–15. https://doi.org/10.1177/074823378500100202.

(12) Benbow, A. W.; Cullis, C. F. The Combustion of Flexible Polyurethane Foams: Mechanisms and Evaluation of Flame Retardance. *Combustion and Flame* **1975**, *24* (C), 217–230. https://doi.org/10.1016/0010-2180(75)90151-0.

(13) Besse, V.; Auvergne, R.; Carlotti, S.; Boutevin, G.; Otazaghine, B.; Caillol, S.; Pascault, J. P.; Boutevin, B. Synthesis of Isosorbide Based Polyurethanes: An Isocyanate Free Method. *Reactive and Functional Polymers* **2013**, *73* (3), 588–594. https://doi.org/10.1016/j.reactfunctpolym.2013.01.002.

(14) Rokicki, G.; Piotrowska, A. A New Route to Polyurethanes from Ethylene Carbonate, Diamines and Diols. *Polymer* **2002**, *43* (10), 2927–2935. https://doi.org/10.1016/S0032-3861(02)00071-X.

(15) Ghasemlou, M.; Daver, F.; Ivanova, E. P.; Adhikari, B. Bio-Based Routes to Synthesize Cyclic Carbonates and Polyamines Precursors of Non-Isocyanate Polyurethanes: A Review. *European Polymer Journal* **2019**, *118* (May), 668–684. https://doi.org/10.1016/j.eurpolymj.2019.06.032.

(16) Blattmann, H.; Fleischer, M.; Bähr, M.; Mülhaupt, R. Isocyanate- and Phosgene-Free Routes to Polyfunctional Cyclic Carbonates and Green Polyurethanes by Fixation of Carbon Dioxide. *Macromolecular Rapid Communications* **2014**, *35* (14), 1238–1254. https://doi.org/10.1002/marc.201400209.

(17) Kathalewar, M. S.; Joshi, P. B.; Sabnis, A. S.; Malshe, V. C. Non-Isocyanate Polyurethanes: From Chemistry to Applications. *RSC Advances* **2013**, *3* (13), 4110–4129. https://doi.org/10.1039/c2ra21938g.

(18) Gomez-Lopez, A.; Panchireddy, S.; Grignard, B.; Calvo, I.; Jerome, C.; Detrembleur, C.; Sardon, H. Poly(Hydroxyurethane) Adhesives and Coatings: State-of-the-Art and Future Directions. *ACS Sustainable Chemistry and Engineering* **2021**, *9* (29), 9541–9562. https://doi.org/10.1021/acssuschemeng.1c02558.

(19) Nohra, B.; Candy, L.; Blanco, J. F.; Guerin, C.; Raoul, Y.; Mouloungui, Z. From Petrochemical Polyurethanes to Biobased Polyhydroxyurethanes. *Macromolecules* **2013**, *46* (10), 3771–3792. https://doi.org/10.1021/ma400197c.

(20) Janvier, M.; Ducrot, P. H.; Allais, F. Isocyanate-Free Synthesis and Characterization of Renewable Poly(Hydroxy)Urethanes from Syringaresinol. *ACS Sustainable Chemistry and Engineering* **2017**, *5* (10), 8648–8656. https://doi.org/10.1021/acssuschemeng.7b01271.

(21) Chen, X.; Li, L.; Jin, K.; Torkelson, J. M. Reprocessable Polyhydroxyurethane Networks Exhibiting Full Property Recovery and Concurrent Associative and Dissociative Dynamic Chemistry: Via Transcarbamoylation and Reversible Cyclic Carbonate Aminolysis. *Polymer Chemistry* **2017**, *8* (41), 6349–6355. https://doi.org/10.1039/c7py01160a.

(22) Martín, R.; Kleij, A. W. Myth or Reality? Fixation of Carbon Dioxide into Complex Organic Matter under Mild Conditions. *ChemSusChem* **2011**, *4* (9), 1259–1263. https://doi.org/10.1002/cssc.201100102.

(23) Versteegen, R. M.; Sijbesma, R. P.; Meijer, E. W. [N]-Polyurethanes: Synthesis and Characterization. *Angewandte Chemie - International Edition* **1999**, *38* (19), 2917–2919. https://doi.org/10.1002/(SICI)1521-3773(19991004)38:19<2917::AID-ANIE2917>3.0.CO;2-7.

(24) Błażek, K.; Datta, J. Renewable Natural Resources as Green Alternative Substrates to Obtain Bio-Based Non-Isocyanate Polyurethanes-Review. *Critical Reviews in Environmental Science and Technology* **2019**, *49* (3), 173–211. https://doi.org/10.1080/10643389.2018.1537741.

(25) Carré, C.; Ecochard, Y.; Caillol, S.; Avérous, L. From the Synthesis of Biobased Cyclic Carbonate to Polyhydroxyurethanes: A Promising Route towards Renewable Non-Isocyanate Polyurethanes. *ChemSusChem* **2019**, *12* (15), 3410–3430. https://doi.org/10.1002/cssc.201900737.

(26) Bähr, M.; Bitto, A.; Mülhaupt, R. Cyclic Limonene Dicarbonate as a New Monomer for Non-Isocyanate Oligo- and Polyurethanes (NIPU) Based upon Terpenes. *Green Chemistry* **2012**, *14* (5), 1447–1454. https://doi.org/10.1039/c2gc35099h.

(27) Magliozzi, F.; Scali, A.; Chollet, G.; Grau, E.; Cramail, H. Enantioselective Crystallization of Diglycerol Dicarbonate: Impact of the Microstructure on Polyhydroxyurethane Properties. *Macromolecular Rapid Communications* **2021**, *42* (3), 1–9. https://doi.org/10.1002/marc.202000533.

(28) Dannecker, P. K.; Meier, M. A. R. Facile and Sustainable Synthesis of Erythritol Bis(Carbonate), a Valuable Monomer for Non-Isocyanate Polyurethanes (NIPUs). *Scientific Reports* **2019**, *9* (1), 1–6. https://doi.org/10.1038/s41598-019-46314-5.

(29) Charbonneau, L.; Foster, X.; Kaliaguine, S. Ultrasonic and Catalyst-Free Epoxidation of Limonene and Other Terpenes Using Dimethyl Dioxirane in Semibatch Conditions. *ACS Sustainable Chemistry and Engineering* **2018**, *6* (9), 12224–12231. https://doi.org/10.1021/acssuschemeng.8b02578.

(30) Danov, S. M.; Kazantsev, O. A.; Esipovich, A. L.; Belousov, A. S.; Rogozhin, A. E.; Kanakov, E. A. Recent Advances in the Field of Selective Epoxidation of Vegetable Oils and Their Derivatives: A Review and Perspective. *Catalysis Science and Technology* **2017**, *7* (17), 3659–3675. https://doi.org/10.1039/c7cy00988g.

(31) Bähr, M.; Mülhaupt, R. Linseed and Soybean Oil-Based Polyurethanes Prepared via the Non-Isocyanate Route and Catalytic Carbon Dioxide Conversion. *Green Chemistry* **2012**, *14* (2), 483–489. https://doi.org/10.1039/c2gc16230j.

(32) Martínez, J.; Fernández-Baeza, J.; Sánchez-Barba, L. F.; Castro-Osma, J. A.; Lara-Sánchez, A.; Otero, A. An Efficient and Versatile Lanthanum Heteroscorpionate Catalyst for Carbon Dioxide Fixation into Cyclic Carbonates. *ChemSusChem* **2017**, *10* (14), 2886–2890. https://doi.org/10.1002/cssc.201700898.

(33) Błażek, K.; Kasprzyk, P.; Datta, J. Diamine Derivatives of Dimerized Fatty Acids and Bio-Based Polyether Polyol as Sustainable Platforms for the Synthesis of Non-Isocyanate Polyurethanes. *Polymer* **2020**, *205*, 122768. https://doi.org/10.1016/j.polymer.2020.122768.

(34) Wang, T.; Deng, H.; Li, N.; Xie, F.; Shi, H.; Wu, M.; Zhang, C. Mechanically Strong Non-Isocyanate Polyurethane Thermosets from Cyclic Carbonate Linseed Oil. *Green Chemistry* **2022**, *24* (21), 8355–8366. https://doi.org/10.1039/d2gc02910c.

(35) Javni, I.; Hong, D. P.; Petrovič, Z. S. Polyurethanes from Soybean Oil, Aromatic, and Cycloaliphatic Diamines by Nonisocyanate Route. *Journal of Applied Polymer Science* **2013**, *128* (1), 566–571. https://doi.org/10.1002/app.38215.

(36) Liang, C.; Gracida-Alvarez, U. R.; Gallant, E. T.; Gillis, P. A.; Marques, Y. A.; Abramo, G. P.; Hawkins, T. R.; Dunn, J. B. Material Flows of Polyurethane in the United States.

Environmental Science and Technology **2021**, *55* (20), 14215–14224. https://doi.org/10.1021/acs.est.1c03654.

(37) Bobbink, F. D.; Van Muyden, A. P.; Dyson, P. J. En Route to CO2-Containing Renewable Materials: Catalytic Synthesis of Polycarbonates and Non-Isocyanate Polyhydroxyurethanes Derived from Cyclic Carbonates. *Chemical Communications* **2019**, *55* (10), 1360–1373. https://doi.org/10.1039/c8cc07907b.

(38) Ecochard, Y.; Caillol, S. Hybrid Polyhydroxyurethanes: How to Overcome Limitations and Reach Cutting Edge Properties? *European Polymer Journal* **2020**, *137* (August), 109915. https://doi.org/10.1016/j.eurpolymj.2020.109915.

(39) Decostanzi, M.; Ecochard, Y.; Caillol, S. Synthesis of Sol-Gel Hybrid Polyhydroxyurethanes. *European Polymer Journal* **2018**, *109* (August), 1–7. https://doi.org/10.1016/j.eurpolymj.2018.08.054.

(40) Rokicki, G.; Parzuchowski, P. G.; Mazurek, M. Non-Isocyanate Polyurethanes: Synthesis, Properties, and Applications. *Polymers for Advanced Technologies* **2015**, *26* (7), 707–761. https://doi.org/10.1002/pat.3522.

(41) Ecochard, Y.; Caillol, S. Hybrid Polyhydroxyurethanes: How to Overcome Limitations and Reach Cutting Edge Properties? *European Polymer Journal* **2020**, *137* (June), 109915. https://doi.org/10.1016/j.eurpolymj.2020.109915.

(42) Cornille, A.; Serres, J.; Michaud, G.; Simon, F.; Fouquay, S.; Boutevin, B.; Caillol, S. Syntheses of Epoxyurethane Polymers from Isocyanate Free Oligo-Polyhydroxyurethane. *European Polymer Journal* **2016**, *75*, 175–189. https://doi.org/10.1016/j.eurpolymj.2015.12.017.

(43) Yadav, N.; Seidi, F.; Crespy, D.; D'Elia, V. Polymers Based on Cyclic Carbonates as Trait d'Union Between Polymer Chemistry and Sustainable CO 2 Utilization. *ChemSusChem* **2019**, *12* (4), 724–754. https://doi.org/10.1002/cssc.201802770.

(44) Schmitt, R.; Rudolf, F. Ueber Die Einwirkung von Chlorkohlenoxyd Auf Pikraminsäure. *Journal für Praktische Chemie* **1893**, *48* (1), 425–446. https://doi.org/10.1002/prac.18930480145.

(45) Garipov, R. M.; Sysoev, V. A.; Mikheev, V. V.; Zagidullin, A. I.; Deberdeev, R. Y.; Irzhak, V. I.; Berlin, A. Al. Reactivity of Cyclocarbonate Groups in Modified Epoxy-

Amine Compositions. *Doklady Physical Chemistry* **2003**, *393* (1–3), 289–292. https://doi.org/10.1023/B:DOPC.0000003463.07883.c9.

(46) Steblyanko, A.; Choi, W.; Sanda, F.; Endo, T. Addition of Five-Membered Cyclic Carbonate with Amine and Its Application to Polymer Synthesis. *Journal of Polymer Science, Part A: Polymer Chemistry* **2000**, *38* (13), 2375–2380. https://doi.org/10.1002/1099-0518(20000701)38:13<2375::AID-POLA100>3.0.CO;2-U.

(47) Tomita, H.; Sanda, F.; Endo, T. Reactivity Comparison of Five- and Six-Membered Cyclic Carbonates with Amines: Basic Evaluation for Synthesis of Poly(Hydroxyurethane). *Journal of Polymer Science, Part A: Polymer Chemistry* **2001**, *39* (1), 162–168. https://doi.org/10.1002/1099-0518(20010101)39:1<162::AID-POLA180>3.0.CO;2-O.

(48) Tomita, H.; Sanda, F.; Endo, T. Polyaddition Behavior of Bis (Five- and Six-Membered Cyclic Carbonate) s with Diamine. *Journal of Polymer Science Part A* **2000**, *39* (6), 860–867.

(49) Mercer, J. H. West Antarctic Ice Sheet and CO2 Greenhouse Effect: A Threat of Disaster. *Nature* **1978**, *271* (5643), 321–325. https://doi.org/10.1080/14702541.2020.1853870.

(50) Cornille, A.; Dworakowska, S.; Bogdal, D.; Boutevin, B.; Caillol, S. A New Way of Creating Cellular Polyurethane Materials: NIPU Foams. *European Polymer Journal* **2015**, *66*, 129–138. https://doi.org/10.1016/j.eurpolymj.2015.01.034.

(51) Beckman, E. J. Supercritical and Near-Critical CO2 in Green Chemical Synthesis and Processing. *Journal of Supercritical Fluids* **2004**, *28* (2–3), 121–191. https://doi.org/10.1016/S0896-8446(03)00029-9.

(52) Cornille, A.; Blain, M.; Auvergne, R.; Andrioletti, B.; Boutevin, B.; Caillol, S. A Study of Cyclic Carbonate Aminolysis at Room Temperature: Effect of Cyclic Carbonate Structures and Solvents on Polyhydroxyurethane Synthesis. *Polymer Chemistry* **2017**, *8* (3), 592–604. https://doi.org/10.1039/c6py01854h.

(53) Tomita, H.; Sanda, F.; Endo, T. Model Reaction for the Synthesis of Polyhydroxyurethanes from Cyclic Carbonates with Amines: Substituent Effect on the Reactivity and Selectivity of Ring-Opening Direction in the Reaction of Five-Membered Cyclic Carbonates with Amine. *Journal of Polymer Science, Part A: Polymer Chemistry* **2001**, *39* (21), 3678–3685. https://doi.org/10.1002/pola.10009.

(54) Diakoumakos, C. D.; Kotzev, D. L. Non-Isocyanate-Based Polyurethanes Derived upon the Reaction of Amines with Cyclocarbonate Resins. *Macromolecular Symposia* **2004**, *216* (1), 37–46. https://doi.org/10.1002/masy.200451205.

(55) Webster, D. C.; Crain, A. L. Synthesis and Applications of Cyclic Carbonate Functional Polymers in Thermosetting Coatings. *Progress in Organic Coatings* **2000**, *40* (1–4), 275–282. https://doi.org/10.1016/S0300-9440(00)00114-4.

(56) Nohra, B.; Candy, L.; Blanco, J. F.; Raoul, Y.; Mouloungui, Z. Aminolysis Reaction of Glycerol Carbonate in Organic and Hydroorganic Medium. *JAOCS, Journal of the American Oil Chemists' Society* **2012**, *89* (6), 1125–1133. https://doi.org/10.1007/s11746-011-1995-5.

(57) Lamarzelle, O.; Durand, P. L.; Wirotius, A. L.; Chollet, G.; Grau, E.; Cramail, H. Activated Lipidic Cyclic Carbonates for Non-Isocyanate Polyurethane Synthesis. *Polymer Chemistry* **2016**, *7* (7), 1439–1451. https://doi.org/10.1039/c5py01964h.

(58) Besse, V.; Camara, F.; Méchin, F.; Fleury, E.; Caillol, S.; Pascault, J.; Boutevin, B. How to Explain Low Molar Masses in PolyHydroxyUrethanes (PHUs). *European Polymer Journal* **2015**, *71*, 1–11. https://doi.org/10.1016/j.eurpolymj.2015.07.020.

(59) Corma, A.; García, H. Lewis Acids: From Conventional Homogeneous to Green Homogeneous and Heterogeneous Catalysis. *Chemical Reviews* **2003**, *103* (11), 4307–4365. https://doi.org/10.1021/cr030680z.

(60) Kamber, N. E.; Jeong, W.; Waymouth, R. M.; Pratt, R. C.; Lohmeijer, B. G. G.; Hedrick, J. L. Organocatalytic Ring-Opening Polymerization. **2007**.

(61) Miao, Y.; Phuphuak, Y.; Rousseau, C.; Bousquet, T.; Mortreux, A.; Chirachanchai, S.; Zinck, P. Ring-Opening Polymerization of Lactones Using Binaphthyl-Diyl Hydrogen Phosphate as Organocatalyst and Resulting Monosaccharide Functionalization of Polylactones. *Journal of Polymer Science, Part A: Polymer Chemistry* **2013**, *51* (10), 2279–2287. https://doi.org/10.1002/pola.26612.

(62) Kiesewetter, M. K.; Shin, E. J.; Hedrick, J. L.; Waymouth, R. M. Organocatalysis: Opportunities and Challenges for Polymer Synthesis. *Macromolecules* **2010**, *43* (5), 2093–2107. https://doi.org/10.1021/ma9025948.

(63) Ashton, P. R.; Calcagno, P.; Spencer, N.; Harris, K. D. M.; Philp, D. Using Polarization Effects to Alter Chemical Reactivity: A Simple Host Which Enhances Amine

Nucleophilicity. *Organic Letters* **2000**, *2* (10), 1365–1368. https://doi.org/10.1021/ol005604m.

(64) Kikuchi, H.; Uyarna, H. Lipase-Catalyzed Ring-Opening Polymerization of 1,3-Dioxan-2-One. **1997**, *579*, 575–579.

(65) Blain, M.; Auvergne, R.; Benazet, D.; Caillol, S.; Andrioletti, B. Rational Investigations in the Ring Opening of Cyclic Carbonates by Amines. *Green Chemistry* **2014**, *16* (9), 4286–4291. https://doi.org/10.1039/c4gc01032a.

(66) Bossion, A.; Aguirresarobe, R. H.; Irusta, L.; Taton, D.; Cramail, H.; Grau, E.; Mecerreyes, D.; Su, C.; Liu, G.; Müller, A. J.; Sardon, H. Unexpected Synthesis of Segmented Poly(Hydroxyurea-Urethane)s from Dicyclic Carbonates and Diamines by Organocatalysis. *Macromolecules* **2018**, *51* (15), 5556–5566. https://doi.org/10.1021/acs.macromol.8b00731.

(67) Maisonneuve, L.; Lamarzelle, O.; Rix, E.; Grau, E.; Cramail, H. Isocyanate-Free Routes to Polyurethanes and Poly(Hydroxy Urethane)s. *Chemical Reviews* **2015**, *115* (22), 12407–12439. https://doi.org/10.1021/acs.chemrev.5b00355.

(68) Rokicki, G.; Parzuchowski, P. G.; Mazurek, M. Non-Isocyanate Polyurethanes: Synthesis, Properties, and Applications. *Polymers for Advanced Technologies* **2015**, *26* (7), 707–761. https://doi.org/10.1002/pat.3522.

(69) Bizet, B.; Grau, E.; Asua, J. M.; Cramail, H. Hybrid Nonisocyanate Polyurethanes (H-NIPUs): A Pathway towards a Broad Range of Novel Materials. *Macromolecular Chemistry and Physics* **2022**, 2100437. https://doi.org/10.1002/macp.202100437.

(70) Figovsky, O.L. and Shapovalov, L.D. Features of Reaction Amino-Cyclocarbonate for Production of New Type Nonisocyanate Polyurethane Coatings. *Macromolecular Symposia* **2002**, *187* (1), 325–332.

(71) Carré, C.; Zoccheddu, H.; Delalande, S.; Pichon, P.; Avérous, L. Synthesis and Characterization of Advanced Biobased Thermoplastic Nonisocyanate Polyurethanes, with Controlled Aromatic-Aliphatic Architectures. *European Polymer Journal* **2016**, *84*, 759–769. https://doi.org/10.1016/j.eurpolymj.2016.05.030.

(72) Rokicki, G.; Lewandowski, M. Epoxy Resins Modified by Carbon Dioxide. *Die Angewandte Makromolekulare Chemie* **1987**, *148* (1), 53–66. https://doi.org/10.1002/apmc.1987.051480105.

(73) Rokicki, G.; Wojciechowski, C. Epoxy Resin Modified by Aliphatic Cyclic Carbonates. *Journal of Applied Polymer Science* **1990**, *41* (3–4), 647–659. https://doi.org/10.1002/app.1990.070410315.

(74) Bürgel, T.; Fedtke, M. Reactions of Cyclic Carbonates with Amines: Model Studies for Curing Process. *Polymer Bulletin* **1991**, *27* (2), 171–177. https://doi.org/10.1007/BF00296027.

(75) Ke, J.; Li, X.; Wang, F.; Jiang, S.; Kang, M.; Wang, J.; Li, Q.; Wang, Z. Non-Isocyanate Polyurethane/Epoxy Hybrid Materials with Different and Controlled Architectures Prepared from a CO2-Sourced Monomer and Epoxy via an Environmentally-Friendly Route. *RSC Advances* **2017**, *7* (46), 28841–28852. https://doi.org/10.1039/c7ra04215a.

(76) Zhang, C.; Wang, H.; Zhou, Q. Waterborne Isocyanate-Free Polyurethane Epoxy Hybrid Coatings Synthesized from Sustainable Fatty Acid Diamine. *Green Chemistry* **2020**, *22* (4), 1329–1337. https://doi.org/10.1039/c9gc03335a.

(77) Wazarkar, K.; Kathalewar, M.; Sabnis, A. Development of Epoxy-Urethane Hybrid Coatings via Non-Isocyanate Route. *European Polymer Journal* **2016**, *84*, 812–827. https://doi.org/10.1016/j.eurpolymj.2016.10.021.

(78) Schmid, H.; Michel, B. Siloxane Polymers for High-Resolution, High-Accuracy Soft Lithography. *Macromolecules* **2000**, *33* (8), 3042–3049. https://doi.org/10.1021/ma982034l.

(79) Ochiai, B.; Kojima, H.; Endo, T. Synthesis and Properties of Polyhydroxyurethane Bearing Silicone Backbone. *Journal of Polymer Science, Part A: Polymer Chemistry* **2014**, *52* (8), 1113–1118. https://doi.org/10.1002/pola.27091.

(80) Chen, X.; Li, L.; Wei, T.; Venerus, D. C.; Torkelson, J. M. Reprocessable Polyhydroxyurethane Network Composites: Effect of Filler Surface Functionality on Cross-Link Density Recovery and Stress Relaxation. *ACS Applied Materials and Interfaces* **2019**, *11* (2), 2398–2407. https://doi.org/10.1021/acsami.8b19100.

(81) Li, Z.; Yang, R. Flame Retardancy, Thermal and Mechanical Properties of Sulfonate-Containing Polyhedral Oligomeric Silsesquioxane (S-POSS)/Polycarbonate Composites. *Polymer Degradation and Stability* **2015**, *116*, 81–87. https://doi.org/10.1016/j.polymdegradstab.2015.03.023.

(82) Liu, G.; Wu, G.; Chen, J.; Kong, Z. Synthesis, Modification and Properties of Rosin-Based Non-Isocyanate Polyurethanes Coatings. *Progress in Organic Coatings* **2016**, *101*, 461–467. https://doi.org/10.1016/j.porgcoat.2016.09.019.

(83) Liu, G.; Wu, G.; Chen, J.; Huo, S.; Jin, C.; Kong, Z. Synthesis and Properties of POSS-Containing Gallic Acid-Based Non-Isocyanate Polyurethanes Coatings. *Polymer Degradation and Stability* **2015**, *121*, 247–252. https://doi.org/10.1016/j.polymdegradstab.2015.09.013.

(84) Chen, F.; Lin, F.; Zhang, Q.; Cai, R.; Wu, Y.; Ma, X. Polyhedral Oligomeric Silsesquioxane Hybrid Polymers: Well-Defined Architectural Design and Potential Functional Applications. *Macromolecular Rapid Communications* **2019**, *40* (17), 1–20. https://doi.org/10.1002/marc.201900101.

(85) Younes, G. R.; Price, G.; Dandurand, Y.; Maric, M. Study of Moisture-Curable Hybrid NIPUs Based on Glycerol with Various Diamines: Emergent Advantages of PDMS Diamines. *ACS Omega* **2020**, *5* (47), 30657–30670. https://doi.org/10.1021/acsomega.0c04689.

(86) Younes, G. R.; Maric, M. Moisture Curable Hybrid Polyhydroxyurethanes from Sugar-Derived Dicarbonates. *Macromolecular Materials and Engineering* **2021**, *306* (4), 1–14. https://doi.org/10.1002/mame.202000715.

(87) Mehravar, S.; Ballard, N.; Tomovska, R.; Asua, J. M. Polyurethane/Acrylic Hybrid Waterborne Dispersions: Synthesis, Properties and Applications. *Industrial and Engineering Chemistry Research* **2019**, *58* (46), 20902–20922. https://doi.org/10.1021/acs.iecr.9b02324.

(88) Besse, V.; Camara, F.; Voirin, C.; Auvergne, R.; Caillol, S.; Boutevin, B. Synthesis and Applications of Unsaturated Cyclocarbonates. *Polymer Chemistry* **2013**, *4* (17), 4545–4561. https://doi.org/10.1039/c3py00343d.

(89) Kalinina, F. E.; Mognonov, D. M.; Radnaeva, L. D. Poly(Hydroxy Urethane) Coatings Prepared from Copolymers of 3-(2-Vinyloxyethoxy)-l,2-Propylene Carbonate and N-Phenylmaleimide. *Russian Journal of Applied Chemistry* **2008**, *81* (7), 1302–1304. https://doi.org/10.1134/S1070427208070367.

(90) Webster, D. C. Cyclic Carbonate Functional Polymers and Their Applications. *Progress in Organic Coatings* **2003**, *47* (1), 77–86. https://doi.org/10.1016/S0300-9440(03)00074-2.

(91) Kihara, N.; Endo, T. Synthesis and Reaction of Polymethacrylate Bearing Cyclic Carbonate Moieties in the Side Chain. *Die Makromolekulare Chemie* **1992**, *193*, 1481–1492.

(92) Seo, J.; Jang, E. S.; Song, J. H.; Choi, S.; Khan, S. B.; Han, H. Preparation and Properties of Poly(Urethane Acrylate) Films for Ultraviolet-Curable Coatings. *Journal of Applied Polymer Science* **2010**, *118* (4), 2454–2460. https://doi.org/10.1002/app.32344.

(93) Islam, M. R.; Beg, M. D. H.; Jamari, S. S. Development of Vegetable-Oil-Based Polymers. *Journal of Applied Polymer Science* **2014**, *131* (18), 9016–9028. https://doi.org/10.1002/app.40787.

(94) Younes, G. R.; Kamel, M.; Titi, H. M.; Farkhondehnia, M.; Marić, M. Sugar-Based Thermoplastic Polyhydroxyurethanes: Effects of Sorbitol and Mannitol Diastereomers on Polymer Properties and Applications in Melt Blending. *ACS Applied Polymer Materials* **2022**, *4* (7), 5161–5172. https://doi.org/10.1021/acsapm.2c00673.

(95) Poussard, L.; Mariage, J.; Grignard, B.; Detrembleur, C.; Jéroîme, C.; Calberg, C.; Heinrichs, B.; De Winter, J.; Gerbaux, P.; Raquez, J. M.; Bonnaud, L.; Dubois, P. Non-Isocyanate Polyurethanes from Carbonated Soybean Oil Using Monomeric or Oligomeric Diamines to Achieve Thermosets or Thermoplastics. *Macromolecules* **2016**, *49* (6), 2162–2171. https://doi.org/10.1021/acs.macromol.5b02467.

(96) Guan, J.; Song, Y.; Lin, Y.; Yin, X.; Zuo, M.; Zhao, Y.; Tao, X.; Zheng, Q. Progress in Study of Non-Isocyanate Polyurethane. *Industrial and Engineering Chemistry Research* **2011**, *50* (11), 6517–6527. https://doi.org/10.1021/ie101995j.

(97) Research, G. view. *Polyurethane Market Size, Share & Trends Analysis Report By Product (Flexible Foam, Rigid Foam), By End Use (Construction, Electronics & Appliances), By Region (APAC, North America), And Segment Forecasts, 2021 - 2028*. https://doi.org/978-1-68038-262-4.

(98) Cornille, A.; Guillet, C.; Benyahya, S.; Negrell, C.; Boutevin, B.; Caillol, S. Room Temperature Flexible Isocyanate-Free Polyurethane Foams. *European Polymer Journal* **2016**, *84*, 873–888. https://doi.org/10.1016/j.eurpolymj.2016.05.032.

(99) Coman, A. E.; Peyrton, J.; Hubca, G.; Sarbu, A.; Gabor, A. R.; Nicolae, C. A.; Iordache, T. V.; Averous, L. Synthesis and Characterization of Renewable Polyurethane Foams Using Different Biobased Polyols from Olive Oil. *European Polymer Journal* **2021**, *149* (March), 110363. https://doi.org/10.1016/j.eurpolymj.2021.110363.

(100) Khatoon, H.; Iqbal, S.; Irfan, M.; Darda, A.; Rawat, N. K. A Review on the Production, Properties and Applications of Non-Isocyanate Polyurethane: A Greener Perspective. *Progress in Organic Coatings* **2021**, *154* (December 2020), 106124. https://doi.org/10.1016/j.porgcoat.2020.106124.

(101) Pfister, D. P.; Xia, Y.; Larock, R. C. Recent Advances in Vegetable Oil-Based Polyurethanes. *ChemSusChem* **2011**, *4* (6), 703–717. https://doi.org/10.1002/cssc.201000378.

(102) Cornille, A.; Michaud, G.; Simon, F.; Fouquay, S.; Auvergne, R.; Boutevin, B.; Caillol, S. Promising Mechanical and Adhesive Properties of Isocyanate-Free Poly(Hydroxyurethane). *European Polymer Journal* **2016**, *84*, 404–420. https://doi.org/10.1016/j.eurpolymj.2016.09.048.

(103) Maisonneuve, L.; Wirotius, A. L.; Alfos, C.; Grau, E.; Cramail, H. Fatty Acid-Based (Bis) 6-Membered Cyclic Carbonates as Efficient Isocyanate Free Poly(Hydroxyurethane) Precursors. *Polymer Chemistry* **2014**, *5* (21), 6142–6147. https://doi.org/10.1039/c4py00922c.

(104) Bähr, M.; Mülhaupt, R. Linseed and Soybean Oil-Based Polyurethanes Prepared via the Non-Isocyanate Route and Catalytic Carbon Dioxide Conversion. *Green Chemistry* **2012**, *14* (2), 483–489. https://doi.org/10.1039/c2gc16230j.

(105) Benyahya, S.; Habas, J. P.; Auvergne, R.; Lapinte, V.; Caillol, S. Structure-Property Relationships in Polyhydroxyurethanes Produced from Terephthaloyl Dicyclocarbonate with Various Polyamines. *Polymer International* **2012**, *61* (11), 1666–1674. https://doi.org/10.1002/pi.4257.

(106) Helou, M.; Carpentier, J. F.; Guillaume, S. M. Poly(Carbonate-Urethane): An Isocyanate-Free Procedure from α,ω-Di(Cyclic Carbonate) Telechelic Poly(Trimethylene Carbonate)s. *Green Chemistry* **2011**, *13* (2), 266–271. https://doi.org/10.1039/c0gc00686f.

(107) Tomita, H.; Sanda, F.; Endo, T. Polyaddition of Bis(Seven-Membered Cyclic Carbonate) with Diamines: A Novel and Efficient Synthetic Method for Polyhydroxyurethanes.

Journal of Polymer Science, Part A: Polymer Chemistry **2001**, *39* (23), 4091–4100. https://doi.org/10.1002/pola.10058.

(108) Younes, G. R.; Marić, M. Bio-Based Thermoplastic Polyhydroxyurethanes Synthesized from the Terpolymerization of a Dicarbonate and Two Diamines: Design, Rheology, and Application in Melt Blending. *Macromolecules* **2021**, *54* (21), 10189–10202. https://doi.org/10.1021/acs.macromol.1c01640.

(109) Suryawanshi, Y.; Sanap, P.; Wani, V. Advances in the Synthesis of Non-Isocyanate Polyurethanes. *Polymer Bulletin* **2019**, *76* (6), 3233–3246. https://doi.org/10.1007/s00289-018-2531-7.

(110) Gomez-Lopez, A.; Elizalde, F.; Calvo, I.; Sardon, H. Trends in Non-Isocyanate Polyurethane (NIPU) Development. *Chemical Communications* **2021**, *57* (92), 12254–12265. https://doi.org/10.1039/d1cc05009e.

(111) Lambeth, R. H. Progress in Hybrid Non-Isocyanate Polyurethanes. *Polymer International* **2021**, *70* (6), 696–700. https://doi.org/10.1002/pi.6078.

(112) Métafiot, A.; Gérard, J. F.; Defoort, B.; Marić, M. Synthesis of β-Myrcene/Glycidyl Methacrylate Statistical and Amphiphilic Diblock Copolymers by SG1 Nitroxide-Mediated Controlled Radical Polymerization. *Journal of Polymer Science, Part A: Polymer Chemistry* **2018**, *56* (8), 860–878. https://doi.org/10.1002/pola.28963.

(113) Sahu, P.; Sarkar, P.; Bhowmick, A. K. Design of a Molecular Architecture via a Green Route for an Improved Silica Reinforced Nanocomposite Using Bioresources. *ACS Sustainable Chemistry and Engineering* **2018**, *6* (5), 6599–6611. https://doi.org/10.1021/acssuschemeng.8b00383.

(114) Ivanković, M.; Brnardić, I.; Ivanković, H.; Huskić, M.; Gajović, A. Preparation and Properties of Organic-Inorganic Hybrids Based on Poly(Methyl Methacrylate) and Sol-Gel Polymerized 3-Glycidyloxypropyltrimethoxysilane. *Polymer* **2009**, *50* (12), 2544–2550. https://doi.org/10.1016/j.polymer.2009.03.059.

(115) Afzal, A.; Siddiqi, H. M. A Comprehensive Study of the Bicontinuous Epoxy-Silica Hybrid Polymers: I. Synthesis, Characterization and Glass Transition. *Polymer* **2011**, *52* (6), 1345–1355. https://doi.org/10.1016/j.polymer.2011.01.046.

(116) G. Odian. In Principles of Polymerization, 4th Ed. In *John Wiley & Sons: Hoboken, NJ*; 2004; p 466. https://doi.org/10.1017/CBO9781139237031.013.

(117) Pablo-Morales, Á.; Treviño, M. E.; Saldívar-Guerra, E. Toward Bio-Sourced Elastomers with Reactive/Polar Groups. Myrcene – Glycidyl Methacrylate Copolymerization: Reactivity Ratios, Properties, and Preliminary RAFT Emulsion Polymerization. *Macromolecular Reaction Engineering* **2022**, *2200007*, 2200007. https://doi.org/10.1002/mren.202200007.

(118) Madrid, J. F.; Barba, B. J. D.; Pomicpic, J. C.; Cabalar, P. J. E. Immobilization of an Organophosphorus Compound on Polypropylene-g-Poly(Glycidyl Methacrylate) Polymer Support and Its Application in Scandium Recovery. *Journal of Applied Polymer Science* **2021**, No. August 2021. https://doi.org/10.1002/app.51597.

(119) Sarkar, P.; Bhowmick, A. K. Synthesis, Characterization and Properties of a Bio-Based Elastomer: Polymyrcene. *RSC Advances* **2014**, *4* (106), 61343–61354. https://doi.org/10.1039/c4ra09475a.

(120) H. KH, M. Method for Gel Permeation Chromatography Calibration and the Evaluation of Mark-Houwink-Sakurada Constants. *J. Appl. Polym. Sci.* **1985**, *30* (4), 1535–1544.

(121) Hattam, P.; Gauntlett, S.; Mays, J. W.; Hadjichristidis, N.; Young, R. N.; Fetters, L. J. Conformational Characteristics of Some Model Polydienes and Polyolefins. *Macromolecules* **1991**, *24* (23), 6199–6209. https://doi.org/10.1021/ma00023a022.

(122) Hutchinson, R. A.; Beuermann, S.; Paquet, D. A.; McMinn, J. H.; Jackson, C. Determination of Free-Radical Propagation Rate Coefficients for Cycloalkyl and Functional Methacrylates by Pulsed-Laser Polymerization. *Macromolecules* **1998**, *31* (5), 1542–1547. https://doi.org/10.1021/ma971307u.

(123) Pasch, H.; Trathnigg, B. Multidimensional HPLC of Polymers Springer Laboratory Manuals in Polymer Science; 2013; pp 37–90.

(124) Kamachi, M.; Kajiwara, A. ESR Study on Radical Polymerizations of Diene Compounds, Determination of Propagation Rate Constants. *Macromolecules* **1996**, *29* (7), 2378–2382. https://doi.org/10.1021/ma951280j.

(125) van Büren, B.; Brandl, F.; Beuermann, S. Propagation Kinetics of Isoprene Radical Homopolymerization Derived from Pulsed Laser Initiated Polymerizations. *Macromolecular Reaction Engineering* **2020**, *14* (1). https://doi.org/10.1002/mren.201900030.

(126) Beuermann, S.; Buback, M.; Davis, T. P.; García, N.; Gilbert, R. G.; Hutchinson, R. A.; Kajiwara, A.; Kamachi, M.; Lacík, I.; Russell, G. T. Critically Evaluated Rate Coefficients for Free-Radical Polymerization, 4: Propagation Rate Coefficients for Methacrylates with Cyclic Ester Groups. *Macromolecular Chemistry and Physics* **2003**, *204* (10), 1338–1350. https://doi.org/10.1002/macp.200390107.

(127) Feist, W. *Exterior Wood Finishes*; Coatings Materials and Surface Coatings, 2006. https://doi.org/10.1201/9781420044058.ch66.

(128) Safa, K. D.; Nasirtabrizi, M. H. Ring Opening Reactions of Glycidyl Methacrylate Copolymers to Introduce Bulky Organosilicon Side Chain Substituents. *Polymer Bulletin* **2006**, *57* (3), 293–304. https://doi.org/10.1007/s00289-006-0564-9.

(129) L. J. Fetters, D. J. Lohse, D. Richter, T. A. Witten, A. Z. Connection between Polymer Molecular Weight, Density, Chain Dimensions, and Melt Viscoelastic Properties. *Macromolecules* **1994**, *27* (17), 4639–4647.

(130) Banik, B. K.; Banerjee, B.; Kaur, G.; Saroch, S.; Kumar, R. Tetrabutylammonium Bromide (TBAB) Catalyzed Synthesis of Bioactive Heterocycles. *Molecules (Basel, Switzerland)* **2020**, *25* (24). https://doi.org/10.3390/molecules25245918.

(131) Mazo, P.; Rios, L. Carbonation of Epoxidized Soybean Oil Improved by the Addition of Water. *JAOCS, Journal of the American Oil Chemists' Society* **2013**, *90* (5), 725–730. https://doi.org/10.1007/s11746-013-2214-3.

(132) Yoshida, Y.; Endo, T. Radical Polymerization Behavior and Thermal Properties of Vinyl Ethylene Carbonate Derivatives Bearing Aromatic Moieties. *Polymer* **2016**, *102*, 167–175. https://doi.org/10.1016/j.polymer.2016.09.002.

(133) Mori, Y.; Houda, T.; Tsuge, A.; Endo, T. Properties of Poly (Methacrylate) s Bearing Hydroxyurethane Structures Synthesized by Various Amines with Poly (Methacrylate) s Containing Five - Membered Cyclic. *Polymer Bulletin* **2021**, No. 0123456789. https://doi.org/10.1007/s00289-021-03943-z.

(134) Lai, Z.; Sudol, E. D.; Dimonie, V. L.; El-Aasser, M. S. Determination of the Extent of Incorporation of a Reactive Surfactant in Polystyrene Latex Particles via GPC. *Journal of Polymer Science, Part A: Polymer Chemistry* **2005**, *43* (12), 2675–2678. https://doi.org/10.1002/pola.20738.

(135) Stachak, P.; Łukaszewska, I.; Hebda, E.; Pielichowski, K. Recent Advances in Fabrication of Non-Isocyanate Polyurethane-Based Composite Materials. *Materials* **2021**, *14* (13). https://doi.org/10.3390/ma14133497.

(136) Chen, H.; Chauhan, P.; Yan, N. "Barking" up the Right Tree: Biorefinery from Waste Stream to Cyclic Carbonate with Immobilization of CO2for Non-Isocyanate Polyurethanes. *Green Chemistry* **2020**, *22* (20), 6874–6888. https://doi.org/10.1039/d0gc02285c.

(137) Maisonneuve, L.; More, A. S.; Foltran, S.; Alfos, C.; Robert, F.; Landais, Y.; Tassaing, T.; Grau, E.; Cramail, H. Novel Green Fatty Acid-Based Bis-Cyclic Carbonates for the Synthesis of Isocyanate-Free Poly(Hydroxyurethane Amide)s. *RSC Advances* **2014**, *4* (49), 25795–25803. https://doi.org/10.1039/c4ra03675a.

(138) Chen, Q.; Gao, K.; Peng, C.; Xie, H.; Zhao, Z. K.; Bao, M. Preparation of Lignin/Glycerol-Based Bis(Cyclic Carbonate) for the Synthesis of Polyurethanes. *Green Chemistry* **2015**, *17* (9), 4546–4551. https://doi.org/10.1039/c5gc01340b.

(139) Błażek, K.; Beneš, H.; Walterová, Z.; Abbrent, S.; Eceiza, A.; Calvo-Correas, T.; Datta, J. Synthesis and Structural Characterization of Bio-Based Bis(Cyclic Carbonate)s for the Preparation of Non-Isocyanate Polyurethanes. *Polymer Chemistry* **2021**, *12* (11), 1643–1652. https://doi.org/10.1039/d0py01576h.

(140) Yi, Z.; Zhu, L.; Xu, Y.; Jiang, J.; Zhu, B. Polypropylene Glycol: The Hydrophilic Phenomena in the Modification of Polyethersulfone Membranes. *Industrial and Engineering Chemistry Research* **2011**, *50* (19), 11297–11305. https://doi.org/10.1021/ie201238c.

(141) Mert, E. H.; Kekevi, B. Synthesis of PolyHIPEs through High Internal Phase Emulsions of β-Myrcene. *Colloid and Polymer Science* **2020**, *298* (10), 1423–1432. https://doi.org/10.1007/s00396-020-04730-4.

(142) Knorr, D. B.; Masser, K. A.; Elder, R. M.; Sirk, T. W.; Hindenlang, M. D.; Yu, J. H.; Richardson, A. D.; Boyd, S. E.; Spurgeon, W. A.; Lenhart, J. L. Overcoming the Structural versus Energy Dissipation Trade-off in Highly Crosslinked Polymer Networks: Ultrahigh Strain Rate Response in Polydicyclopentadiene. *Composites Science and Technology* **2015**, *114*, 17–25. https://doi.org/10.1016/j.compscitech.2015.03.021.

(143) van der Sanden, M. C. M.; Meijer, H. E. H. Deformation and Toughness of Polymeric Systems: 3. Influence of Crosslink Density. *Polymer* **1993**, *34* (24), 5063–5072. https://doi.org/10.1016/0032-3861(93)90249-A.

(144) Farkhondehnia, M.; Marić, M. Design of Crosslinked Networks with Hydroxyurethane Linkages via Bio-Based Alkyl Methacrylates and Diamines. *Journal of Applied Polymer Science* **2023**, *140* (28). https://doi.org/10.1002/app.54039.

(145) Lombardo, V. M.; Dhulst, E. A.; Leitsch, E. K.; Wilmot, N.; Heath, W. H.; Gies, A. P.; Miller, M. D.; Torkelson, J. M.; Scheidt, K. A. Cooperative Catalysis of Cyclic Carbonate Ring Opening: Application towards Non-Isocyanate Polyurethane Materials. *European Journal of Organic Chemistry* **2015**, *2015* (13), 2791–2795. https://doi.org/10.1002/ejoc.201500313.

(146) Wang, S.; Liu, Q.; Li, L.; Urban, M. W. Recent Advances in Stimuli-Responsive Commodity Polymers. *Macromolecular Rapid Communications* **2021**, *42* (18), 1–20. https://doi.org/10.1002/marc.202100054.

(147) Otto Bayer. Das Di-Lsocganat-Poluadditionsverfahren (Polyurethane). *Angewandte Chemie* **1947**, *59* (9), 257–272.

(148) Cotarca, L.; Eckert, H. *Phosgenations : A Handbook*; John Wiley & Sons, 2006.

(149) Dong, T.; Dheressa, E.; Wiatrowski, M.; Pereira, A. P.; Zeller, A.; Laurens, L. M. L.; Pienkos, P. T. Assessment of Plant and Microalgal Oil-Derived Nonisocyanate Polyurethane Products for Potential Commercialization. *ACS Sustainable Chemistry and Engineering* **2021**, *9* (38), 12858–12869. https://doi.org/10.1021/acssuschemeng.1c03653.

(150) Maisonneuve, L.; Lamarzelle, O.; Rix, E.; Grau, E.; Cramail, H. Isocyanate-Free Routes to Polyurethanes and Poly(Hydroxy Urethane)s. *Chemical Reviews* **2015**, *115* (22), 12407–12439. https://doi.org/10.1021/acs.chemrev.5b00355.

(151) Bähr, M.; Mülhaupt, R. Linseed and Soybean Oil-Based Polyurethanes Prepared via the Non-Isocyanate Route and Catalytic Carbon Dioxide Conversion. *Green Chemistry* **2012**, *14* (2), 483–489. https://doi.org/10.1039/c2gc16230j.

(152) Tomita, H.; Sanda, F.; Endo, T. Structural Analysis of Polyhydroxyurethane Obtained by Polyaddition of Bifunctional Five-Membered Cyclic Carbonate and Diamine Based on the Model Reaction. *Journal of Polymer Science, Part A: Polymer Chemistry* **2001**, *39* (6),

851–859. https://doi.org/10.1002/1099-0518(20010315)39:6<851::AID-POLA1058>3.0.CO;2-3.

(153) Beniah, G.; Heath, W. H.; Torkelson, J. M. Functionalization of Hydroxyl Groups in Segmented Polyhydroxyurethane Eliminates Nanophase Separation. *Journal of Polymer Science, Part A: Polymer Chemistry* **2017**, *55* (20), 3347–3351. https://doi.org/10.1002/pola.28722.

(154) Tomita, H.; Sanda, F.; Endo, T. Polyaddition of Bis(Seven-Membered Cyclic Carbonate) with Diamines: A Novel and Efficient Synthetic Method for Polyhydroxyurethanes. *Journal of Polymer Science, Part A: Polymer Chemistry* **2001**, *39* (23), 4091–4100. https://doi.org/10.1002/pola.10058.

(155) Li, C.; Sablong, R. J.; Koning, C. E. Chemoselective Alternating Copolymerization of Limonene Dioxide and Carbon Dioxide: A New Highly Functional Aliphatic Epoxy Polycarbonate. *Angewandte Chemie* **2016**, *128* (38), 11744–11748. https://doi.org/10.1002/ange.201604674.

(156) Yadollahi, M.; Bouhendi, H.; Zohuriaan-Mehr, M. J.; Farhadnejad, H.; Kabiri, K.; Mirabedini, S. M. Glycidyl Methacrylate Copolymers Modified with CO2. *Soft Materials* **2013**, *11* (4), 430–439. https://doi.org/10.1080/1539445X.2012.688783.

(157) Froidevaux, V.; Negrell, C.; Caillol, S.; Pascault, J. P.; Boutevin, B. Biobased Amines: From Synthesis to Polymers; Present and Future. *Chemical Reviews* **2016**, *116* (22), 14181–14224. https://doi.org/10.1021/acs.chemrev.6b00486.

(158) Pan, T.; Dutta, S.; Kamble, Y.; Patel, B. B.; Wade, M. A.; Rogers, S. A.; Diao, Y.; Guironnet, D.; Sing, C. E. Materials Design of Highly Branched Bottlebrush Polymers at the Intersection of Modeling, Synthesis, Processing, and Characterization. *Chemistry of Materials* **2022**, *34* (5), 1990–2024. https://doi.org/10.1021/acs.chemmater.1c04030.

(159) Iwasaki, T.; Yoshida, J. I. Free Radical Polymerization in Microreactors. Significant Improvement in Molecular Weight Distribution Control. *Macromolecules* **2005**, *38* (4), 1159–1163. https://doi.org/10.1021/ma048369m.

(160) Payne, K. A.; D'Hooge, D. R.; Van Steenberge, P. H. M.; Reyniers, M. F.; Cunningham, M. F.; Hutchinson, R. A.; Marin, G. B. ARGET ATRP of Butyl Methacrylate: Utilizing Kinetic Modeling to Understand Experimental Trends. *Macromolecules* **2013**, *46* (10), 3828–3840. https://doi.org/10.1021/ma400388t.

(161) Yu, Q.; Zeng, F.; Zhu, S. Atom Transfer Radical Polymerization of Poly (Ethylene Glycol) Dimethacrylate. *Macromolecules* **2001**, *34* (6), 1612–1618.

(162) Rooney, T. R.; Hutchinson, R. A. Monomer Structure and Solvent Effects on Copolymer Composition in (Meth)Acrylate Radical Copolymerization. *Industrial and Engineering Chemistry Research* **2018**, *57* (15), 5215–5227. https://doi.org/10.1021/acs.iecr.8b00451.

(163) Haehnel, A. P.; Schneider-baumann, M.; Arens, L.; Misske, A. M.; Fleischhaker, F.; Barner-kowollik, C. Haehnel, A.P., Schneider-Baumann, M., Hiltebrandt, K.U., Misske, A.M. and Barner-Kowollik, C., 2013. Global Trends for Kp? Expanding the Frontier of Ester Side Chain Topography in Acrylates and Methacrylates. *Macromolecules* **2013**, *46* (1), 15–28.

(164) Tajbakhsh, S.; Hajiali, F.; Marić, M. Epoxy-Based Triblock, Diblock, Gradient and Statistical Copolymers of Glycidyl Methacrylate and Alkyl Methacrylates by Nitroxide Mediated Polymerization. *Reactive and Functional Polymers* **2021**, *167*, 105008. https://doi.org/10.1016/j.reactfunctpolym.2021.105008.

(165) Dorota Neugebauer, Katarzyna Bury, M. W. Atom Transfer Radical Copolymerization of Glycidyl Methacrylate and Methyl Methacrylate. *Journal of Applied Polymer Science* **2012**, *124* (3), 2209–2215. https://doi.org/10.1002/app.

(166) Tcharkhtchi, A.; Nony, F.; Khelladi, S.; Fitoussi, J.; Farzaneh, S. *Epoxy/Amine Reactive Systems for Composites Materials and Their Thermomechanical Properties*; Elsevier Ltd., 2015; Vol. 1. https://doi.org/10.1016/B978-1-78242-307-2.00013-0.

(167) Dai, X.; Yu, L.; Zhang, Y.; Zhang, L.; Tan, J. Polymerization-Induced Self-Assembly via RAFT-Mediated Emulsion Polymerization of Methacrylic Monomers. *Macromolecules* **2019**, *52* (19), 7468–7476. https://doi.org/10.1021/acs.macromol.9b01689.

(168) Levy, F.; Donaldson, J. T. Morphology, Geographic Distribution, and Conservation Status of the Southern Appalachian Endemic, Solidago Lancifolia (Asteraceae). *Journal of the Torrey Botanical Society* **2018**, *145* (4), 281–295. https://doi.org/10.3159/TORREY-D-18-00011.1.

(169) Kim, K.; Yu, S.; Kim, S. W.; Kim, T.; Kim, S. M.; Kang, S. Y.; Han, S. M.; Jang, J. H. Highly Transparent Poly(Glycidyl Methacrylate-: Co -Acryloisobutyl POSS) for 100 Mm-Thick Submicron Patterns with an Aspect Ratio over 100. *Chemical Communications* **2017**, *53* (58), 8172–8175. https://doi.org/10.1039/c7cc02937c.

(170) Tajbakhsh, S.; Hajiali, F.; Maric, M. Nitroxide-Mediated Miniemulsion Polymerization of Bio-Based Methacrylates. *Industrial and Engineering Chemistry Research* **2020**, *59* (19), 8921–8936. https://doi.org/10.1021/acs.iecr.0c00840.

(171) Hajiali, F.; Tajbakhsh, S.; Marić, M. Epoxidized Block and Statistical Copolymers Reinforced by Organophosphorus-Titanium-Silicon Hybrid Nanoparticles: Morphology and Thermal and Mechanical Properties. *ACS Omega* **2021**, *6* (17), 11679–11692. https://doi.org/10.1021/acsomega.1c00993.

(172) Hempel, E.; Huth, H.; Beiner, M. Interrelation between Side Chain Crystallization and Dynamic Glass Transitions in Higher Poly(n-Alkyl Methacrylates). *Thermochimica Acta* **2003**, *403* (1), 105–114. https://doi.org/10.1016/S0040-6031(03)00098-4.

(173) Beiner, M.; Schröter, K.; Hempel, E.; Reissig, S.; Donth, E. Multiple Glass Transition and Nanophase Separation in Poly(Ra-Alkyl Methacrylate) Homopolymers. *Macromolecules* **1999**, *32* (19), 6278–6282. https://doi.org/10.1021/ma981780n.

(174) Reimschuessel, H. K. On the Glass Transition Temperature of Comblike Polymers: Effects of Side Chain Length and Backbone Chain Structure. *J Polym Sci Polym Chem Ed* **1979**, *17* (8), 2447–2457. https://doi.org/10.1002/pol.1979.170170817.

(175) Çayli, G.; Meier, M. A. R. Polymers from Renewable Resources: Bulk ATRP of Fatty Alcohol-Derived Methacrylates. *European Journal of Lipid Science and Technology* **2008**, *110* (9), 853–859. https://doi.org/10.1002/ejlt.200800028.

(176) Mao, H.; Wang, H.; Li, J.; Zhang, L.; Shi, J.; Shi, H. Side-Chain Crystallization and Segment Packing of Poly(Isobutylene-Alt-Maleic Anhydride)-g-Alkyl Alcohol Comb-like Polymers. *Polymer* **2020**, *202*, 122721. https://doi.org/10.1016/j.polymer.2020.122721.

(177) Gupta, G.; Danke, V.; Babur, T.; Beiner, M. Interrelations between Side Chain and Main Chain Packing in Different Crystal Modifications of Alkoxylated Polyesters. *Journal of Physical Chemistry B* **2017**, *121* (17), 4583–4591. https://doi.org/10.1021/acs.jpcb.7b00928.

(178) Zulfiqar, S.; Zulfiqar, M.; Nawaz, M.; McNeill, I. C.; Gorman, J. G. Thermal Degradation of Poly(Glycidyl Methacrylate). *Polymer Degradation and Stability* **1990**, *30* (2), 195–203. https://doi.org/10.1016/0141-3910(90)90075-I.

(179) Podkościelna, B. Synthesis, Modification, and Porous Properties of NewGlycidyl Methacrylate Copolymers. *Journal of Applied Polymer Science* **2011**, *120* (5), 3020–3026. https://doi.org/10.1002/app.33420.

(180) Dhal, P. K.; Babu, G. N. Glycidyl Methacrylate-Tert-Butyl Acrylate Thermal Studies. *Journal of Polymer Science: Polymer Chemistry Edition* **1984**, *22* (8), 1817–1829.

(181) Nakabayashi, N. Reactive Fiber. *Sen-ito Kogyo* **1969**, *2* (7), 507–511. https://doi.org/10.2115/fiber1968.2.507.

(182) Wu, S. Chain Structure and Entanglement. *Journal of Polymer Science Part B: Polymer Physics* **1989**, *27* (4), 723–741. https://doi.org/10.1002/polb.1989.090270401.

(183) Yadollahi, M.; Bouhendi, H.; Zohuriaan-Mehr, M. J.; Kabiri, K. Spectral and Chemical Monitoring of Cyclo-Addition Reaction of CO 2 with Poly(MMA-Co-GMA) Copolymers. *Chinese Journal of Polymer Science (English Edition)* **2012**, *30* (5), 727–734. https://doi.org/10.1007/s10118-012-1174-7.

(184) Jana, S.; Yu, H.; Parthiban, A.; Chai, C. L. L. Controlled Synthesis and Functionalization of PEGylated Methacrylates Bearing Cyclic Carbonate Pendant Groups. *Journal of Polymer Science, Part A: Polymer Chemistry* **2010**, *48* (7), 1622–1632. https://doi.org/10.1002/pola.23928.

(185) Barkakaty B, Morino K, Sudo A, E. T. Synthesis of a Methacrylic Monomer Having Pendant Cyclohexene CyclicCarbonate—Easy CO2Fixation and Radical Polymerization. *Journal of Polymer Science: Part A: Polymer Chemistry* **2011**, *46* (2), 545–549. https://doi.org/10.1002/pola.

(186) Kihara, N. and Endo, T. Synthesis and Properties of Poly (Hydroxyurethane). *Journal of Polymer Science Part A: Polymer Chemistry* **1993**, *31* (11), 2765–2773.

(187) Doley, S.; Dolui, S. K. Solvent and Catalyst-Free Synthesis of Sunflower Oil Based Polyurethane through Non-Isocyanate Route and Its Coatings Properties. *European Polymer Journal* **2018**, *102* (March), 161–168. https://doi.org/10.1016/j.eurpolymj.2018.03.030.

(188) Tryznowski, M.; widerska, A.; Zołek-Tryznowska, Z.; Gołofit, T.; Parzuchowski, P. G. Facile Route to Multigram Synthesis of Environmentally Friendly Non-Isocyanate Polyurethanes. *Polymer* **2015**, *80*, 228–236. https://doi.org/10.1016/j.polymer.2015.10.055.

(189) Das, M.; Mandal, B.; Katiyar, V. Environment-Friendly Synthesis of Sustainable Chitosan-Based Nonisocyanate Polyurethane: A Biobased Polymeric Film. *Journal of Applied Polymer Science* **2020**, *137* (36), 49050. https://doi.org/10.1002/app.49050.

(190) Hill, L. W. Calculation of Crosslink Density in Short Chain Networks. *Progress in Organic Coatings* **1997**, *31* (3), 235–243. https://doi.org/10.1016/S0300-9440(97)00081-7.

(191) Jones, F.; Nichols, M.; Pappas, S. *Organic Coatings: Science and Technology*; 2017.

(192) Farkhondehnia, M.; Marić, M. Effect of Alkyl Methacrylate / Glycidyl Methacrylate Copolymer Backbone Structure on Mechanical Properties of Hydroxyurethane-Crosslinked Networks. *Reactive and Functional Polymers* **2023**, *191*, 105683. https://doi.org/10.1016/j.reactfunctpolym.2023.105683.

(193) Mhatre, S. V.; Mahajan, J. S.; Epps, T. H.; Korley, L. S. T. J. Lignin-Derivable Alternatives to Petroleum-Derived Non-Isocyanate Polyurethane Thermosets with Enhanced Toughness. *Materials Advances* **2022**, *4* (1), 110–121. https://doi.org/10.1039/d2ma00895e.

(194) Zhang, W.; Wang, T.; Zheng, Z.; Quirino, R. L.; Xie, F.; Li, Y.; Zhang, C. Plant Oil-Based Non-Isocyanate Waterborne Poly(Hydroxyl Urethane)s. *Chemical Engineering Journal* **2023**, *452*, 138965. https://doi.org/10.1016/j.cej.2022.138965.

(195) Fortman, D. J.; Brutman, J. P.; Cramer, C. J.; Hillmyer, M. A.; Dichtel, W. R. Mechanically Activated, Catalyst-Free Polyhydroxyurethane Vitrimers. *Journal of the American Chemical Society* **2015**, *137* (44), 14019–14022. https://doi.org/10.1021/jacs.5b08084.

(196) Chen, B.; Chuang, S. S. C. In Situ Infrared Study of Oxidative Carbonylation of Aniline with Methanol on Cu-Based Catalysts. *Green Chemistry* **2003**, *5* (4), 484–489. https://doi.org/10.1039/b303283c.

(197) Schmidt, S.; Ritter, B. S.; Kratzert, D.; Bruchmann, B.; Mülhaupt, R. Isocyanate-Free Route to Poly(Carbohydrate-Urethane) Thermosets and 100% Bio-Based Coatings Derived from Glycerol Feedstock. *Macromolecules* **2016**, *49* (19), 7268–7276. https://doi.org/10.1021/acs.macromol.6b01485.

(198) Shan, S.; Wu, X.; Lin, Y.; Zhang, A. Tough, Self-Healing, Recyclable Bottlebrush Polyurethane Elastomer with a Skin-like Strain-Adaptive-Strengthening Property. *ACS*

Applied Polymer Materials **2022**, *4* (10), 7554–7563. https://doi.org/10.1021/acsapm.2c01234.

(199) Zhang, J.; Chen, J.; Yao, M.; Jiang, Z.; Ma, Y. Hydrolysis-Resistant Polyurethane Elastomers Synthesized from Hydrophobic Bio-Based Polyfarnesene Diol. *Journal of Applied Polymer Science* **2019**, *136* (25), 47673. https://doi.org/10.1002/app.47673.

(200) MacInnis, C. M.; Younes, G. R.; Marić, M. The Effect of Polyhedral Oligomeric Silsesquioxane Fillers in Non-Isocyanate Polyurethane Hybrid Resins. *Journal of Applied Polymer Science* **2022**, *139* (48), 1–20. https://doi.org/10.1002/app.53225.

(201) Bogdanova, E.; Kocherbitov, V. Assessment of Activation Energy of Enthalpy Relaxation in Sucrose-Water System: Effects of DSC Cycle Type and Sample Thermal History. *Journal of Thermal Analysis and Calorimetry* **2022**, *147* (17), 9695–9709. https://doi.org/10.1007/s10973-022-11250-6.

(202) Yang, Y. N.; Zhu, C. X.; Zhou, Y. N.; Luo, Z. H. Deterministic Modeling of Non-Adiabatic Solution Radical Polymerization of n-Butyl Acrylate in Light of Runaway Prevention. *Chemical Engineering Journal* **2022**, *450*, 138110. https://doi.org/10.1016/j.cej.2022.138110.

(203) Braunecker, W. A.; Matyjaszewski, K. Controlled/Living Radical Polymerization: Features, Developments, and Perspectives. *Progress in Polymer Science (Oxford)* **2007**, *32* (1), 93–146. https://doi.org/10.1016/j.progpolymsci.2006.11.002.

(204) Fukuda, Takeshi, Keiji Kubo, and Y.-D. M. Kinetics of Free Radical Copolymerization. *Progress in polymer science* **1992**, *17* (5), 875–916.

(205) Ledesma-González, T.; Pérez-Camacho, O.; Treviño, M. E.; Torres-Lubián, R.; Saldívar-Guerra, E. Toward Functionalized Polyolefins from the Hydrogenation of Isoprene-Glycidyl Methacrylate Copolymers Prepared by Reversible Deactivation Radical Polymerization in Heterogeneous Media. *Industrial and Engineering Chemistry Research* **2021**, *60* (29), 10826–10833. https://doi.org/10.1021/acs.iecr.1c00620.

(206) Geurts, J. M.; Jacobs, P. E.; Muijs, J. C.; Steven Van Es, J. J. G.; German, A. L. Molecular Mass Control in Methacrylic Copolymer Latexes Containing Glycidyl Methacrylate. *Journal of Applied Polymer Science* **1996**, *61* (1), 9–19. https://doi.org/10.1002/(sici)1097-4628(19960705)61:1<9::aid-app2>3.0.co;2-p.

(207) Morton Fineman, S. D. R. Linear Method for Determining Monomer Reactivity Ratios in Copolymerization. *Journal of Polymer Science* **1950**, *15* (5), 259–262. https://doi.org/10.1097/01241398-199509000-00028.

(208) Kelen, T.; Tüdős, F. A New Improved Linear Graphical Method for Determing Copolymerization Reactivity Ratios. *Reaction Kinetics and Catalysis Letters* **1974**, *1* (4), 487–492. https://doi.org/10.1007/BF02074484.

(209) Tidwell, P. W.; Mortimer, G. A. An Improved Method of Calculating Copolymerization Reactivity Ratios. *Journal of Polymer Science Part A: General Papers* **1965**, *3* (1), 369–387. https://doi.org/10.1002/pol.1965.100030137.

(210) Mayo, F. R.; Lewis, F. M.; Lewis, M. Copolymerization. I. A Basis for Comparing the Behavior of Monomers in Copolymerization; the Copolymerization of Styrene and Methyl Methacrylate. *Journal of the American Chemical Society* **1944**, *66* (9), 1594–1601.

(211) Lynd, N. A.; Ferrier, R. C.; Beckingham, B. S. Recommendation for Accurate Experimental Determination of Reactivity Ratios in Chain Copolymerization. *Macromolecules* **2019**, *52* (6), 2277–2285. https://doi.org/10.1021/acs.macromol.8b01752.

(212) De La Fuente, J. L.; Canamero, P. F.; Fernández-García, M. Synthesis and Characterization of Glycidyl Methacrylate/Butyl Acrylate Copolymers Obtained at a Low Temperature by Atom Transfer Radical Polymerization. *Journal of Polymer Science, Part A: Polymer Chemistry* **2006**, *44* (6), 1807–1816. https://doi.org/10.1002/pola.21294.

(213) Abdollahi, H.; Najafi, V.; Amiri, F. Determination of Monomer Reactivity Ratios and Thermal Properties of Poly(GMA-Co-MMA) Copolymers. *Polymer Bulletin* **2021**, *78* (1), 493–511. https://doi.org/10.1007/s00289-020-03123-5.

(214) Fox, T. G. Influence of Diluent and of Copolymer Composition on the Glass Temperature of a Poly-Mer System. *Bull. Am. Phys. Soc* **1956**, *1*, 123.

(215) Condo, P. D.; Johnston, K. P. In Situ Measurement of the Glass Transition Temperature of Polymers with Compressed Fluid Diluents. *Journal of Polymer Science Part B: Polymer Physics* **1994**, *32* (3), 523–533. https://doi.org/10.1002/polb.1994.090320313.

(216) Kitayama, Tatsuki, Koichi Ute, Masanori Yamamoto, Nobutaka Fujimoto, and K. H. Highly Isotactic and Living Polymerization of Ethyl Methacrylate with T-C4h9mgbr in Toluene and the Preparation of Block and Random Copolymers with High

Stereoregularity. *Polymer Journal* **1990**, *22* (5), 386–396. https://doi.org/10.1295/polymj.22.386.

(217) Grabowski, C. A.; Mukhopadhyay, A. Size Effect of Nanoparticle Diff Usion in a Polymer Melt. *Macromolecules* **2014**, *47* (20), 7238–7242.

(218) Saramolee, P.; Lopattananon, N.; Sahakaro, K. Preparation and Some Properties of Modified Natural Rubber Bearing Grafted Poly(Methyl Methacrylate) and Epoxide Groups. *European Polymer Journal* **2014**, *56* (1), 1–10. https://doi.org/10.1016/j.eurpolymj.2014.04.008.

(219) Dawlee, S.; Jayabalan, M. Studies on Inherently Radiopaque Acrylate Copolymers for Biomedical Applications. *Journal of Applied Polymer Science* **2012**, *125* (3), 2252–2261. https://doi.org/10.1002/app.

(220) Hasanzadeh, R.; Moghadam, P. N.; Bahri-Laleh, N.; Ziaee, F. A Reactive Copolymer Based on Glycidylmethacrylate and Maleic Anhydride: 1-Synthesis, Characterization and Monomer Reactivity Ratios. *Journal of Polymer Research* **2016**, *23* (8), 1–19. https://doi.org/10.1007/s10965-016-1048-8.

(221) Kaya, I.; Ilter, Z.; Enol, D. Thermodynamic Interactions and Characterisation of Poly[(Glycidyl Methacrylate-Co-Methyl, Ethyl, Butyl) Methacrylate] by Inverse Gas Chromatography. *Polymer* **2002**, *43* (24), 6455–6463. https://doi.org/10.1016/S0032-3861(02)00554-2.

(222) Helbling, P.; Hermant, F.; Petit, M.; Tassaing, T.; Vidil, T.; Cramail, H. Unveiling the Reactivity of Epoxides in Carbonated Epoxidized Soybean Oil and Application in the Stepwise Synthesis of Hybrid Poly(Hydroxyurethane) Thermosets. *Polymer Chemistry* **2023**, 500–513. https://doi.org/10.1039/d2py01318e.

(223) Sun, J.; Li, H.; Wang, C.; Yuan, D.; Stubbs, L. P.; He, C. The Effect of Residual Solvent N,N′-Dimethylformamide on the Curing Reaction and Mechanical Properties of Epoxy and Lignin Epoxy Composites. *Macromolecular Chemistry and Physics* **2016**, *217* (9), 1065–1073. https://doi.org/10.1002/macp.201500453.

(224) Javni, Ivan, Doo Pyo Hong, and Z. S. P. Soy-Based Polyurethanes by Nonisocyanate Route. *Journal of Applied Polymer Science* **2008**, *108* (6), 3867–3875. https://doi.org/10.1002/app.

(225) Yadollahi, M.; Bouhendi, H.; Zohuriaan-Mehr, M. J.; Farhadnejad, H.; Kabiri, K. Investigation of Viscoelastic and Thermal Properties of Cyclic Carbonate Bearing Copolymers. *Polymer Science - Series B* **2013**, *55* (5–6), 327–335. https://doi.org/10.1134/S1560090413060109.

(226) Ghasemi, S.; Ghezelsofloo, M. Isocyanate - Free Urethane Vinyl Ester Resin : Preparation , Characterization and Thermal and Mechanical Properties Investigation. *Chemical Papers* **2022**, 1–16. https://doi.org/10.1007/s11696-022-02547-9.

(227) Delebecq, E., Pascault, J.P., Boutevin, B. and Ganachaud, F. On the Versatility of Urethane/Urea Bonds: Reversibility, Blocked Isocyanate, and Non-Isocyanate Polyurethane. *Chemical reviews* **2013**, *113* (1), 80–118.

(228) Lambeth, R. H.; Henderson, T. J. Organocatalytic Synthesis of (Poly) Hydroxyurethanes from Cyclic Carbonates and Amines. *Polymer* **2013**, *54* (21), 5568–5573. https://doi.org/10.1016/j.polymer.2013.08.053.

(229) Tomita, H.; Sanda, F.; Endo, T. Structural Analysis of Polyhydroxyurethane Obtained by Polyaddition of Bifunctional Five-Membered Cyclic Carbonate and Diamine Based on the Model Reaction. *Journal of Polymer Science, Part A: Polymer Chemistry* **2001**, *39* (6), 851–859. https://doi.org/10.1002/1099-0518(20010315)39:6<851::AID-POLA1058>3.0.CO;2-3.

(230) Pavlinec, J.; Lazar, M. Cross-linking of Poly(Methyl Methacrylate) by Aminolysis of Ester Functions with Diamines. *Journal of Applied Polymer Science* **1995**, *55* (1), 39–45. https://doi.org/10.1002/app.1995.070550104.

(231) Yu, Youlu, and G. R. B. Carbon-13 NMR Studies of the Reactions of Crosslinked Poly (Methyl Acrylate) Beads with Multifunctional Amines. *Macromolecules* **1993**, *26* (5), 1037–1041.

(232) Carré, C., Bonnet, L. and Avérous, L. Original Biobased Nonisocyanate Polyurethanes: Solvent-and Catalyst-Free Synthesis, Thermal Properties and Rheological Behaviour. *RSC advances* **2014**, *4* (96), 54018–54025. https://doi.org/10.1039/c4ra09794g.

(233) Xiao, X., Kong, D., Qiu, X., Zhang, W., Zhang, F., Liu, L., Liu, Y., Zhang, S., Hu, Y. and Leng, J. Shape-Memory Polymers with Adjustable High Glass Transition Temperatures. *Macromolecules* **2022**, *43* (13), 3582–3589. https://doi.org/10.1002/marc.202100833.

(234) Fei, X.; Wei, W.; Tang, Y.; Zhu, Y.; Luo, J.; Chen, M.; Liu, X. Simultaneous Enhancements in Toughness, Tensile Strength, and Thermal Properties of Epoxy-Anhydride Thermosets with a Carboxyl-Terminated Hyperbranched Polyester. *European Polymer Journal* **2017**, *90* (February), 431–441. https://doi.org/10.1016/j.eurpolymj.2017.03.022.

(235) Zhang, Q.; Chen, G.; Wu, K.; Shi, J.; Liang, L.; Lu, M. Biphenyl Liquid Crystal Epoxy Containing Flexible Chain: Synthesis and Thermal Properties. *Journal of Applied Polymer Science* **2020**, *137* (38), 1–12. https://doi.org/10.1002/app.49143.

(236) Carré, C.; Bonnet, L.; Avérous, L. Solvent- and Catalyst-Free Synthesis of Fully Biobased Nonisocyanate Polyurethanes with Different Macromolecular Architectures. *RSC Advances* **2015**, *5* (121), 100390–100400. https://doi.org/10.1039/c5ra17638g.

(237) Lian, Q.; Chen, H.; Luo, Y.; Li, Y.; Cheng, J.; Liu, Y. Toughening Mechanism Based on the Physical Entanglement of Branched Epoxy Resin in the Non-Phase-Separated Inhomogeneous Crosslinking Network: An Experimental and Molecular Dynamics Simulation Study. *Polymer* **2022**, *247* (March), 124754. https://doi.org/10.1016/j.polymer.2022.124754.

(238) Dokukin, M. E.; Sokolov, I. On the Measurements of Rigidity Modulus of Soft Materials in Nanoindentation Experiments at Small Depth. *Macromolecules* **2012**, *45* (10), 4277–4288. https://doi.org/10.1021/ma202600b.

(239) Boisaubert, P.; Kébir, N.; Schuller, A. S.; Burel, F. Polyurethane Coatings from Formulations with Low Isocyanate Content Using a Transurethane Polycondensation Route. *Polymer* **2022**, *240*, 124522. https://doi.org/10.1016/j.polymer.2022.124522.

(240) Dolci, E.; Froidevaux, V.; Michaud, G.; Simon, F.; Auvergne, R.; Fouquay, S.; Caillol, S. Thermoresponsive Crosslinked Isocyanate-Free Polyurethanes by Diels-Alder Polymerization. *Journal of Applied Polymer Science* **2017**, *134* (5), 1–11. https://doi.org/10.1002/app.44408.

(241) Kotanen, S.; Poikelispää, M.; Efimov, A.; Harjunalanen, T.; Mills, C.; Laaksonen, T.; Sarlin, E. Hydrolytic Stability of Polyurethane/Polyhydroxyurethane Hybrid Adhesives. *International Journal of Adhesion and Adhesives* **2021**, *110*, 102950. https://doi.org/10.1016/j.ijadhadh.2021.102950.

(242) Zhao, W.; Chen, B.; Zhang, K. Biobased Bisbenzoxazine Resins Derived from Natural Renewable Monophenols and Diamine: Synthesis and Property Investigations. *ACS Sustainable Chemistry and Engineering* **2022**, *10* (45), 14783–14793. https://doi.org/10.1021/acssuschemeng.2c04103.

(243) Farkhondehnia, M., Marić M. Utilizing Bio-Derived Amine-Terminated Thermoplastic Polyhydroxyurethanes as Crosslinkers for Hybrid Thermosets. *Journal of Polymer Science* **2023,** Just Accepted. https://doi.org/10.1002/pol.20230382.

(244) Guan, J.; Song, Y.; Lin, Y.; Yin, X.; Zuo, M.; Zhao, Y.; Tao, X.; Zheng, Q. Progress in Study of Non-Isocyanate Polyurethane Progress in Study of Non-Isocyanate Polyurethane. *Industrial & Engineering Chemistry* **2017**, *50* (May 2011), 6517–6527.

(245) Yang, X.; Ren, C.; Liu, X.; Sun, P.; Xu, X.; Liu, H.; Shen, M.; Shang, S.; Song, Z. Recyclable Non-Isocyanate Polyurethanes Containing a Dynamic Covalent Network Derived from Epoxy Soybean Oil and CO2. *Materials Chemistry Frontiers* **2021**, *5* (16), 6160–6170. https://doi.org/10.1039/d1qm00765c.

(246) Miao, P.; Jiao, Z.; Liu, J.; He, M.; Song, G.; Wei, Z.; Leng, X.; Li, Y. Mechanically Robust and Chemically Recyclable Polyhydroxyurethanes from CO2-Derived Six-Membered Cyclic Carbonates. *ACS Applied Materials and Interfaces* **2022**, *15*, 2246–2255. https://doi.org/10.1021/acsami.2c19251.

(247) Santos, J. J.; Lopes, J. H.; De Aguiar, K. M. F. R.; Simões, M. B.; Mpeko, J. C.; Jasinevicius, R. G.; Cavalheiro, E. T.; Imasato, H.; Rodrigues-Filho, U. P. Hybrid Bisphenol A Non-Isocyanate Polyurethane Composite with Mica Powder: A New Insulating Material. *Journal of CO2 Utilization* **2023**, *67* (September 2022). https://doi.org/10.1016/j.jcou.2022.102303.

(248) Hernández, A.; Houck, H. A.; Elizalde, F.; Guerre, M.; Sardon, H.; Du Prez, F. E. Internal Catalysis on the Opposite Side of the Fence in Non-Isocyanate Polyurethane Covalent Adaptable Networks. *European Polymer Journal* **2022**, *168*, 111100. https://doi.org/10.1016/j.eurpolymj.2022.111100.

(249) Xu, W.; Ding, Y.; You, S.; Chao, C.; Wu, B.; Chen, F. Customized Thermoplastic Polyhydroxyurethanes Synthesized from Ene-Containing Cyclic Carbonate, Dithiol and Diamine: Design, Mechanical Property and Application in Adhesive. *Polymer Chemistry* **2023**. https://doi.org/10.1039/d3py00134b.

(250) Ochiai, B.; Utsuno, T. Non-Isocyanate Synthesis and Application of Telechelic Polyurethanes via Polycondensation of Diurethanes Obtained from Ethylene Carbonate and Diamines. *Journal of Polymer Science, Part A: Polymer Chemistry* **2013**, *51* (3), 525–533. https://doi.org/10.1002/pola.26418.

(251) Liu, X.; Xu, K.; Liu, H.; Cai, H.; Fu, Z.; Guo, Y.; Chen, M. The Antihydrolytic Effect and Properties of Crosslinked Polyurethane Containing Natural Dimer Fatty Acids Building Blocks. *Macromolecular Research* **2012**, *20* (6), 642–649. https://doi.org/10.1007/s13233-012-0083-5.

(252) Bueno-Ferrer, C.; Hablot, E.; Garrigós, M. D. C.; Bocchini, S.; Averous, L.; Jiménez, A. Relationship between Morphology, Properties and Degradation Parameters of Novative Biobased Thermoplastic Polyurethanes Obtained from Dimer Fatty Acids. *Polymer Degradation and Stability* **2012**, *97* (10), 1964–1969. https://doi.org/10.1016/j.polymdegradstab.2012.03.002.

(253) Elif Hamurcu, E. and Baysal, B. M. Solubility Parameter of a Poly (Dimethylsiloxane) Network. *Journal of Polymer Science Part B: Polymer Physics* **1994**, *32* (3), 591–594.

(254) Ashworth, A. J.; Price, G. J. Comparison of Static with Gas Chromatographic Interaction Parameters and Estimation of the Solubility Parameter for Poly(Dimethylsiloxane). *Macromolecules* **1986**, *19* (2), 362–363. https://doi.org/10.1021/ma00156a022.

(255) Van Krevelen, D. W.; Te Nijenhuis, K. Cohesive Properties and Solubility. In *Properties of polymers*; Elsevier: New York, 2009; pp 189–227.

(256) Hansen, C. M. /. *Solubility Parameters : A User's Handbook*; CRC press, 2007.

(257) Delebecq, E.; Pascault, J. P.; Boutevin, B.; Ganachaud, F. On the Versatility of Urethane/Urea Bonds: Reversibility, Blocked Isocyanate, and Non-Isocyanate Polyurethane. *Chemical Reviews* **2013**, *113* (1), 80–118. https://doi.org/10.1021/cr300195n.

(258) Guillame, S. M.; Khalil, H.; Misra, M. Green and Sustainable Polyurethanes for Advanced Applications. *Journal of Applied Polymer Science* **2017**, *134* (45), 44958. https://doi.org/10.1002/app.45646.

(259) Ecochard, Y.; Leroux, J.; Boutevin, B.; Auvergne, R.; Caillol, S. From Multi-Functional Siloxane-Based Cyclic Carbonates to Hybrid Polyhydroxyurethane Thermosets. *European*

Polymer Journal **2019**, *120* (August), 109280. https://doi.org/10.1016/j.eurpolymj.2019.109280.

(260) Krishnakumar, B.; Pucci, A.; Wadgaonkar, P. P.; Kumar, I.; Binder, W. H.; Rana, S. Vitrimers Based on Bio-Derived Chemicals: Overview and Future Prospects. *Chemical Engineering Journal* **2022**, *433* (P2), 133261. https://doi.org/10.1016/j.cej.2021.133261.

(261) Wang, X.; Gao, S.; Wang, J.; Xu, S.; Li, H.; Chen, K.; Ouyang, P. The Production of Biobased Diamines from Renewable Carbon Sources: Current Advances and Perspectives. *Chinese Journal of Chemical Engineering* **2021**, *30*, 4–13. https://doi.org/10.1016/j.cjche.2020.12.009.

(262) Younes, G. R.; Maric, M. Bio-Based and Hydrolytically Degradable Hydroxyurethane Acrylates as Photocurable Thermosets. *Journal of Applied Polymer Science* **2022**, *139* (18), 1–10. https://doi.org/10.1002/app.52044.

(263) Xie, K.; Tang, D.; Zhang, G. A Nonisocyanate Strategy toward Polyurethane Vitrimers from Alkylene Bisurea and Epoxide through Eutectic-Assisted Melting. *Macromolecular Chemistry and Physics* **2022**, *223* (7), 1–9. https://doi.org/10.1002/macp.202100452.

(264) Magliozzi, F.; Chollet, G.; Grau, E.; Cramail, H. Benefit of the Reactive Extrusion in the Course of Polyhydroxyurethanes Synthesis by Aminolysis of Cyclic Carbonates. *ACS Sustainable Chemistry and Engineering* **2019**, *7* (20), 17282–17292. https://doi.org/10.1021/acssuschemeng.9b04098.

(265) Karanam, S.; Goossens, H.; Klumperman, B.; Lemstra, P. "Controlled" Synthesis and Characterization of High Molecular Weight Methyl Methacrylate/Tert-Butyl Methacrylate Diblock Copolymers via ATRP. *Macromolecules* **2003**, *36* (22), 8304–8311. https://doi.org/10.1021/ma034768q.

(266) Clark, J. H.; Farmer, T. J.; Ingram, I. D. V.; Lie, Y.; North, M. Renewable Self-Blowing Non-Isocyanate Polyurethane Foams from Lysine and Sorbitol. *European Journal of Organic Chemistry* **2018**, *2018* (31), 4265–4271. https://doi.org/10.1002/ejoc.201800665.

APPENDIX A

SUPPORTING INFORMATION FOR DEVELOPMENT OF MYRCENE-BASED RESINS WITH AMINE ENDED POLY(PROPYLENE GLYCOL) SIDE CHAINS BONDED THROUGH HYDROXYURETHANE LINKAGES

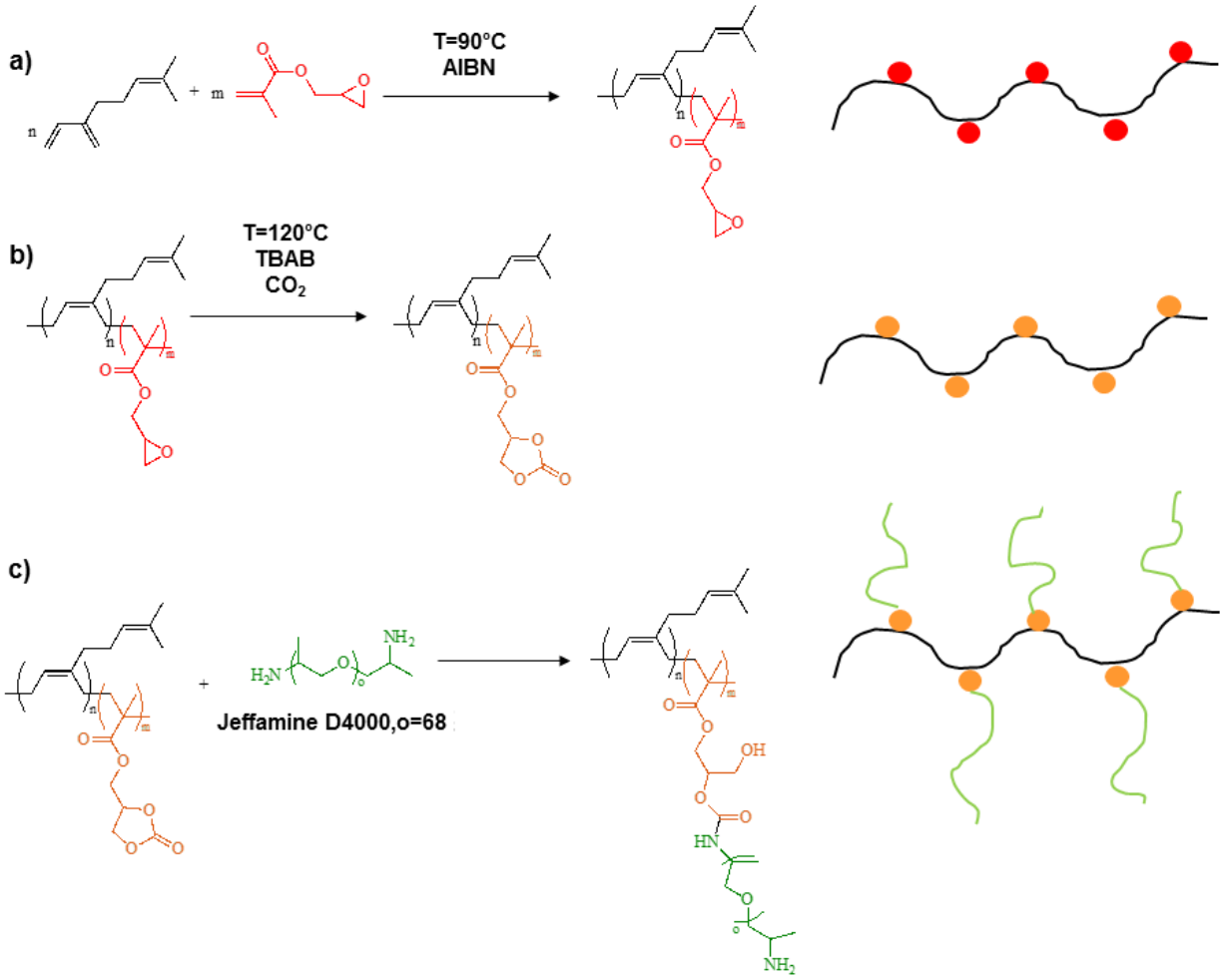

Figure A 1. Polymerization steps overview, a) Bulk copolymerization of Myr and GMA using AIBN as initiator at 90°C, b) cyclo-addition reaction of CO2 with poly(Myr-co-GMA), c) reaction of five membered cyclic carbonates with diamines at 120°C to produce corresponding hybrid poly(hydroxyurethanes).

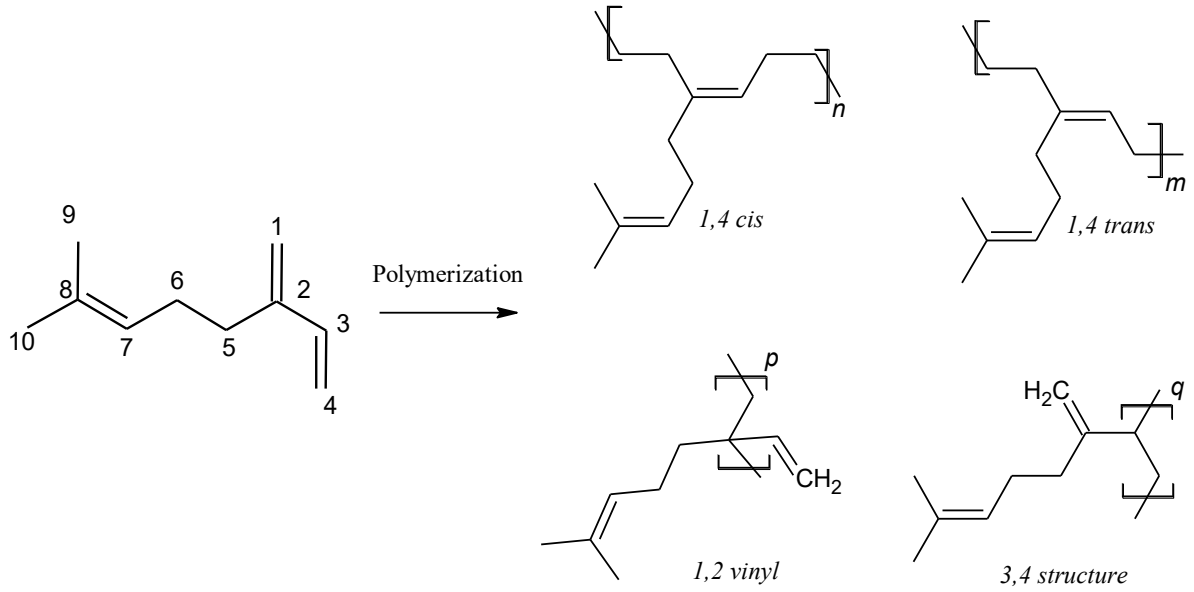

Figure A 2. Regioselectivity of myrcene in poly(*Myr*).

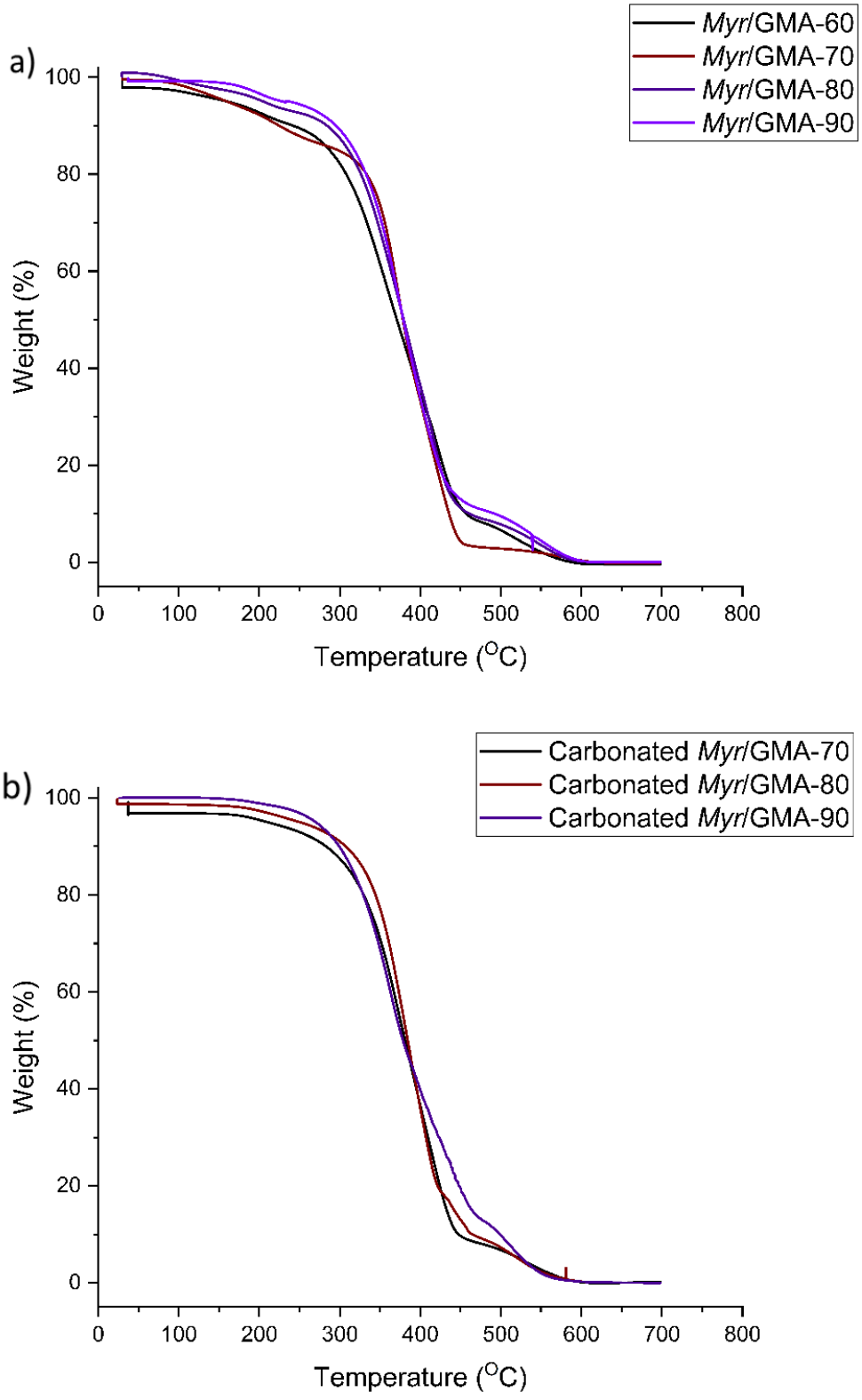

Figure A 3. TGA thermograms for *Myr*/GMA copolymers before and after carbonation, a) TGA thermograms of poly(*Myr*-co-GMA)s, b) TGA thermograms of carbonated poly(*Myr*-co-GMA)s.

Table A 1. Thermal Characterization of Poly(Myr-co-GMA).

ID[a]	F_{Myr}	$T_{dec,10\%}$ [a)] (°C)	$T_{dec,max}$ [a)] (°C)	$T_{dec,final}$ [a)] (°C)	Residual (%)
Myr/GMA-90	0.91	293	378	604	0.0
Myr/GMA-80	0.84	285	390	595	0.0
Myr/GMA-70	0.77	226	372	615	0.0
Myr/GMA-60	0.61	248	351	605	0.0
Carbonated *Myr*/GMA-90	0.91	296	360	590	0.0
Carbonated *Myr*/GMA-80	0.84	303	380	615	0.0
Carbonated *Myr*/GMA-70	0.77	280	375	605	0.0
EC-90	0.91	333	374	624	0.98
EC-80	0.84	318	375	620	1.20
EC-70	0.77	337	372	610	1.18

([a)] $T_{dec,10\%}$ (decomposition temperature for 10% weight loss), $T_{dec,max}$ (maximum decomposition temperature) and $T_{dec,final}$ (end of decomposition) measured by TGA under N_2 atmosphere at a heating rate of 10 °C min).

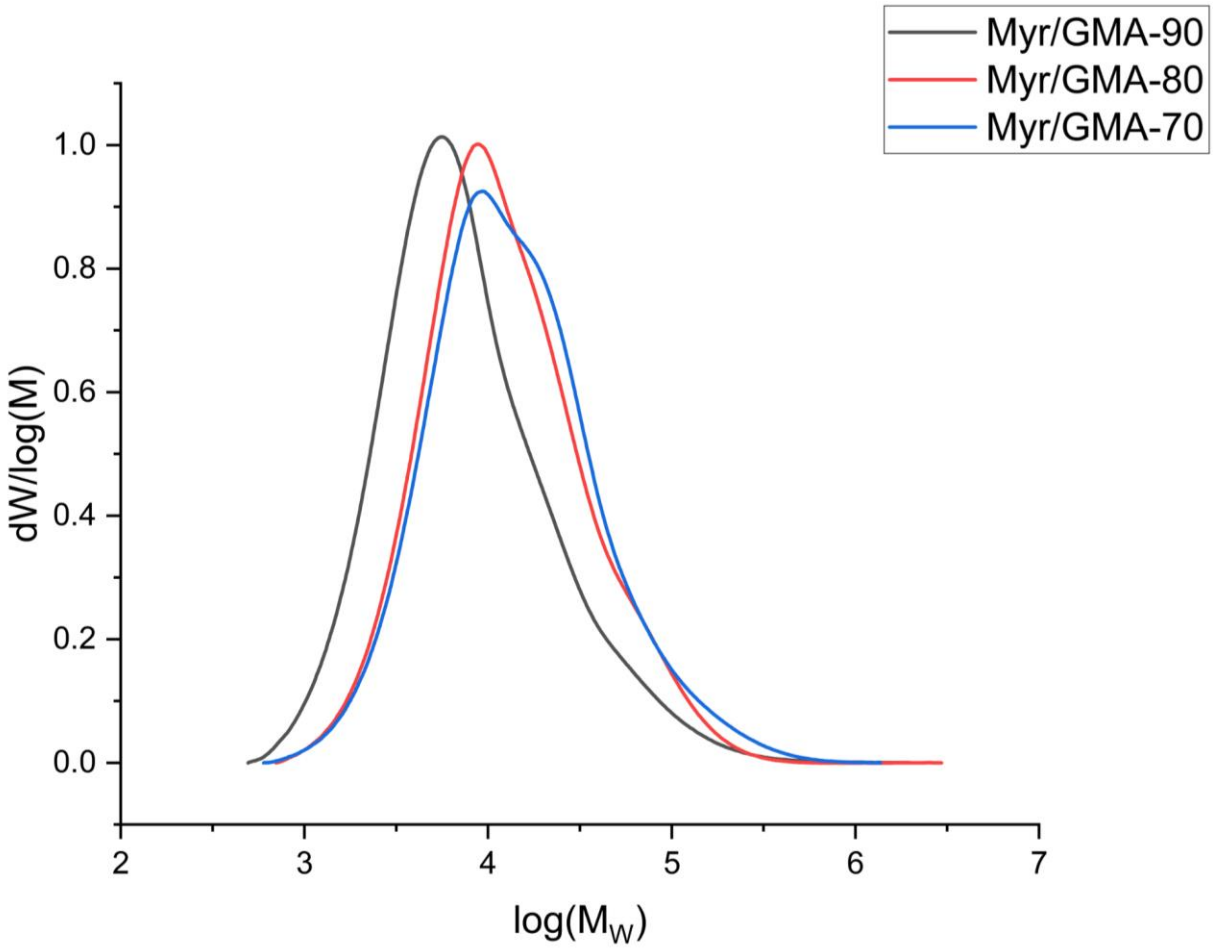

Figure A 4. GPC peaks for Myr/GMA copolymers with different molar ratio.

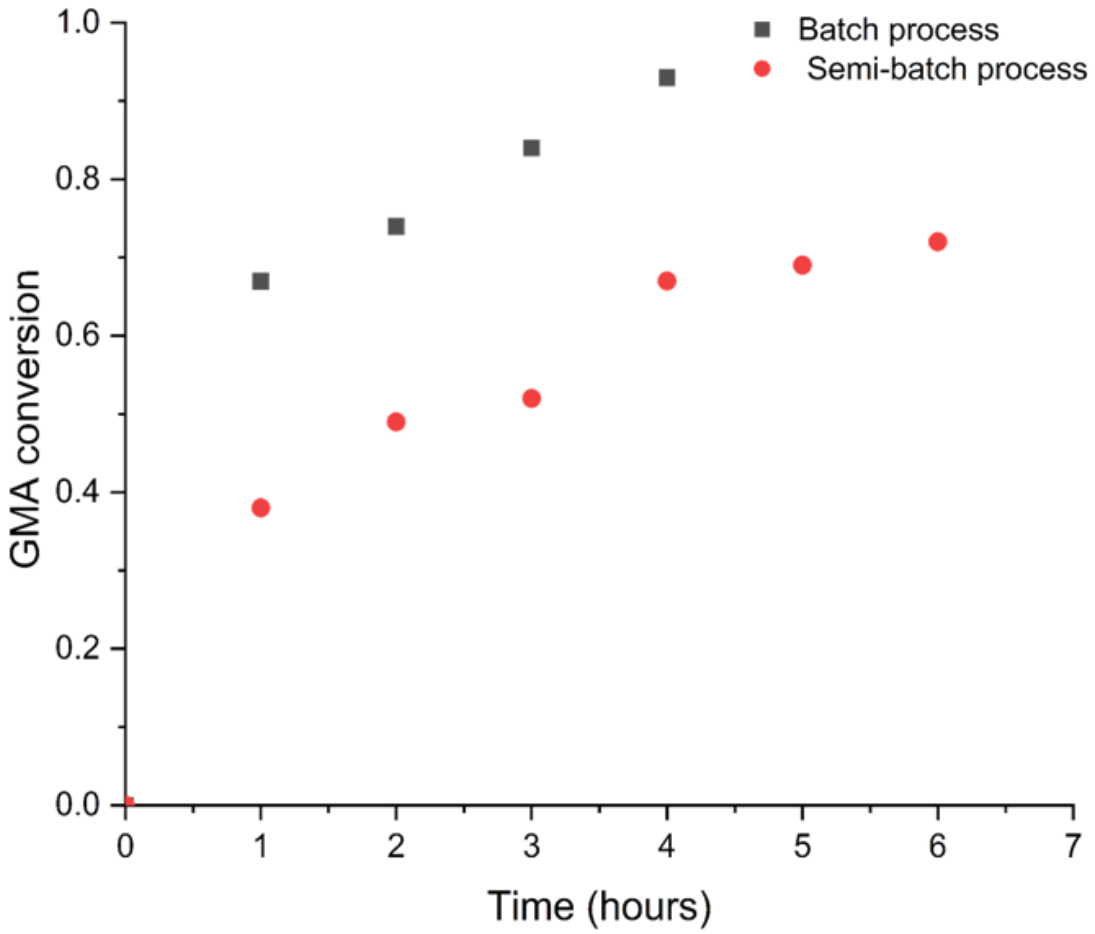

Figure A 5. Comparison of poly(GMA) conversion in batch and semi-batch processes for *Myr*/GMA-90 (GMA conversion is 100% after almost four hours in batch process).

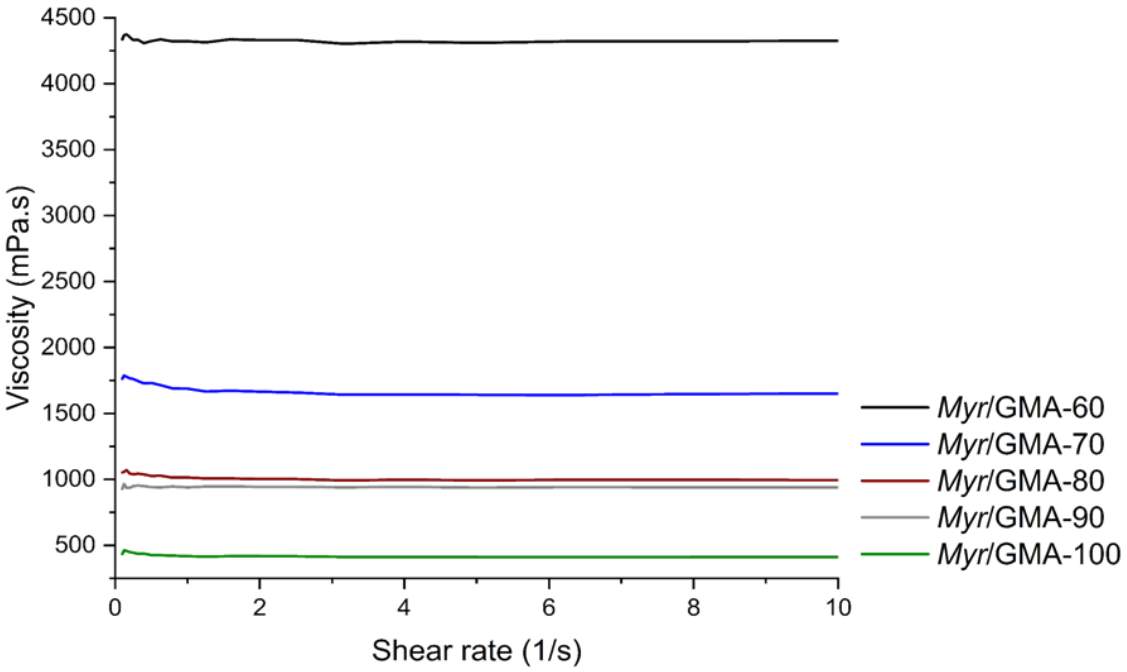

Figure A 6. Viscosity as a function of steady shear rate for the various poly(Myr-co-GMA) at ambient temperature (*Myr*/GMA-100 refers to poly(myrcene) homopolymer).

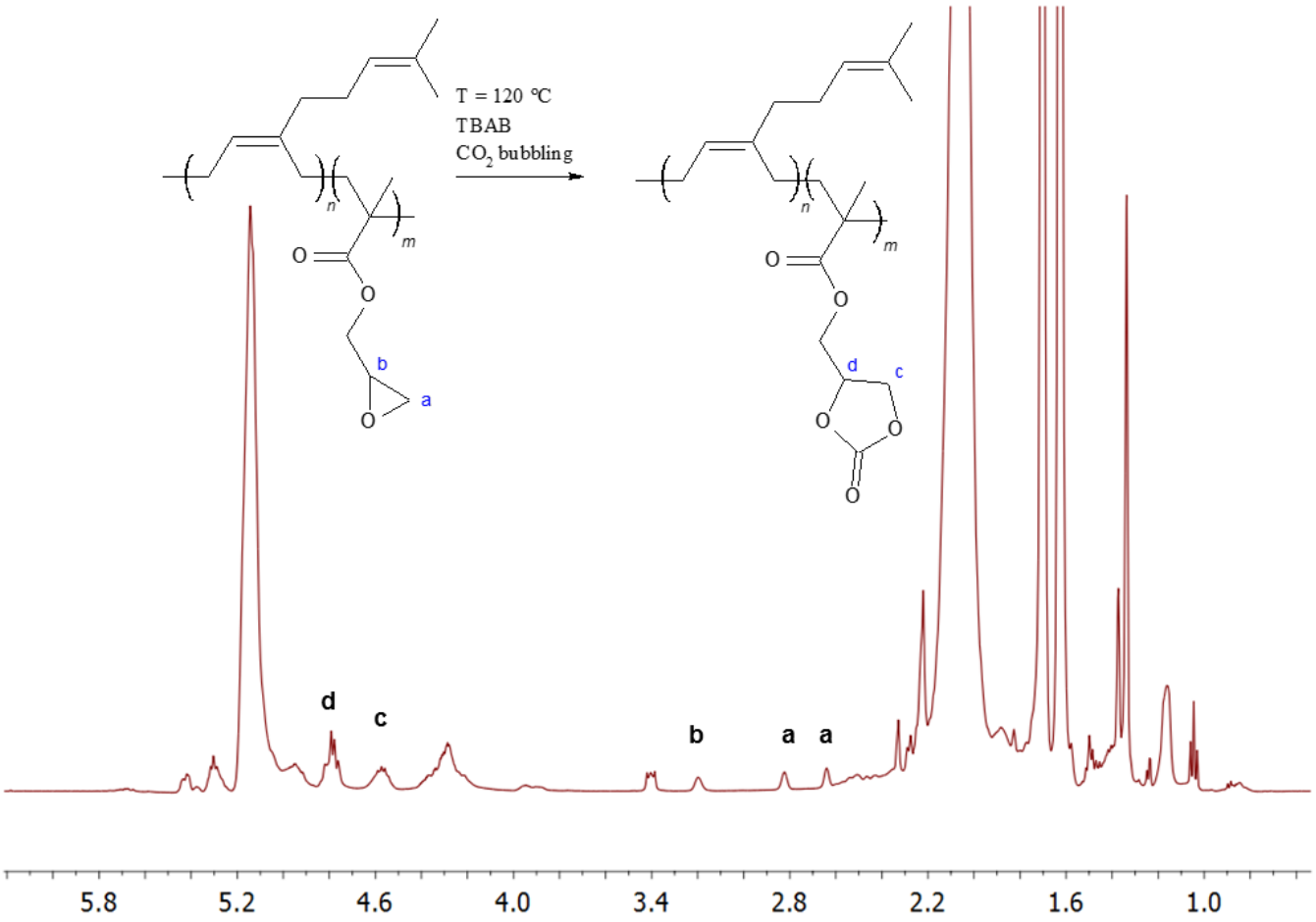

Figure A 7. ^{1}H NMR spectrum of the carbonated Myr/GMA-90 after 10 hours.

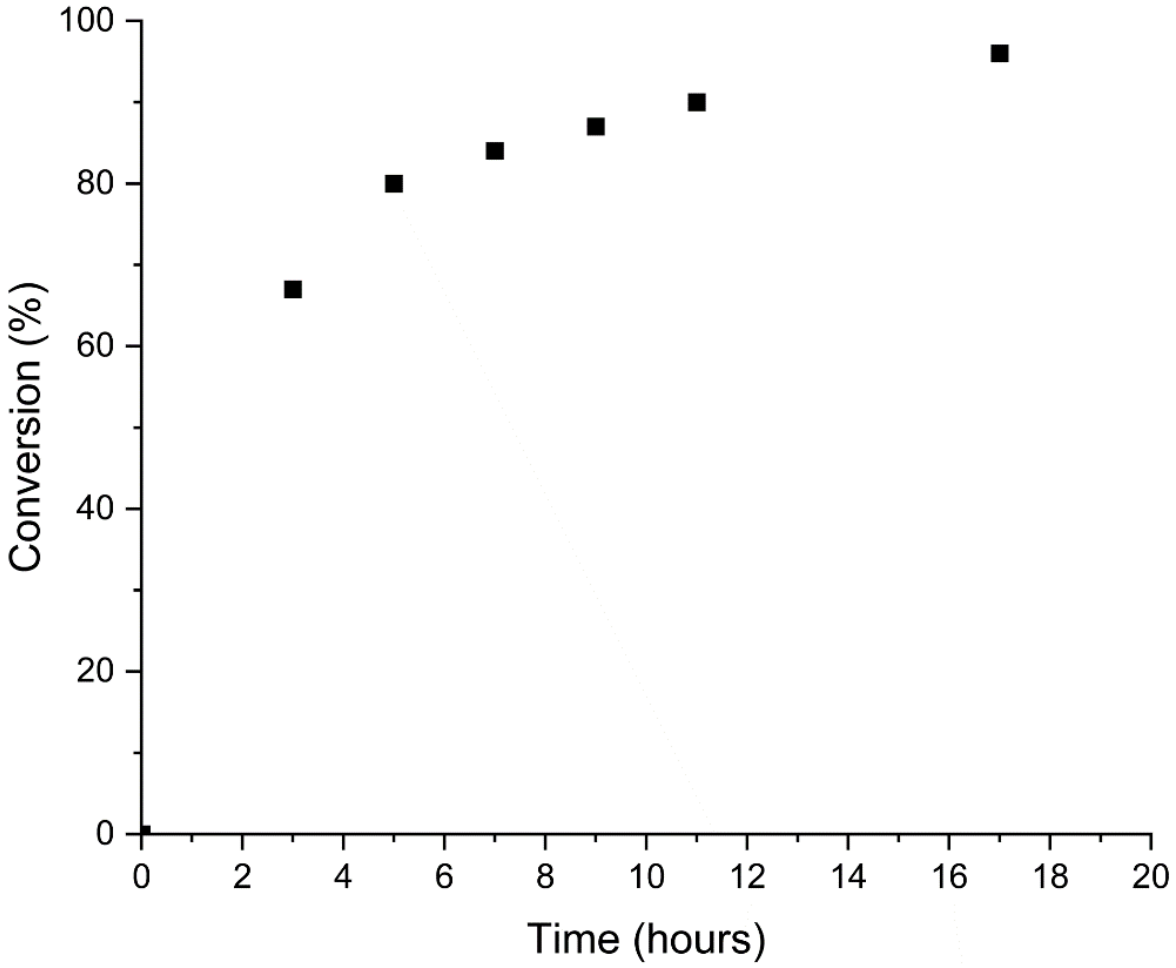

Figure A 8. Carbonation conversion versus time for carbonated Myr/GMA-90.

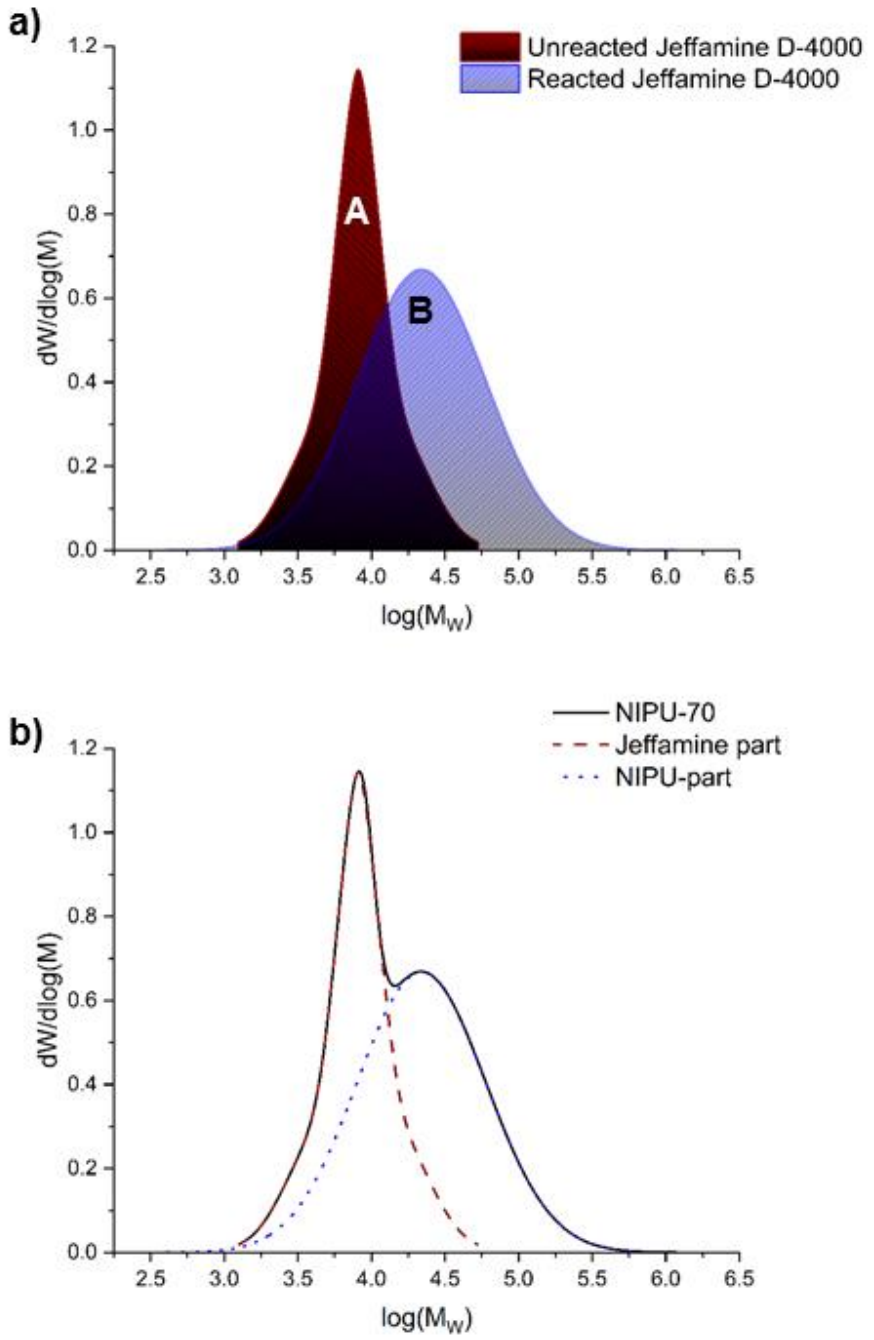

Figure A 9. GPC traces for NIPUs and Jeffamine D-4000, a) Separate distribution fit of GPC trace for both NIPU and Jeffamine D-4000 part of the mixture (NIPU-90), b) GPC trace of NIPU-70 and its distribution for NIPU and Jeffamine D-4000.

GPC curve of the synthesized NIPU (NIPU-70) was plotted on MATLAB and maximum peaks were identified. Gaussian model with four terms was fitted on the curve with 95% confidence bound. Numerical integration method was used to find the area under the two Gaussian curves in MATLAB (Integral function in MATLAB). The area under the unreacted Jeffamine D-4000 curve (area A) was calculated as 0.59. The area under the reacted Jeffamine D-4000 curve (area B) was calculated as 0.73.

The functions for the unreacted Jeffamine D-4000 and reacted Jeffamine D-4000 which were found through Gaussian curve fitting can be found in **Euqation A 1 a**nd **Euqation A 2,** respectively.

$$F1(x) = a1 * \exp\left(-\left(\frac{x-b1}{c1}\right)^2\right) + a2 * \exp\left(-\left(\frac{x-b2}{c2}\right)^2\right) + a3 * \exp\left(-\left(\frac{x-b3}{c3}\right)^2\right) + a4 * \exp\left(-\left(\frac{x-b4}{c4}\right)^2\right) \quad \textbf{(A1)}$$

$$F2(x) = a1 * \exp\left(-\left(\frac{x-b1}{c1}\right)^2\right) + a2 * \exp\left(-\left(\frac{x-b2}{c2}\right)^2\right) + a3 * \exp\left(-\left(\frac{x-b3}{c3}\right)^2\right) + a4 * \exp\left(-\left(\frac{x-b4}{c4}\right)^2\right) \quad \textbf{(A2)}$$

The constants for F1 and F2 can be find in **Table A 2**.

Table A 2. Constants values for the Gaussian models.

Const. / Functions	a1	b1	c1	a2	b2	c2	a3	b3	c3	a4	b4	c4
F1	-0.01702	3.824	0.04135	0.6723	3.909	0.1765	-0.008087	3.166	0.1044	0.4611	3.91	0.4783
F2	0.6657	4.34	0.6175	0.00599	93.06	528.1	-0.007034	7.021	2.337	-0.00636	1.956	2.169

The fraction of Jeffamine D-4000 that is chemically bounded can be calculated using **Equation A 3**:

$$\%\ chemically\ bounded\ Jeffamine\ D-4000 = \frac{area\ B}{area\ A + area\ B} * 100 \qquad \textbf{(A3)}$$

$$\%\ chemically\ bounded\ Jeffamine\ D-4000 = \frac{0.73}{0.73 + 0.59} * 100 = 55.3\%$$

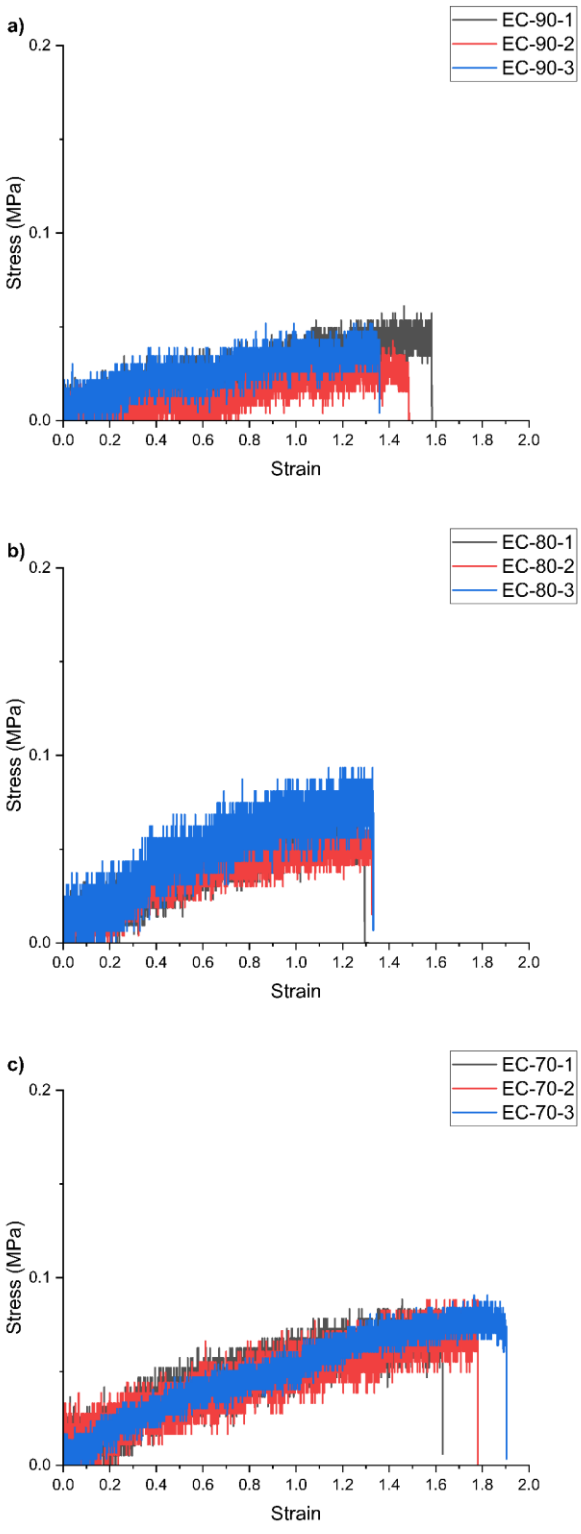

Figure A 10. Tensile test results of the crosslinked NIPUs, a) EC-90, b) EC-80 and c) EC-70 (the error is due to the loading cell used to measure the mechanical properties).

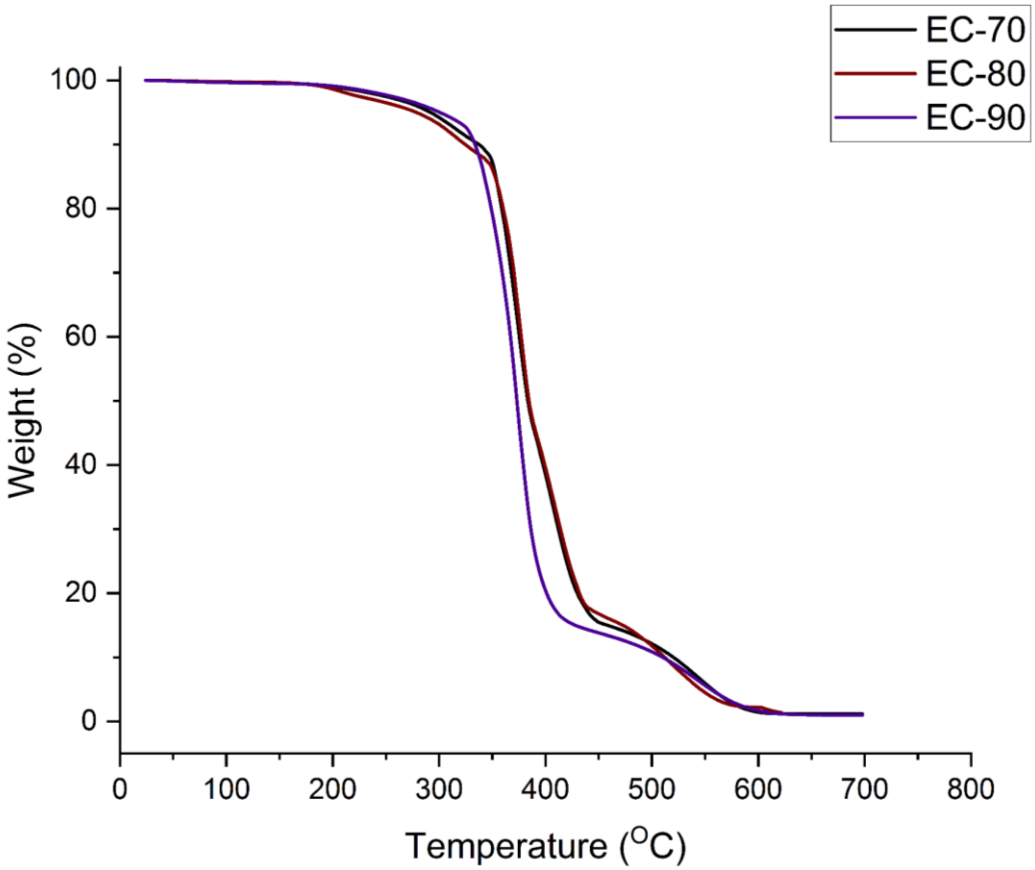

Figure A 11. TGA thermograms of end-capped NIPUs from room temperature to 700 °C under nitrogen purge.

Table A 3. Myr/GMA copolymerization formulations for different compositions at 90°C in bulk using AIBN as initiator.

ID[a)]	[*Myr*]$_0$ (M)	[GMA]$_0$ (M)	[AIBN](M)	t(min)	$f_{Myr,0}$[b)]
Myr/GMA-90	0.9367	0.1626	0.0320	360	0.9
Myr/GMA-80	0.6120	0.1573	0.0158	360	0.8
Myr/GMA-70	0.6518	0.3161	0.0259	360	0.7
Myr/GMA-60	0.6366	0.4218	0.0295	360	0.6

([a)] Experimental identification given by *Myr*/GMA-XX, where XX refers to the rounded % initial molar fraction of *Myr* in the mixture ($f_{Myr,0}$)); ([b)] Initial molar ratio of myrcene in the feed).

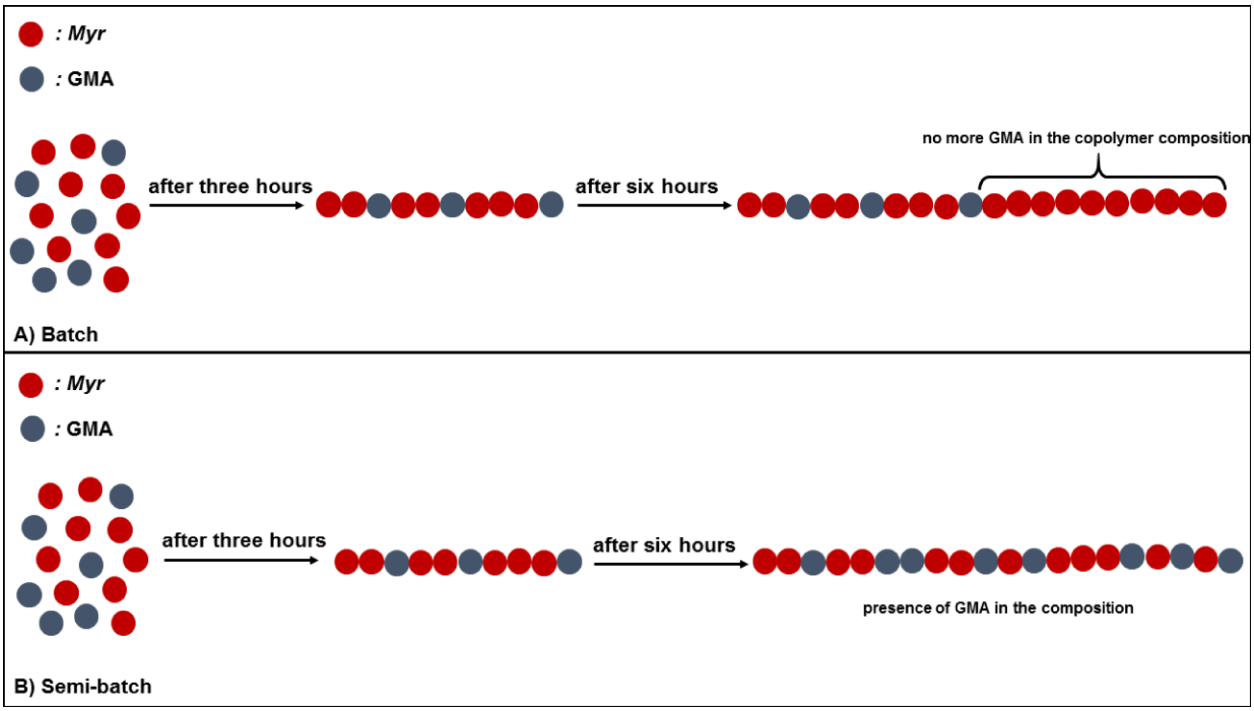

Scheme A 1. Summary of ideal copolymer microstructure in two different polymerization processes A) batch and B) semi-batch (since conventional free radical polymerization was used to synthesize *Myr*/GMA copolymers, it is expected to have some poly(myrcene) homopolymers after six hours in the batch process, since the GMA would be depleted, but in the scheme this compositional drift is represented by poly(*Myr*) homopolymer segment at the tail end of each chain).

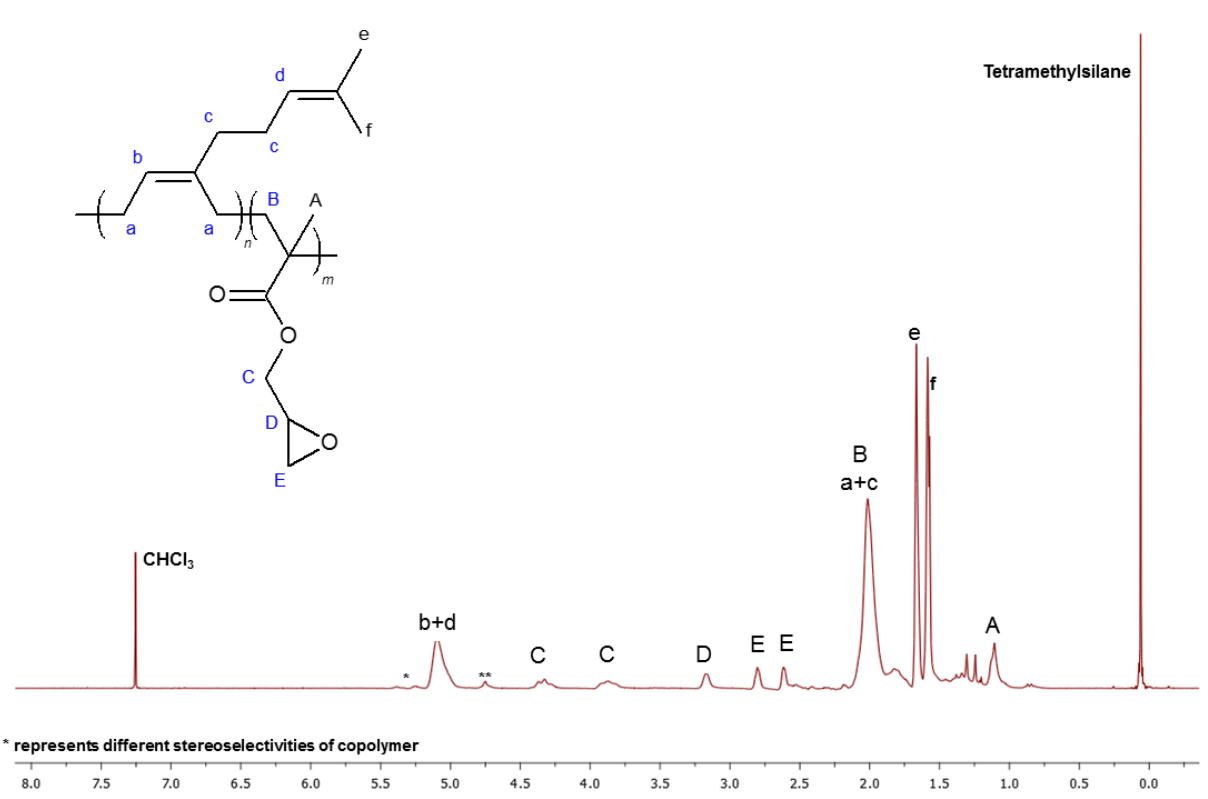

Figure A 12. ^{1}H NMR spectra of the *Myr*/GMA-90.

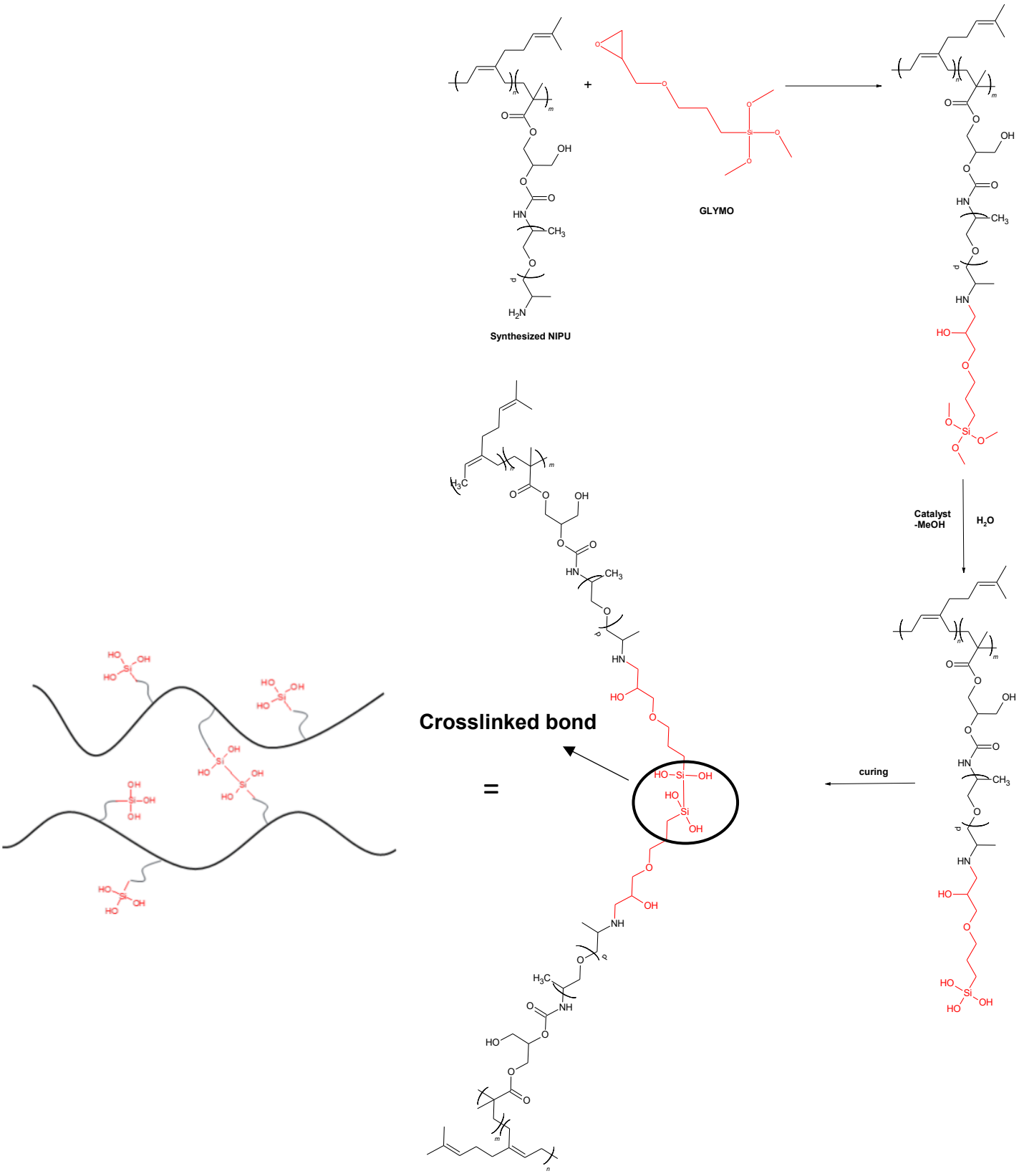

Figure A 13. Reaction schematic of GLYMO with the synthesized NIPU.

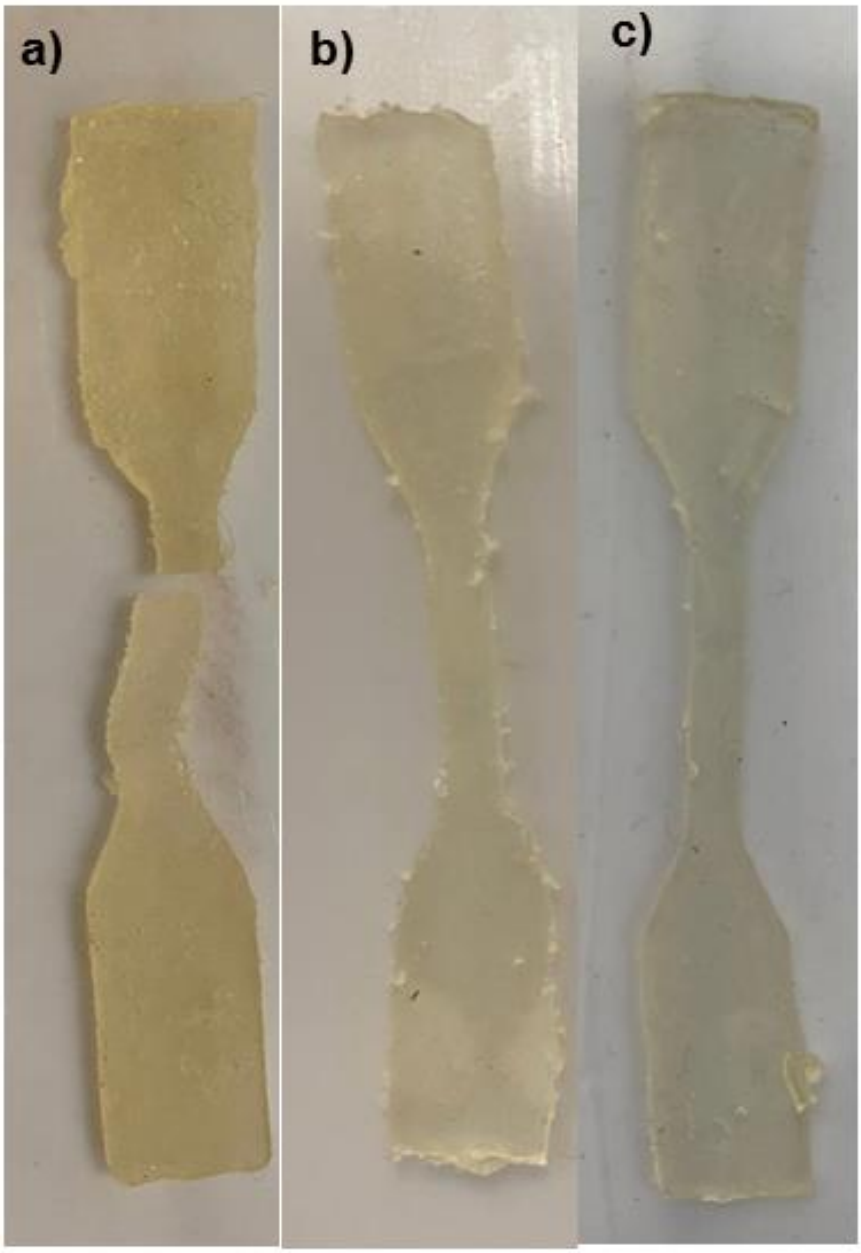

Figure A 14. Tensile bars for the synthesized films, a) EC-70, b) EC-80 and c) EC-90.

APPENDIX B

SUPPORTING INFORMATION FOR DESIGN OF CROSSLINKED NETWORKS WITH HYDROXYURETHANE LINKAGES VIA BIO-BASED ALKYL METHACRYLATES AND DIAMINES

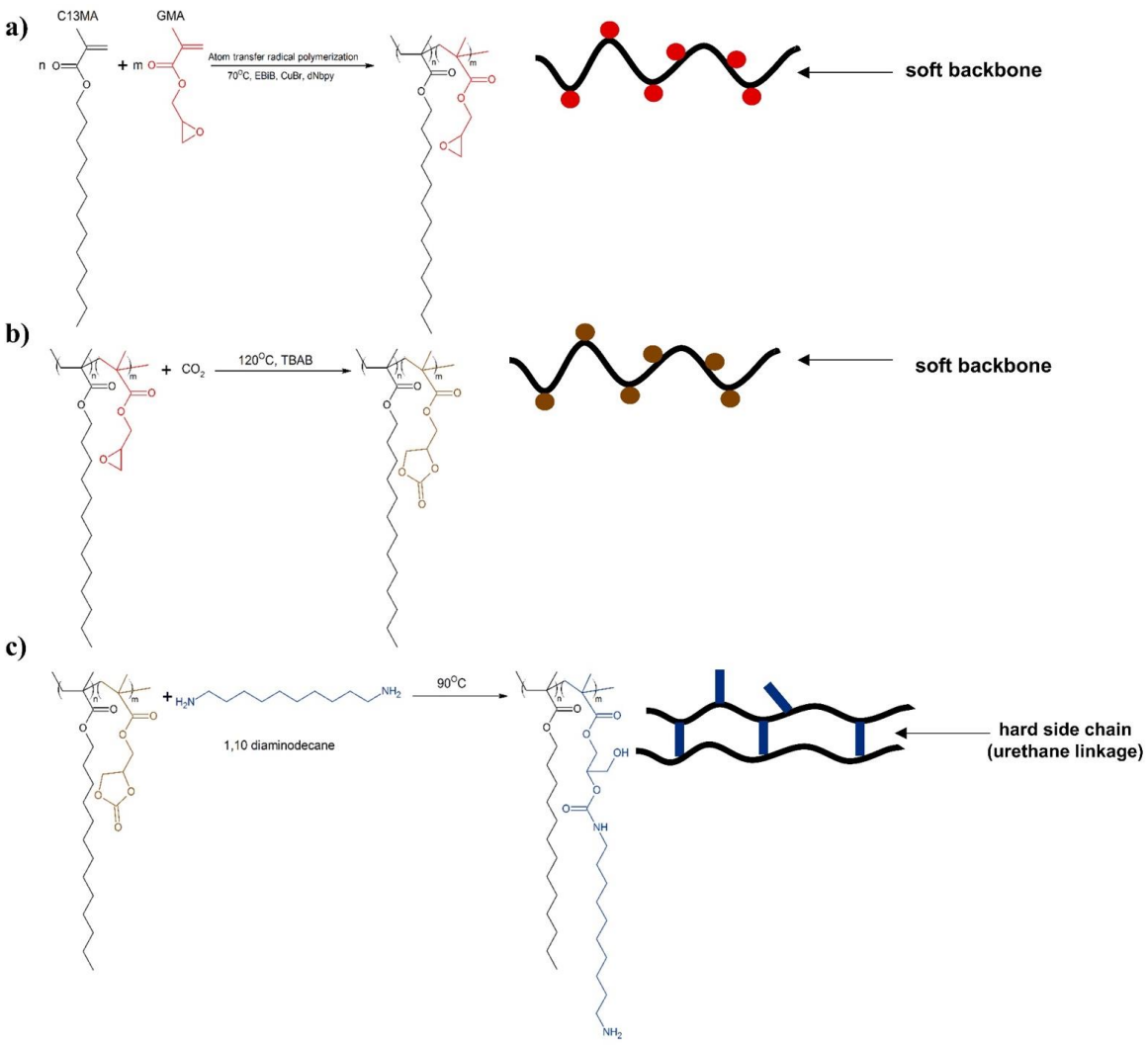

Figure B 1. Overall schematic of the study.

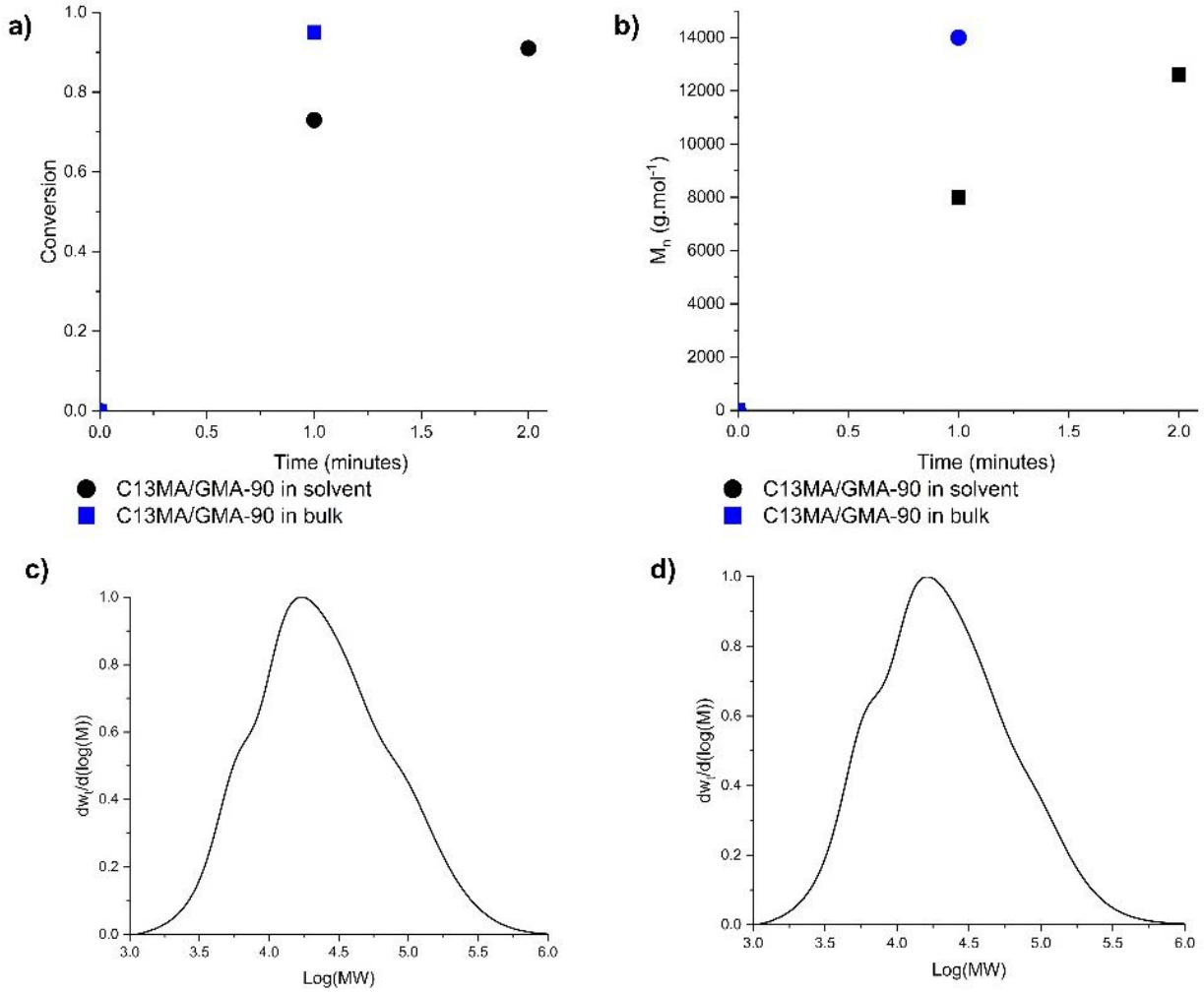

Figure B 2. Free radical polymerization (FRP) of C13MA/GMA-90 in bulk and dioxane as solvent, a) Conversion of copolymers vs time in bulk and dioxane, b) M_n vs time for copolymers in bulk and dioxane, c) GPC trace of C13MA/GMA-90 synthesized in bulk after two minutes, d) GPC trace of C13MA/GMA-90 synthesized in dioxane after two minutes.

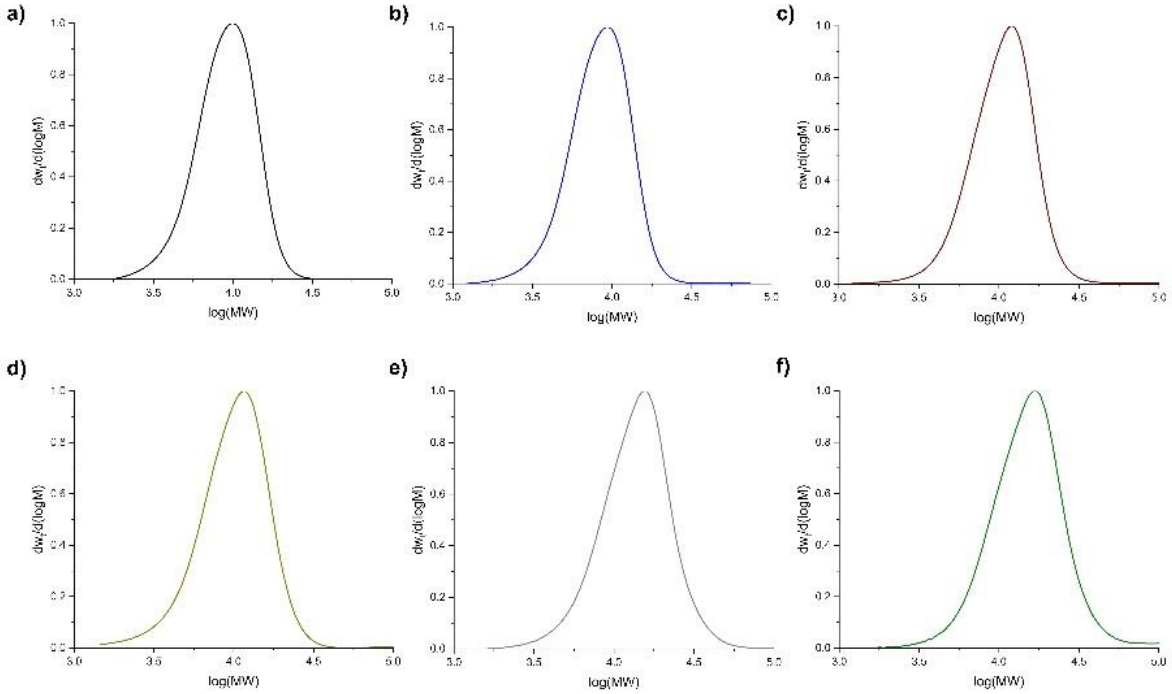

Figure B 3. GPC traces of C13MA/GMA copolymers, a) C13MA/GMA-90, b) C13MA/GMA-80, c) C13MA/GMA-70, d) C13MA/GMA-60, e) C13MA/GMA-50 and e) C13MA/GMA-40.

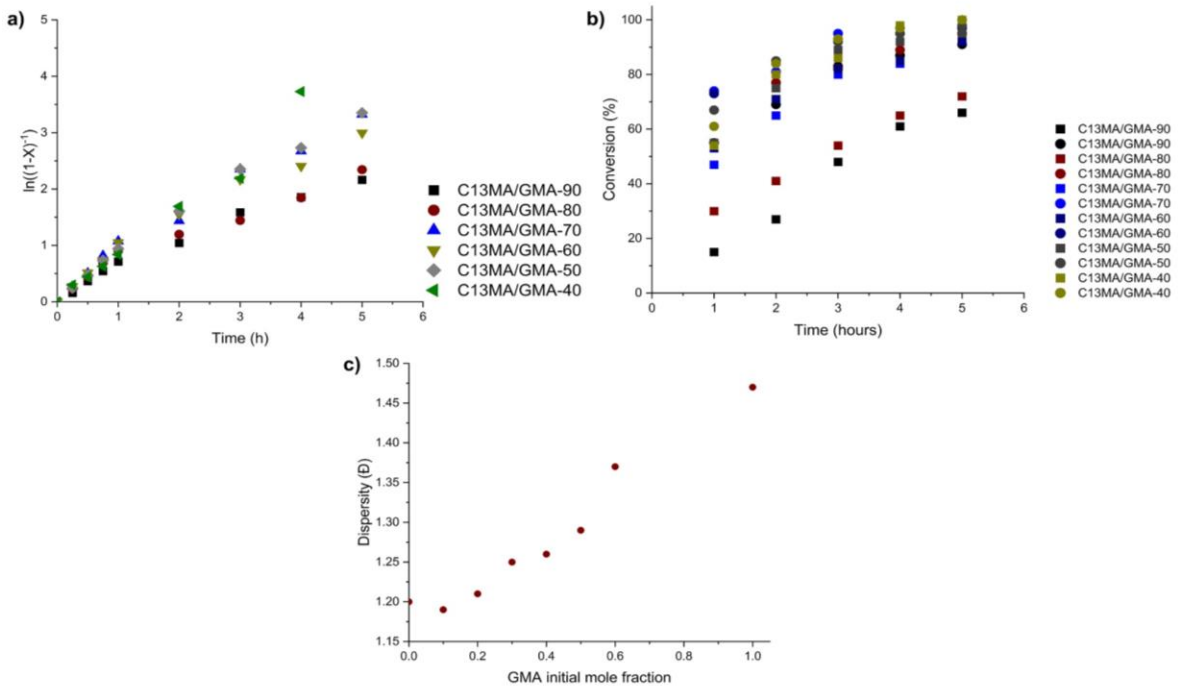

Figure B 4. ATRP copolymerization of C13MA/GMA at 70°C. The complete conditions are given in **Table 4.1** and **Table B 1**. a) semi-logarithmic kinetic plots of $\ln[(1-X)^{-1}]$ (X is conversion) versus reaction time, b) individual conversions for each monomers (C13MA and GMA) versus reaction time (■ is for GMA conversion and ● is for C13MA conversion), c) dispersity (Đ) of poly(C13MA-co-GMA)s as a function of GMA initial fraction in the feed.

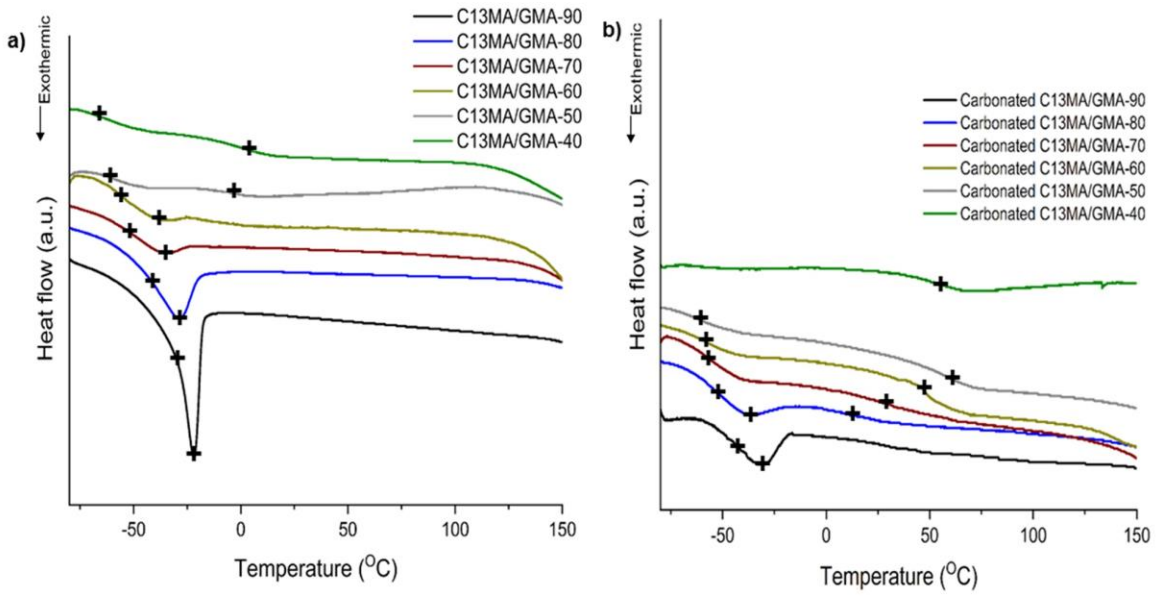

Figure B 5. Comparison of DSC curves for C13MA/GMA before and after carbonation; b) carbonated poly(C13MA-*co*-GMA) copolymers (all data are reported in **Table 4.2**).

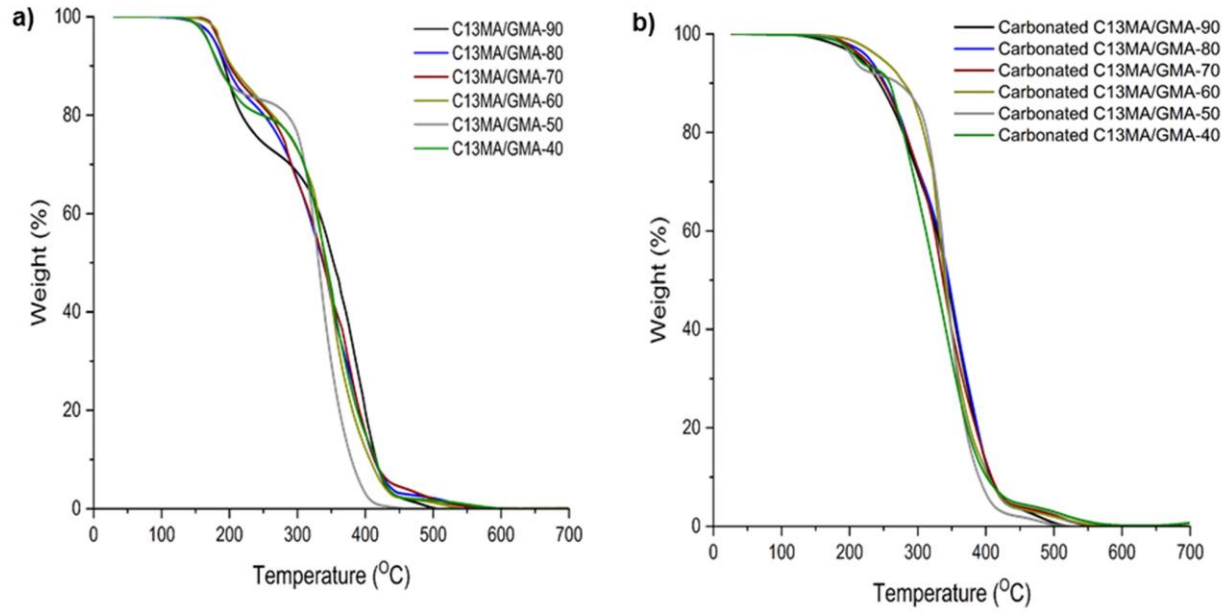

Figure B 6. TGA curves for C13MA/GMA copolymers before and after carbonation; a) synthesized poly(C13MA-*co*-GMA) copolymers and b) carbonated poly(C13MA-*co*-GMA) copolymers with heating rate of 10 °C min^{-1} from room temperature to 700°C (all data are reported in **Table 4.2**).

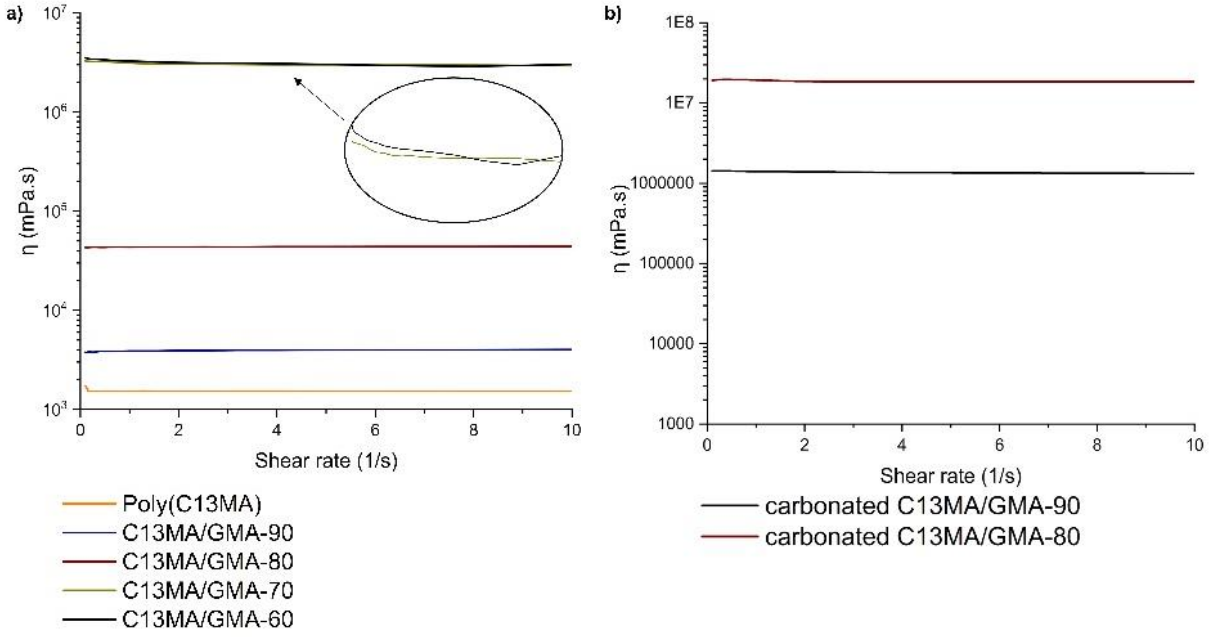

Figure B 7. Viscosity tests comparing C13MA/GMA copolymers after and before carbonation; a) poly(C13MA-co-GMA)s versus b) carbonated poly(C13MA-co-GMA)s (η is viscosity (mPa·s)).

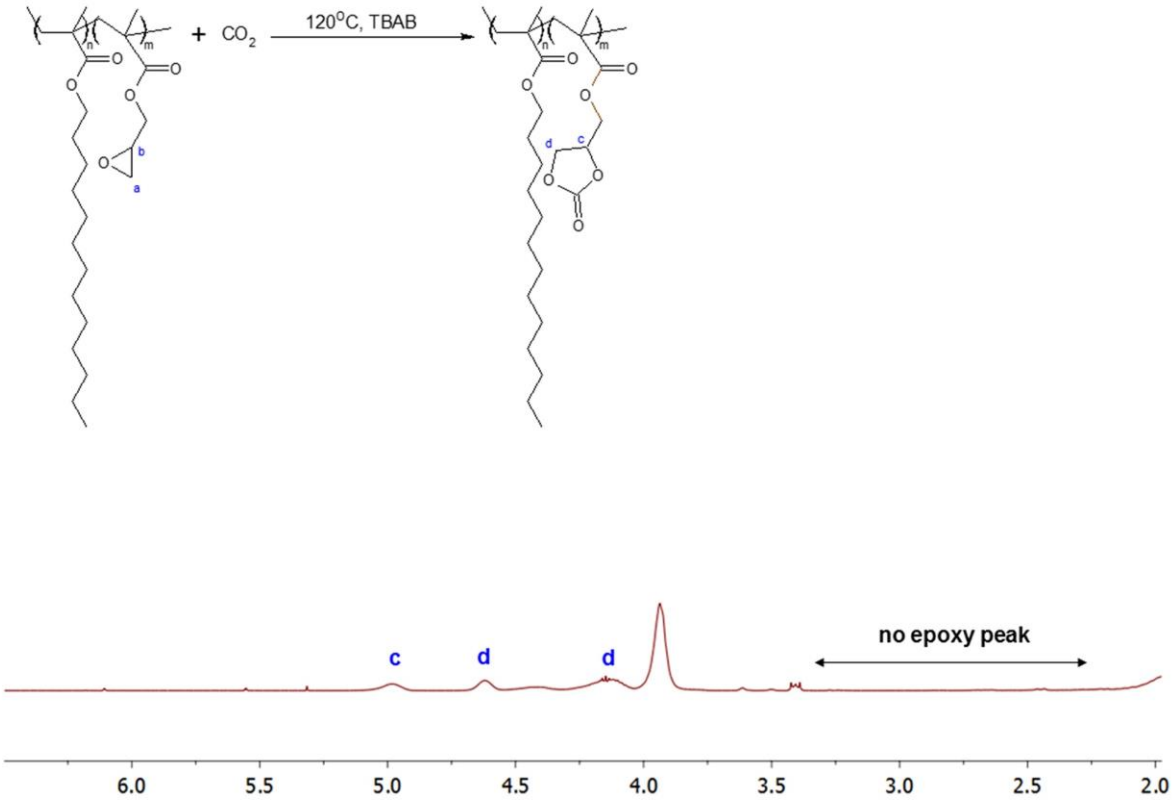

Figure B 8. ^{1}H NMR spectrum of carbonated C13MA/GMA-90 copolymer after 24 hours.

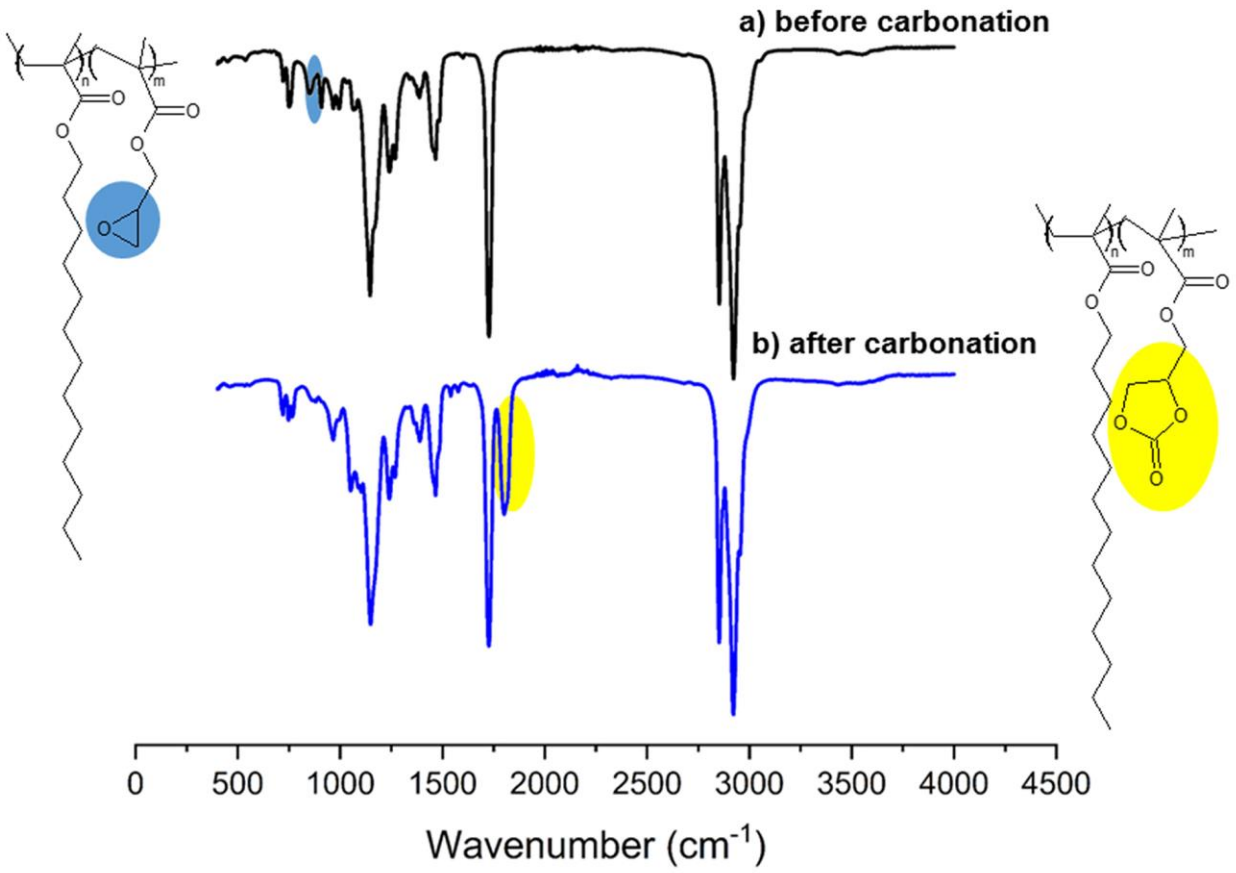

Figure B 9. FTIR spectra for C13MA/GMA copolymer before and after carbonation; a) FTIR spectrum of C13MA/GMA-60, b) FTIR spectrum of carbonated C13MA/GMA-60 after 24 hours at 120°C.

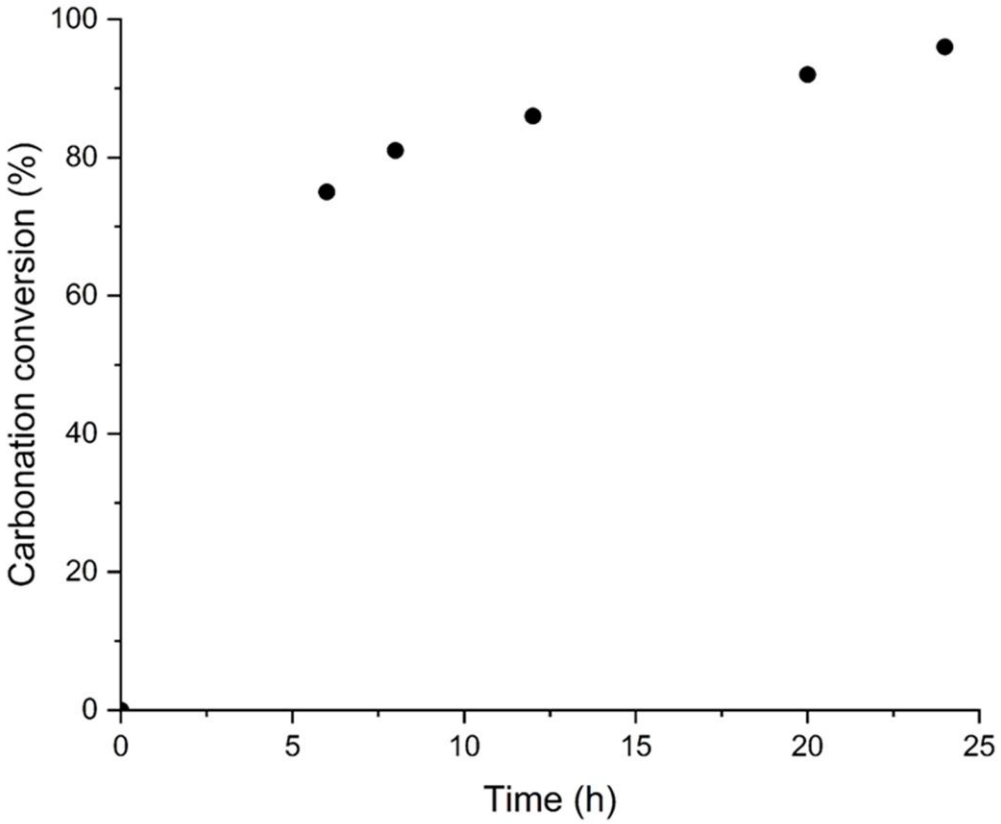

Figure B 10. Carbonation conversion versus time for C13MA/GMA-90 at 120°C.

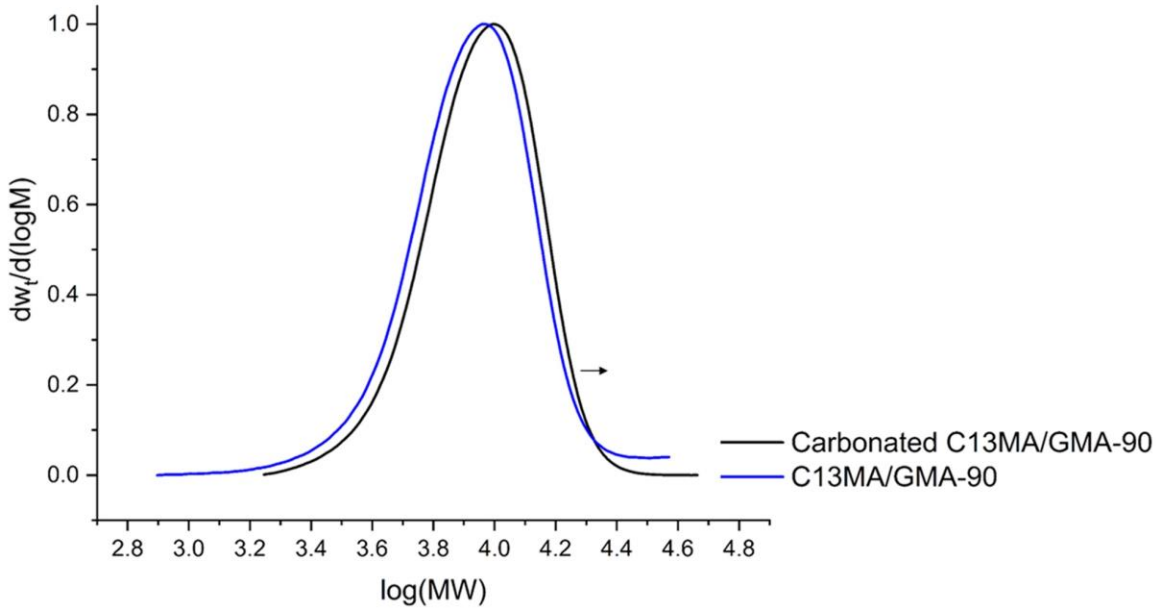

Figure S11.

Figure B 11. Normalized GPC peaks for carbonated C13MA/GMA-90 versus its precursor C13MA/GMA-90.

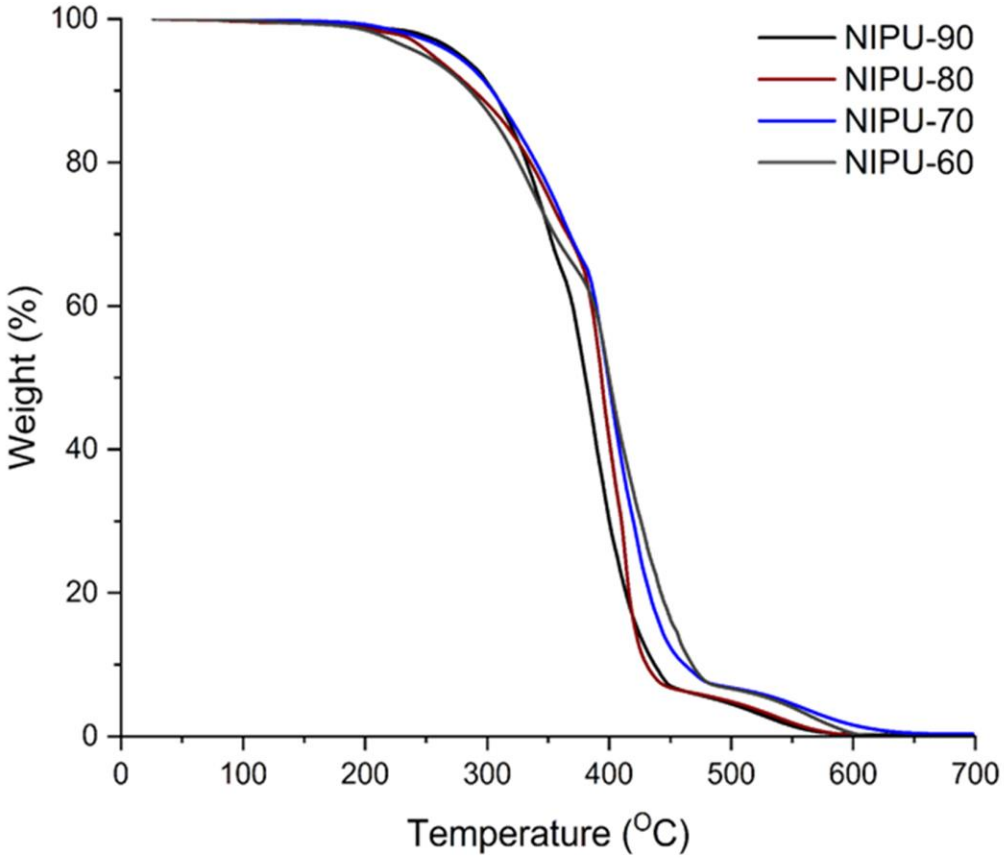

Figure B 12. TGA curves for the crosslinked networks with the values which are reported in **Table 4.4**.

Table B 1. C13MA/GMA copolymerization formulations for different compositions at 70°C using ATRP.

ID[a)]	$[C13MA]_0$ (mol)	$[GMA]_0$ (mol)	[EBiB] (mol)	[Cu(I)Br] (mol)	[dNbpy] (mol)	[Anisole] (mol)	t(min)	$f_{C13MA,0}$[b)]
C13MA/GMA-90	0.270	0.030	0.015	7.5×10^{-4}	1.5×10^{-3}	0.154	300	0.9
C13MA/GMA-80	0.189	0.046	0.011	5.7×10^{-4}	1.1×10^{-3}	0.129	300	0.8
C13MA/GMA-70	0.167	0.072	0.011	5.9×10^{-4}	1.2×10^{-3}	0.12	300	0.7
C13MA/GMA-60	0.154	0.100	0.011	6.4×10^{-4}	1.3×10^{-3}	0.106	300	0.6
C13MA/GMA-50	0.134	0.134	0.011	6.6×10^{-4}	1.3×10^{-3}	0.106	300	0.5
C13MA/GMA-40	0.114	0.171	0.011	7.2×10^{-4}	1.4×10^{-3}	0.100	300	0.4

([a)] Experimental identification given by C13MA/GMA-XX, where XX refers to the rounded % initial molar fraction of C13MA in the mixture ($f_{C13MA,0}$)); ([b)] Initial molar ratio of C13MA in the feed).

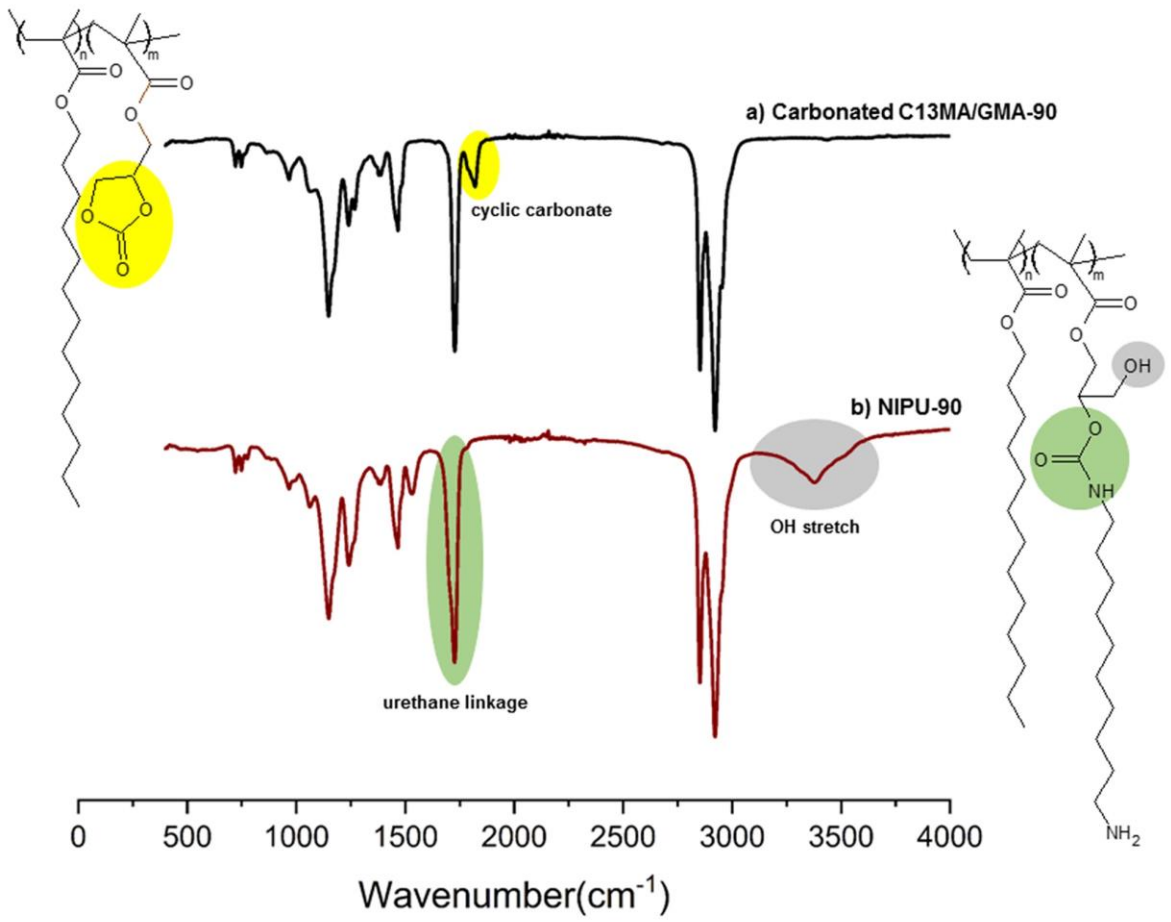

Figure B 13. FT-IR spectra for carbonated C13MA/GMA-90 and NIPU-90.

APPENDIX C

SUPPORTING INFORMATION FOR EFFECT OF ALKYL METHACRYLATE/GLYCIDYL METHACRYATE COPOLYMER BACKBONE STRUCTURE ON MECHANICAL PROPERTIES OF HYDROXYURETHANE-CROSSLINKED NETWORKS

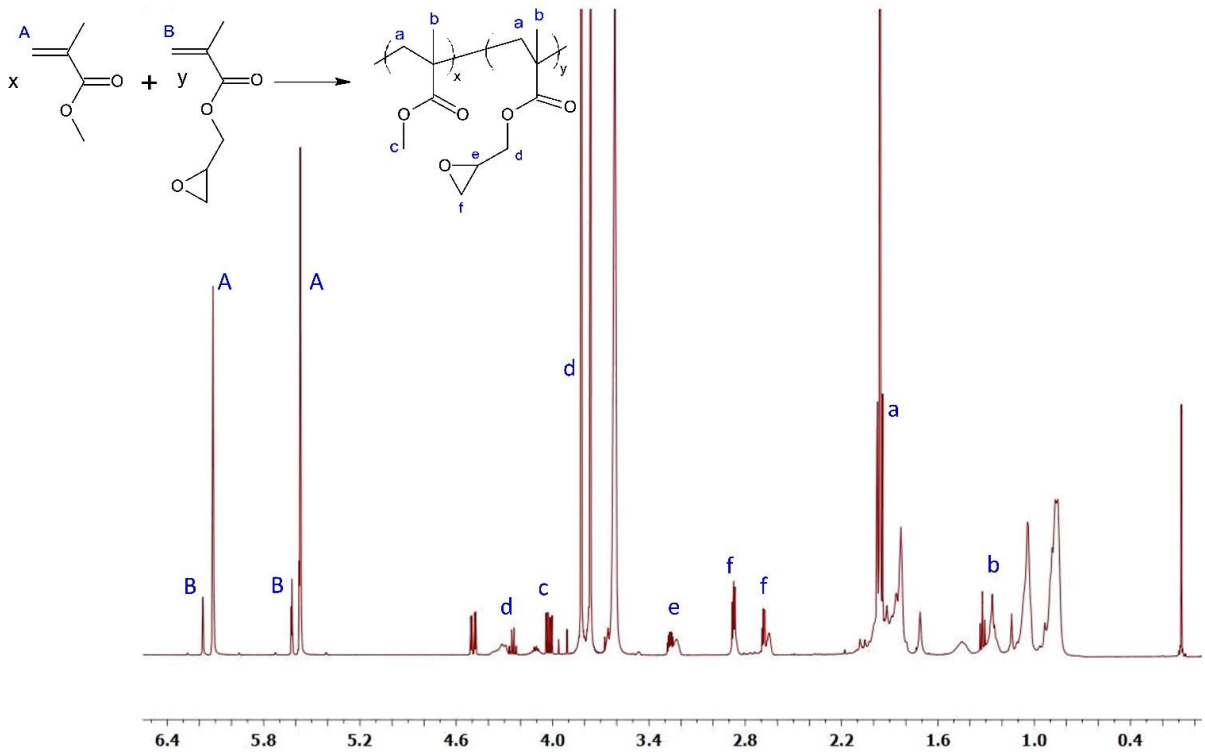

Figure C 1. ^{1}H NMR spectrum for MMA/GMA-90 after two hours. ^{1}H NMR ($CDCl_3$, ppm): 6.13- 6.20 ppm (m, $1H^{GMA}$), 6.04- 6.12 ppm (m, $1H^{MMA}$), 5.50- 5.65 ppm (m, $1H^{GMA}$), 5.48-5.61 ppm (m, $1H^{MMA}$), 4.4−4.2 (br, $1H^{P(GMA)}$), 4.15-3.95 (br, $3H^{P(MMA)}$), 3.92−3.75 (br, $1H^{P(GMA)}$), 3.3−3.18 (br, $1H^{P(GMA)}$), 2.95−2.8 (br, $1H^{P(GMA)}$), 2.75−2.65 (br, $1H^{P(GMA)}$), 2.2−1.8 (br, $3H^{P(GMA)+P(MMA)}$), 1.15, 0.93 (br, $3H^{P(GMA)+P(MMA)}$).

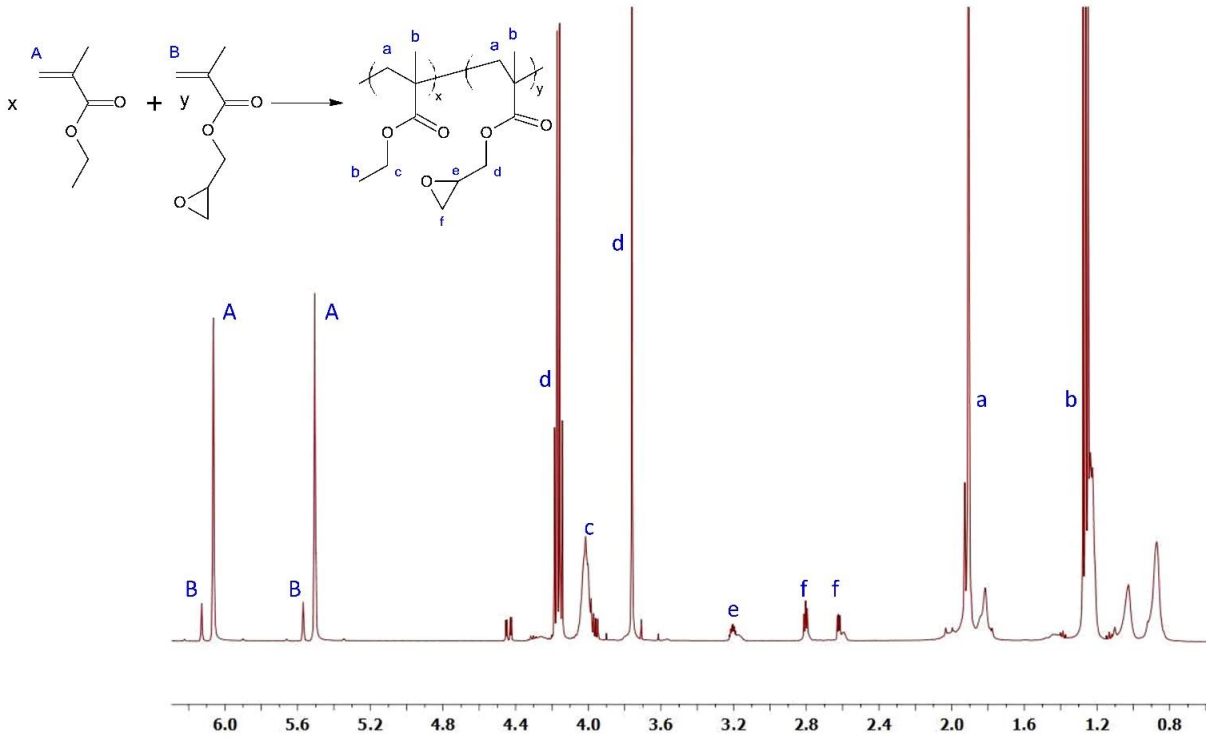

Figure C 2. ^{1}H NMR spectrum for EMA/GMA-90 after four hours. ^{1}H NMR ($CDCl_3$, ppm): 6.13- 6.20 ppm (m, $1H^{GMA}$), 6.04- 6.12 ppm (m, $1H^{EMA}$), 5.50- 5.65 ppm (m, $1H^{GMA}$), 5.45-5.65 ppm (m, $1H^{EMA}$), 4.35−4.12 (br, $1H^{P(GMA)}$), 4.1−3.85 (br, $2H^{P(EMA)}$), 3.85-3.75 (br, $1H^{P(GMA)}$), 3.35−3.15 (br, $1H^{P(GMA)}$), 2.95−2.75 (br, $1H^{P(GMA)}$), 2.75−2.55 (br, $1H^{P(GMA)}$), 2.25−1.75 (br, $3H^{P(GMA)+P(EMA)}$), 1.15, 0.95 (br, $6H^{P(GMA)+P(EMA)}$).

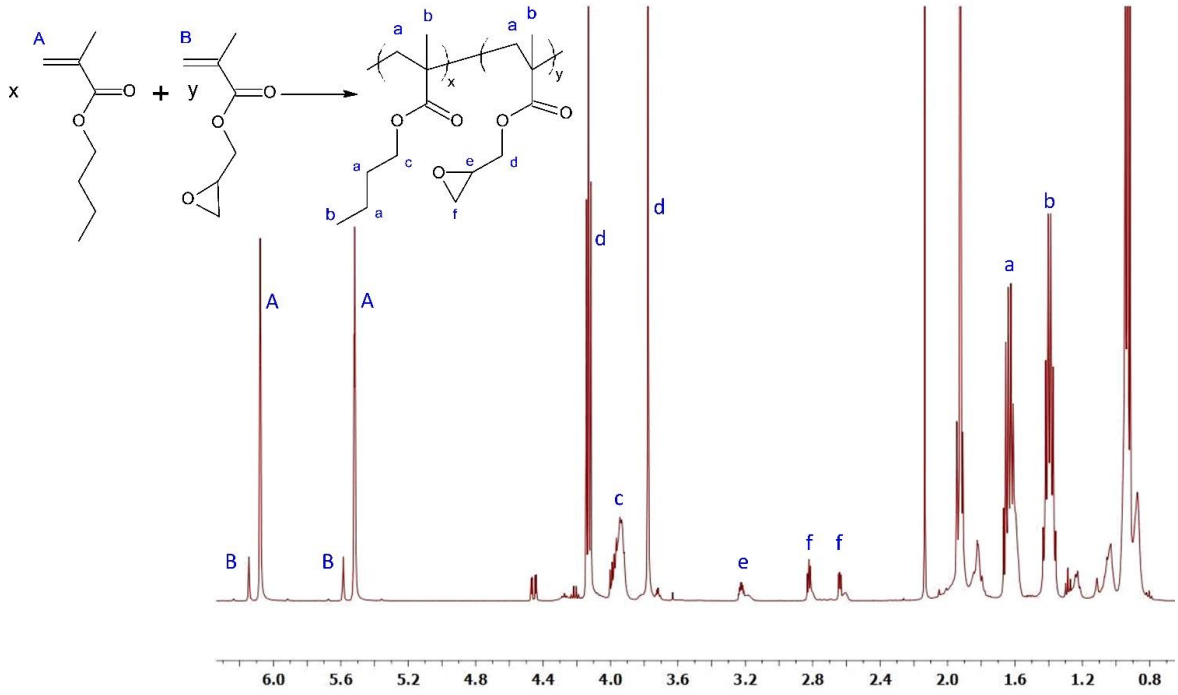

Figure C 3. ^{1}H NMR spectrum for BMA/GMA-90 after four hours. ^{1}H NMR ($CDCl_3$, ppm): 6.11- 6.22 ppm (m, $1H^{GMA}$), 6.04- 6.12 ppm (m, $1H^{BMA}$), 5.50- 5.65 ppm (m, $1H^{GMA}$), 5.45-5.65 ppm (m, $1H^{BMA}$), 4.3−4.1 (br, $1H^{P(GMA)}$), 4.1−3.85 (br, $2H^{P(BMA)}$), 3.85-3.7 (br, $1H^{P(GMA)}$), 3.3−3.1 (br, $1H^{P(GMA)}$), 2.85−2.75 (br, $1H^{P(GMA)}$), 2.7−2.55 (br, $1H^{P(GMA)}$), 2.25−1.75 (br, $6H^{P(GMA)+P(BMA)}$), 1.15, 0.95 (br, $6H^{P(GMA)+P(BMA)}$).

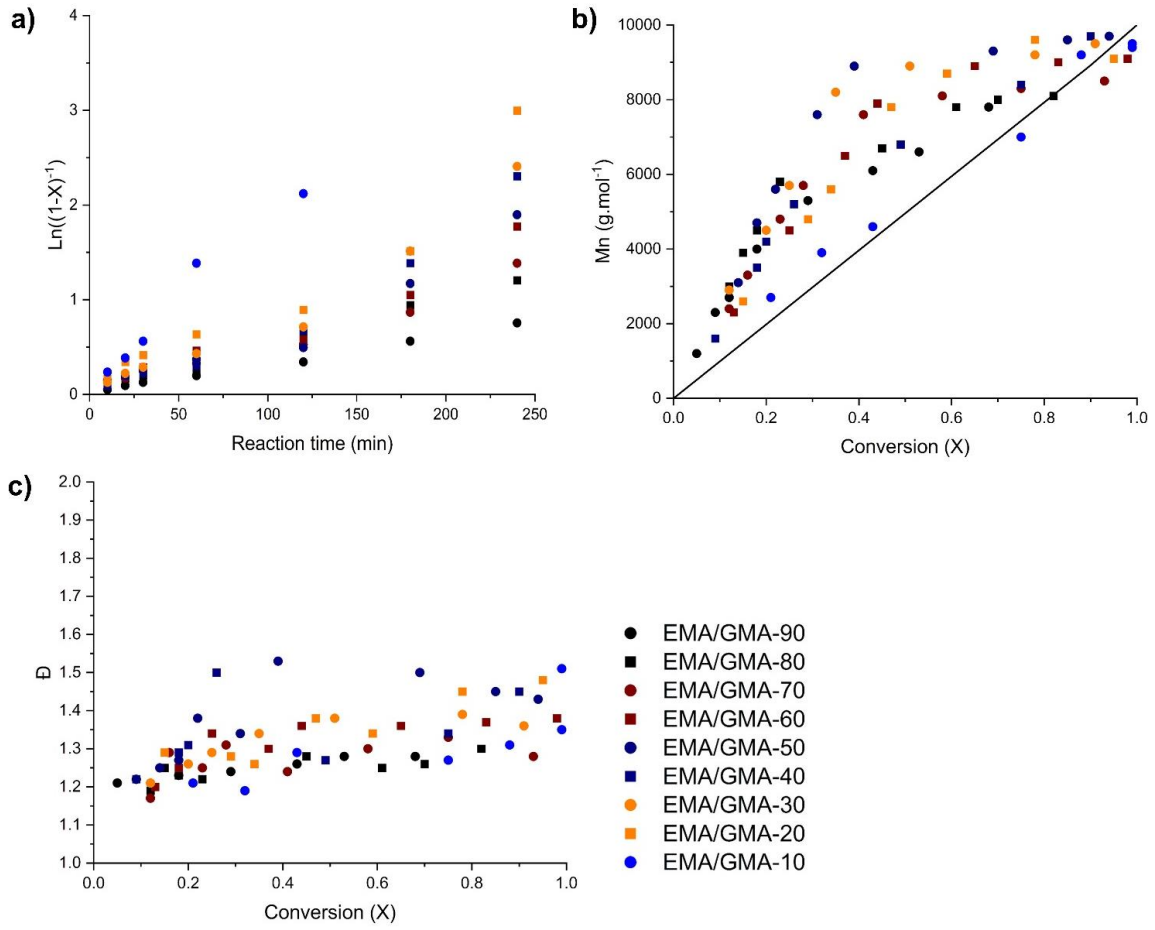

Figure C 4. Kinetic studies for EMA/GMA copolymers at 70°C. All kinetic results are reported in **Table 1**. a) semi-logarithmic kinetic plots of $\ln[(1-X)^{-1}]$ versus reaction time, where X is monomer conversion, b) M_n versus X for the various EMA/GMA copolymers (the line indicates the theoretical M_n ($M_{n,theo}$) versus X based on the monomers to initiator ratio for EMA/GMA copolymerizations ($M_{n,target} \sim 10$ kg.mol^{-1} at $X = 1$), c) dispersity ($Đ$) versus conversion (X).

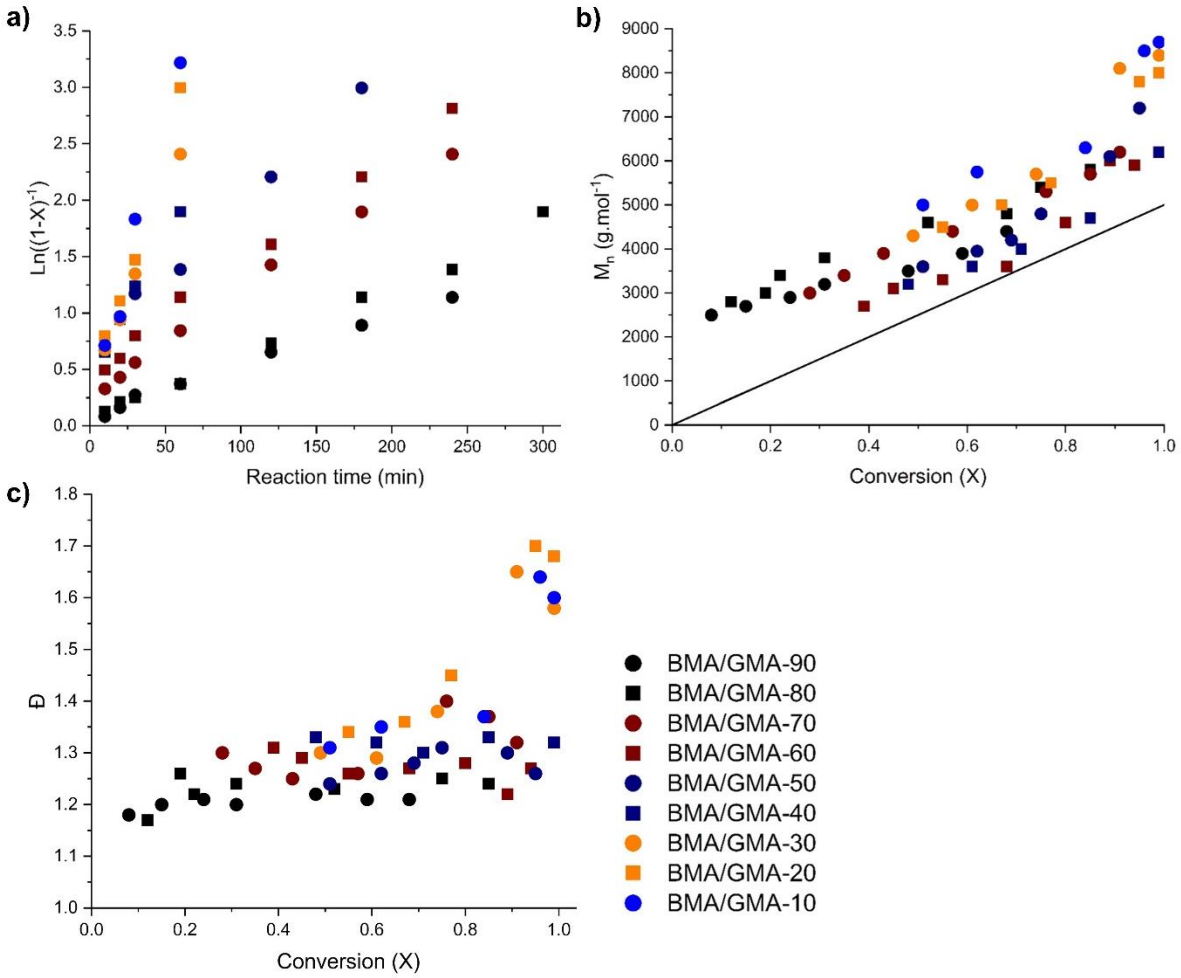

Figure C 5. Kinetic studies for EMA/GMA copolymers at 70°C. All kinetic results are reported in **Table 1**. a) semi-logarithmic kinetic plots of $\ln[(1-X)^{-1}]$ versus reaction time, where X is monomer conversion, b) M_n versus X for the various BMA/GMA copolymers (the line indicates the theoretical M_n ($M_{n,theo}$) versus X based on the monomers to initiator ratio for BMA/GMA copolymerizations ($M_{n,target}$ ~ 5 kg.mol^{-1} at X = 1), c) dispersity ($Đ$) versus conversion (X).

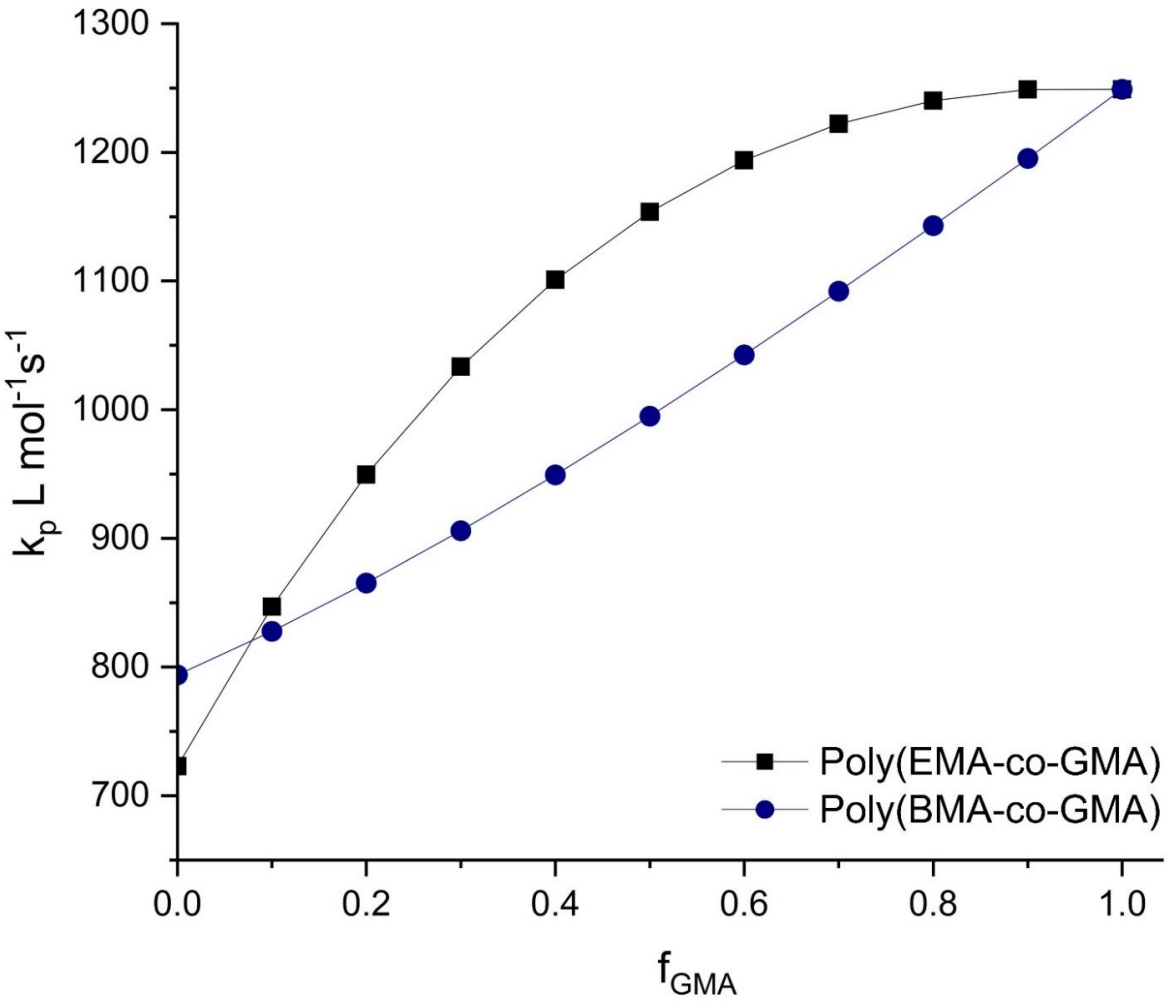

Figure C 6. Plot of kp vs fGMA for EMA/GMA and BMA/GMA copolymers using equation proposed by Fukuda (**Equation C1):**

$$k_p = \frac{r_{1f_1^2+r_1f_2^2+2f_1f_2}}{\frac{r_1f_1}{k_{p,1}}+\frac{r_2f_2}{k_{p,2}}} \quad \text{(C1)}$$

Equation C1 shows the terminal model equation proposed by Fukuda et. al., where r_1 is the reactivity ratio for GMA, r_2 is the reactivity ratio of EMA or BMA (reactivity ratios are reported in this study), f_1 and f_2 are the initial molar fraction of comonomers in the feed and $k_{p,1}$ and $k_{p,2}$ are the propagation rate coefficients for GMA and EMA or BMA, respectively.

A) Determination of reactivity ratios of EMA and GMA by Fineman–Ross (FR), Kelen–Tüdös (KT) and non-linear least square (NLLS) model

Terminal models (FR and KT):

All formulations that were used to calculate the reactivity ratios of EMA (r_{EMA}) and GMA (r_{GMA}) are tabulated in **Table C 1**. It was assumed that the selected copolymers had low conversions that the monomer composition was unchanged. Reactivity ratios of the monomers were first calculated by Fineman-Ross (FR) method and then Kelen-Tüdös (KT) approach was used. FR approach is basically rearrangement of Mayo-Lewis copolymer equation into a linear form. In KT method, a positive parameter between (0,1) is introduced into the linearized equation, giving equal weight to all experimental data points (in FR method, any positive value can be assumed). To calculate reactivity ratios via FR approach, two variables of G and H are defined as provided in **Equation C2** and **C3**. There is a linear relationship between G and H, which gives the reactivity ratios as the slope and intercept as shown in **Equation C4**. G versus H is plotted and shown in **Figure 5.1**.

$$G = \left(\frac{f_{GMA}}{f_{EMA}}\right)\left[\frac{(2F_{GMA}-1)}{F_{GMA}}\right] \quad \text{(C2)}$$

$$H = \left(\frac{f_{GMA}}{f_{EMA}}\right)^2\left[\frac{1-F_{GMA}}{F_{GMA}}\right] \quad \text{(C3)}$$

$$G = r_{GMA} \times H - r_{EMA} \quad \text{(C4)}$$

Equation C5, **C6**, **C7**and **C8** show the additional parameters used in KT method to calculate reactivity ratios.

$$\eta = \frac{G}{H+\alpha} \quad \text{(C5)}$$

$$\varepsilon = \frac{H}{H+\alpha} \quad \text{(C6)}$$

$$\alpha = \sqrt{H_{min}H_{max}} \quad \text{(C7)}$$

$$\eta = \left(\frac{(r_{GMA}+r_{EMA})}{\alpha}\right)\varepsilon - \frac{r_{EMA}}{\alpha} \quad \text{(C8)}$$

As it can be seen from **Equation C8**, by plotting η versus ε the reactivity ratios of EMA and GMA can be calculated. It should be noted that in **Equation C7**, H_{max} and H_{min} are the highest and lowest values of the set of experimental data, respectively.

Non-linear least square (NLLS) model:

Due to shortcomings of linearization methods, a non-linear least squares fit (NLLS) was performed. Such a fitting to the Mayo-Lewis equation is a prominent method to calculate the reactivity ratios and a commercial software package MATLAB 2021b was used to solve Mayo-Lewis equation (**Equation C9**) for EMA/GMA copolymers.

$$F_{GMA} = \frac{(r_{GMA}f_{GMA}^2 + f_{GMA}f_{EMA})}{(r_{GMA}f_{GMA}^2 + 2f_{GMA}f_{EMA} + r_{EMA}f_{EMA}^2)} \quad \text{(C9)}$$

Using the reactivity ratios found by the FR method as initial guesses, the statistical fit to the data yielded reactivity ratios of $r_{GMA} = 1.17 \pm 0.13$ and $r_{EMA} = 0.46 \pm 0.13$ with 95% confident bounds and with a regression coefficient $R^2 = 0.99$.

All the experimental data which were used to calculate the reactivity ratios are tabulated in **Table C 1**.

Table C 1. Copolymer samples used to determine reactivity ratios of GMA and EMA via ATRP at 70°C.

f_{GMA} [a)]	F_{GMA} [b)]	X [c)] (%)	t (min)
0.1	0.24	3	~2
0.2	0.31	6	~2
0.3	0.4	5	~2
0.4	0.47	7	~2
0.5	0.57	10	~2
0.6	0.71	8	~2
0.7	0.76	11	~2
0.8	0.87	10	~2
0.9	0.92	12	~2

[a)] Initial molar ratio of GMA in the feed

[b)] Final molar ratio of GMA in the dried copolymer

[c)] Overall monomer conversion ($X=X_{GMA}f_{GMA} + X_{EMA}f_{EMA}$) determined by ^{1}H NMR in $CDCl_3$

B) Determination of reactivity ratios of BMA and GMA by Fineman–Ross (FR), Kelen–Tüdös (KT) and non-linear least square (NLLS) model

In order to calculate the reactivity ratios of BMA and GMA, same equations of **C1** to C8 was used. It should be noted that r_{BMA} was substituted by r_{EMA} in the equations. **Table C 2** shows the copolymer characterizations of the samples which were used to find the reactivity ratios of BMA and GMA.

Table C 2. Copolymer samples used to determine reactivity ratios of GMA/BMA and MMA/GMA via ATRP at 70°C.

Poly(BMA-*stat*-GMA)				Poly(MMA-*stat*-GMA)			
f_{GMA}[a)]	F_{GMA}[b)]	X [c)] (%)	t (min)	f_{GMA}	F_{GMA}	X (%)	t (min)
0.1	0.13	5	~2	0.1	0.15	4	~2
0.2	0.28	9	~2	0.2	0.25	8	~2
0.3	0.38	12	~2	0.3	0.39	15	~2
0.4	0.56	15	~2	0.4	0.46	11	~2
0.5	0.61	14	~2	0.5	0.62	16	~2
0.6	0.69	11	~2	0.6	0.69	15	~2
0.7	0.78	19	~2	0.7	0.76	21	~2
0.8	0.88	17	~2	0.8	0.85	20	~2
0.9	0.93	21	~2	0.9	0.92	24	~2

[a)] Initial molar ratio of GMA in the feed

[b)] Final molar ratio of GMA in the dried copolymer

[c)] Overall monomer conversion ($X=X_{GMA}f_{GMA} + X_{BMA}f_{BMA}$) determined by ^1H NMR in $CDCl_3$

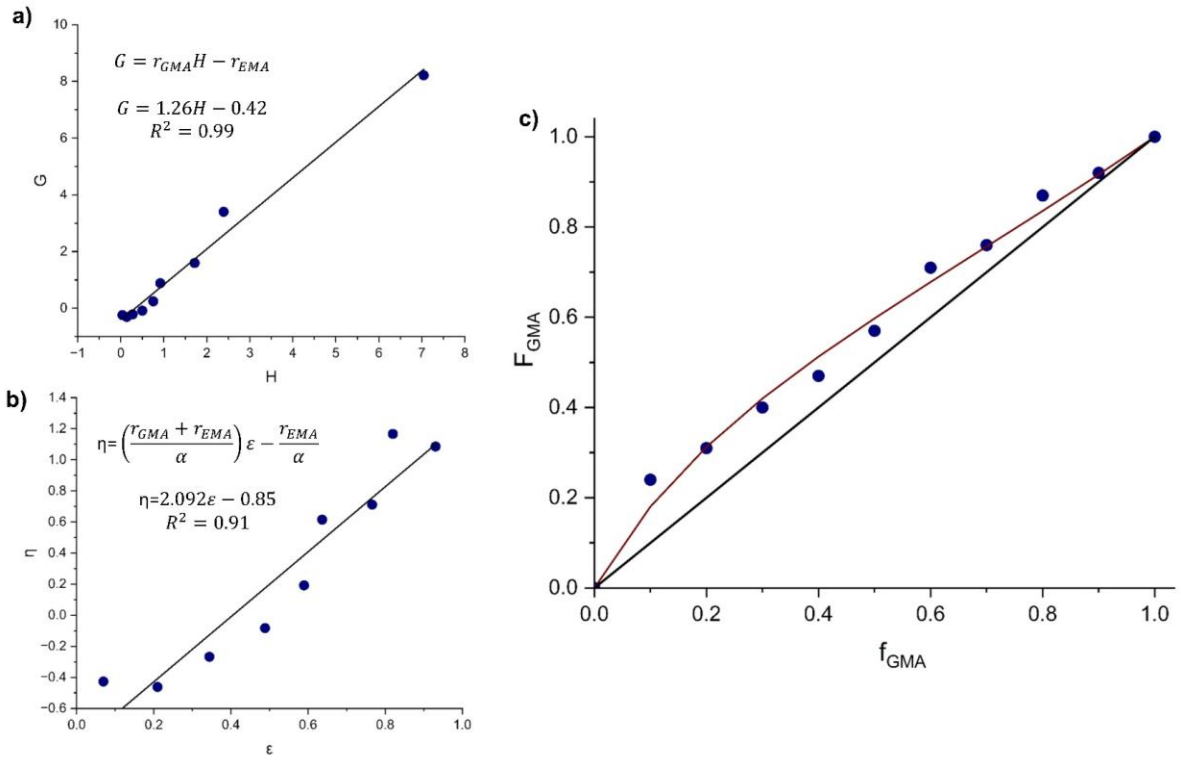

Figure C 7. Plots used to estimate reactivity ratios for EMA/GMA copolymerizations by ATRP at 70°C in anisole:, a) Fineman-Ross plot, b) Kelen-Tudos plot (filled circles ( ) are the experimental data and the solid line is the fit) and c) Mayo-Lewis plot of copolymer composition with respect to final molar fraction of GMA (F_{GMA}) in the copolymer versus initial GMA feed composition (blue circles ( ) are the experimental data while the red solid line is the associated trend line; the solid straight black line is the azeotropic composition where $F_{GMA} = f_{GMA,0}$).

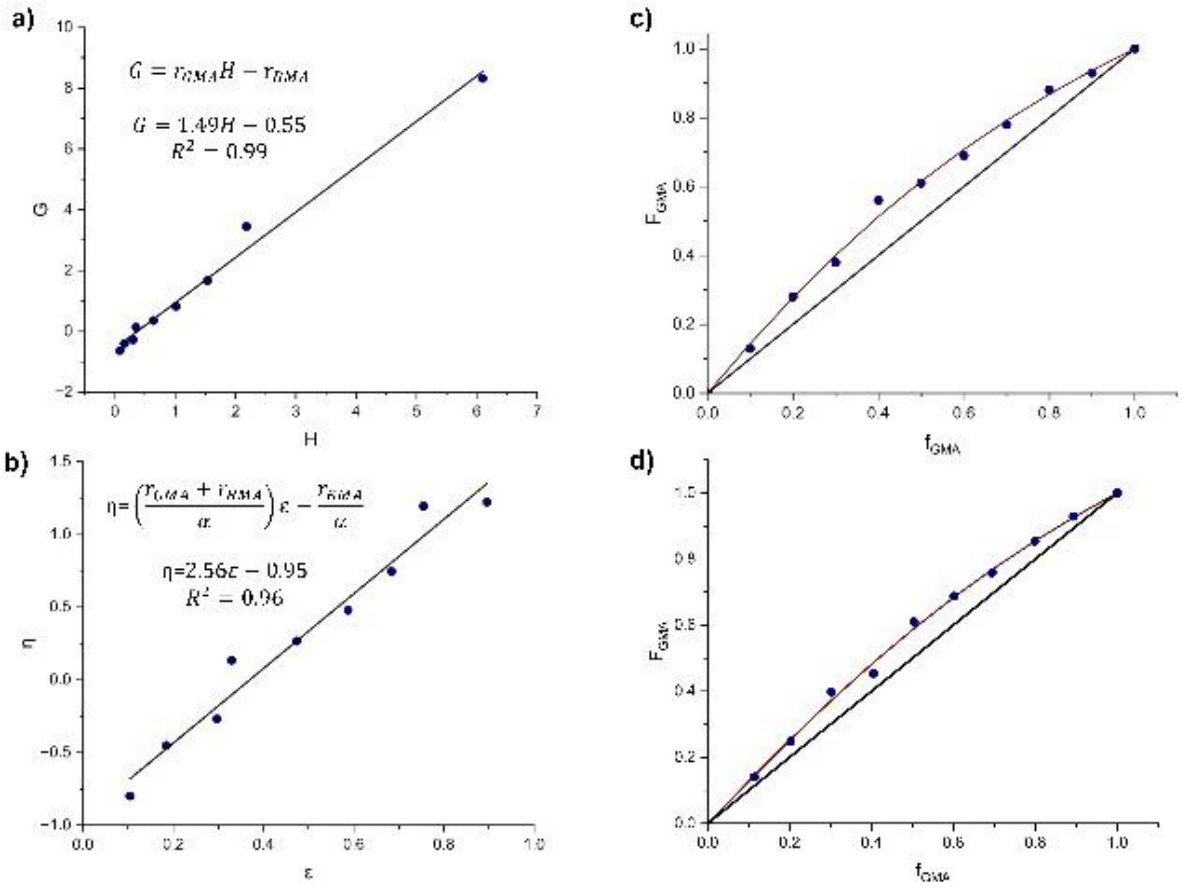

Figure C 8. Plots used to estimate reactivity ratios for BMA/GMA and MMA/GMA copolymerizations by ATRP at 70°C in anisole:, a) Fineman-Ross plot, b) Kelen-Tudos plot (filled circles (●) are the experimental data and the solid line is the fit), c) Mayo-Lewis plot of copolymer composition with respect to final molar fraction of GMA (F_{GMA}) in the copolymer versus initial GMA feed composition (blue circles (●) are the experimental data while the red solid line is the associated trend line; the solid straight black line is the azeotropic composition where $F_{GMA} = f_{GMA,0}$) and d) Mayo-Lewis plot of copolymer composition for poly(MMA-*stat*-GMA) with respect to final molar fraction of GMA (F_{GMA}) in the copolymer versus initial GMA feed composition (blue circles (●) are the experimental data while the red solid line is the associated trend line; the solid straight black line is the azeotropic composition where $F_{GMA} = f_{GMA,0}$).

Table C 3. Thermal characterization of EMA/GMA copolymers via ATRP at 70 °C in anisole as solvent.

Sample ID	T_g [a] (°C)	$T_{d,10\%}$ [b] (°C)	$T_{d,max}$ [b] (°C)	$T_{d,1}$ [b] (°C)	$T_{d,2}$ [b] (°C)	$T_{d,3}$ [b] (°C)	$T_{d,final}$ [b] (°C)	F_{GMA} [c]	Ash content (%)
EMA/GMA-90	46	315	367	180	367	-	550	0.13	0
EMA/GMA-80	49	257	345	181	345	-	580	0.81	0
EMA/GMA-70	51	308	334	172	334	-	570	0.73	0
EMA/GMA-60	53	293	348	178	348	495	560	0.58	0
EMA/GMA-50	59	295	340	180	340	505	585	0.43	0
EMA/GMA-40	63	275	339	165	339	478	600	0.45	0
EMA/GMA-30	67	270	328	151	328	530	590	0.34	0
EMA/GMA-20	69	272	330	150	330	539	585	0.24	0
EMA/GMA-10	70	250	327	139	327	545	560	0.13	0
Carbonated EMA/GMA-90	50	245	364	198	364	-	540	-	0
Carbonated EMA/GMA-80	58	200	326	176	326	-	520	-	0
Carbonated EMA/GMA-70	70	216	331	182	331	-	550	-	0

[a] Glass transition temperature (T_g) determined by DSC under nitrogen atmosphere using three cycle (heat/cool/heat) with heating rate of 5 °C min^{-1}

[b] $T_{d,10\%}$ (decomposition temperature for 10% weight loss), $T_{d,max}$ (temperature at maximum decomposition rate), $T_{d,1}$, $T_{d,2}$ and $T_{d,3}$ (the first, second and third peaks in derivative weight (%/°C) versus temperature (°C) obtained from TGA) and $T_{d,final}$ (temperature at the end of decomposition) measured by TGA under nitrogen purge at a heating ramp rate of 10 °C min^{-1}

[c] Final molar composition of GMA in EMA/GMA copolymers

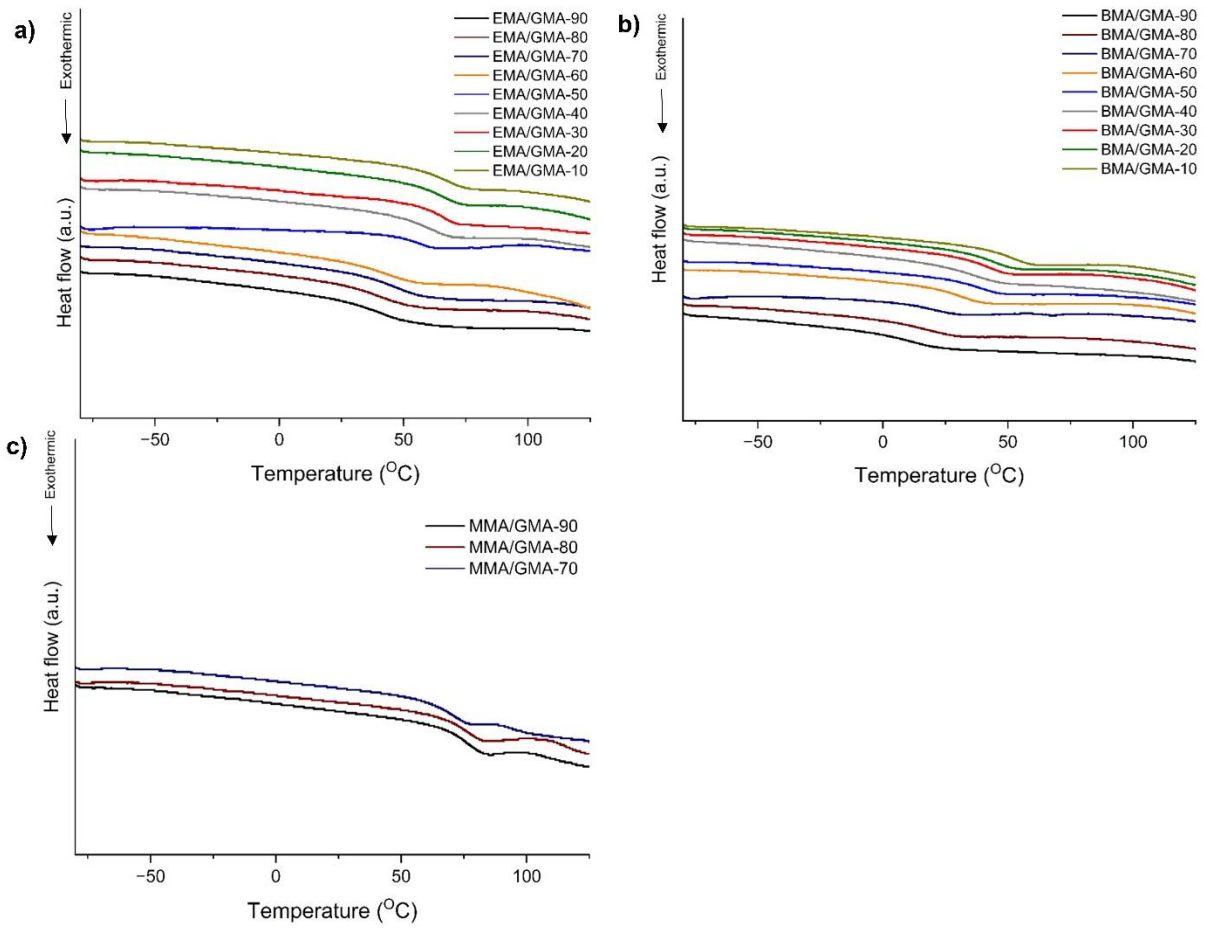

Figure C 9. DSC curves for the synthesized copolymers, a) poly(EMA-*stat*-GMA)s, b) poly(BMA-*stat*-GMA)s and c) poly(MMA-*stat*-GMA)s.

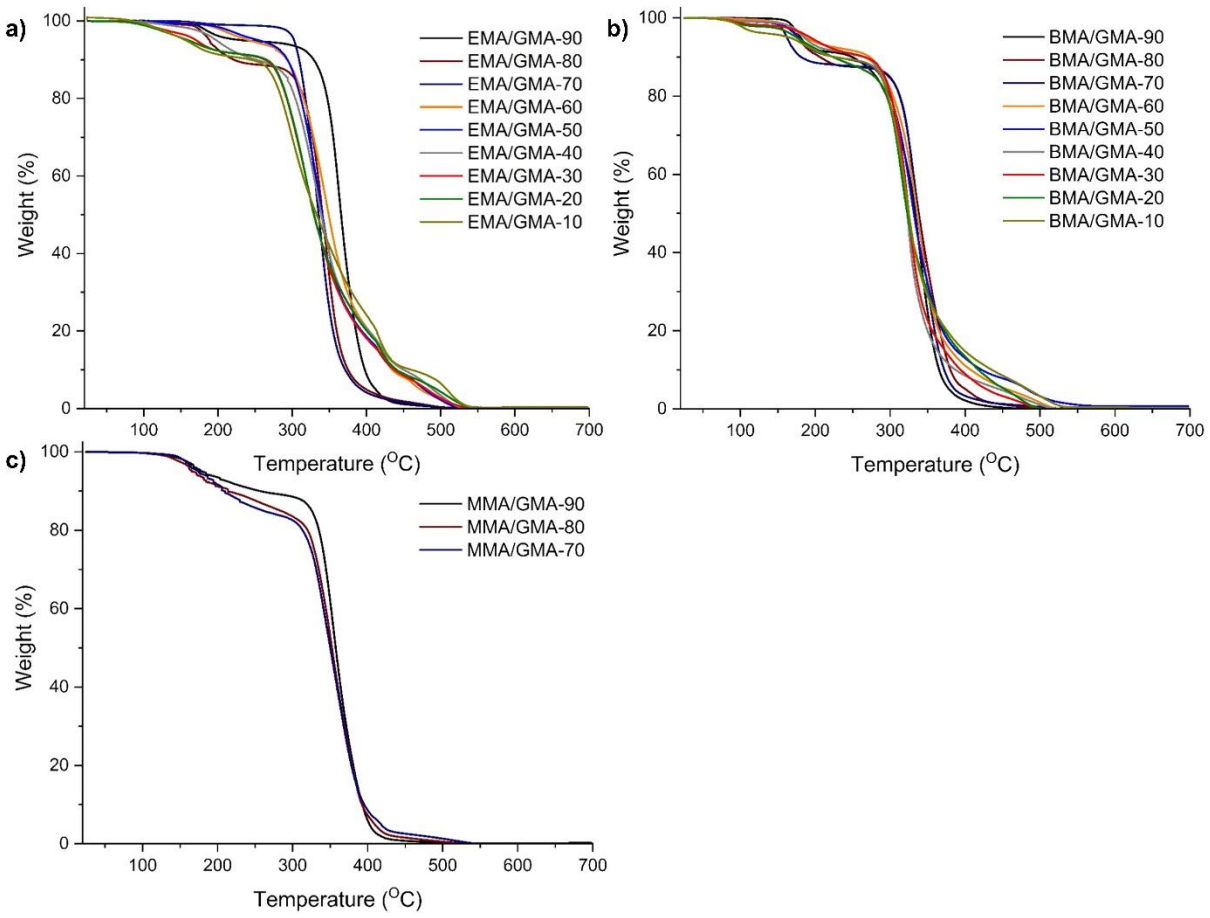

Figure C 10. TGA curves for the synthesized copolymers, a) poly(EMA-*stat*-GMA)s, b) poly(BMA-*stat*-GMA)s and c) poly(MMA-*stat*-GMA)s.

Table C 4. Thermal characterization of BMA/GMA and MMA/GMA copolymers via ATRP at 70 °C in anisole as solvent.

Sample ID	T_g [a] (°C)	$T_{dec,10\%}$ [b] (°C)	$T_{dec,max}$ [b] (°C)	$T_{dec,1}$ [b] (°C)	$T_{dec,2}$ [b] (°C)	$T_{dec,final}$ [b] (°C)	F_{GMA} [c]	Ash content (%)
BMA/GMA-90	15.5	246	330	143	330	498	0.06	0
BMA/GMA-80	20.5	203	345	175	345	514	0.13	0
BMA/GMA-70	22	181	340	160	340	516	0.20	0
BMA/GMA-60	32.5	255	335	153	335	525	0.32	0
BMA/GMA-50	38.5	230	332	154	332	540	0.35	0
BMA/GMA-40	40	244	322	147	322	530	0.45	0
BMA/GMA-30	43	250	329	160	329	525	0.59	0
BMA/GMA-20	44.5	223	330	155	330	517	0.76	0
BMA/GMA-10	51.5	216	327	150	327	535	0.86	0
Carbonated BMA/GMA-90	28.5	280	345	168	345	460	-	0
Carbonated BMA/GMA-80	42	214	345	175	345	490	-	0
Carbonated BMA/GMA-70	45	195	340	180	340	505	-	0
MMA/GMA-90	78.5	237	360	180	360	525	0.08	0
MMA/GMA-80	77	222	357	183	357	540	0.16	0
MMA/GMA-70	70	210	354	185	354	540	0.29	0
Carbonated MMA/GMA-90	117.5	320	363	-	363	480	-	0
Carbonated MMA/GMA-80	112	220	337	210	337	540	-	0
Carbonated MMA/GMA-70	105	210	322	215	322	537	-	0

[a] Glass transition temperature (T_g) determined by DSC under nitrogen atmosphere using three cycle (heat/cool/heat) with heating rate of 5°C min^{-1}

[b] $T_{d,10\%}$ (decomposition temperature for 10% weight loss), $T_{d,max}$ (temperature at maximum decomposition rate), $T_{d,1}$ and $T_{d,2}$ (the first and second peaks in derivative weight (%/°C) versus temperature (°C) obtained from TGA) and $T_{d,final}$ (temperature at the end of decomposition) measured by TGA under nitrogen purge at a heating ramp rate of 10 °C min^{-1}

[c] Final molar composition of GMA in copolymers

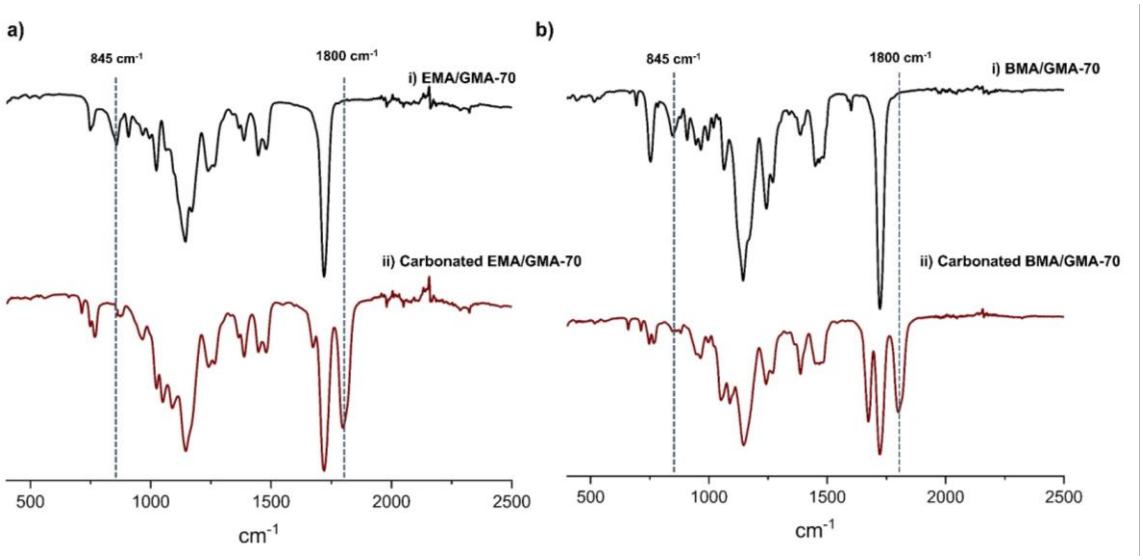

Figure C 11. FTIR spectra for synthesized copolymers, a) EMA/GMA-70 and its carbonated form and b) BMA/GMA-70 and its carbonated form.

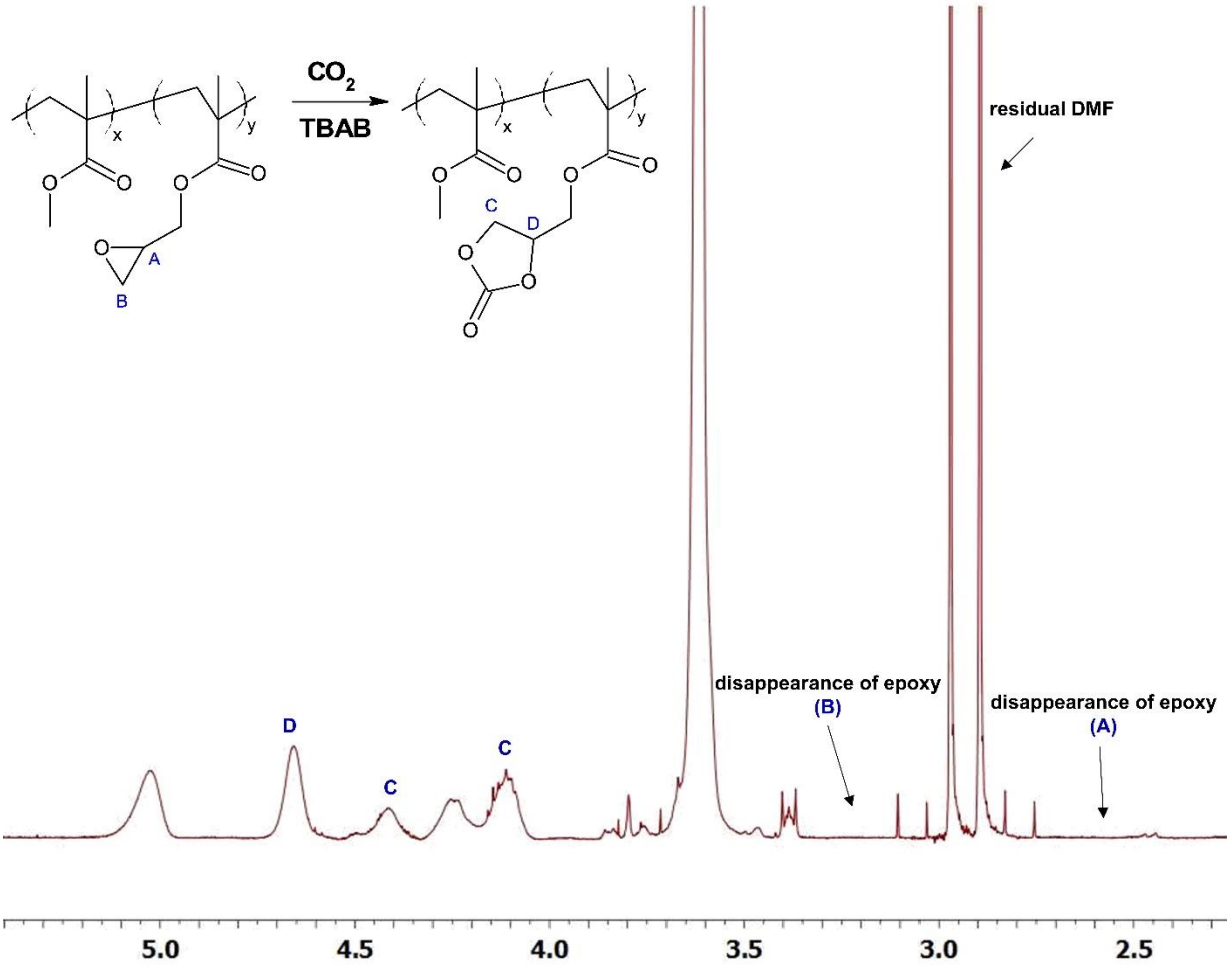

Figure C 12. 1H NMR spectrum of carbonated MMA/GMA-90 after 24 hours.

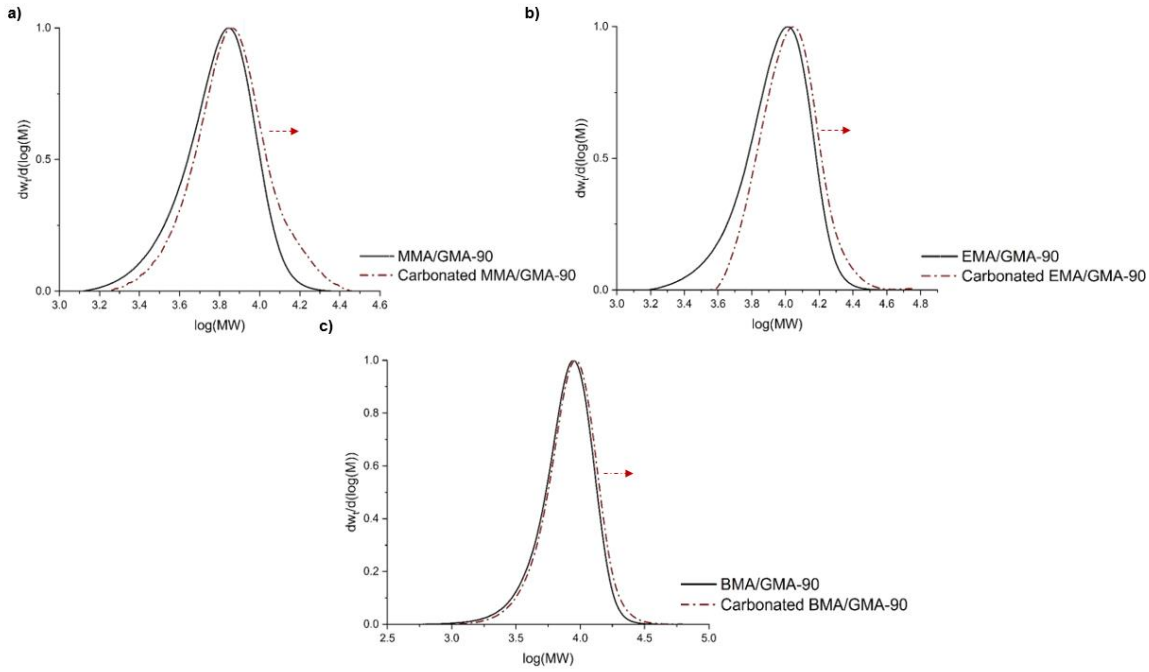

Figure C 13. GPC traces for copolymers before and after carbonation; a) MMA/GMA-90 and carbonated MMA/GMA-90, b) EMA/GMA-90 and carbonated EMA/GMA-90 and c) BMA/GMA-90 and carbonated BMA/GMA-90.

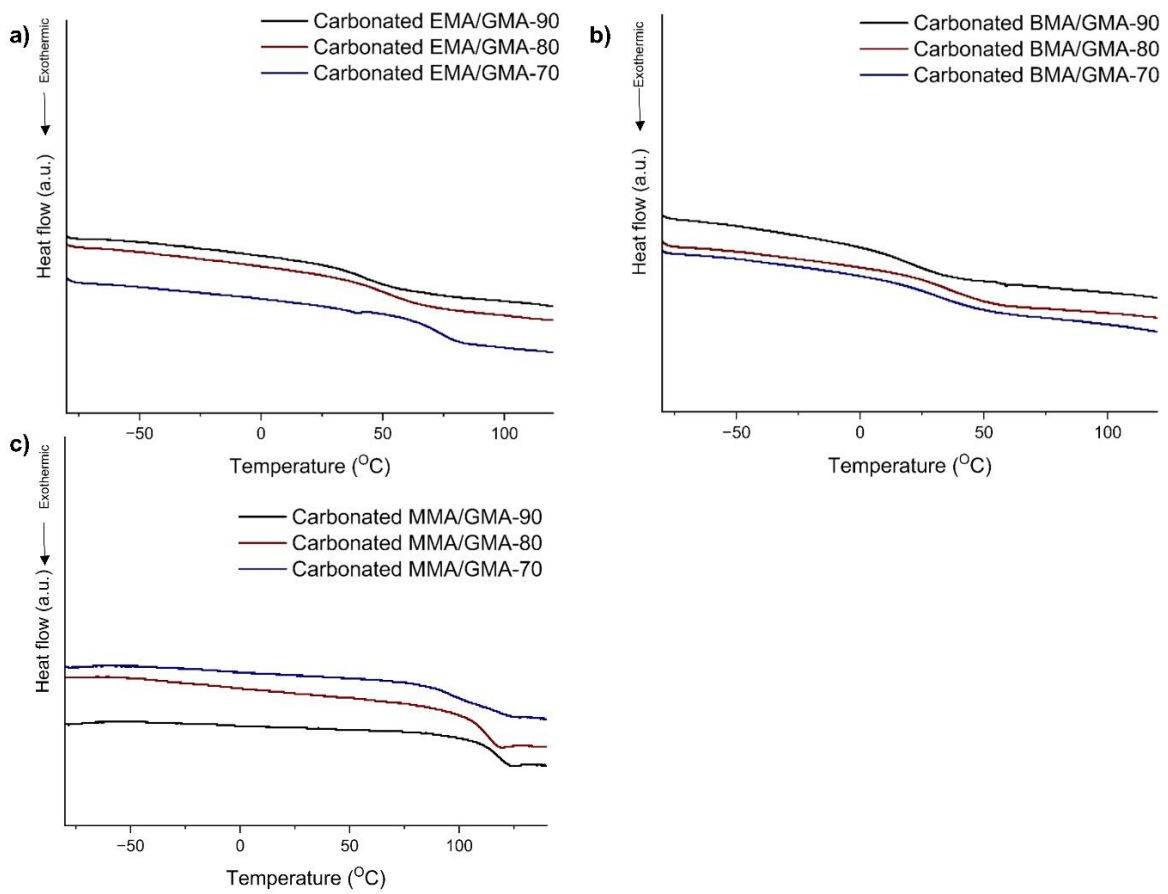

Figure C 14. DSC curves for the carbonated copolymers, a) carbonated poly(EMA-*stat*-GMA)s, b) carbonated poly(BMA-*stat*-GMA)s and c) carbonated poly(MMA-*stat*-GMA)s.

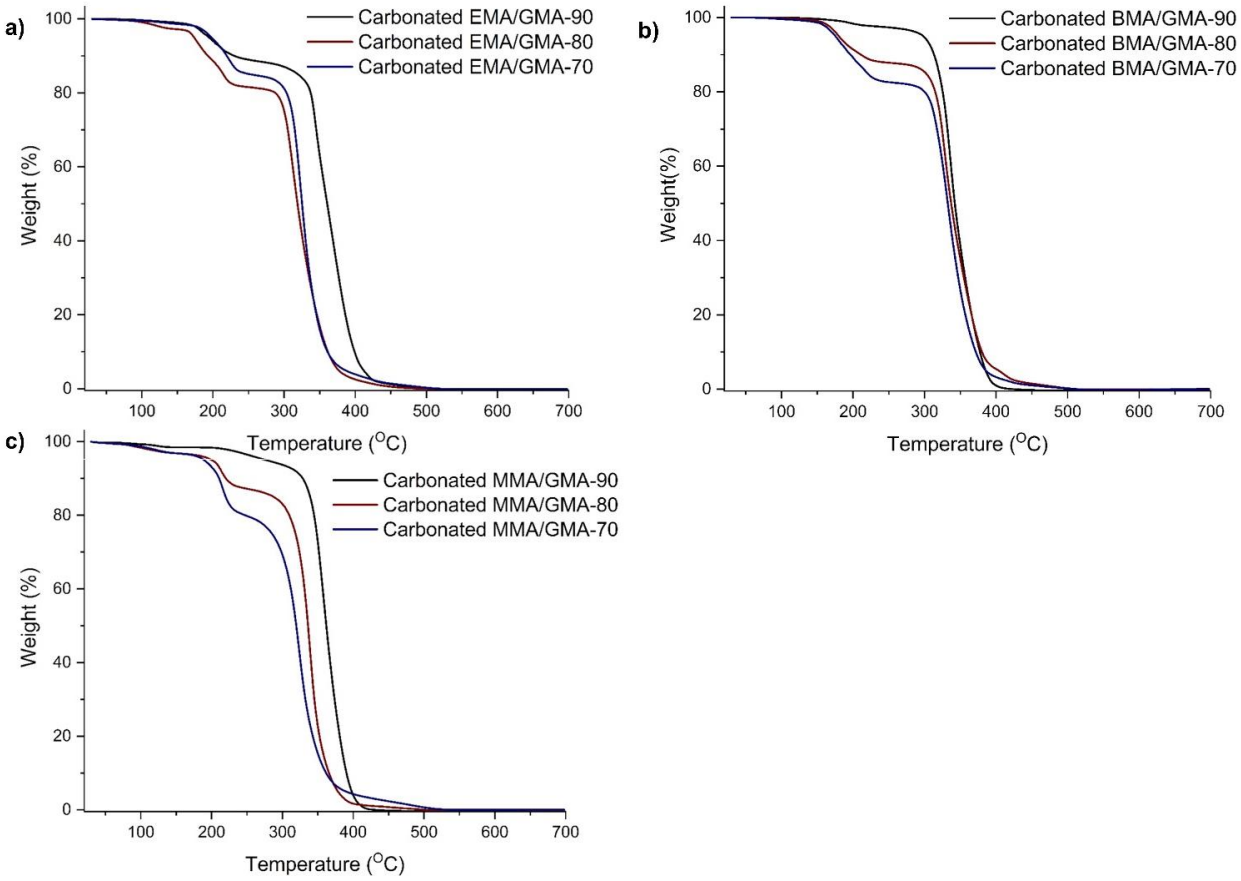

Figure C 15. TGA curves for the carbonated copolymers, a) carbonated poly(EMA-*stat*-GMA)s, b) carbonated poly(BMA-*stat*-GMA)s and c) carbonated poly(MMA-*stat*-GMA)s.

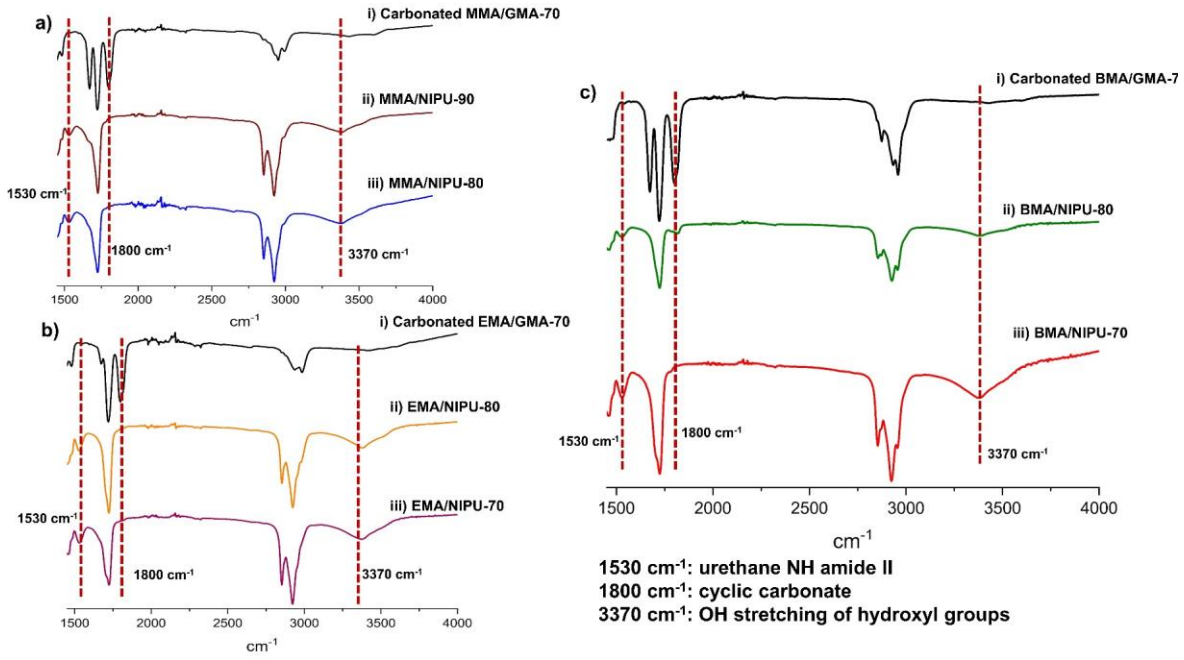

Figure C 16. FTIR spectra for synthsized samples;a) FTIR spectra for i) carbonated MMA/GMA-70, ii) MMA/NIPU-90, iii) MMA/NIPU-80, b) FTIR spectra for i) carbonated EMA/GMA-70, ii) EMA/NIPU-80, iii) EMA/NIPU-70 and c) FTIR spectra for i) carbonated BMA/GMA-70, ii) BMA/NIPU-80, iii) BMA/GMA-70.

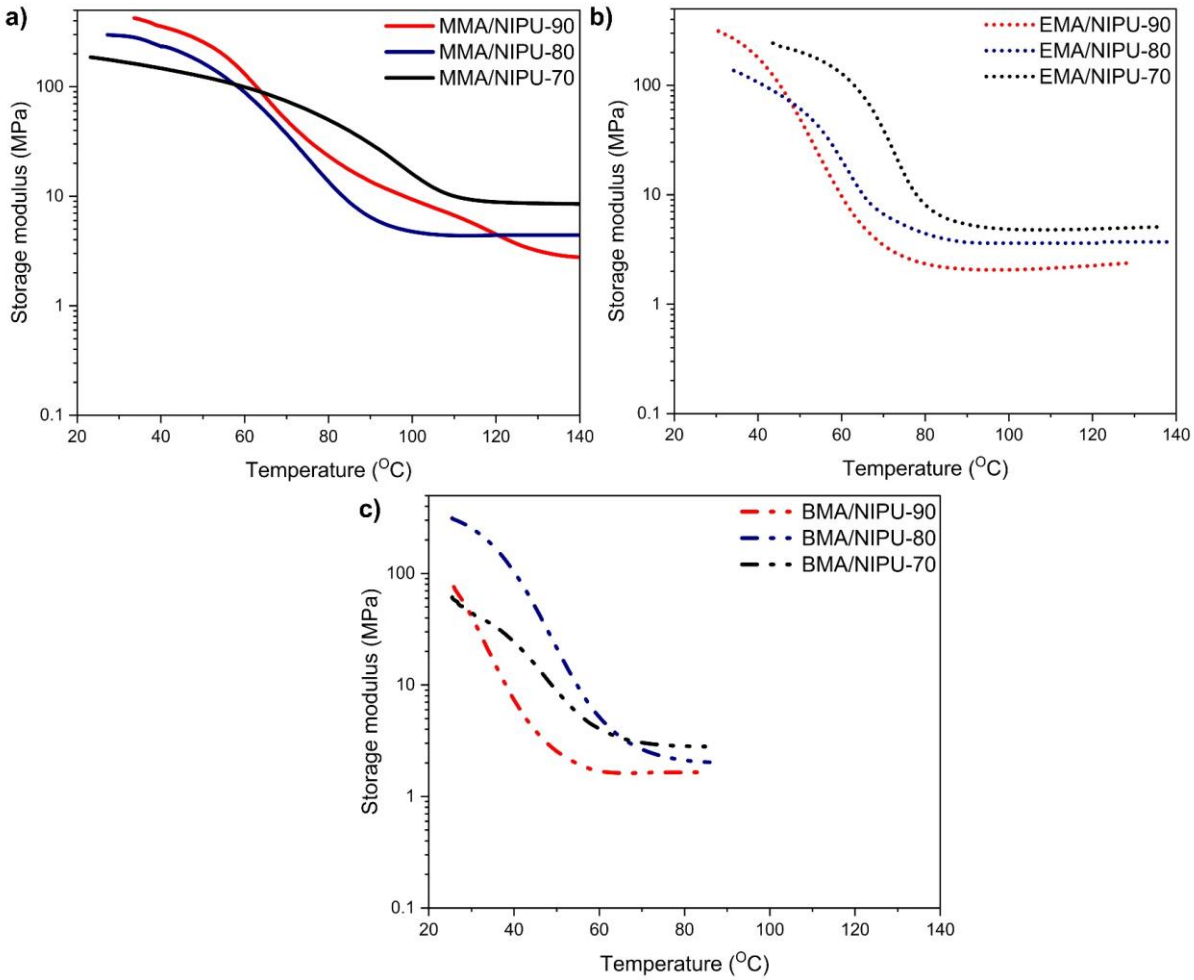

Figure C 17. DMTA results for the crosslinked networks; storage moduli as a function of temperature.

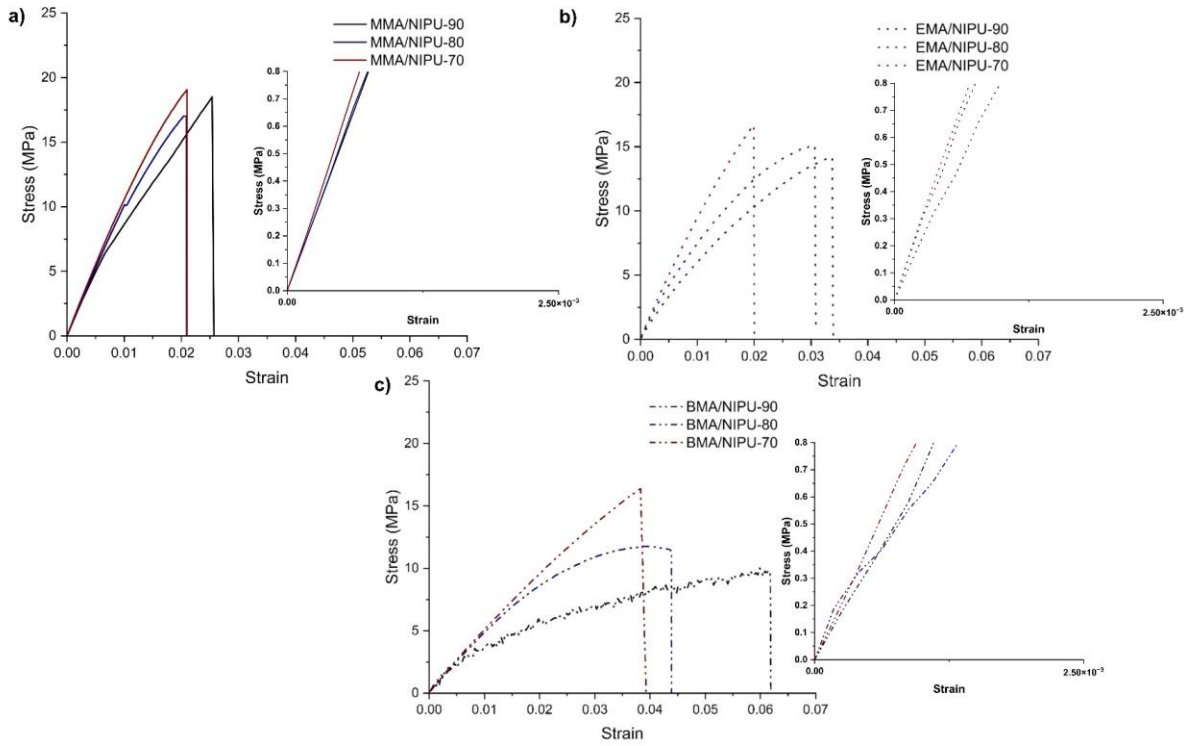

Figure C 18. Tensile testing for the crosslinked samples; a) MMA/NIPU, b) EMA/NIPU and c) BMA/NIPU crosslinked networks.

Calculation for number of urethane linkages on the backbone

Knowing the M_n which is molecular weight of the synthesized copolymers extracted by GPC and the M_m which is the molecular weight of the repeating unit in the copolymer calculated from **Equation C10**, the number average degree of polymerization (*DP*) can be calculated using **Equation C11.**

$$M_m = f_1 M_1 + f_2 M_2 \quad \textbf{(C10)}$$

$$DP = \frac{M_n}{M_m} \quad \textbf{(C11)}$$

In **Equation C10**, f_1 and f_2 are the initial molar fraction of monomers in the feed and M_1 and M_2 are the molecular weight of each monomer.

The calculation of the number of epoxy functional groups can be achieved by multiplying *DP* with F_1, where F_1 represents the molar fraction of GMA in the copolymer in our study. Knowing complete conversion of all epoxy functional groups to cyclic carbonate (carbonation conversion = 1), and subsequent conversion of all cyclic carbonates to urethane linkages during the diamine addition step, the number of urethane linkages on the backbone can be determined.

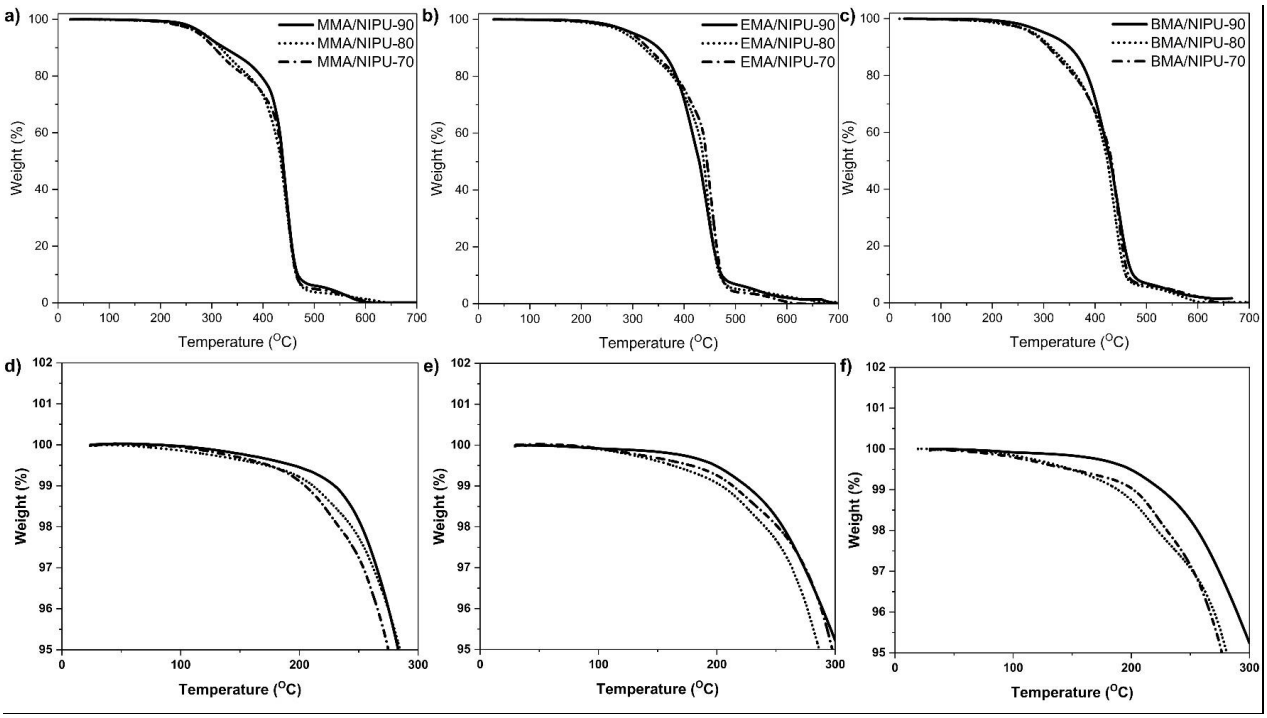

Figure C 19. TGA thermograms for the crosslinked networks; a) MMA/GMA-based crosslinked networks ("d" is the inset of the region between 0 and 300°C), b) EMA/GMA-based crosslinked networks ("e" is the inset of the region between 0 and 300°C version) and c) BMA/GMA-based crosslinked networks ("f" is the inset of the region between 0 and 300°C).

APPENDIX D

SUPPORTING INFORMATION FOR UTILIZING BIO-DERIVED AMINE-TERMINATED THERMOPLASTIC POLYHYDROXYURETHANES AS CROSSLINKERS FOR HYBRID THERMOSETS

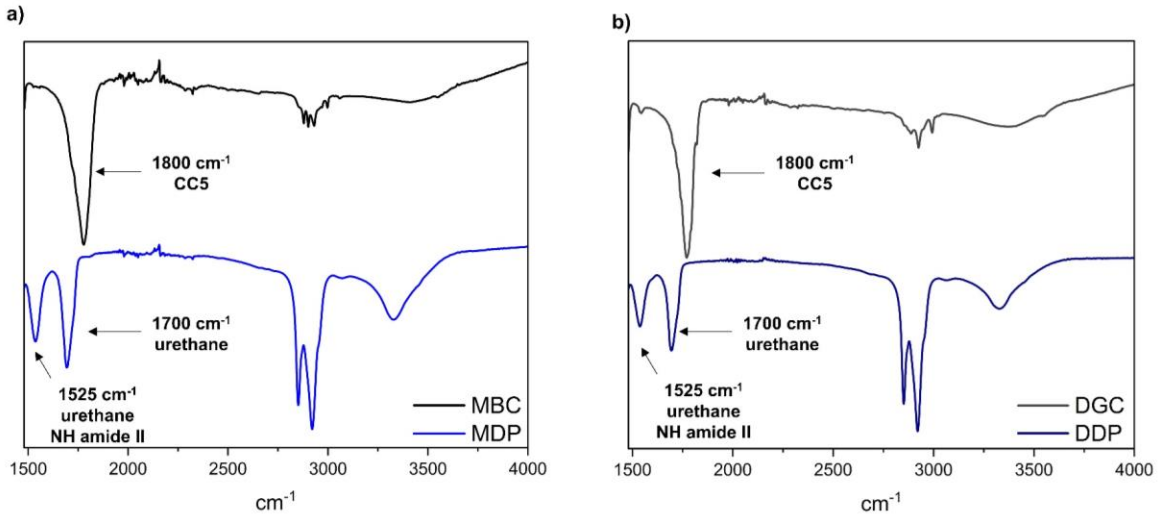

Figure D 1. FTIR spectra for MDP and DDP; a) MDP, b) DDP.

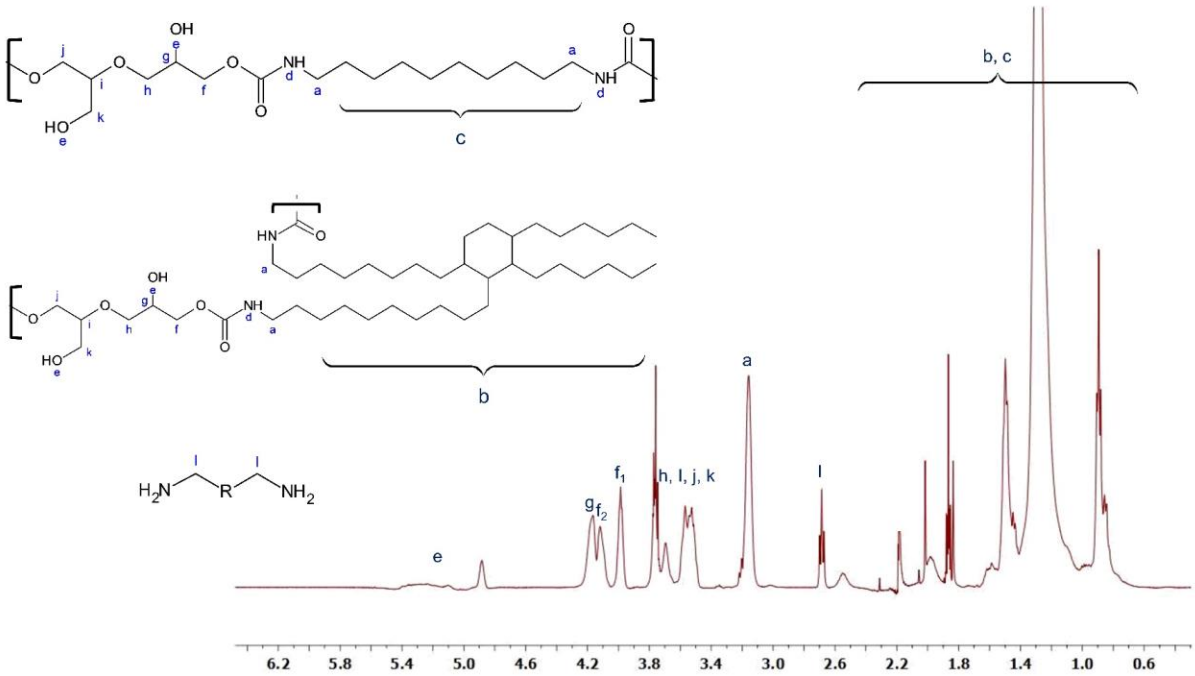

Figure D 2. ^{1}H NMR spectrum of unpurified DDP after 24 hours in $CDCl_3$.

A) DDP analysis including calculation of conversion and the primary to secondary alcohol ratio

The synthesized PHUs were characterized using ^{1}H NMR to determine the ratio of primary to secondary alcohols in the structure. First, the ratio of secondary to primary alcohol was calculated. **Equation D1** was used to calculate the secondary alcohol fraction in DDP.

$$Secondary\ alcohol = \frac{\int g + \int f + \int h}{\int g + \int f + \int h + \int i + \int j + \int k} \quad \text{(D1)}$$

In **Equation D1**, the chemical shifts of *g, f*, and *h*, falling within the range of 3.8-4.2 ppm, are associated with the presence of secondary hydroxyl groups. These hydroxyl groups are formed as a result of the ring-opening reaction of cyclic carbonates with amines. The chemical shifts of *i, j*, and *k* are indicative of the presence of primary hydroxyl groups. Therefore, by dividing the sum of peaks associated with secondary alcohols by the total integral of peaks attributed to both secondary and primary alcohols, it is possible to determine the fraction of secondary alcohols present in the mixture. The integrals of *f* and *g* can be determined, while the integral of *h* is equal to integral of *f*. Therefore, the sum of integrals of *i, j* and *k* can be found.

Using **Equation D2**,fraction of primary alcohol in the structure was determined.

$$Primary\ alcohol = 1 - secondary\ alcohol \quad \text{(D2)}$$

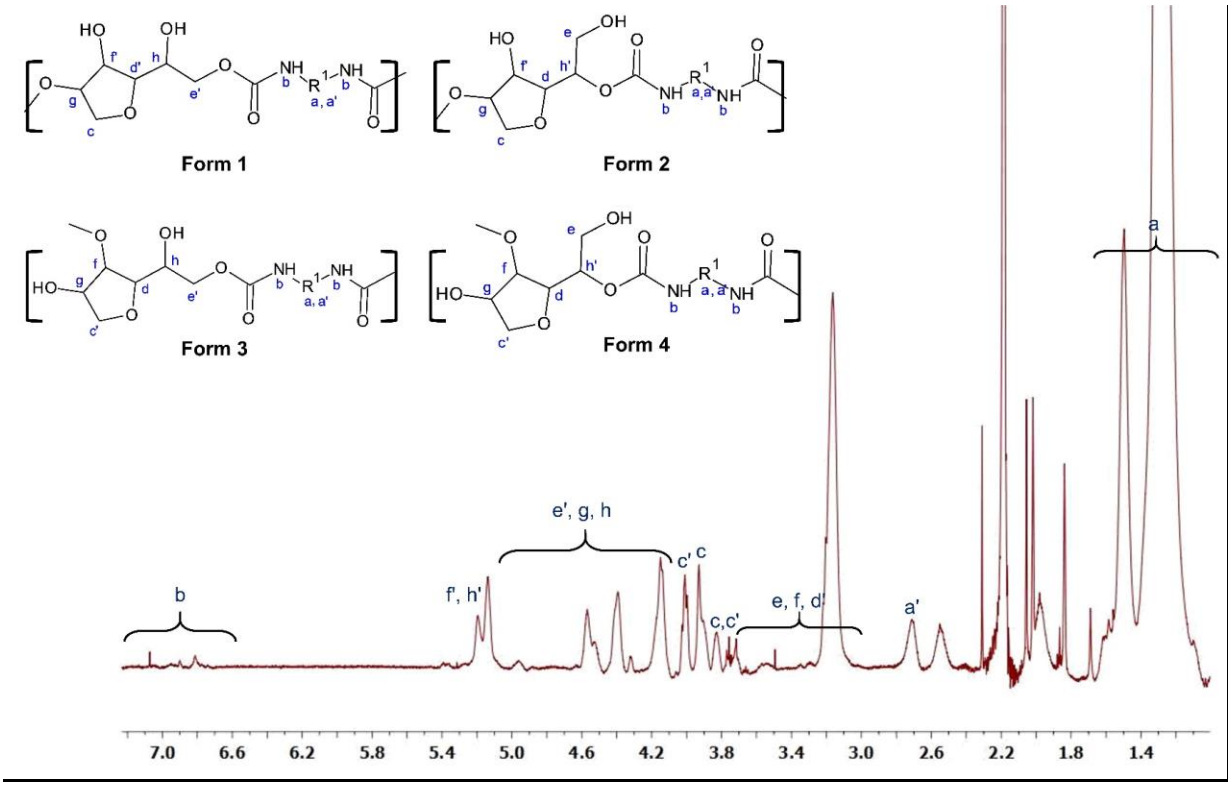

Figure D 3. ^{1}H NMR spectrum of unpurified MDP after 24 hours in $CDCl_3$.

B) MDP analysis including calculation of conversion and the primary to secondary alcohol ratio

The synthesized PHUs were characterized using ^{1}H NMR to determine the ratio of primary to secondary alcohols in the structure. The calculations were done based on our previous work [94]. During the polyaddition of cyclic carbonates with diamines, the cyclic carbonates rings of the nonsymmetric MBC open in two different ways. As a result, four different forms of urethane segments are generated, which has been discussed elsewhere [86,266]. These forms are shown in **Figure D 3**. The fractions of the different forms of sugar-based TPHUs were determined by employing the following equations.

$$F_1 + F_2 + F_3 + F_4 = \frac{\int c + \int c'}{2} \quad \text{(D3)}$$

By taking integral of c and c' (3.85ppm and 4ppm, respectively):

$$F_1 + F_2 = \int c \quad \text{(D4)}$$

$$F_3 + F_4 = \int c' \quad \text{(D5)}$$

To determine the fraction of primary hydroxyl groups, the peak at 5.4 ppm was utilized in the following equation.

$$F_1 + 2F_2 + F_4 = \int f' + \int h' \quad \text{(D6)}$$

To calculate the fraction of primary alcohols, **Equation D7** can be defined by subtracting **Equation D4** from **Equation D6.**

$$F_2 + F_4 = \int f' + \int h' - \int c \quad \text{(D7)}$$

Therefore, the fraction of primary hydroxyl groups can be found using **Equation D8.**

$$Primary\ alcohol = \frac{F_2 + F_4}{2} \quad \text{(D8)}$$

Sum of both primary and secondary hydroxyl groups is two. Therefore, sum of F_2 and F_4 was divided by 2. By subtracting **Equation D8** from one, fraction of secondary alcohols would be determined.

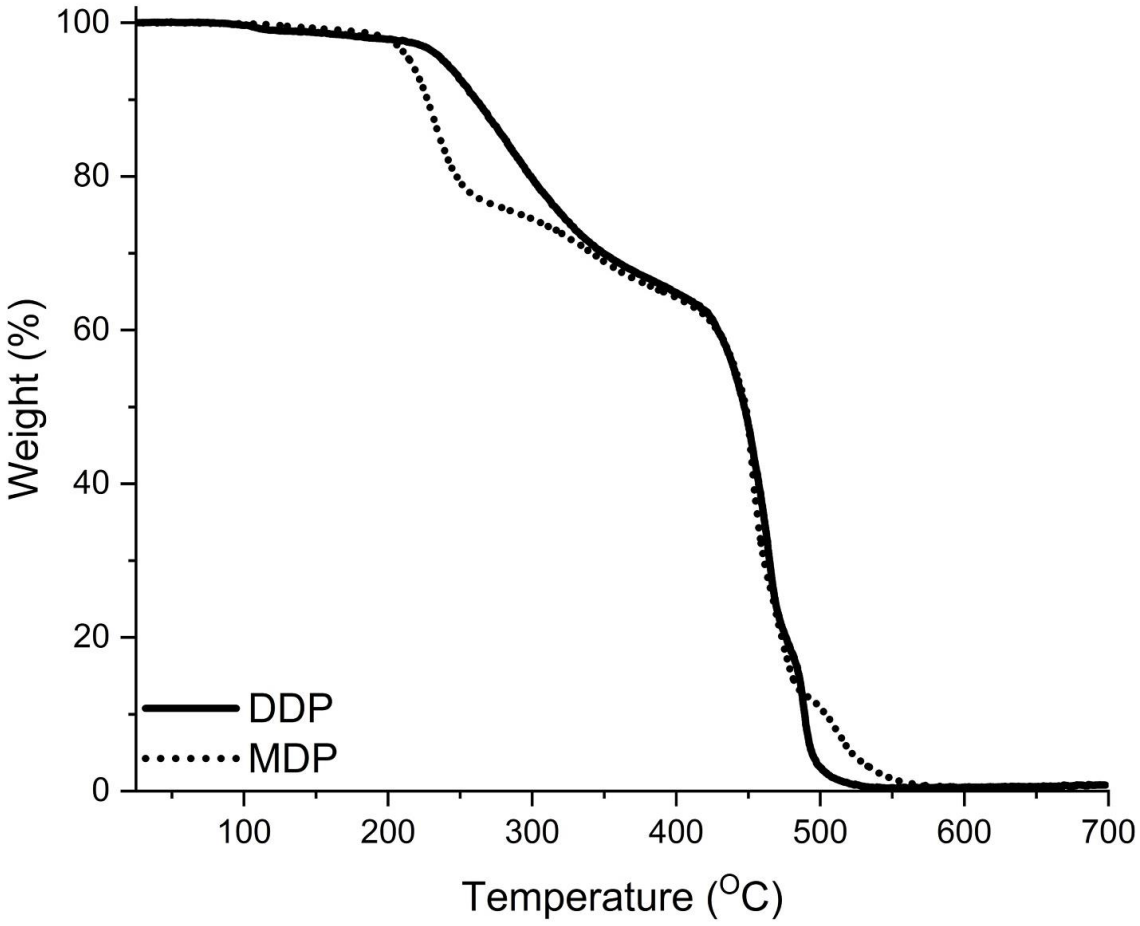

Figure D 4. TGA thermograms for DDP and MDP.

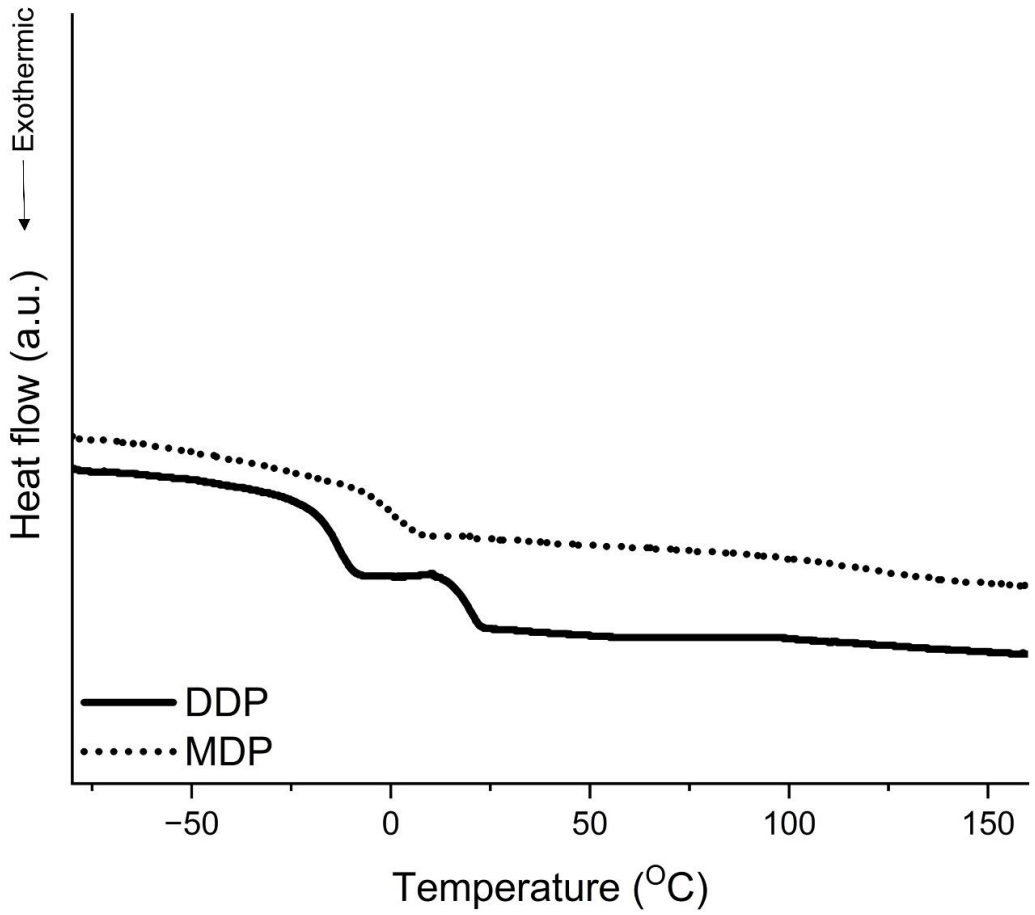

Figure D 5. DSC results for DDP and MDP.

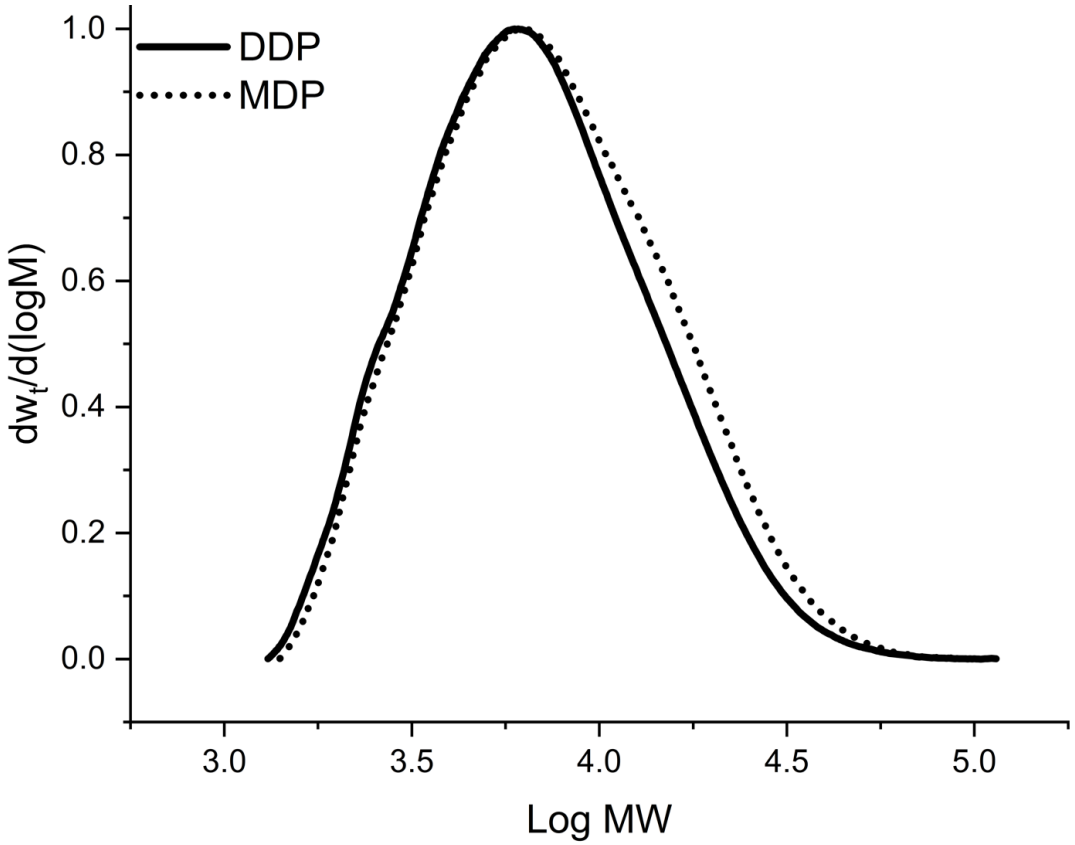

Figure D 6. Normalized GPC traces of DDP and MDP.

Table D 1. Calculation of solubility parameters using the Hoftyzer-Van Krevelen group for DDP.

Monomer	M_w ($g.mol^{-1}$)	Density ($g.cm^{-3}$)	Molar volume ($cm^3.mol^{-1}$)	Number of group	Group contribution	F_{di} ($MJ.m^{-3})^{0.5}.mol^{-1}$	F^2_{pi} ($MJ.m^{-3}).mol^{-2}$	E_{hi} ($J.mol^{-1}$)	δ_d ($MJ.m^{-3})^{0.5}$	δ_p ($MJ.m^{-3})^{0.5}$	δ_h ($MJ.m^{-3})^{0.5}$	δ ($MJ.m^{-3})^{0.5}$
Priamine 1074				1	Cyclic aliphatic	1620	0	0				
				2	-NH-	160	44100	3100				
				28	$-CH_2-$	270	0	0				
DGC				1	-O-	100	160000	3000				
				4	$-CH_2-$	270	0	0				
				2	>CH	80	0	0				
				2	-OH	210	250000	20000				
				2	-COO-	390	240100	7000				
PHU linkage	534	0.92	580						20.7	1.91	10.4	23.3

DAD				2	-NH-	160	44100	3100				
				10	$-CH_2-$	270	0	0				
DGC				1	-O-	100	160000	3000				
				4	$-CH_2-$	270	0	0				
				2	>CH	80	0	0				
				2	-OH	210	250000	20000				
				2	-COO-	390	240100	7000				
PHU linkage	390	1.3	300.2						18.51	3.69	14.51	23.81

In order to calculate Hansen solubility parameters **Equation D9-D11** were used.

$$\delta_d = \frac{\sum F_{di}}{V} \tag{D9}$$

$$\delta_p = \sqrt{\sum F_{pi}^2} \tag{D10}$$

$$\delta_h = \sqrt{\sum E_{ni}} \tag{D11}$$

$$\delta = \sqrt{\delta_d^2 + \delta_p^2 + \delta_h^2} \tag{D12}$$

$$\Delta\delta = \sqrt{(\delta_{d,P1} - \delta_{d,P2})^2 + (\delta_{p,P1} - \delta_{p,P2})^2 + (\delta_{h,P1} - \delta_{h,P2})^2} \tag{D13}$$

δ_d is the contribution of dispersion forces, δ_p is the contribution of polar forces and δ_h is the contribution of hydrogen bonding.

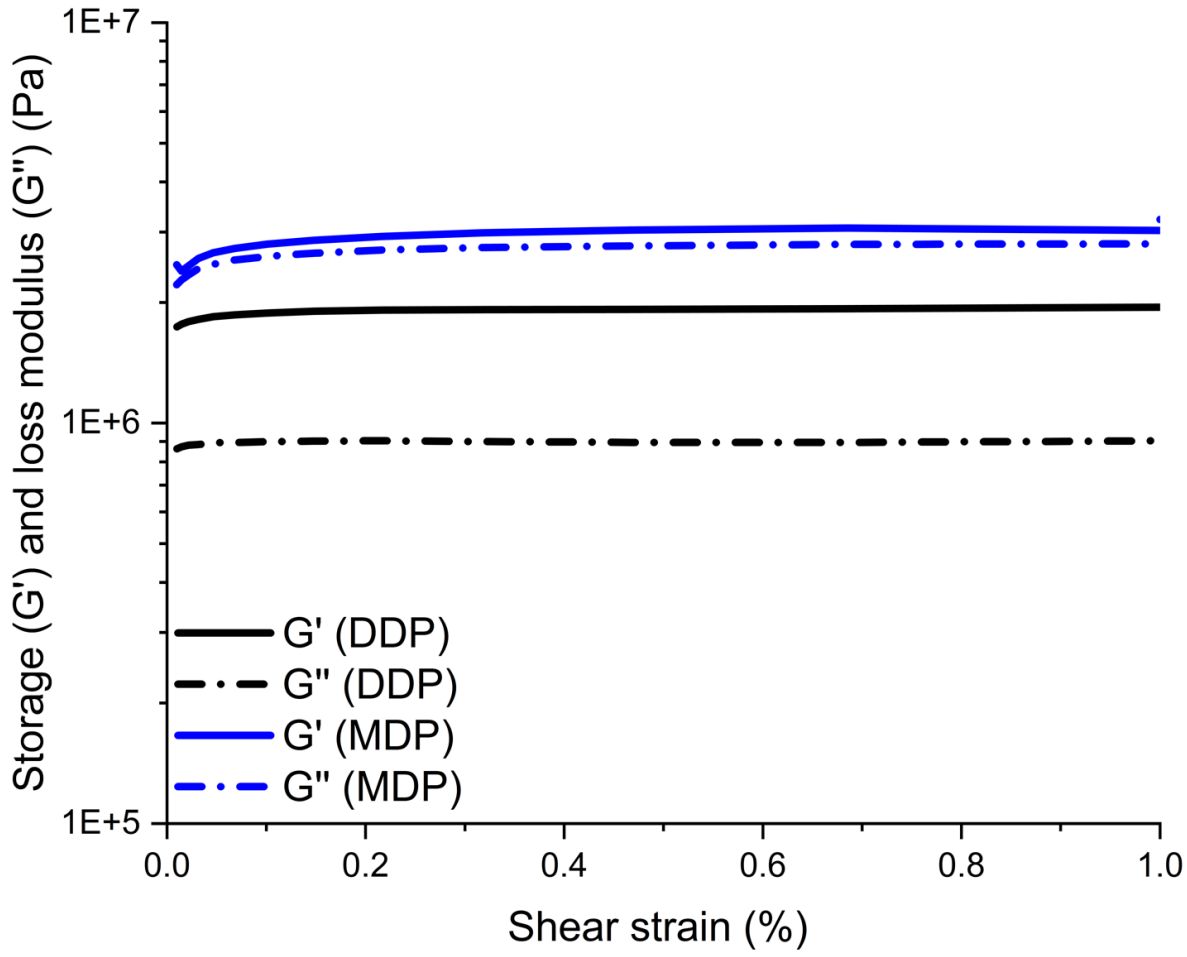

Figure D 7. Amplitude sweep performed on the synthesized PHUs at 25°C with frequence of 1 Hz.

Table D 2. Mechanical properties of each crosslinked NIPU sample.

Sample ID	*E* (MPa)	*EB* (%)	Ultimate stress (MPa)	Swelling ratio in THF (%)	Swelling ratio in water (%)
NIPUDDP-90-1	2.80	105	1.1	543	7.65
NIPUDDP-90-2	2.15	92	0.83	524	11.60
NIPUDDP-90-3	2.10	88	0.86	525	8.50
NIPUDDP-80-1	4.25	85	1.20	455	12.50
NIPUDDP-80-2	5.18	97	1.95	476	11.35
NIPUDDP-80-3	3.86	88	1.50	480	9.30
NIPUDDP-70-1	21.60	52	4.00	185	17.50
NIPUDDP-70-2	21.83	55	4.52	190	12.60
NIPUDDP-70-3	19.12	46	3.93	192	15.80
NIPUMDP-90-1	1.60	52	0.32	390	7.20
NIPUMDP-90-2	1.50	55	0.35	411	9.80
NIPUMDP-90-3	0.63	43	0.17	391	5.50
NIPUMDP-80-1	2.31	40	0.58	325	14.70
NIPUMDP-80-2	1.95	36	0.45	322	13.45
NIPUMDP-80-3	1.91	35	0.32	335	16.10
NIPUMDP-70-1	5.60	21	0.91	250	18
NIPUMDP-70-2	6.25	23	1.05	205	15.85
NIPUMDP-70-3	7.50	28	1.07	243	22.58

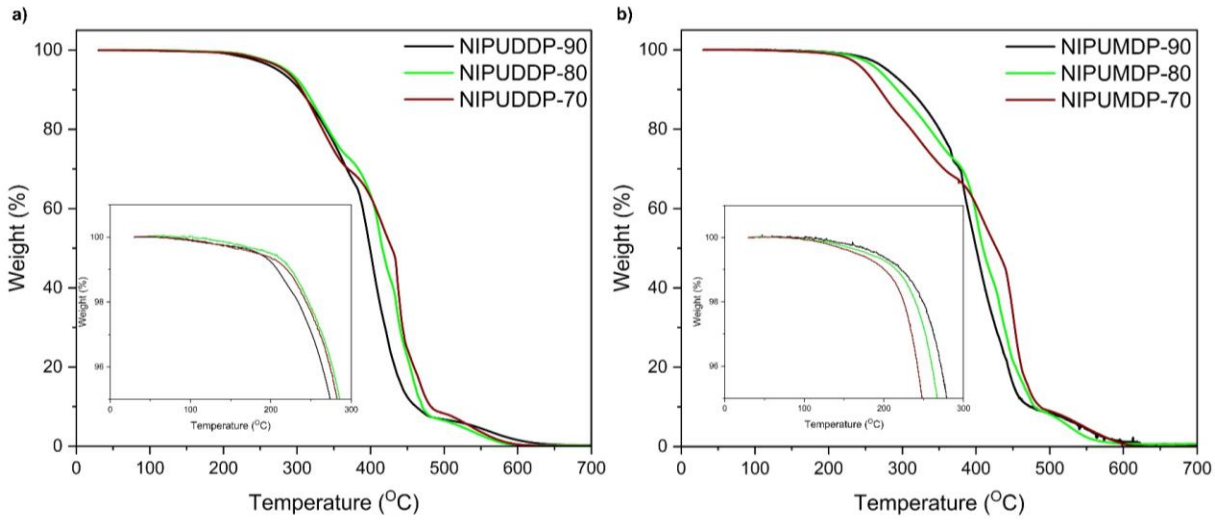

Figure D 8. TGA thermograms for the crosslinked NIPUs; a) DDP-based NIPUs and b) MDP-based NIPUs.

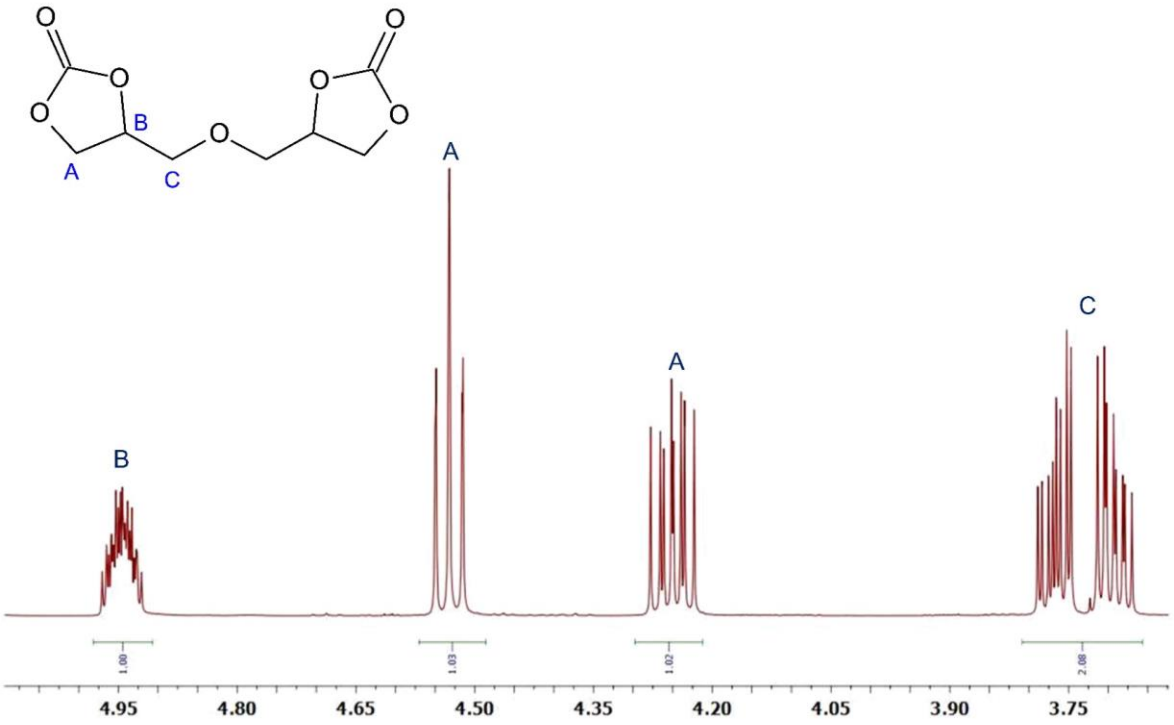

Figure D 9. ^{1}H NMR spectrum for the synthesized DGC. ^{1}H NMR (DMSO-d_6, ppm): 4.92-4.98 (m, 2H), 4.50-4.56 (t, 2H, cis or trans), 4.20-4.30 (ddd, 2H, cis or trans), 3.80-3.65 (m, 4H).

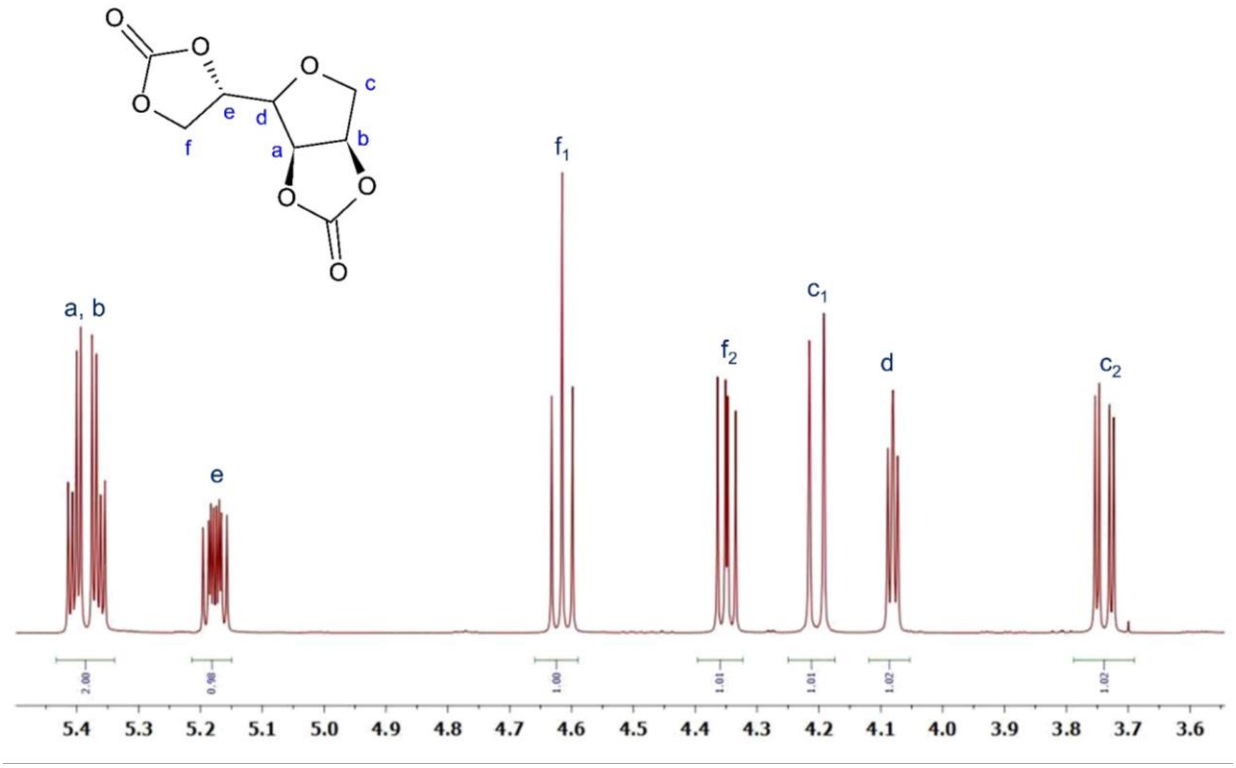

Figure D 10. ^{1}H NMR spectrum for the synthesized MBC. ^{1}H NMR (DMSO-d_6, ppm): 5.40-5.45 (m, 2H), 5.34-5.40 (m, 2H), 5.15-5.22 (m, 1H), 4.58-4.67 (t, 2H), 4.32-4.40 (dd, 2H), 4.18-4.26 (d, 2H), 4.05-4.12 (t, 1H), 3.68-3.78 (m, 2H).

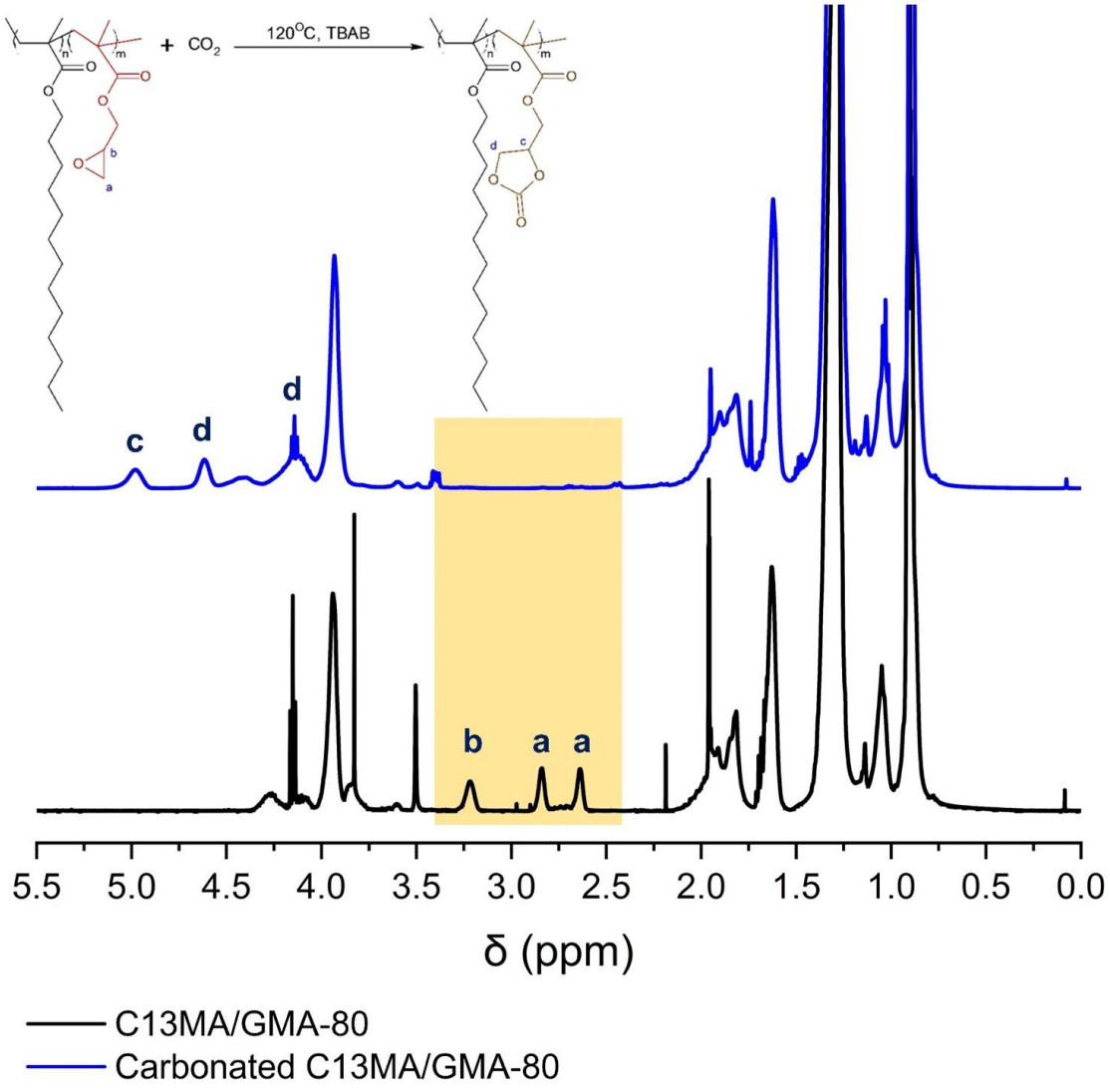

Figure D 11. [1]H NMR spectrum for carbonated C13MA/GMA-80 after 24 hours.

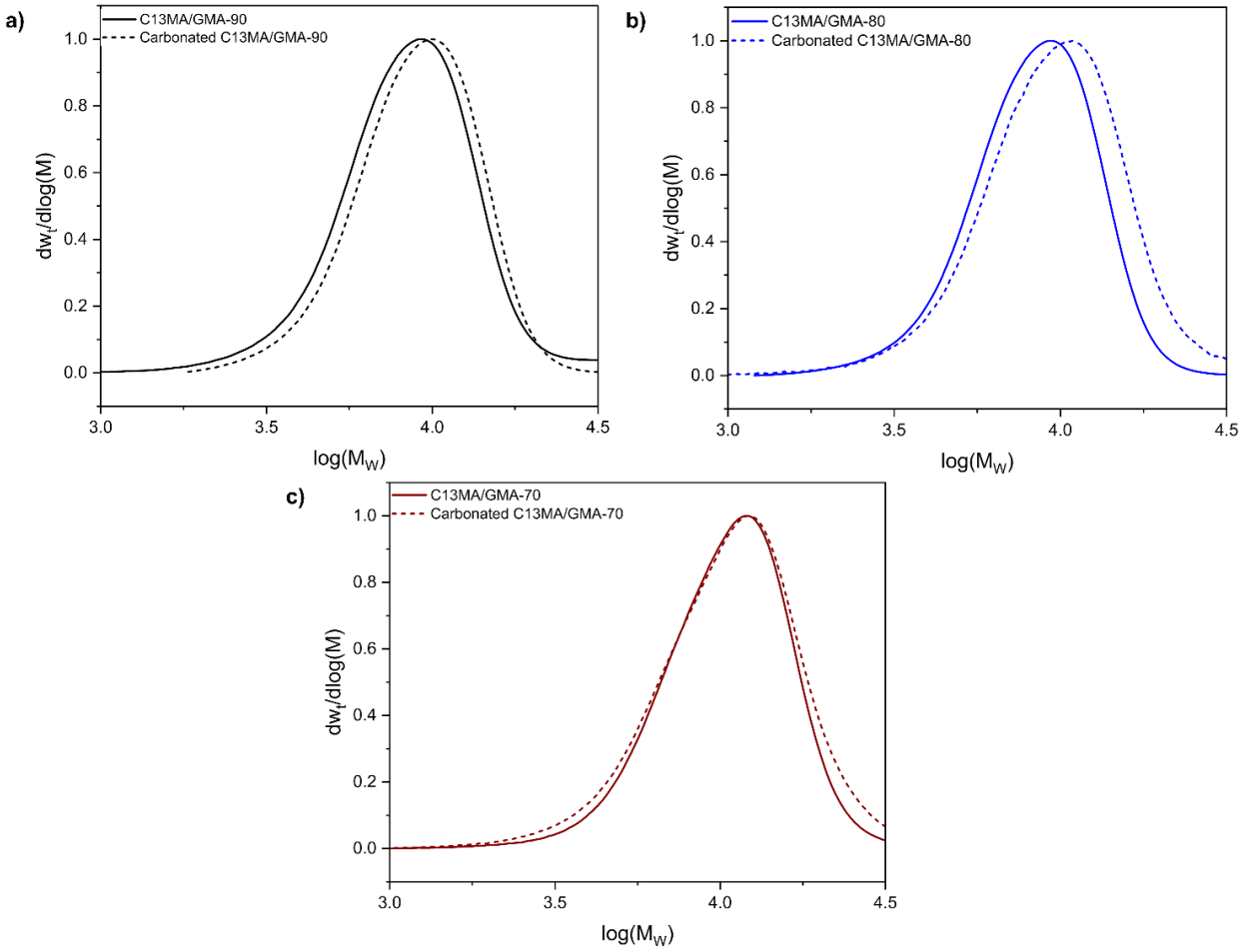

Figure D 12. Normalized GPC results for C13MA/GMA copolymers before and after carbonation.

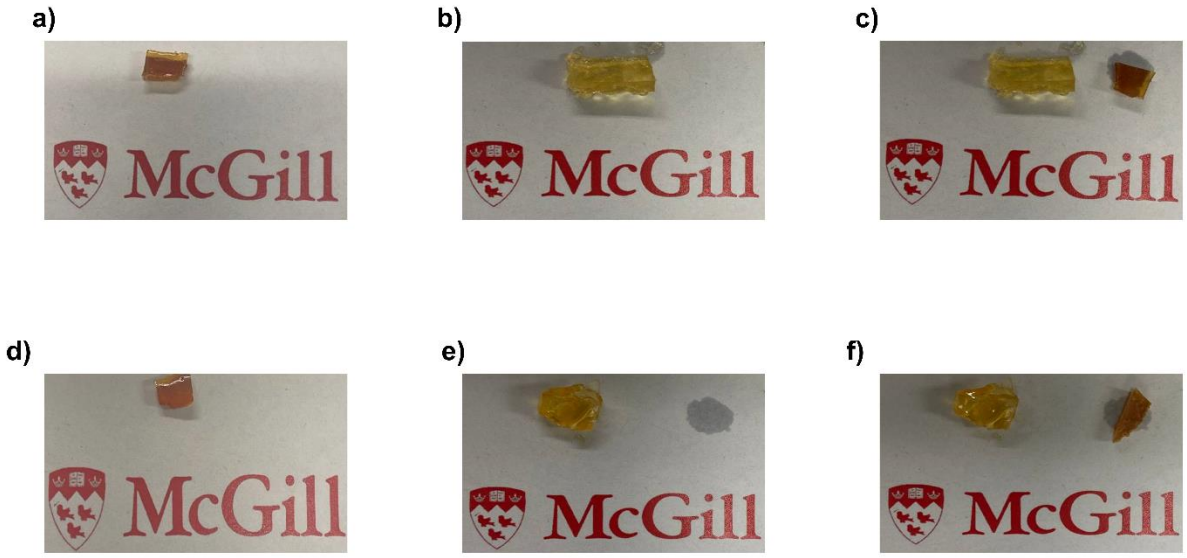

Figure D 13. Swelled samples in solvent, a) NIPUDDP-80 before swelling, b) NIPUDDP-80 after being soaked for 24 hours in THF, c) comparison of NIPUDDP-80 after being soaked in THF and RO water (left sample was soaked in THF and the right samples was soaked in RO water), d) NIPUMDP-70 before swelling, e) NIPUMDP-70 after being soaked for 24 hours in THF and f) comparison of NIPUMDP-70 after being soaked in THF and RO water (left sample was soaked in THF and the right samples was soaked in RO water).